U.PORTO

FEUP FACULDADE DE ENGENHARIA
UNIVERSIDADE DO PORTO

lepabe Laboratory for Process Engineering,
Environment, Biotechnology and Energy

Chemical Engineering Department

DEVELOPMENT AND STUDY OF PHOTOCATALYSTS FOR PHOTO-INACTIVATION OF MICROORGANISMS

Pedro José Martins Cardoso de Magalhães

Dissertation presented to obtain the degree of
DOCTOR IN CHEMICAL AND BIOLOGICAL ENGINEERING
by the
UNIVERSITY OF PORTO

SUPERVISORS:

Adélio Miguel Magalhães Mendes, Full Professor

2018

ACKNOWLEDGEMENTS

I would like to express my gratitude to Professor Adélio Mendes, my supervisor, for the opportunity to work in this topic, for our helpful discussions and for his continuous interest on my work that led me to finsh this thesis. I also like to acknowledge the great contribution of Professor Olga Nunes, who always helped me to grow as both a person and a professional. I would like to point out the role of Dr. Luisa Andrade on the completion of this thesis. The professional support given by her helped me to achieve the results presented here. I gratefully acknowledge Professor Bo Iversen, who accepted me in his research group for three months.

This thesis would not be possible if my parents did not always give me their full support and encouraged me to pursue this goal. All of their belief in me made me the person that I am today. My sister, who is to me like a second mother, was always with me in all the decisions that I made throughout these years and helped to do much of the work.

To the one and only Rute, that always put up with my bad moods and was always with me in the great achievements. I am indeed a better person when I am with you. I love you for who you are and for who I am when I am with you.

To all the people that worked with me during this long journey, who were always available to help me when needed. I also have to point out the role of Joana Ângelo, who made this journey with me, and who was a great co-worker and a very good friend during the whole process

I would also like to thank my whole family for the great fun, discussions and conversations that we all shared throughout these years. I would like to mainly acknowledge Gena for putting up with me during almost three long years, I will never forget that.

To all my friends that, everyday, make my life so special making everything I do so unique.

Last, but not least, I thank all my current co-workers in NDtech.

To all that crossed my path and made me the person I am today…

PREFACE

The present work was developed in Laboratory for Process, Environmental and Energy Engineering (LEPABE) facilities, in the Chemical Engineering Department of Faculty of Engineering of the University of Porto (FEUP), between 2012 and 2017 and under the grant SFRH/BD/ 78827/2011.

Part of the studies was also performed in Center for Materials and Cristallography (CMC), under the supervision of Prof. Bo Iversen (Head of the Laboratory).

This work results from a compilation of three scientific papers and a chapter concerning the work developed during my stay in Denmark. A final chapter with the overall conclusions and perpectives for future work is also presented.

Statement

The PhD thesis presented by Pedro José Martins Cardoso de Magalhães and entitled "Development and study of Photocatalysts for photo-Inactivation of microorganisms", supervised by Professor Adélio Miguel Magalhães Mendes, comprises three scientific articles - one accepted and two submitted for publication - and one unpublished chapter. Since the articles included in the thesis have several co-authors, the contribution of thesis author is explained. The co-authors of each article do agree with this statement. The information presented on this thesis is not included in any other PhD thesis

Articles

Pedro Magalhães, Luísa Andrade, Olga C. Nunes*, Adélio Mendes*, Titanium dioxide photocatalysis: fundamentals and application on photoinactivation. Submitted to Reviews on Advanced Materials Science in March 2017.

Pedro Magalhães was involved on the writing of all of the chapters that comprise this review article. The author was also responsible to the bibliographic search. Contribution of 40 %.

Pedro Magalhães, Joana Ângelo, Vera M. Sousa, Olga C. Nunes, Luísa Andrade, Adélio Mendes, Synthesis and Assessment of a Graphene-based Composite Photocatalyst, Biochemical Engineering Journal 2015, 104, 20-26.

Pedro Magalhães contributed to the planning and execution of all the experiments described in this article. The author was also involved on the discussion and interpretation of results, as well as on the preparation of the manuscript. Contribution of 70 %.

Pedro Magalhães, Joana Ângelo, Olga Nunes, Adélio Mendes*, Enhanced methylene blue photodegradation with propylene carbonate as a solvent. To be submitted in March 2017.

Pedro Magalhães contributed to the planning and execution of all the experiments described in this article. The author was also involved on the discussion and interpretation of results, as well as on the preparation of the manuscript. Contribution of 50 %.
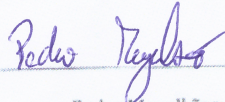
Unpublished chapters

Synthesis of a novel TiO_2/graphene composite under supercritical conditions – This work was conducted in Aarhus Universitet (Denmark) under the supervision of Prof. Bo B. Iversen, assisted by Doctor Henrik L. Hellstern, and supervision of Prof. Adélio Mendes. Characterization trials of the produced photocatalyst were also conducted in Portugal. Contribution of 60 %.

The thesis also includes a section of a chapter that is included on a submitted article - Joana Ângelo, Pedro Magalhães, Luísa Andrade, Luís M. Madeira, Adélio Mendes. Modelling of NO photoabatement using commercial titanium dioxide. Submitted in March 2017.
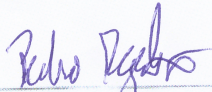
Porto, 13th of March of 2017

Pedro Magalhães
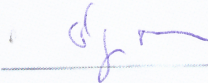
The co-authors agree with the contributions of the thesis author for the mentioned articles

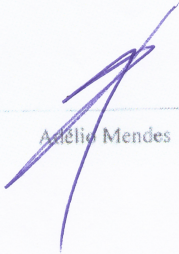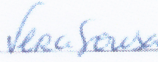Pedro Magalhães   Luísa Andrade   Olga Nunes

Adélio Mendes   Vera Sousa   Joana Ângelo

CONTENTS

PART III: PHOTOCATALYITIC MECHANISM

PART IV: GENERAL CONCLUSIONS AND FUTURE WORK SUGGESTIONS

ABSTRACT

In the past four decades photoelectrochemistry and photocatalysis fundamentals and applications developed tremendously. Presently, photoelectrochemical systems are researched and entering in several emergent fields such as energy production (*e.g.* photoelectrochemical cells for fuel production from solar energy), environmental protection (e.g. photo abatement of atmospheric pollutants such as NO_x, volatile and halogenated hydrocarbons), water purification (e.g. photooxidation of micropollutants, volatile organohalide compounds, pesticides) and for microorganisms inactivation.

In the last decade many studies reported the use of photocatalysis for disinfection purposes; especially the antimicrobial application of titanium dioxide has been widely discussed in many reviews and research articles. In this thesis, the microorganism photoinactivation main issues are reviewed, namely regarding the development of materials with enhanced visible light harvesting to foster photocatalysis for indoor applications (e.g. hospitals, health centres, etc.).

A novel composite photocatalyst prepared from graphene and commercial TiO_2 (P25 from Evonik) was synthesized, exhibiting enhanced photocatalytic activity for methylene blue degradation, when compared with pristine P25. Additionally, the new catalyst showed 20 % more NO conversion under UV light than P25. The band gap of the catalyst, obtained from diffuse reflectance, was 2.95 eV indicating an extended light absorption up to 420 nm. The novel photocatalyst was further tested for inactivating microorganisms showing better results than the reference photocatalyst. Under visible light, the viability loss of the reference bacterial strain *Escherichia coli* DSM 1103 was two times higher than with the bare P25; it was observed 29 % of inactivation with the P25/graphene composite and 14 % with the P25 sample, following standard ISO 27447:2009.

A novel method for producing TiO_2/graphene composites under supercritical conditions is described. This method allows the use of nontoxic reactants to prepare a high quality TiO_2/graphene photocatalyst and uses an easily scalable reactor. The produced composite presented a lower band gap -3.0 eV when compared with the TiO_2 produced under supercritical conditions -3.2 eV. The morphology of the composite was

thoroughly characterized. When compared with pristine TiO_2 produced under the same conditions, the composite showed enhanced methylene blue degradation.

The role of water in the TiO_2-based photocatalytic phenomenon is not yet fully understood. The photocatalysis of methylene blue dissolved in propylene carbonate and different concentrations of water was studied. It was observed that the photocatalytic activity of TiO_2 (P25 from Evonik) peaks when propylene carbonate solvent is used with minute amounts of water; the maximum photodegradation rate was ca. 6.5 times higher than when just water solvent was used. The conventional interpretation of the methylene blue photooxidation intermediated by free radical OH• cannot explain these results. Alternately, the experimental results were interpreted based on the recently proposed "direct–indirect" (D-I) model and a mathematical model was successfully developed and fitted to the experimental results. Finally, new insights on the role of water in the photocatalytic phenomenon were withdrawn.

SUMÁRIO

Nas últimas quatro décadas os fundamentos e aplicações da fotoeletroquímica e fotocatálise foram extensamente desenvolvidos. Atualmente, os sistemas fotoeletroquímicas são estudados e ocupam diversas áreas emergentes, tais como a produção de energia (por exemplo, células fotoeletroquímicas para a produção de combustível a partir de energia solar), a proteção do ambiente (por exemplo foto redução de poluentes atmosféricos, tais como NO_x, voláteis e hidrocarbonetos halogenados), purificação de água (por exemplo foto-oxidação de micropoluentes, compostos voláteis, pesticidas) e inativação de microrganismos.

Na última década, muitos estudos descreveram a utilização de fotocatálise para fins de desinfecção; especialmente a aplicação antimicrobiana do dióxido de titânio tem sido amplamente discutida em diversos artigos científicos. Nesta tese, as questões principais sobre a fotoinativação de microrganismos são revistas, nomeadamente no que respeita ao desenvolvimento de materiais que ativos sob luz visível para fomentar a fotocatálise para aplicações de interiores (por exemplo, hospitais, centros de saúde, etc.).

Um novo fotocatalisador compósito preparado a partir de grafeno e TiO_2 comercial (P25 da Evonik) foi sintetizado, exibindo aumento da atividade fotocatalítica para a degradação do azul de metileno, quando comparado com o P25. Além disso, o novo catalisador mostrou 20% mais conversão de NO sob a luz UV do que o P25. O hiato energético do catalisador, obtido a partir de refletância difusa, foi de 2,95 eV indicando uma absorção de luz estendida até o comprimento de onda de 420 nm. O novo fotocatalisador foi ainda testado para inativação de microrganismos exibindo melhores resultados do que o fotocatalisador de referência. Sob luz visível, a perda de viabilidade da referência bacteriana *Escherichia coli* DSM 1103 foi duas vezes maior do que com o P25; observou-se 29% de inativação com o P25/grafeno e 14% com o P25, seguindo a norma ISO 27447: 2009.

Um novo método para a preparação de compósitos de TiO_2/grafeno sob condições supercríticas é descrito. Este método permite o uso de reagentes não tóxicos para preparar um fotocatalisador compósito de TiO_2/grafeno de alta qualidade e usando um reator de fácil dimensionamento. O compósito produzido apresenta um hiato energético mais pequeno -3.0 eV, quando comparado com o hiato energético do TiO_2

produzido sob condições supercríticas -3.2 eV. A morfologia do compósito foi extensamente caracterizada. Quando comparado com o TiO_2 produzido sob as mesmas condições, o compósito produzido apresentou uma melhor eficiência foto catalítica para a degradação de azul metileno.

O papel desempenhado pela água no fenómeno foto catalítico ainda não é completamente compreendido. No trabalho realizado, a degradação de azul de metileno com a utilização de um solvente orgânico – carbonato de propileno – foi estudada. A atividade foto catalítica do dióxido de titânio comercial – P25 da Evonik – apresentou um valor máximo com a utilização deste solvente orgânico e quantidades diminutas de água; o valor máximo para foto degradação de azul de metileno foi cerca de 6.5 vezes superior ao valor obtido utilizando apenas água como solvente. A interpretação tradicional da foto oxidação de azul de metileno intermediada pelo radical livre OH• não explica os resultados obtidos. Assim, os resultados experimentais foram interpretados tendo como base o recentemente proposto modelo de transporte direto-indireto (DT-IT) e um modelo matemático foi desenvolvido e aproximado com sucesso aos resultados experimentais obtidos.

TABLE CAPTIONS

LIST OF ABBREVIATIONS

ABBREVIATIONS	DEFINITION
7HC	7- hydroxycoumarin
CB	conduction band
CFU	colony forming units
C_{MB}	concentration of methylene blue
COU	coumarin
C_W	concentration of water
D-I	direct-indirect
DT	direct transfer
e^-	electrons
EDX	energy dispersive X-Ray spectroscopy
E_g	band gap
FTIR	Fourier-transform infrared spectroscopy
GNP	graphene nano-platelets
GNP_{ox}	oxidized graphene nano-platelets
h^+	holes
HPLC	high-performance liquid chromatography
ISO	international organization for standardization
IT	indirect transfer
MB	methylene blue
NHE	normal hydrogen electrode
NO	nitrogen monoxide
NO_x	nitrogen oxides
$O_2^{\cdot-}$	superoxide anion

$O_{br}{}^{\bullet-}$	bridging oxygen radicals
$O_{br}{}^{2-}$	bridging oxygen ions
OH·	hydroxyl radical
OH_s	bridging hydroxyl group
PCA	plate counting agar
PL	photoluminescence
RH	relative humidity
SC	semiconductor
SEM	scanning electron microscopy
SPR	surface plasmon ressonance
TEM	transmission electron microscopy
TiO_2	titanium dioxide
UV	ultra violet
VB	valence band
XRD	x-ray diffraction

PART I:

INTRODUCTION

Chapter 1

INTRODUCTION[1]

In the past four decades photocatalysis fundamentals and applications developed tremendously. Presently, there is a deeper understanding of the photocatalysis fundamentals and, consequently, the use of photocatalysts in several emergent fields such as energy production (*e.g.* photocatalytic water splitting [1]), environmental protection (*e.g.* self-cleaning materials [2] and photo abatement of atmospheric pollutants such as NO_x [3], volatile and halogenated hydrocarbons [4]), water purification (*e.g.* photooxidation of micropollutants [5], volatile organohalide compounds, pesticides [6]) and for microorganisms inactivation [7].

Even though the environmental applications are leading the photocatalysis, microorganism photoinactivation is also catching more and more attention within the scientific community. In fact, there is an alarming increase in the number of hospital-acquired infections, also known as nosocomial infections [8]. This increase was caused by an uncontrolled use of substances that promote the propagation of antibiotic resistance, strongly motivated by a lack of adequate legislation [9]. Infectious diseases are becoming again a real threat, with new infections appearing at an alarming rate [10], and the exponential movement of people across countries, oceans and continents are intensively contributing to their propagation.

In the past decade many studies reported the photocatalysis use for disinfection purposes; especially the antimicrobial application of titanium dioxide has been widely discussed in many reviews and research papers [11]. In this chapter, the microorganism photoinactivation main issues will be reviewed, namely regarding the development of materials with enhanced visible light harvesting to foster photocatalysis for indoor applications (*e.g.* hospitals, health centres, etc.). Since the use of TiO_2 for disinfection purposes is being limited to its ability of absorbing only UV light and by the rapid recombination of separated positive and negative charges, doping, decoration and the

---

[1] Adapted from Magalhães, P., Andrade, L., Nunes, O.C., Mendes, A., "**Titanium dioxide photocatalysis: fundamentals and application on photoinactivation"**

use of TiO$_2$/graphene composites are addressed below as mechanisms for mitigating these drawbacks.

1.1 Fundamentals of photocatalysis

The pioneer work developed by Fujishima *et al.* [12] describing water splitting with a TiO$_2$ photoelectrode caught the attention of several research groups working on this field and rapidly TiO$_2$ became the most used semiconductor for photocatalysis. Titanium dioxide exhibits three crystalline structures: rutile, anatase and brookite. Rutile is the most thermodynamically stable crystal structure of titanium dioxide but anatase is the preferred form for photocatalysis because it presents higher photocatalytic activity and it is easier to prepare. Brookite is the least stable phase and normally not used in photocatalysis. There are studies that indicate the benefits of mixings different crystalline phases of TiO$_2$ for obtaining a higher photoactivity [13, 14]. When different crystalline phases are coupled, it is mostly believed that the movement of electrons from the rutile phase to the anatase phase occurs, which causes a more efficient e$^-$/h$^+$ separation and consequently an increased photocatalytic activity [15]. However, there are other studies defending that the electron movement is from anatase to rutile [16].

The anatase band gap is *ca*. 3.2 eV while the band gap of rutile is *ca*. 3.0 eV. Upon excitation with photons presenting energy higher than the band gap energy, an electron is injected from the valence to the conduction band, generating an electron-hole pair in the conduction and valence bands, respectively. The photogenerated charges diffuse to the surface of the semiconductor particle where they promote redox reactions; holes may generate vacancies on TiO$_2$ surface or excited reduced species, while excited electrons normally react with oxygen to produce free radical O$^{2-\bullet}$. These are responsible for the photodecomposition of organic compounds, where adsorbed water and oxygen have been described to play an important role. There are, nowadays, several proposed pathways for the photodegradation of pollutants [17, 18]. The most commonly assumed photodegradation mechanism is based on Langmuir-Hinshelwood kinetic model, as described by Ollis and Turchi [19]. There are however, nowadays works that question the role of hydroxyl radicals in photocatalysis [20] Montoya and co-workers [21] made a strong case against the direct reaction of a photogenerated hole with adsorbed water or OH$^-$ to form OH·, suggesting a novel direct-indirect model (D-

I). The role of water in the TiO_2-based photocatalytic phenomenon will be further addressed and developed on Chapter 4.

As previously mentioned, improving the TiO_2 photocatalytic activity for attaining visible light activity is being targeted; this improvement can be achieved by: i) avoiding the recombination of photogenerated electrons/holes; ii) narrowing the semiconductor band gap (E_g) [22]. While the first permits to efficiently generate more free radicals, the later allows the photocatalyst to absorb a larger fraction of the solar spectrum. Even though the recombination rate of e^-/h^+ has been neglected in many works due to difficulties in its estimation, it has been proved that the recombination rate has a strong contribution for the net photocatalytic activity [23, 24]. The majority of the authors working on this topic defend that the crystal structure of the photocatalyst is a dominant factor of the photocatalytic activity since the recombination of e^- and h^+ is facilitated at the traps on the surface and in the bulk of the particles [25]. Indeed, it is assumed that the recombination process occurs at the crystal defects, explaining why amorphous TiO_2 presents almost negligible photocatalytic activity. Nevertheless, there are few works discussing this point since the defects of the photocatalytic powders are very difficult to determine. Anatase absorbs only wavelengths smaller than 386 nm, which falls in the UV range. Sunlight spectrum comprises only 5-7 % of UV light, 46 % of visible light and 47 % of infrared radiation [26]. So, TiO_2 modifications to allow visible absorption are fundamental to enhance the photocatalytic rate. Targeting this enhancement the research was directed for the use visible light instead of only UV radiation, and of proper immobilization of the photocatalyst. TiO_2 doping and/or decoration with the objective of increasing photoactivity and photoabsorbance is addressed below. Doping concerns adding foreign chemical elements (impurities) to modify in the inner-structure of the photocatalyst, while decoration concerns adding materials to the photocatalyst surface. Both modifications target the same objectives: preventing e^-/h^+ recombination and red-shift of the light absorption. TiO_2/graphene composite photocatalysts reduces the charge recombination and originates Ti-O-C bonds that promotes significant red-shift.

1.1.1 Doping and decoration

Doping of TiO₂ can help the improvement of photocatalytic activity by enhancing the optical absorption of wide band gap semiconductors, increasing the minority carrier diffusion length or enhancing the catalytic activity at the surface of the semiconductor [27]. However, in some cases, these dopants can also promote e^-/h^+ recombination with the creation of mid gap surface states that actually act as recombination centres [27]. High values of dopant concentration (not above 10^{-6} mol·dm⁻³ [27]) should be avoided since may lead to segregation of the dopant phase. There are two possible doping sites in TiO₂: at the titanium site (cation doping) or at the oxygen site (anion doping). Thus, there are two main types of TiO₂ doping: cation-doping [28-37] and anion-doping [38-47]. Various studies have been performed to explain the band gap narrowing mechanism in TiO₂ doping [26, 38, 48]. Nitrogen doping is the most used approach for obtaining visible light activity; [49-51] however, there is no established mechanism that explains the visible light activity of N-doped TiO₂. While some authors state that substitutional N-doping results in band gap narrowing due to the efficient mixing of orbitals 2p of N and O, others argue that band gap narrowing through modifications in the energy levels of valence and conduction bands can only occur with high concentrations of dopants and strong interactions among impurity energy states, valence and conduction bands [50]. Di Valentin and co-workers [52] based on the density functional theory (DFT) predicted that N atoms could occupy either substitutional or interstitial sites in the TiO₂ lattice and thus generate localized energy states. When substitutional sites are occupied, a higher energy level extending the valence band is formed, while in the case of interstitial sites occupation, discrete energy levels above the valence band are created. Doping with other anions, such as carbon, can also show gap narrowing [53]. Some authors suggest that the use of doping agents results in modifications of (101) TiO₂ surface [54]. These modifications can increase the transfer of photogenerated electrons to the outer surface regions, facilitating the photocatalytic reactions and improving the quantum efficiency of the photocatalytic processes.

Another approach used for obtaining visible light activity is metal ion doping. Some theories explain the visible light response obtained with this type of doping such

as, the occurrence of band gap narrowing and intrinsic defects by either substitutional or interstitial substitution in the TiO_2 matrix [50]. Metal ion doping induces, however, recombination of charge carriers lowering the overall efficiency of photocatalysis. Additionally, some reports point to differences in the photocatalytic phenomena under visible light and UV radiation. For UV radiation, both superoxide and hydroxyl radicals are produced. Nevertheless, for the case of visible light activity, a less oxidative superoxide radical was suggested to be formed and being the main responsible for the photocatalytic activity [50, 55, 56]. Renguifo-Herrera and co-workers [55] developed N and S co-doped TiO_2 presenting an intense visible-light absorption. However, its photocatalytic activity was low, similar to P25 under solar simulated light. These results can be ascribed to the fact that the photogenerated holes on the intermediary energy levels formed by N and S co-doping under visible light do not present sufficient redox potential to oxidize water and thus are not able to produce OH· radicals.

The main difference between doping and decoration is related to which part of the TiO_2 is modified. In the case of doping, the modifications are conducted inside the crystalline structure of TiO_2, while in the case of decoration the modifications are made on the TiO_2 surface. After excitation of TiO_2, electrons migrate to the attached decorating particle where they become trapped, minimizing the electron-hole recombination [57]. The migration of electrons to the decorating particles was confirmed in several studies [58-60], which showed an improved photocatalytic activity of the decorated TiO_2 when compared to pristine TiO_2; the holes migrate then to the semiconductor surface without recombining [58-60]. Few review articles analysing doping and decorating effects on photocatalysis have been published recently [61-64].

An effect that worth to be explained and that has been gathering interest in the scientific community is the surface plasmon resonance effect - SPR effect. When a metal nanoparticle is subjected to an oscillating electric field as the case of incident light, the free electrons in the nanoparticle will answer to that electric field also by oscillating. This behavior is called localized surface plasmon resonance and it can be adjusted by manipulating the size, shape and dielectric environment to change the

interaction of the nanoparticles with incident light. Thus, it is possible to scatter the incident light with metal nanoparticles and increase the optical path of photons, leading to an absorption enhancement in certain wavelengths. SPR effect also promotes changes in the energy of the Fermi level caused by the electron storage effects in the metal nanoparticle [50]. Localized SPR of gold and silver nanoparticles normally results in strong and broad absorption bands in the visible light region, which can be exploited to attain visible light-activated photocatalysts [57, 65-67].

Important to mention that one of the possible disadvantages of TiO_2 decoration is the corrosion and dissolution of decorating metal particles during the photocatalytic reaction [68]. The decorative particles can also act as co-catalysts, reducing the overvoltage of the redox reactions involved in photocatalysis. The use of co-catalysts allow a given electrochemical reaction to progress faster [69]. For instance, in photoelectrochemical water splitting, the lower level of the conduction band must be more negative than the redox potential of H^+/H_2 (0 V vs. NHE, at pH = 0) and the top level of the valence band must be more positive than the redox potential of O_2/H_2O (1.23 V, at pH = 0). Since this reaction is very difficult to accomplish using TiO_2 photocatalyst, the use of co-catalysts such as Pt, Au and Rh for H_2 evolution [70] and RuO_2 for O_2 evolution [71] is essential.

1.1.2. TiO₂/graphene composite

TiO_2 photoactivity can also be enhanced with the production of TiO_2 composites. The most notable case is the production of TiO_2/graphene composites. In TiO_2/graphene composites, the electron–hole pairs are generated upon TiO_2 excitation under UV light irradiation. These photogenerated electrons are then injected into graphene due to the more positive Fermi level of graphene [72] The high carrier mobility of graphene accelerates excited electron transport that enhances the photocatalytic performance [73]. Simultaneously, Ti-O-C bonds formed in the TiO_2/graphene photocatalyst originate a red shift of few dozens of nanometers in the solar spectrum, reducing its bandgap and making it sensitive to longer-wavelength light [74, 75]. The resulted photocatalyst presents then an extended photoresponse of up to *ca.* 440 nm

TiO$_2$ photooxidation is normally assigned intermediated free radicals OH$^{\bullet}$ (oxidation potential of 2.8 V [76]) and O$_2^{\bullet-}$ (reduction potential of -0.137 V [77]), making necessary a thermodynamic minimum band gap of 2.94 eV for generating both radicals. Since most of band gap shortening approaches consider the creation of intermediate energy levels, cf. section 1.1.1, making the electron energy gain a stepwise process, the lowest and highest energy levels are still available. This means that, despite the band gap shortening below e.g. 2.8 eV, the photocatalyst is still active towards OH$^{\bullet}$ and O$_2^{\bullet-}$ generation [78]. Nevertheless, the visible light activity of the TiO$_2$/graphene composites is not fully understood [79, 80]. When graphene is bounded to TiO$_2$ the overall photocatalytic performance is largely improved. This is mainly attributed to three effects: i) efficient charge separation and transportation; ii) extended light absorption range; and iii) enhanced adsorptivity of the reactant species [75].

For photocatalytic indoor applications, such as for photoinactivation of microorganisms, a very promising photocatalyst is Au/TiO$_2$/graphene. The use of gold nanoparticles is expected to promote increased values of photoactivity due to the high surface plasmon resonance effect observed with these nanoparticles [57, 81]. The Au/TiO$_2$/graphene, already described for the H$_2$ production [82], shows enhanced photocatalytic activity due to the surface plasmon resonance effect of the Au nanoparticles, that broadens the visible light response of the TiO$_2$, and the excellent electron transport properties of graphene, which decreases the recombination of electron and hole pairs. Au nanoparticles, as explained before, can also reduce redox overpotentials [83].

1.2. Photoinactivation

1.2.1 Rationale of using TiO₂ photocatalysis as the basis of new disinfection methods

The intensive use of antimicrobial agents, including antibiotics in human and veterinary chemo-biotherapy, aquaculture and animal husbandry have been pointed out as the main cause behind the tremendous increase of antibiotic resistance in clinical settings and in the environment [84]. The emergence and spread of antibiotic resistant bacteria is not only of paramount public health concern, but it leads also to high costs for the national health services. Organic disinfectants are among the substances that may promote antibiotic resistance dissemination, given the occurrence of co-selection due to genetic linkage between antibiotics and biocides [85-88]. Therefore, the development of new disinfection techniques based on biocides naturally occurring in the human immune system is very attractive.

Phagocytic cells of the human immune system use the cytotoxic effects of ROS as a component of their host defence mechanism [89-91]. When a phagocyte encounters a microorganism, a portion of the phagocyte membrane surrounds it – the first step of a phagolysosome formation. This process leads to increased phagocyte oxygen consumption and activates a unique membrane-associated NADPH-dependent oxidase complex [92]. This enzymatic complex univalently reduces O_2 to $O_2^{\bullet-}$, which further dismutes to H_2O_2 [92]. Another mechanism involved in phagocyte-mediated oxidant generation and microbial toxicity involves the iron-catalysed intra- or extracellular reaction of $O_2^{\bullet-}$ and H_2O_2 to form $OH^{\bullet}$ [90]. These ROS are known to be highly reactive with biological molecules and various authors proposed that $OH^{\bullet}$ radical is the most toxic [93-96]. During the photocatalysis process similar ROS are formed. Hence, photoinactivation seems a good alternative to commonly used disinfection methods.

Matsunaga and co-workers in 1985 were the first authors assessing the feasibility of using UV-activated TiO_2 for photoinactivation [7]. This study reported the successful photoinactivation of both Gram negative and Gram positive bacteria (*Escherichia coli* and *Lactobacillus acidophilus,* respectively) and yeasts (*Saccharomyces cerevisiae*) cells by a semiconductor powder (platinum-doped

titanium dioxide, Pt-TiO$_2$). This pioneer work triggered numerous studies to assess the efficiency of TiO$_2$ photocatalysis on the inactivation of microorganisms and viruses (Tables 1.1-1.3) as well as microbial toxins and prions [11, 97]. A representative summary of the studies performed up to now on photoinactivation, as well as a comparison of this technique with traditional disinfection methods is given below.

1.2.2 Target test organisms and TiO$_2$ matrices

Given the commercial availability of TiO$_2$ nanoparticles, most of the studies assessing the efficacy of photoinactivation have been carried out with P25 (Table 1.1), which shows high performance and stability when excited with UV radiation [98]. Most of the studies used axenic suspensions of bacteria as target organisms, being *Escherichia coli*, the well characterized and universally used faecal contamination indicator, the most used. However, domain *Bacteria* accommodates an immense diversity of organisms, reflected in a wide variety of phylogenetic, genotypic and phenotypic groups. Therefore, differences in cellular structure, metabolism, pathogenicity, or tolerance against stressful conditions, including resistance to antimicrobial agents, may influence the susceptibility of bacteria to photocatalysis. This explains why other bacteria, including Gram positive bacteria (phyla *Firmicutes* and *Actinobacteria*), endospore formers (a restricted group of *Firmicutes,* including genera such as *Bacillus* and *Clostridium*), pathogens or opportunistic pathogens (such as *Legionella pneumophila* and *Pseudomonas aeruginosa*)*,* and antibiotic resistant bacteria have been used as test organisms in photoinactivation trials (Table 1.1, [99-102]). Given the complexity of the bacterial communities in natural environments, some studies assessed the efficacy of photocatalysis in mixed suspensions of known composition, or in a more realistic way, in wastewater (Table 1.1). The efficacy of photocatalysis in the inactivation of eukaryotic microorganisms, both in axenic or mixed suspensions has also been assessed. In fact, the differences in the cellular structure of prokaryotic and eukaryotic organisms may lead to distinct tolerances to photocatalysis. Similar reasons are behind the studies performed with prokaryotic and eukaryotic dormant forms (spores, cysts). Indeed, the inactivation of these structures,

particularly the bacterial endospores, has been a challenge due to their well-known resistance to chemical and physical antimicrobial agents [103, 104].

TiO_2 photoinactivation is expected to be the basis of different processes and materials compatible with commercial applications for disinfection. Indeed, photocatalysis-based new disinfection processes can be potentially used in several fields, such as water disinfection [93, 105-117], medical applications [115, 118-121], and pharmaceutical and food industry [120]. Given the wide variety of potential applications, assessment of photoinactivation has been carried out in different matrices. The majority of the studies assessed the efficacy of TiO_2 nanoparticles in aqueous suspension. This happens mainly because it is well known that the photoinactivation process is favored when cells are in direct contact with the photocatalyst. However, and primarily due to the potential harmful effects of nanoparticles in human health [122] and environment [123], immobilization of TiO_2 has been studied (Tables 1.1-1.3). Indeed, TiO_2 immobilization is very important for commercial applications [124], also due to two main reasons. Firstly, it is difficult to recover the photocatalyst when used as powder; this requires a post-treatment solid-liquid separation stage, which will add complexity and costs to the overall process [105]. Secondly, when it is not possible to recover the photocatalyst, the total loss of this material implies economical losses and it becomes itself a pollutant.

TiO_2 has been immobilized in different materials such as glass (plates, beads), polymers (polypropylene, polycarbosilane, cellulose acetate), paint and quartz disks [124-138]. These materials have been employed in surface coatings (glass, cellulose acetate sheets), paint coating and impregnated membranes. These approaches can be used for the inactivation of organisms in aqueous solutions (e.g. reactor wall), air (e.g. air filters) and fomites (e.g. paint coating). In the specific case of water treatment, the advantage of using coated glass beads is the larger specific surface area, which allows a more efficient photoinactivation of microorganisms. However, the use of glass beads can increase the cost and complexity of the process. In impregnated membranes, TiO_2 is deposited in the interstices of the membrane, improving the surface contact area between TiO_2 and the microorganisms. This method seems to be useful for wastewater treatment [139] but can also be used for the photoinactivation of air microorganisms

[132]. Paint coating seems to be, currently, the most promising immobilization matrix for commercial applications. Paint is a readily available material, easy to be applied onto surfaces and does not react with the photocatalyst nor interfere with the photocatalytic efficiency [140]. Furthermore, paint provides a good support for the photocatalyst in a 3D arrangement and can be applied in hospitals and other buildings where infections should be prevented.

1.2.3 Photoinactivation mechanism

To better understand the effect of TiO_2 photocatalysis on the differential inactivation of the cells and thereof dormant forms, the mechanism of action of photoinactivation is summarized as follows. All the cellular constituents, such as polysaccharides, lipids, proteins and nucleic acids can be attacked by ROS formed during photocatalysis. However, cell wall is the initial target for the photocatalytic attack. Considering as example the Gram-negative bacteria, the oxidation of components of the outer membrane by ROS promotes an increase in cell permeability. Consequently, ROS easily reach the cytoplasmic membrane, where peroxidation of membrane lipids also occurs. The consequent structural and functional disorders of the cytoplasmic membrane lead to ROS entrance in the cell, where they negatively interfere with DNA replication [11, 141] and respiratory activity [7, 142] due to the direct oxidation of coenzyme A into its dimeric form. Ultimately, ROS attack leads to the loss of cell viability and cell death [143-145]. The initial process of *E. coli* photoinactivation by the action of TiO_2 photocatalysis is depicted in Figure 1.1. Evidences indicate that the TiO_2 photocatalytic reaction results in continued bactericidal activity, well after the UV illumination terminates [144].
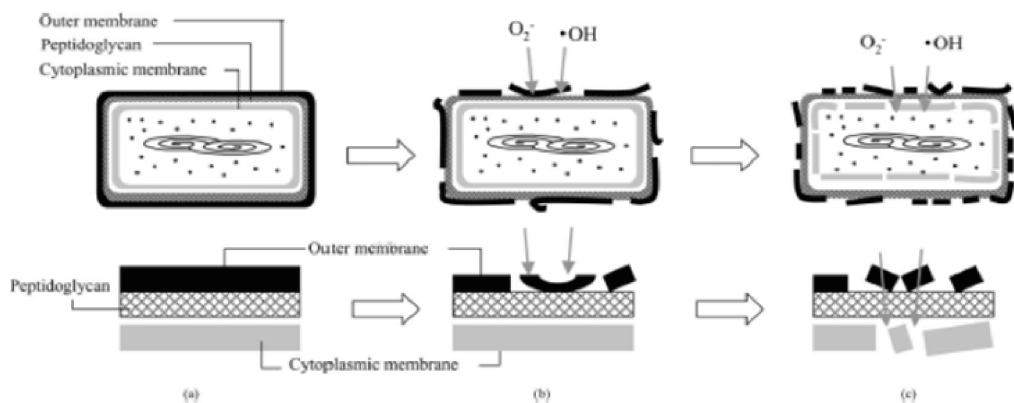
Figure 1.1. Free radicals mode of action (reprinted from [145] with permission).

In what concerns Gram-positive bacteria, the majority of the studies showed that they are more resistant to photocatalytic inactivation than Gram-negative [11]. However, some authors reported opposite observations [137, 146, 147]. Some of the differences encountered in the susceptibility to photoinactivation between Gram-negative and Gram-positive bacteria may be caused by the experimental conditions. For instance, van Grieken and co-workers [148] showed that the susceptibility of *E. coli* and *Enterococcus faecalis* to photocatalysis in natural waters was similar, whereas in distilled water the Gram-positive was more resistant. Nevertheless, the different cell wall structure of Gram-negative and positive bacteria is actually cited as the main reason for the distinction on ROS attack susceptibility. Gram-negative bacteria have a triple-layer, with an inner cytoplasmic membrane, and a cell wall composed by a thin peptidoglycan layer and an outer membrane. Besides the inner cytoplasmic membrane, the Gram-positive bacteria have a thick peptidoglycan layer. The high porosity of peptidoglycan allows solutes, such as ROS, to permeate. Therefore, also Gram-positive cells become susceptible to radical attack [149, 150]. However, the thickness of the peptidoglycan layer in these bacteria may allow a delay in the loss of cell permeability, and/or retard oxidants diffusion to vital sites. Indeed, both mechanisms would explain the higher resistance of Gram-positive bacteria to TiO_2 photoinactivation when compared with Gram-negative ones. On the other hand, the presence of an outer membrane in Gram-negative cells may explain why under certain circumstances these bacteria are more resistant to ROS attack than Gram-positive cells [7, 137, 146]. The

rigid cell wall of filamentous and unicellular fungi, composed mainly of soluble and insoluble polysaccharide polymers, make them more resistant to ROS attack than bacterial cells [11, 131]. Generally, dormant forms, such as fungal spores [127], cysts [131] and bacterial endospores [127], are even more resistant than the vegetative cells which proves the role of cell wall thickness and complexity in ROS defence.

1.2.4 Efficiency of photoinactivation

In this section, a summary of the studies carried out on the efficiency of photoinactivation under UV and visible radiation is given. Given the high number of studies published up to now in this field, a selection was made. The selection criteria included the type of tested microorganism, light sources and testing conditions, and the utilization of novel TiO_2 based photocatalysts. A more extensive literature review on this topic can be found elsewhere [11].

The factors affecting cell death, caused by an antimicrobial agent, include the agent concentration, time of exposure, and type and density of cells. Therefore, for a rigorous comparison of efficiency among antimicrobial agents and/or type of target organisms, standardized methods should be used. Even though there is already a standard for testing photocatalytic materials [151], most studies does not follow this standard, probably because this standard is referred to surfaces and most of studies are based on the use of suspensions, as previously mentioned. Hence, it is very difficult to compare the photoinactivation efficiency against different target organisms in different conditions, even when the same photocatalyst (e.g., P25) is used (Table 1.1-1.3). For example, studies reporting the inactivation of *E. coli* in suspension used photocatalyst concentrations ranging from 50 to 1000 mg/L, values of UV irradiance from 2 to 1000 W/m^2, time of contact from 5 min up to 144 h, and cell densities ranging between 10^3 to 10^7 colony forming units (CFU)/mL. In addition, different strains of this species were used ([101, 102, 112, 116, 127, 133, 137, 152-155], Table 1.1). Nevertheless, most of the studies performed up to now included controls and, in some cases, the inactivation of different organisms or matrices were tested under the same conditions allowing a better comparative assessment and thus valuable data to conclude on the efficacy of photoinactivation.

1.2.4.1 UV-TiO₂ photoinactivation

Photocatalytic experiments under UV radiation produce high levels of photoinactivation for the majority of the different microorganisms tested. As mentioned previously, P25 has been the most used photocatalyst. However, synthetized, pristine, doped or decorated TiO_2 were also reported.

As referred to above, despite the difficulties encountered on comparing the results obtained in the different studies shown in Tables 1.1 and 1.2, some conclusions can be drawn. UV-TiO₂ photocatalysis seems to be effective on the inactivation of all the types of microorganisms. Studies carried out by Herrera Mélian *et al.* [139], Dillert *et al.* [114] and Rincón *et al.* [117] should be highlighted since high values of inactivation of total heterotrophic bacteria and coliforms were reported for real wastewater samples.

But care must be taken to define the operating conditions since organisms with different cellular structure and complexity, such as *E. coli*, *Bacillus subtilis* endospores and the yeast *Candida albicans*, have very different susceptibility to photoinactivation. Total inactivation of *E. coli* cellular at a density of 10^6 CFU/mL was achieved within 40 minutes of contact in suspension, with a photocatalyst concentration of 0.1 g/L and irradiance of 55 W/m^2 [112]. However, to completely inactivate *Bacillus subtilis* endospores at a similar initial spore density (10^6 spore/mL), a photocatalyst concentration of 0.25 g/L, an irradiance of 70 W/m^2 and 540 minutes were needed [156]. Despite of shorter time of contact (30 minutes) and photocatalyst concentration (0.02 g/L) a very high irradiance value (330 W/m^2) was necessary to achieve 96 % inactivation of *Candida albicans* at and initial cellular density of 10^3 CFU/mL [157]. On the contrary, pathogenicity seems to have less influence on bacterial susceptibility against photoinactivation. For example, Cheng et al. [158] reported that total inactivation of pathogenic *Legionella pneumophila* serotype 1 at an initial cellular density of 10^7 CFU/mL was attained after 105 minutes with a photocatalyst concentration of 0.2 g/L and an irradiance of 1.65 W/m^2, conditions comparable to the ones used by Ibañez et al. [112] for the photoinactivation of *E. coli*.

Some antibiotic resistant bacteria are also susceptible to TiO₂ photocatalytic inactivation. Photoinactivation values of susceptible and antibiotic resistant strains of

E. coli [101] and *S. aureus* (MRSA) [102] were not significantly different (Table 1.1). However, differences between antibiotic resistant and sensitive counterparts have also been reported [102]. A multidrug-resistant *Acinetobacter baumannii* (MDRAB) was ca. 2 times more susceptible to photoinactivation than the antibiotic sensitive *Acinetobacter baumannii* control strain. Opposite results were obtained for *Enterococcus faecalis,* where the vancomycin resistant strain (VRE) showed ca. 2 times less susceptibility against photoinactivation than the susceptible strain [102]. Indeed, different susceptibility against oxidative stress was already reported among strains of the same microbial species [159, 160]. Hence, despite the utmost importance of comparing the response of a wide variety of these organisms against photoinactivation, to the best of our knowledge, such studies were not reported yet.

Table 1.1. Photoinactivation studies conducted under the influence of UV radiation (<380 nm).

Suspension type	Domain	Phylum	Organism	Initial cellular density (CFU/mL)	Photocatalyst	Photocatalyst concentration (mg/L)	Irradiance (W/m²)	Contact time (min)	Reduction (%)	Type of Trial	Ref.
Axenic	*Bacteria*	*Proteobacteria*	Susceptible and multidrug resistant *Acinetobacter baumannii*	10^3 - 10^5	TiO₂ (P25, other commercial TiO₂ and produced TiO₂)	62.5 and 125	4 and 8	5 to 80	99	Suspension	[102]
			Enterobacter cloacae	10^6-10^7		100	55	40	99.9	Suspension	[112]
			Susceptible and multiantibiotic resistant *Escherichia coli*	10^3 to 10^9, [a,b]		25 to 2500, [c,d]	2 to 1000, [e,f,g]	5 to 8640	99-100 (20[h])	Surface coating Suspension Paint Coating	[102, 112, 116, 127, 133, 137, 138, 152-155, 157, 161-165]
				10^6		9000	10	40	98.7 -99	Paint coating	[101]
			Salmonella typhimurium	10^6-10^7		100	55	40	99.9	Suspension	[112]
			Legionella pneumophila	10^7		1000	1.65	1	100	Suspension	[158]
			Pseudomonas aeruginosa	10^3-10^7		1000 - 10000	8 – 30, [c,i]	60 - 120	99.9 - 100	Surface coating Suspension	[116, 133, 137, 161]
			Salmonella enteritidis	10^7		1000	[c]	120	99.9	Suspension	[116]
			Salmonella choleraesuis	10^7		250 - 1250	1	180	> 99	Suspension	[166]
			Vibrio parahaemolyticus	10^7		250 - 1250	1	180	> 99	Suspension	[166]
		Firmicutes	*Bacillus anthracis*	10^3-10^6		1000, 1500	[j]	60, 90	4[k]	Suspension	[167]
			Bacillus cereus endospores	10^5		250	34	540	> 5[k]	Suspension	[156]
			Bacillus subtilis	$10^{5, l}$		[d]	74-318	8640	> 80, 20[h]	Surface coating Impregnated Membrane	[127, 132]
			Bacillus subtilis endospores	10^6		250	70	540	> 5[k]	Suspension	[156]

a - 1.3 mg/mL, b - 1000 microbial cells (mc)/mL, c - 0.02% suspension of uncovered 100-nm TiO₂ nanoparticles, d - 15-25 mg of TiO₂ per disk, e - 3.42 x 10^{-5} Einsteins.s^{-1}, f - 100 W high-pressure Hg lamp, g - 3900 lux, h – reduction in CO₂ mass balance, i - 2 x15 W, white light 356 nm peak emission, j - UVA - 9 W lamp; UVC -11 W lamp, k - log reduction, l - 1.5 mg/mL, n.a. – not available

Table 1.1 (Continuation). Photoinactivation studies conducted under the influence of UV radiation (<380 nm).

Suspension type	Domain	Phylum	Organism	Initial Cellular Density (CFU/mL)	Photocatalyst	Photocatalyst Concentration (mg/L)	Irradiance (W/m^2)	Contact Time (min)	Reduction (%)	Type of Trial	Ref.
Axenic	Bacteria	Firmicutes	Geobacillus stearothermophilus endospores	10^7	TiO$_2$ (P25, other commercial TiO$_2$ and produced TiO$_2$)	50 to 1000	91± 2	90	100	Suspension	[168]
			Clostridium difficile endospores	10^3		n.a.	30	300	3[a]	Surface coating	[137]
			Enterococcus hirae	10^7		10 000	8	60	100	Suspension	[161]
			Lactobacillus acidophilus	10^7		n.a.	[b]	60	100	Surface coating	[169]
			Listeria monocytogenes	10^7		250 - 1250	1	180	> 99	Suspension	[166]
			Susceptible and Vancomycin-resistant Enterococcus faecalis	10^3- 10^5		62.5 and 125	4 and 8	5 to 80	99	Suspension	[102]
			Enterococcus faecium	10^7		n.a.	[c]	n.a.	3[a]	Surface coating	[133]
			Staphylococcus aureus	10^3- 10^7		62.5 – 10 000	4 and 8	5 to 80	99 - 100	Suspension	[102, 157, 161, 163]
				10^5		n.a.	[c]	n.a.	>4[a]	Surface coating	[133]
			Methicillin resistant Staphylococcus aureus	10^3- 10^5		62.5 and 125	4 - 330	5 to 80	99	Suspension	[102]
				10^3		n.a.	30	80	99.8	Surface coating	[137]
			Streptococcus sobrinus	10^5		1000	[d]	3	5[a]	Suspension	[170]
		Actinobacteria	Micrococcus luteus	[h]		[e]	104	8640	20[f]	Surface coating	[127]
		Bacteroidetes	Bacteroides fragilis	10^7		10 000	8	60	100	Suspension	[161]
		Cyanobacteria	Anabaena	n.a.		n.a.	6 and 43	60	100[g]	Surface coating	[134]
			Microcystis								

a - log reduction, b - UVA light - 2 x 15 W black light, c - 2 x15 W, white light 356 nm peak emission, d - UV light (300-400 nm, peak emission: 352 nm), e - 15-25 mg of TiO$_2$ per disk, f - reduction in CO$_2$ mass balance, g - relative ^{14}C-assimilation, h – 1.77 mg/mL, i – 0.15 mg/mL, n.a. – not available

Table 1.1 (Continuation). Photoinactivation studies conducted under the influence of UV radiation (<380 nm).

Suspension Type	Domain	Phylum	Organism	Initial Cellular Density (CFU/mL)	Photocatalyst	Photocatalyst Concentration (mg/L)	Irradiance (W/m²)	Contact Time (min)	Reduction (%)	Type of Trial	Ref.
Axenic	Eukarya	Ascomycota	*Candida albicans*	$10^3 - 10^5$	TiO₂ (P25, other commercial TiO₂ and produced TiO₂)	20 (n.a.)	315 and 330, [a]	30, n.a.	96 (1.2 [b])	Suspension Surface coating	[133, 157]
			Aspergillus niger spores	[c]		[d]	104	8640	0 [e]	Surface coating	[127]
			Fusarium (5 different strains)	10^3		35	34	360	3 [b]	Suspension	[171]
			Penicillium citrinum	10^5		n.a.	74 and 318	n.a.	< 60	Impregnated Membrane	[132]
		Apicomplexa	*Cryptosporidium parvum*	Variable		n.a.	100	Variable	100	Impregnated membrane	[130]
		Stramenopiles	*Melosira*	n.a.		n.a.	6 and 43	60	60 [f]	Surface coating	[134]
		Metamonada	*Giardia lamblia*	10^5		[g]	24 and 100	60	100	Surface coating Impregnated membrane	[130, 172]
Mixed	Bacteria	Proteobacteria	*Escherichia coli*	10^5		25 [h]	[i]	90	5.5 [b]	Surface coating	[131]
			Pseudomonas aeruginosa	10^4				120	5 [b]		
		Firmicutes	*Bacillus subtilis* endospores	10^6				480	1.7 [b]		
	Eukarya	Amoebozoa	*Acanthamoeba Polyphaga* (Trophozoites)	10^4				120	4 [b]		
			Acanthamoeba Polyphaga (Cysts)	10^4				480	0		
		Ascomycota	*Candida albicans*	10^5				240	5.4 [b]		
			Fusarium solani (Conidia)	10^5				240	5.5 [b]		
Wastewater	Bacteria	Proteobacteria	*Escherichia coli*	Variable		100	38	360	100	Suspension	[173]
Wastewater	Bacteria	Firmicutes	*Enterococcus faecalis*	n.a.		250	[j]	180	99.6	Impregnated membrane	[139]
		Proteobacteria	Total coliforms	$10^4 - 10^7$		0.2 - 2000	1.5 (n.a.), [k]	3 -150	100	Suspension	[117, 174-176]
		-	Total heterotrophic bacteria	10^4		5000	[l]	360	100	Suspension	[114]

a - 2 x15 W, white light 356 nm peak emission, b - log reduction, c – 0.6 mg/mL, d - 25 mg of TiO₂ per disk, e - reduction in CO_2 mass balance, f - relative ^{14}C-assimilation, g - 3 % colloidal solution, h - mg/cm², i - 70 W/m² in the 300 nm–10 mm range, 200W/m² in the 300–400nm UV range, j - 800 W UV lamp, k - 36 W UV Lamp, l-Photon flux: 0.2 mmol/h < 280 nm, 18 mmol/h 280±315 nm, 390 mmol/h 315±380 nm or 5 mmol/h < 280 nm, 150 mmol/h 280±315 nm, 220 mmol/h 315±380 nm, n.a. – not available

Even though efficient, high photocatalyst concentrations, powerful light sources or high contact times are needed when P25 or other synthetized pristine TiO_2 are used. Thus, in order to achieve higher photoinactivation performances with less severe conditions, modified titanium dioxide (doped and/or decorated) has been studied (Table 1.2). As discussed in detail in section 1.1.1, these TiO_2 modifications enhance the photocatalytic activity of the photocatalyst. Much lower irradiance (0.5 *versus* 55 W/m^2, respectively) and lower contact times (35 *versus* 40 minutes) were necessary to achieve total inactivation of *E. coli* at a higher cellular density (10^9 *versus* 10^6 CFU/mL, respectively) with a TiO_2 decorated with silver nanoparticles [177] compared with pristine TiO_2 [112]. However, a final conclusion concerning the performance of the modified photocatalyst cannot be retrieved because a 10 times higher concentration of TiO_2 decorated with Ag (1 g/L) [177] than of pristine TiO_2 [112] was used. Nevertheless, other studies suggest that modification of the photocatalyst improve, in fact, their inactivation performance. For the complete inactivation of *S. aureus* at an initial cellular density of 10^6 CFU/mL, 10 g/L of synthetized pristine TiO_2 and irradiance of 8 W/m^2 for 60 minutes were necessary [161], while 2.5 g/L of Fe_3O_4 decorated TiO_2 and an irradiance of 4 W/m^2 for 20 minutes were sufficient to inactivate 93 % of *S. aureus* viable cells at an initial higher concentration (10^9 CFU/mL).

Table 1.2. Photoinactivation studies conducted under the influence of UV radiation (<380 nm) with TiO_2 modified photocatalysts. The modification types are: doping (x-TiO_2) and decoration (x/TiO_2).

Suspension Type	Domain	Phylum	Organism	Initial Cellular Density (CFU/mL)	Photocatalyst	Photocatalyst Concentration (mg/L)	Irradiance (W/m^2)	Contact Time (min)	Reduction (%)	Type of Trial	Ref.
Axenic	Bacteria	Proteobacteria	Escherichia coli	10^9	Ag/TiO_2	1000	0.5	35	6[a]	Suspension	[177]
			Bacillus cereus endospores	10^4 - 10^5	Ag-TiO_2	n.a.	50	1440	100	Surface coating	[128]
		Firmicutes	Staphylococcus aureus	10^9 – 10^{10}	Fe$_3$O$_4$@TiO_2[b]	2500	4	20	93	Suspension	[178]
			Streptococcus pyogenes						96		
			Staphylococcus saprophyticus						99.5		
			Lactococcus lactis	10^4	TiO$_2$, In$_2$O$_3$-TiO$_2$, Ag/TiO_2,Ag/Ni/ TiO$_2$	n.a.	150	10	99.98	Surface coating	[129]
		Proteobacteria	Pseudomonas fluorescens								
		Firmicutes	Escherichia coli	10^3	Pt -P25	250	[c]	60 and 120	100	Suspension	[7]
			Lactobacillus acidophilus						100		
	Eukarya	Ascomycota	Saccharomyces cerevisiae						100		
		Chlorophyta	Chlorella vulgaris						45		
			Tetraselmis suecica	10^3	Ag/TiO_2, Ag-TiO_2	500	[d]	60	100	Suspension	[179]
		Dinoflagellata	Amphidinium carterae								

a –log reduction, b – core/shell magnetic nanoparticles, c -300-W xenon lamp, a 400-W metal halide lamp and a 500-W white fluorescent lamp, d - 20 W A-type UV lamps, n.a. - not available

1.2.5 Visible Light-TiO$_2$ photoinactivation

Despite the success of UV-photocatalysis in disinfection, the mutagenic action of this type of radiation hampers its use in the majority of the indoor spaces [109]. On the other hand, the negligible UV irradiancy under common internal lighting conditions prevents the use of pure photocatalytic TiO$_2$ in indoor spaces. Even in outdoor events, the low fraction of solar UV compared to the total solar irradiation advises the use of visible light photocatalysts. To overcome this major drawback, several studies focused on the development of modified titanium dioxide with enhanced visible light photoactivity have been conducted, as mentioned in section 1.1.

Among the modified photocatalysts tested up to now, carbon doped TiO$_2$, decorated [180] or not [181] with silver nanoparticles was shown to respectively fully inactivate *E. coli* and *S. aureus* under visible light. Also manganese-, cobalt doped or co-doped Mn/Co-TiO$_2$ was shown to fully inactivate *Klebsiella pneumonia* [100]. The use of graphene for photocatalytic applications by Akhavan *et al.* [182] resulted in a novel graphene oxide/TiO$_2$ composite with an increased antibacterial activity under solar light irradiation when compared to bare TiO$_2$ (roughly 7.5 times more).

Nevertheless, the disinfection performance of modified TiO$_2$ under visible light is still lower than under UV radiation. Indeed, the inactivation fraction of vegetative cells of a wide variety of microorganisms under UV irradiation varies between 96 % and 100 % (Table 1.1), while under visible light ranges from 65 % to 90% (Table 1.3). Moreover, to attain these inactivation values extreme conditions were necessary, i.e, very high values of irradiance (up to 15 000 lux), photocatalyst concentration (1 g/L) and/or contact time (1440 minutes). Finally, inactivation of dormant forms such as spores of *Aspergillus niger* under visible light was also not attained yet (Table 1.3).

Thus, optimization of photoinactivation under visible light envisaging a future commercial application of this technique is still needed.

Table 1.3. Photoinactivation studies conducted under the influence of visible light (>380 nm) with TiO_2 modified photocatalysts.

Suspension Type	Domain	Phylum	Organism	Initial Cellular Density (CFU/mL)	Photocatalyst	Photocatalyst Concentration (mg/L)	Irradiance (W/m^2)	Contact Time (min)	Reduction (%)	Type of Trial	Ref.
Axenic	Bacteria	Proteobacteria	*Escherichia coli*	10^2-10^9	Ag/C-TiO$_2$, AgBr/TiO$_2$, I-TiO$_2$, PdO-TiO$_2$, CNT-doped TiO$_2$, N-TiO$_2$, C-TiO$_2$ Pt-TiO$_2$, S-TiO$_2$, N-F-TiO$_2$, Mn-TiO$_2$, Co-TiO$_2$, Fe-TiO$_2$ Mn/Co-TiO$_2$,Cathecol/TiO$_2$ TiO$_2$/Graphene	10-1000, [a]	1.31×10^{-2} – 1100, 3900 - 15 000[b], [c,d,e]	15-1440, [f]	100	Impregnated Membrane Suspension Surface coating	[124, 125, 135, 136, 180, 182-193]
			Erwinia; Carotovora	10^4-10^5	Synthesized TiO$_2$	n.a.	724[b]	20-60	> 90	Thin films	[126]
			Enterobacter cloacae	10^4-10^5	Synthesized TiO$_2$	n.a.	724[b]	20-60	> 90	Thin films	[126]
			Shigella flexneri	10^4	C-TiO$_2$	200	100 and 900	5	> 80	Suspension	[181]
			Klebsiella pneumoniae	10^2 – 10^8	Mn-TiO$_2$, Co-TiO$_2$, Mn/Co-TiO$_2$	25-250	1.31×10^{-2}	60	100	Suspension	[187]
			Acinetobacter baumannii	10^4 – 10^5	C-TiO$_2$, Pt-TiO$_2$	50, 200	100 - 900	5, 75	< 90	Suspension	[181, 194]
			Staphylococcus aureus	10^3-10^8	P25, PdO-TiO$_2$, C-TiO$_2$, AgBr/TiO$_2$, Pt-TiO$_2$, Cathecol/TiO$_2$	50 – 200, [c]	10 - 900	5 - 1440	100	Paint coating Surface coating Suspension	[125, 136, 181, 186, 189, 194]
			Streptococcus pyogenes	10^5	Pt-TiO$_2$	50	480	75	> 90	Suspension	[194]
			Enterococcus faecalis	10^6 -10^9	Ag/C-TiO$_2$, N-TiO$_2$, C-TiO$_2$	1000	450 -500, 15 000[b]	300	4[g]	Suspension Surface coating	[135, 180]
	Eukarya	Ascomycota	*Saccharomyces cerevisiae*	10^2	PdO-TiO$_2$	n.a.	100	180	65	Thin films	[136]
			Aspergilus niger spores	10^2	PdO-TiO$_2$	n.a.	100	480	0	Thin films	[136]

a - 2 wt% in paint, b - lux, c - 4 x 24 W fluorescence lamps, d - portion of UV (290–400 nm) of 0.05–0.12 W m^{-2} intensity, and visible light (400–700 nm) with a range of intensity 2.70–3.99 W m^{-2}, e - UVA - 3 mW/cm^2 (SSL) VL-162 370 lux, f - months of May-September in Tehran (IRAN) at around noon, g – log reduciton, n.a. – not available

1.2.6 Traditional disinfection methods

Traditional disinfection methods are based on the utilization of heat, radiation or chemical compounds. Chlorine, hydrogen peroxide, ozone, and UV radiation are amongst the most used agents currently used to disinfect water, air or fomites. The disinfection methods based on each of these antimicrobial agents will be briefly overviewed next.

1.2.6.1 Chlorination

Chlorination as a disinfection technique is mainly based on the use of gaseous chlorine and/or hypochlorite. Chlorine gas (Cl_2) is the elemental form of chlorine at standard temperature and pressure. Chlorine gas is approximately 2.5 times heavier than air and is highly toxic. Hypochlorite (ClO^-) is usually obtained from sodium hypochlorite and calcium hypochlorite [195].

Chlorine gas hydrolyzes in water according to the following reaction (Eq. 1.1):

$$Cl_2 + H_2O \rightarrow HOCl + Cl^- + H^+ \qquad (1.1)$$

while hypochlorous acid, resulting from the previous reaction, is a weak acid, which dissociates in aqueous solution:

$$HOCl \rightarrow ClO^- + H^+ \qquad (1.2)$$

Under typical water treatment conditions in the pH range 6–9, hypochlorous acid and hypochlorite are the main chlorine species. Depending on the temperature and pH level, different distributions of aqueous chlorine species (Cl_2, HOCl and ClO^-) are observed [196]. In addition to these major chlorine species, other chlorine intermediates including trichloride (Cl_3^-) and chlorine hemioxide (Cl_2O) can also be formed - Figure 1.2. In solution, ratios of these intermediates are a function of temperature, pH and chloride concentration. Under typical water treatment conditions, the concentrations of Cl_3^- and Cl_2O are very low, accounting, at most, to 20% of all the chlorine species in solution [196, 197].

$$H_2OCl^+ \qquad Cl_2O$$

$$Cl_3^- \rightleftharpoons Cl_2 \rightleftharpoons HOCl$$

$$OCl^-$$
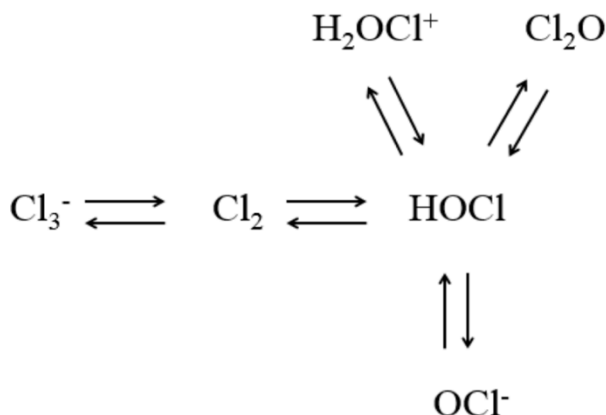
Figure 1.2. Equilibrium of chlorine and its derivatives in solution at 25 ºC (adapted from [196]).

Chlorination as a water disinfection method was first introduced in 1902 in Middlekerke, Belgium [198]. Chlorination is mainly used in water disinfection, however, hypochlorite is also used for the disinfection of some surfaces (mostly for countertops and floors), mainly in health care facilities [199]. A leading advantage of chlorination is that it is effective against a wide variety of bacteria and viruses. However, it cannot inactivate all microbes, being some protozoan cysts resistant to the effects of chlorine [200]. In cases where protozoan cysts are not a major concern, chlorination seems to be a good water disinfection method because it is inexpensive.

The precise mechanism by which microorganisms are inactivated by chlorine has not yet been fully explained. However, some studies show that the bacterial cell membrane changes its permeability in the presence of chlorine [201, 202]. The presence of suspended solids influences the action of chlorine because the particles and organic compounds usually provide protection to microorganisms. This protection usually comes from stabilization of the cell membranes, which reduces the access of chlorine to key cellular components for inactivation [202]. Indeed, microbial aggregates or microorganisms attached to or embedded in particles have been shown to have increased resistance to inactivation by chlorine, when compared to non-attached, free-swimming microorganisms. Dietrich and co-workers [202] reported, however, that chlorine is capable of penetrating particles in wastewater by radial diffusion. Greater

chlorine penetration into wastewater particles was observed with increasing initial chlorine concentration, indicating that chlorine application could be tailored to penetrate particles of known size in order to achieve inactivation [202].

Some of the studies reported in the literature on the efficiency of chlorination on disinfection are summarized in Table 1.4. Koivunen and co-workers [203] studied the chlorination of *Enterococcus faecalis, Escherichia coli* and *Salmonella enteritidis* in aqueous solution. In this work, concentrations of chlorine of 12 mg/L with a contact time of 10 minutes were used in order to achieve a log reduction value of around 3 for *Enterococcus faecalis*. But, even with a higher chlorine concentration (18 mg/L), lower reduction values were registered for *Escherichia coli* and *Salmonella enteritidis* (0.3 and 0.44, respectively) for the same contact time, demonstrating that microorganisms have distinct tolerance against chlorination. In wastewater samples, Hassen and co-workers [204] registered log reduction values up to 3.7 and 4.4 for fecal coliforms and enterococci, respectively, when using chlorine concentrations ranging from 6.5 and 13.6 mg/L and contact times up to 40 minutes.

Table 1.4. Inactivation of several microorganisms by chlorination.

Domain	Phylum	Organism	Type of suspension	Type of Trial	Chlorine concentration (mg/l)	Contact time (min)	Final chlorine concentration (mg/L)	Initial cellular density (CFU/mL	Reduction (log)	Reference
Bacteria	Firmicutes	*Clostridium perfringens* Spores	Axenic	Suspension	5	1440	n.a.	10^4	4	[205]
		Enterococci	Wastewater	Suspension	6.5-25	15-40	1.2-3	10^4-10^5	4.5(99[a])	[204, 206]
		Enterococcus faecalis	Axenic; Wastewater	Suspension	8 - 30	30	0.2-0.3	10^5-10^7	5	[207, 208]
		Staphylococcus aureus	Axenic	Suspension	1 - 5	30	0.5-3	10^8-10^9	[b]	[203]
		Enterococcus faecalis	Axenic	Suspension	1 - 5	30	0.5-3	10^8-10^9	[b]	[203]
	Proteobacteria	*Campylobacter jejuni*	Axenic	Suspension	0 -4	120	n.a.	10^3-10^4	99[a]	[209]
		Citrobacter freundii	Axenic	Suspension	0-10	120	n.a.	10^3-10^4	99[a]	[209]
		Enterobacter agglomerans	Axenic	Suspension	0-10	120	n.a.	10^3-10^4	99[a]	[209]
		Enterobacter cloacae,	Axenic	Suspension	0-10	120	n.a.	10^3-10^4	99[a]	[209]
		Escherichia coli	Axenic; Wastewater	Suspension	1 - 30	2.5 - 120	0.2-3	10^5-10^9	>5 (99[a])[b]	[165, 203, 207-209]
		Fecal coliforms	Wastewater	Suspension	6.5-25	15- 5760	1.2-3	10^4-10^5[c]	7 (99[a])	[204, 206, 210]
		Klebsiella oxytoca	Axenic	Suspension	0-10	120	n.a.	10^3-10^4	99[a]	[209]
		Klebsiella pneumoniae	Axenic	Suspension	0-10	120	n.a.	10^3-10^4	99[a]	[209]
		Legionella gormanii	Axenic	Suspension	0 -4	120	n.a.	10^3-10^4	99[a]	[209]
		Pseudomonas aeruginosa	Axenic	Suspension	1 - 5	30	0.5-3	10^8-10^9	[b]	[203]
		Salmonella enterica	Axenic	Suspension	0 -4	120	n.a.	10^3-10^4	99[a]	[209]
		Salmonella enteritidis	Axenic	Suspension	18	n.a.	0.2-0.3	10^5-10^7	0.5	[208]
		Shigella sonnei	Axenic	Suspension	0 -4	120	n.a.	10^3-10^4	99[a]	[209]
		Total coliforms	Wastewater	Suspension	11-21	15-5760	n.a.	[c]	7(99[a])	[206, 210]
		Yersinia enterocolitica	Axenic	Suspension	0 -4	120	n.a.	10^3-10^4	99[a]	[209]
Eukarya	Apicomplexa	*Cryptosporidium parvum* Cysts	Axenic	Suspension	5	1440	n.a.	10^4	4	[205]

a-%, b – evaluated through the consumption of chlorine and presence of residual chlorine, c- 1 million to 20 millions per 100 ml, n.a. – not available

1.2.6.2 Ozonation

Ozone is produced when oxygen molecules are dissociated by an energy source into oxygen atoms and subsequently collide with the non-dissociated oxygen molecules. Ozone is one of the most powerful oxidizing agents ($E^0 = 2.07$ V) and it is mostly used to destroy organic compounds [211].

The oxidation of the target compounds can occur through two different mechanisms: i) direct reaction with molecular ozone or ii) indirect reaction with secondary oxidants formed upon the decomposition of ozone in water. Such decomposition is catalyzed by hydroxide ions (OH^-) and other solutes. Highly reactive secondary oxidants, such as hydroxyl radicals ($OH^•$), are thereby formed. These radicals and their reaction products can cause the decomposition of ozone. Consequently, radical-type chain reactions may occur, which consume ozone concurrently with the direct reaction of ozone with dissolved organic material and contributing to the formation of additional hydroxyl radicals – Figure 1.3 [212].
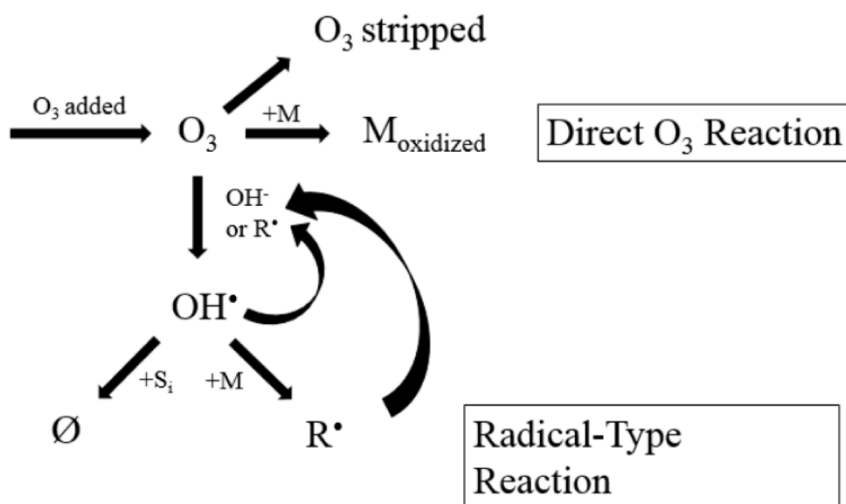

Figure 1.3. Mechanisms involved in the ozonation process. In the figure, M is referred to the solute, M_{oxid} to the oxidized solute, S_i to the free radical scavenger, Ø to products that do not catalyze the ozone decomposition and R to the free radicals that catalyze the ozone decomposition. (Reprinted from [212] with permission)

Ozone reacts with polysaccharides slowly, leading to breakage of glycosidic bonds and formation of aliphatic acids and aldehydes. The reaction of ozone with primary and secondary aliphatic alcohols may lead to formation of hydroxy-hydroperoxides, precursors to hydroxyl radicals, which in turn react strongly with the hydrocarbons [213]. However, it was already shown that N-acetyl glucosamine, a compound present in the peptidoglycan of bacterial cell walls, was resistant to the action of ozone in aqueous solution at pH 3 to 7. This explains the higher resistance of Gram-positive bacteria compared to Gram negative ones, because the former contains higher amounts of peptidoglycan in their cell walls than the later. Ozone can react significantly with amino acids and peptides, especially at neutral and basic pH. Furthermore, ozone reacts quickly with nucleobases, especially thymine, guanine, and uracil. Reaction of ozone with the nucleotides releases the carbohydrate and phosphate ions [213].

Ozone is mainly used for water treatment, however the use of ozone for surface disinfection was already reported [214]. Water disinfection by ozonation has been extensively reported, and some of the works are summarized in Table 1.5. Low ozone concentrations (0.15-0.20 mg/L) and contact time (180 s) were sufficient to inactivate several Gram negative bacteria in suspension to values up to 99.99% [215]. Nebel and co-workers [216] reported one of the first works describing the treatment of wastewater by ozonation. In this work, with an ozone dose of 14 mg/L and a contact time of 5 minutes it was possible to achieve log reduction values of up to 3 log for enterococci, total coliforms and fecal coliforms.

Table 1.5. Inactivation of several microorganisms by ozonation.

Domain	Phylum	Organism	Type of suspension	Type of trial	Disinfection O$_3$ dose (mg/l)	Contact time (min)	Final Ozone Concentrations (mg/L)	Initial cellular density (CFU/mL)	Reduction (log)	Reference
Bacteria	*Firmicutes*	*Bacillus subtilis* spores	Axenic	Surface	16	150	n.a.	10^5-10^6	0.5	[214]
		Enterococci	Wastewater	Suspension	2-14	5-30	0.05-0.4	n.a.	1-3	[216-219]
		Leuconostoc mesenteroides	Axenic	Suspension	0.2 – 3.8	2	0	10^9	7	[220]
		Listeria monocytogenes	Axenic	Suspension	0.2 – 3.8	2	0	10^9	7	[220]
		Staphylococcus aureus	Axenic	Suspension	a	n.a.	2	10^7	7	[221]
	Proteobacteria	*Aeromonas salmonicida*	Axenic	Suspension	0.15-0.20	3	0.05-0.07	10^9	4	[215]
		Escherichia coli	Axenic Wastewater	Surface Suspension	0.2 – 4	2-30	0.1-0.4	10^5-10^9	2-7	[214, 217, 219-222]
		Fecal coliforms	Wastewater	Suspension	7-14	5	0.05	n.a.	1-3	[216, 218]
		Pseudomonas fluorescens	Axenic	Suspension	0.2 – 3.8^a	2	2	10^9	7	[220, 221]
		Salmonella enterica	Axenic	Suspension	a	n.a.	2	10^7	7	[221]
		Shigella flexneri	Axenic	Suspension	a	n.a.	2	10^7	7	[221]
		Total coliforms	Wastewater	Suspension	7-14	5	0.05	n.a.	2-3	[216, 222]
		Vibrio anguillarum	Axenic	Suspension	0.15-0.20	3	0.05-0.07	10^9	4	[215]
		Vibrio cholerae	Axenic	Suspension	a	n.a.	2	10^7	7	[221]
		Vibrio salmonicida	Axenic	Suspension	0.15-0.20	3	0.05-0.07	10^9	4	[215]
		Yersinia ruckeri	Axenic	Suspension	0.15-0.20	3	0.05-0.07	10^9	4	[215]
	-	Total heterotrophic bacteria	Treated wastewater	Suspension	50^b	30	0	10^6	6	[219]
Eukarya	*Apicomplexa*	*Cryptosporidium parvum*	Axenic	Suspension	0.36-2.2	1	n.a.	n.a.	6	[223]
	Ascomycota	*Aspergillus niger*	Wastewater	Suspension	50^b	30	0	10^3	3	[219]
		Penicillium citrinum	Axenic	Surface	16	120	n.a.	10^5-10^9	2	[214]
	Basidiomycota	*Rhodotorula rubra*	Wastewater	Suspension	50^b	30	0	10^3	3	[219]

a – Flow rate of 152.4 cm^3/h, b - grams of ozone per normal cubic meter, n.a. – not available

1.2.6.3 UV

Ultraviolet processing involves the use of radiation from the ultraviolet region of the electromagnetic spectrum for purposes of disinfection. Usually, the range of UV refers to wavelengths between 100 and 400 nm. This range can be further subdivided. UVA corresponds to wavelengths between 315 and 400 nm and it is normally responsible for change in human skin that cause tanning; UVB refers to wavelengths between 280 and 315 nm and is the main responsible for skin burning and can also lead ultimately to skin cancer. UVC – 200 to 280 nm – is called the germicidal range, because it is considered to be the most effective towards the inactivation of bacteria and viruses. Finally, the vacuum UV range (100 to 200 nm), can be absorbed by almost all substance and can only be transmitted in the vacuum [224].

Among the above mentioned disinfection methods, UV light has been adopted as the most appropriate treatment process for drinking water because it is simple to use, highly effective for inactivating microbes and it does not introduce chemicals or cause the production of harmful disinfection by-products in the water [225]. This method promotes additional security after traditional treatment processes [226, 227]. UV radiation is responsible for a wide range of biological effects [228-230], including modifications in the protein structure and in the DNA [231]. Regarding DNA damage, it may result on inhibition of cell replication and, in case of lethal doses, on the loss of ability to reproduce. Although the UV-A wavelengths bordering on visible light are not sufficiently energetic to directly modify DNA bases, cellular membrane damage can be induced through the production of ROS, such as singlet oxygen, superoxide, hydrogen peroxide and hydroxyl radical, generated via excitation of dissolved oxygen in water [173, 232]. Furthermore, according to several authors, the damage induced by UV radiation continues even after the end of the irradiation period [232, 233]. Bacterial DNA is a critical target of UV radiation and its effects depend on several parameters, such as UV spectrum, dissolved oxygen concentration, salt concentration and post-irradiation growth conditions [232]. Different microorganisms respond differently to the lethal effects of UV. It is known that the effectiveness of a UV disinfection system depends on the sensitivity of the target microorganisms to UV, microbial content, antibiotic resistance phenotypes, light source, UV radiation intensity, exposure time of

microorganisms to radiation and their ability to re-growth [116, 219, 232-234]. UV treatment can be used for the inhibition of microorganisms in surfaces, in the air or in water [235-237].

Some works reporting the use of UV radiation on the inactivation of microorganisms are presented in Table 1.6. When using a light intensity of 2 W/m^2, it was possible to achieve high values of inactivation of different microorganisms in wastewater samples. A contact time of 50 seconds permitted to achieve log reductions of 4 to 5 for methicillin-resistant *Staphylococcus aureus* (MRSA), *E. coli,* and *Pseudomonas aeruginosa.* A higher contact time (100 s) was needed to reach similar log reduction values for vancomycin resistant *Enterococcus faecium* (VRE) [238]. In a study assessing the effectiveness of UV radiation on the inactivation of several vegetative bacteria (*Staphylococcus aureus, Enterococcus faecalis, E. coli, Salmonella enterica, Shigella sonnei) Bacillus subtilis* spores*, Acanthamoeba castellanii* cysts and viruses (poliovirus type 1 and simian rotavirus SAil), Chang and co-workers [239] reported that viruses, spores and cysts were 3-4, 9 and 15 times more resistant than the vegetative bacteria, respectively.

Table 1.6. Inactivation of several microorganisms with the use of UV radiation.

Domain	Phylum	Microorganism	Type of suspension	Type of trial	Irradiance (W/m^2)	Contact time (min)	Initial cellular density (CFU/mL)	Log reduction	Reference
Bacteria	Firmicutes	*Bacillus subtilis spores*	Axenic	Suspension	45[a]	a	10^5-10^6	99.9[b]	[239]
		Clostridium difficile Spores	Axenic	Surface	36000[c]	17	10^6-10^7	3	[237]
		Enterococci	Wastewater	Suspension	[e,g]	180	10^5	2	[139, 219]
		Vancomycin-resistant *Enterococcus*	Wastewater Axenic	Suspension Surface	12000[c]	17(100[d])	10^5-10^7	5	[237, 238]
		Enterococcus faecalis	Axenic	Suspension	80-100 (45[a])	10 (a)	10^5-10^7	1.2 (99.9[b])	[208, 239]
		Staphylococcus aureus	Axenic	Suspension	45[a]	a	10^5-10^6	99.9[b]	[239]
		Methicillin-resistant *Staphylococcus aureus (MRSA)*	Wastewater Axenic	Suspension Surface	12000[c]	17(50[d])	10^5-10^7	4	[237, 238]
	Proteobacteria	*Acinetobacter baumannii*	Axenic	Surface	12000[c]	17	10^6-10^7	4	[237]
		Escherichia coli	Wastewater Axenic	Suspension	100- 140[f,g]	10-120(50[d])	10^5-10^7	5	[116, 208, 219, 238, 239]
		Pseudomonas aeruginosa	Wastewater Axenic	Suspension	f	120(50[d])	10^7	5	[116, 238]
		Salmonella enterica	Axenic	Suspension	f	120	10^7	3	[116, 239]
		Salmonella enteritidis	Axenic	Suspension	60-100	10	10^5-10^7	3	[208]
		Shigella sonnei	Axenic	Suspension	45[a]	a	10^5-10^6	99.9[b]	[239]
		Total Coliforms	Wastewater Axenic	Suspension	1.5 - 45[a] (e)	2, a	10^5-10^6	3 (99.9[b])	[139, 176, 239]
		Vibrio anguillarum,	Axenic	Suspension	30	n.a.	10^7	5	[215]
		Vibrio salmonicida,	Axenic	Suspension	30	n.a.	10^7	5	[215]
		Yersinia ruckeri	Axenic	Suspension	30	n.a.	10^7	5	[215]
	-	Total heterotrophic bacteria	Wastewater	Suspension	g	30	10^6	6	[219]
Eukarya		*Acanthamoeba castellanii* cysts	Axenic	Suspension	45[a]	a	10^5-10^6	99.9[b]	[239]
	Ascomycota	*Aspergillus niger*	Wastewater	Suspension	g	30	10^3	3	[219]
	Basidiomycota	*Rhodotorula rubra*	Wastewater	Suspension	g	30	10^3	3	[219]

a- UV dose – mW.s/cm^2, b- %, c- µWs/cm^2, d – seconds, e - 800 W UV-lamp, f –3.42 × 10^{-5} Einsteins s^{-1}, g - low-pressure mercury lamp (emission line at 254 nm), n.a. – not available

1.2.6.4 Hydrogen Peroxide

Hydrogen peroxide is a metastable molecule – it easily decomposes into water and oxygen - with high redox potential (1.77 V) [240]. Even though the mechanism of hydrogen peroxide inactivation towards cells is usually attributed to the production of highly reactive hydroxyl radical, hydrogen peroxide itself presents some cytotoxicity towards cells. H_2O_2 can directly oxidize the catalytic iron atom of dehydratase clusters, precipitating iron loss and enzyme inactivation. H_2O_2 poisons the Isc system, which is responsible for the transfer of [4Fe-4S] clusters to newly synthesized apoenzymes. However, the mechanism of cytotoxic activity of H_2O_2 is generally reported as based on the production of highly reactive hydroxyl radicals from the interaction of the superoxide ($O_2^{\cdot-}$) radical and H_2O_2, a reaction first proposed by Haber and Weiss [241] (Eq. 1.3):

$$O_2^{\cdot-} + H_2O_2 \ \rightarrow \ O_2 + OH^{\cdot} + OH^- \tag{1.3}$$

Further, it is believed that the production of extremely short-lived hydroxyl radicals within the cell by the Haber–Weiss cycle is catalyzed in vivo by the presence of transition metal ions (particularly iron-II) according to Fenton chemistry [242] (Eq. 1.4):

$$Fe^{2+} + H_2O_2 \ \rightarrow \ Fe^{3+} + OH^{\cdot} + OH^- \tag{1.4}$$

The iron released from oxidized metalloproteins enlarges its intracellular pool, favoring the production of hydroxyl radical through the Fenton reaction [243]. The production of hydroxyl radical is, as described before, of utmost importance in the inactivation of microorganisms, accelerating the process of DNA damaging [213].

H_2O_2 can be used in both liquid and vapor phases. Hence, it is used in water disinfection (liquid phase) or in the disinfection of surfaces (vapor phase). Indeed, it is believed that the vapor phase has higher kinetic energies and is uncharged, so it can surround and penetrate the three-dimensional protein structures more easily, oxidizing buried cysteine residues and breaking vulnerable bonds between subunits [244]. Thus, an enhanced antimicrobial activity of hydrogen peroxide vapor when compared to its liquid state is usually reported [245-248].

Some studies reporting the utilization of hydrogen peroxide as a disinfectant are summarized in Table 1.7. Otter and co-workers [247] studied the effectiveness of hydrogen peroxide on the inactivation of nosocomial bacteria and spores on surfaces. After 90 minutes of contact with hydrogen peroxide vapor, all of the tested microorganisms were completely inactivated (Log reduction of 6). However, differences on the resistance against the hydrogen peroxide vapor treatment were observed. *Acinetobacter* showed the highest resistance to this treatment, while vancomycin-resistant enterococci were the first to be completely inactivated, after only 10 minutes of treatment. Hydrogen peroxide is also suitable to disinfect wastewater. Indeed, the density of total coliforms in wastewater was reduced 4 fold when using H_2O_2 up to 2.5 mL/L and a contact time of 3 h [249].

Table 1.7. Inactivation of several microorganisms with the use hydrogen peroxide.

Domain	Phylum	Organism	Type of suspension	Type of trial	Hydrogen peroxide concentration (mL/L)	Contact time (min)	Initial cellular density (CFU/mL)	Log reduction	Reference
Bacteria	Firmicutes	*Bacillus subtilis*	Axenic	Surface	a	32	10^6	100^b	[248]
		Enterococcus faecalis	Axenic	Suspension	3-150	10	10^5-10^7	0.1	[208]
		Enterococcus faecium	Axenic	Surface	a	90	10^6	6	[247]
		Geobacillus stearothermophilus	Axenic	Surface	a	32 - 50	10^4 - 10^6	4 (100^b)	[248, 250]
		Staphylococcus aureus (MRSA)	Axenic	Surface	a	50 - 90	10^4 - 10^6	6	[247, 250]
		Vancomycin-resistant *Enterococcus* (VRE)	Axenic	Surface	a	50 - 90	10^4 - 10^6	6	[247, 250]
		Clostridium difficile	Axenic	Surface	a	50 - 90	10^4 - 10^6	6	[247, 250]
	Proteobacteria	*Acinetobacter baumannii*	Axenic	Surface	a	90	10^6	6	[247]
		Acinetobacter sp.	Axenic	Surface	a	90	10^6	6	[247]
		Fecal Coliforms	Wastewater	Suspension	2.5	240	10^6	4	[249]
		Klebsiella pneumoniae	Axenic	Surface	a	90	10^6	6	[247]

a- Hydrogen Peroxide Vapor (HPV) was used, b-%

1.2.7 Comparison between photoinactivation and traditional disinfection methods

In contrast with the traditional disinfection methods described above, TiO_2-UV photocatalysis is not yet considered as an established water disinfection technology [251]. However, until this date, several reports showed the potential of this technique for disinfecting. Indeed, photocatalysis is a versatile and effective process that can be adapted for use in many applications for disinfection in both air and water matrices. Additionally, improved photocatalytic coatings are being developed, tested and even commercialized for use in the context of "self-disinfecting" materials. In this sense, the strength of photocatalytic disinfection lies in its versatility for use in many different applications [252]. Indeed, photocatalytic-based products already reached a global volume of US$848 Million in 2009 of which over 87 % were related to products with self-cleaning activity used for construction [253]. Among these are glass coatings, cements and textile fibers [253], commercialized by companies such as Pilkington, Italcementi Group and Taiheiyou Cement. Coatings and ceramics with antimicrobial activity are also commercialized by several companies. Deutsche Steinzeug company, which commercializes flags, tiles and sanitary ceramics and, company Kurare, which commercializes textile fibers containing TiO_2 photocatalysts, should be highlighted. Japanese Arc-Flash, the first company commercializing photocatalyst-based materials in 1992, uses a photocatalyst fixation technology that allows spraying the photocatalytic product directly on surfaces. The photocatalytic coating produced by Arc-Flash uses titania nanoparticles as main ingredient and is used to sterilize mildew, sanitize environments such as hospitals, residential kitchens, schools, and floors, killing bacteria with over 98 % efficiency [253].

The versatility mentioned for photocatalysis is also reported for UV radiation. Advances in the optimization of UV reactors permitted to inactivate a high variety of waterborne microorganisms in few seconds [238]. However, there are still some limitations on the use of this technique. Very high values of irradiation (in most cases over 50 W/m^2) must be used to inactivate some microorganisms (Table 1.6), and even under these harsh conditions, inactivation of some microbial forms, such as *Clostridium difficile* spores, is not possible. Several studies where the effectiveness of UV treatment was directly compared with photocatalysis demonstrated that, as

expected, UV treatment was less efficient than TiO_2-UV [101, 112, 114]. The use of a photocatalyst, in most cases decreases the need of high irradiation intensity and promotes the decrease of contact times. Ibanez and co-workers [112] verified that it was not possible to inactivate *Enterobacter cloacae, E. coli, P. aeruginosa and Salmonella typhimurium* with an UV irradiance of 55 W/m^2. However, when coupling UV irradiation with 0.1 g/L TiO_2, log reduction values around 6 were achieved for all the tested strains for the same time of contact. The decrease of contact time from 360 to 50 minutes to achieve 3 log reduction of the total heterotrophic bacteria of wastewater was also reported [114], when using a photon flux of approximately 390 mmol/h and 5 g/L of photocatalyst. More recently, Lin and co-workers [176] showed that it was possible to reduce the load of the total coliforms in wastewater 4 fold, when irradiance of 1.5 W/m^2 and a contact time of 120 s was coupled with the presence of a TiO_2 coated reactor, while a 3 fold reduction was obtained in the absence of the photocatalyst.

Ozonation is a technique that can promote total inactivation of most types of microorganisms under low contact times, in most cases under 20 minutes, and with low O_3 doses, at most 4 mg/L – Table 1.5. However, it is important to note that ozonation may cause the formation of very harmful by products, specially bromide and other brominated compounds [254]. Rizzo and co-workers [255] compared the efficiency of ozonation and photocatalysis for the treatment of urban wastewaters. In this work, it was shown that it was possible to obtain increased degradation of organic matter with the photocatalytic oxidation process, even at low TiO_2 concentrations. Furthermore, a 30 min photocatalytic treatment was found to produce an effluent complying with the trihalomethanes limit set by Italian regulation for wastewater reuse. Furthermore, the cost associated to the use of ozonation is still very high [256]. Additionally, the coupling of ozonation with photocatalysis was already studied. Moreira and co-workers [257] reported the use of photocatalytic ozonation for the disinfection of urban treated wastewaters. In this study, a photocatalytic ozonation system using TiO_2-coated glass Raschig rings with LEDs irradiation - two 10 W UV high intensity LEDs with dominant emission line at 382 nm - was tested in continuous mode. This study reported the reduction of enterococci, enterobacteria, and fungi from 10^5 - 10^6 CFU/100 mL to

values around or below 10^1 CFU/100 mL; total heterotrophs presented lower reductions, but still reaching values of around 10^2 CFU/100 mL after the treatment.

The use of hydrogen peroxide to disinfect water requires, usually, high contact times (up to 240 minutes) or concentrations (up 150 mL/L) (Table 1.7). Lower contact times (90 minutes) are required to inactivate the microorganisms when the vapor phase is used (Table 1.7), suggesting that hydrogen peroxide is a good technique to disinfect surfaces. However, the toxic effects of H_2O_2, require the interdiction of the site to be disinfected [258] for periods up to 1 hour and 40 minutes. Also chlorination requires high contact times (up to 120 minutes) to be effective on the inactivation of microorganisms (Table 1.4). Additionally, some microorganisms are resistant to chlorination treatments [259, 260]. Nevertheless, it is important to note that nowadays chlorination remains as the most used disinfection method [261]. This is mainly due to the fact that the new alternative processes require expensive chemicals or costly equipment to generate the disinfectant onsite. However, chlorination causes the formation of several highly toxic by-products. Among these, it is important to highlight the formation of trihalomethanes and dichloroacetic acid that are believed to be carcinogenic [262]. The existence of these dangerous by-products leads to the necessity of coming up with suitable alternatives to chlorination. The main advantages and disadvantages of each of these techniques are summarized in Table 1.8.

Although promising, photocatalysis still faces some drawbacks when imposing itself as a reference disinfection technique. As for other disinfection methods, re-growth after photocatalytic treatment may occur [219, 257]. In addition, one of the main problems, usually disregarded by most of works conducted up to now in this field, is the absence of knowledge on the long time effect of photoinactivation. Little is known on the type of organisms able to tolerate the oxidative stress imposed by photocatalysis; however, increased tolerance of antibiotic resistant bacteria when compared with the susceptible counterpart is reported [102]. This observation points out for the need of further studies on the type and fate of the organisms surviving the treatment. This is particularly important, because under real conditions it may be not economically feasible to use conditions guaranteeing the inactivation without regrowth of potentially dangerous microorganisms [263]. Furthermore, and in order to be

applied in full scale, the optimization of the photocatalyst to fully take advantage of the visible light spectrum should be achieved. This optimization should be focused in the future either by the optimization of the photocatalytic material (TiO_2) or by the use of suitable supports (for example graphene).

Although being a very promising disinfection technology, the massive use of TiO_2 nanoparticles without a proper evaluation concerning of their antimicrobial potential can produce negative drawbacks. Indeed, using TiO_2 nanoparticles, even in those products not directly designed for disinfection, may cause the propagation of the aforementioned antibiotic and oxidative stress resistant microorganism in a worrisome scale. Thus, the definition of new standards to test the efficacy of photocatalytic systems, including organisms with high tolerance to oxidative stress and antibiotics, is a subject of utmost importance in nowadays society.

Table 1.8. Comparison between the different disinfection techniques.

Disinfection Technique	Chlorination	Ozonation	Ultraviolet radiation	Hydrogen Peroxide	Photocatalysis
Advantages	• Inexpensive; • Relatively easy to handle, simple to dose, measure and control; • Proven to be effective against a wide variety of bacteria and viruses;	• One of the most effective disinfectants; widely used to inactivate pathogens in drinking water; • Needs short contact times; • Generated onsite, leading to fewer safety issues than other techniques;	• Simple to use • Highly effective for inactivating microorganisms; • Does not introduce chemicals or cause the production of harmful disinfection by-products in the water; • High versatility – can be applied to waster, air and surfaces treatment;	• Considered environmentally friendly because it can rapidly degrade into the innocuous products water and oxygen; • Demonstrates broad-spectrum efficacy against viruses, bacteria, yeasts, and bacterial spores	• Capable of inactivating microorganisms, including viruses, bacteria, spores and protozoa; • Does not cause the production of harmful disinfection by-products in water; • TiO_2 is cheap, innocuous and can be attached to different types of inert matrices; • Useful in developing countries where electricity is not available; • High versatility – can be applied to disinfect water, air and surfaces;
Disadvantages	• Some organisms tend to develop resistance and require a concentration higher than normal, diminishing the quality of water; • Formation of hazardous disinfection by-products, specially trihalomethanes (THMs) and nitrosamines; • Residuals are highly toxic to aquatic life; hence, a dechlorination step is needed; • Mainly applied and limited to water treatment and surface cleaning;	• Formation of potentially harmful byproducts including bromate and other brominated disinfection by-products; • Due to its instability, ozone must be generated before use, which leads to high equipment and operating costs; • Low dosage may not effectively inactivate some viruses, spores and cysts; • Lacks long residual activity, limiting its application in large distribution systems; • Mainly limited to water treatment, but can be use also for surface disinfection;	• Needs shortwave radiation (<280 nm), which requires the set up of expensive lighting equipment and is associated with increased energy utilization; • Organisms can sometimes repair and reverse the destructive effects of UV (photo-reactivation); • The presence of solid particles in water can affect severely the UV efficiency; • Low dosage may not effectively inactivate some viruses, spores, and cysts; • During the UV treatments the sites where the treatments are applied are interdicted to humans due to the harmful effect of this type of radiation;	• The presence of catalase or other peroxidases in these organisms can increase tolerance, when conjugated with lower concentrations of H_2O_2; • Higher concentrations of H_2O_2, between 10 and 30 %, and longer contact times are required for inactivation of spores; • During the H_2O_2 treatments the sites where the treatments are applied are interdicted to humans due to the harmful effect of this chemical compound;	• Uses nanoparticles than can be harmful for the general health; • Its mainly active in the UV range, presenting still some limitations using visible light; • When used in suspension, brings complexity to the process for the recuperation of the photocatalyst;
References	[203, 264]	[265-267]	[225, 228-230, 268]	[243, 269]	[261, 270, 271]

Acknowledgements

Bibliography

[1] M. Ni, M.K.H. Leung, D.Y.C. Leung, K. Sumathy, A review and recent developments in photocatalytic water-splitting using for hydrogen production, Renewable and Sustainable Energy Reviews, 11 (2007) 401-425.

[2] S. Banerjee, D.D. Dionysiou, S.C. Pillai, Self-cleaning applications of TiO_2 by photo-induced hydrophilicity and photocatalysis, Applied Catalysis B: Environmental, 176–177 (2015) 396-428.

[3] F. Kapteijn, J. Rodriguez-Mirasol, J.A. Moulijn, Heterogeneous catalytic decomposition of nitrous oxide, Applied Catalysis B: Environmental, 9 (1996) 25-64.

[4] M. Kaneko, I. Okura, in: Photocatalysis: Science and Technology, Kodansha, 2002, pp. 123-155.

[5] J.H. Carey, J. Lawrence, H.M. Tosine, Photodechlorination of PCB's in the presence of titanium dioxide in aqueous suspensions, Bull. Environ. Contam. Toxicol., 16 (1976) 697-701.

[6] M. Kaneko, I. Okura, in: Photocatalysis: Science and Technology, Kodansha, 2002, pp. 157-173.

[7] T. Matsunaga, R. Tomoda, T. Nakajima, H. Wake, Photoelectrochemical sterilization of microbial cells by semiconductor powders, FEMS Microbiol. Lett., 29 (1985) 211-214.

[8] B. Meyer, B. Cookson, Does microbial resistance or adaptation to biocides create a hazard in infection prevention and control?, Journal of Hospital Infection, 76 (2010) 200-205.

[9] B. Spellberg, R. Guidos, D. Gilbert, J. Bradley, H.W. Boucher, W.M. Scheld, J.G. Bartlett, J. Edwards, t.I.D.S.o. America, The Epidemic of Antibiotic-Resistant Infections: A Call to Action for the Medical Community from the Infectious Diseases Society of America, Clinical Infectious Diseases, 46 (2008) 155-164.

[10] W.H. Organization, The world health report 2007 - A safer future: global public health security in the 21st century, in, World Health Organization, Geneva, Switzerland, 2007.

[11] H.A. Foster, I.B. Ditta, S. Varghese, A. Steele, Photocatalytic disinfection using titanium dioxide: spectrum and mechanism of antimicrobial activity, Appl. Microbiol. Biotechnol., 90 (2011) 1847-1868.

[12] A. Fujishima, K. Honda, Electrochemical Photolysis of Water at a Semiconductor Electrode, Nature, 238 (1972) 37-38.

[13] A. Di Paola, M. Bellardita, L. Palmisano, Brookite, the Least Known TiO_2 Photocatalyst, Catalysts, 3 (2013) 36-73.

[14] T.A. Kandiel, L. Robben, A. Alkaim, D. Bahnemann, Brookite versus anatase TiO2 photocatalysts: phase transformations and photocatalytic activities, Photochemical & Photobiological Sciences, 12 (2013) 602-609.

[15] D.C. Hurum, A.G. Agrios, K.A. Gray, T. Rajh, M.C. Thurnauer, Explaining the Enhanced Photocatalytic Activity of Degussa P25 Mixed-Phase TiO_2 Using EPR, The Journal of Physical Chemistry B, 107 (2003) 4545-4549.

[16] T. Kawahara, Y. Konishi, H. Tada, N. Tohge, J. Nishii, S. Ito, A Patterned TiO_2(Anatase)/TiO_2(Rutile) Bilayer-Type Photocatalyst: Effect of the Anatase/Rutile Junction on the Photocatalytic Activity, Angew. Chem., 114 (2002) 2935-2937.

[17] A. Mills, C. O'Rourke, K. Moore, Powder semiconductor photocatalysis in aqueous solution: An overview of kinetics-based reaction mechanisms, Journal of Photochemistry and Photobiology A: Chemistry, 310 (2015) 66-105.

[18] B. Liu, X. Zhao, C. Terashima, A. Fujishima, K. Nakata, Thermodynamic and kinetic analysis of heterogeneous photocatalysis for semiconductor systems, PCCP, 16 (2014) 8751-8760.

[19] C.S. Turchi, D.F. Ollis, Photocatalytic degradation of organic water contaminants: Mechanisms involving hydroxyl radical attack, J. Catal., 122 (1990) 178-192.

[20] P. Salvador, On the Nature of Photogenerated Radical Species Active in the Oxidative Degradation of Dissolved Pollutants with TiO_2 Aqueous Suspensions: A Revision in the Light of the Electronic Structure of Adsorbed Water, The Journal of Physical Chemistry C, 111 (2007) 17038-17043.

[21] J.F. Montoya, M.F. Atitar, D.W. Bahnemann, J. Peral, P. Salvador, Comprehensive Kinetic and Mechanistic Analysis of TiO_2 Photocatalytic Reactions According to the Direct–Indirect Model: (II) Experimental Validation, The Journal of Physical Chemistry C, 118 (2014) 14276-14290.

[22] A. Zaleska, Doped-TiO_2: A Review, Recent Patents on Engineering, 2 (2008) 157-164.

[23] B. Ohtani, Y. Ogawa, S.I. Nishimoto, Photocatalytic activity of amorphous-anatase mixture of titanium(IV) oxide particles suspended in aqueous solutions, J. Phys. Chem. B, 101 (1997) 3746-3752.

[24] B. Ohtani, K. Iwai, S.I. Nishimoto, S. Sato, Role of platinum deposits on titanium(IV) oxide particles: Structural and kinetic analyses of photocatalytic reaction in aqueous alcohol and amino acid solutions, J. Phys. Chem. B, 101 (1997) 3349-3359.

[25] N. Wu, J. Wang, D.N. Tafen, H. Wang, J.G. Zheng, J.P. Lewis, X. Liu, S.S. Leonard, A. Manivannan, Shape-enhanced photocatalytic activity of single-crystalline anatase TiO_2 (101) nanobelts, JACS, 132 (2010) 6679-6685.

[26] S. Rehman, R. Ullah, A.M. Butt, N.D. Gohar, Strategies of making TiO2 and ZnO visible light active, J. Hazard. Mater., 170 (2009) 560-569.

[27] R. Van De Krol, M. Grätzel, in: Photoelectrochemical Hydrogen Production, Springer, 2011, pp. 13-67.

[28] J. Blanco-Galvez, P. Fernandez-Ibanez, S. Malato-Rodriguez, Solar Photocatalytic Detoxification and Disinfection of Water: Recent Overview, Journal of Solar Energy Engineering, 129 (2007) 4-15.

[29] G. Fu, P.S. Vary, C.-T. Lin, Anatase TiO2 Nanocomposites for Antimicrobial Coatings, The Journal of Physical Chemistry B, 109 (2005) 8889-8898.

[30] A. Ghicov, B. Schmidt, J. Kunze, P. Schmuki, Photoresponse in the visible range from Cr doped TiO_2 nanotubes, Chem. Phys. Lett., 433 (2007) 323-326.

[31] J.-M. Herrmann, J. Disdier, P. Pichat, Effect of chromium doping on the electrical and catalytic properties of powder titania under UV and visible illumination, Chem. Phys. Lett., 108 (1984) 618-622.

[32] S.T. Martin, C.L. Morrison, M.R. Hoffmann, Photochemical Mechanism of Size-Quantized Vanadium-Doped TiO_2 Particles, J. Phys. Chem., 98 (1994) 13695-13704.

[33] J. Moser, M. Grätzel, R. Gallay, Inhibition of Electron-Hole Recombination in Substitutionally Doped Colloidal Semiconductor Crystallites, Helv. Chim. Acta, 70 (1987) 1596-1604.

[34] K. Wilke, H.D. Breuer, The influence of transition metal doping on the physical and photocatalytic properties of titania, Journal of Photochemistry and Photobiology A: Chemistry, 121 (1999) 49-53.

[35] J.C.S. Wu, C.-H. Chen, A visible-light response vanadium-doped titania nanocatalyst by sol–gel method, Journal of Photochemistry and Photobiology A: Chemistry, 163 (2004) 509-515.

[36] J. Choi, H. Park, M.R. Hoffmann, Effects of Single Metal-Ion Doping on the Visible-Light Photoreactivity of TiO_2, The Journal of Physical Chemistry C, 114 (2009) 783-792.

[37] S.N.R. Inturi, T. Boningari, M. Suidan, P.G. Smirniotis, Visible-light-induced photodegradation of gas phase acetonitrile using aerosol-made transition metal (V, Cr, Fe, Co, Mn, Mo, Ni, Cu, Y, Ce, and Zr) doped TiO_2, Applied Catalysis B: Environmental, 144 (2014) 333-342.

[38] R. Asahi, T. Morikawa, T. Ohwaki, K. Aoki, Y. Taga, Visible-Light Photocatalysis in Nitrogen-Doped Titanium Oxides, Science, 293 (2001) 269-271.

[39] D. Chen, Z. Jiang, J. Geng, Q. Wang, D. Yang, Carbon and nitrogen co-doped TiO_2 with enhanced visible-light photocatalytic activity, Ind. Eng. Chem. Res., 46 (2007) 2741-2746.

[40] T. Lindgren, J.M. Mwabora, E. Avendaño, J. Jonsson, A. Hoel, C.-G. Granqvist, S.-E. Lindquist, Photoelectrochemical and Optical Properties of Nitrogen Doped Titanium Dioxide Films Prepared by Reactive DC Magnetron Sputtering, The Journal of Physical Chemistry B, 107 (2003) 5709-5716.

[41] R. Nakamura, T. Tanaka, Y. Nakato, Mechanism for Visible Light Responses in Anodic Photocurrents at N-Doped TiO_2 Film Electrodes, The Journal of Physical Chemistry B, 108 (2004) 10617-10620.

[42] W. Zhu, X. Qiu, V. Iancu, X.Q. Chen, H. Pan, W. Wang, N.M. Dimitrijevic, T. Rajh, H.M. Meyer, M.P. Paranthaman, G.M. Stocks, H.H. Weitering, B. Gu, G. Eres, Z. Zhang, Band gap narrowing of titanium oxide semiconductors by noncompensated anion-Cation codoping for enhanced visible-Light photoactivity, Phys. Rev. Lett., 103 (2009).

[43] C. Burda, Y. Lou, X. Chen, A.C.S. Samia, J. Stout, J.L. Gole, Enhanced nitrogen doping in TiO_2 nanoparticles, Nano Lett., 3 (2003) 1049-1051.

[44] T. Tachikawa, S. Tojo, K. Kawai, M. Endo, M. Fujitsuka, T. Ohno, K. Nishijima, Z. Miyamoto, T. Majima, Photocatalytic oxidation reactivity of holes in the sulfur- and carbon-doped TiO_2 powders studied by time-resolved diffuse reflectance spectroscopy, J. Phys. Chem. B, 108 (2004) 19299-19306.

[45] J. Xu, Y. Ao, D. Fu, C. Yuan, Low-temperature preparation of F-doped TiO_2 film and its photocatalytic activity under solar light, Appl. Surf. Sci., 254 (2008) 3033-3038.

[46] J.G. Yu, J.C. Yu, B. Cheng, S.K. Hark, K. Iu, The effect of F--doping and temperature on the structural and textural evolution of mesoporous TiO_2 powders, J. Solid State Chem., 174 (2003) 372-380.

[47] H. Barndõk, D. Hermosilla, C. Han, D.D. Dionysiou, C. Negro, Á. Blanco, Degradation of 1,4-dioxane from industrial wastewater by solar photocatalysis using immobilized NF-TiO_2 composite with monodisperse TiO_2 nanoparticles, Applied Catalysis B: Environmental, 180 (2016) 44-52.

[48] N. Serpone, Is the Band Gap of Pristine TiO_2 Narrowed by Anion- and Cation-Doping of Titanium Dioxide in Second-Generation Photocatalysts?, The Journal of Physical Chemistry B, 110 (2006) 24287-24293.

[49] M. Pelaez, N.T. Nolan, S.C. Pillai, M.K. Seery, P. Falaras, A.G. Kontos, P.S.M. Dunlop, J.W.J. Hamilton, J.A. Byrne, K. O'Shea, M.H. Entezari, D.D. Dionysiou, A review on the visible light active titanium dioxide photocatalysts for environmental applications, Applied Catalysis B: Environmental, 125 (2012) 331-349.

[50] S. Banerjee, S.C. Pillai, P. Falaras, K.E. O'Shea, J.A. Byrne, D.D. Dionysiou, New Insights into the Mechanism of Visible Light Photocatalysis, The Journal of Physical Chemistry Letters, 5 (2014) 2543-2554.

[51] X. Li, P. Liu, Y. Mao, M. Xing, J. Zhang, Preparation of homogeneous nitrogen-doped mesoporous TiO_2 spheres with enhanced visible-light photocatalysis, Applied Catalysis B: Environmental, 164 (2015) 352-359.

[52] C. Di Valentin, G. Pacchioni, A. Selloni, S. Livraghi, E. Giamello, Characterization of Paramagnetic Species in N-Doped TiO_2 Powders by EPR Spectroscopy and DFT Calculations, The Journal of Physical Chemistry B, 109 (2005) 11414-11419.

[53] W. Ren, Z. Ai, F. Jia, L. Zhang, X. Fan, Z. Zou, Low temperature preparation and visible light photocatalytic activity of mesoporous carbon-doped crystalline TiO_2, Applied Catalysis B: Environmental, 69 (2007) 138-144.

[54] X. Ma, Y. Dai, M. Guo, B. Huang, Insights into the Role of Surface Distortion in Promoting the Separation and Transfer of Photogenerated Carriers in Anatase TiO_2, The Journal of Physical Chemistry C, 117 (2013) 24496-24502.

[55] J.A. Rengifo-Herrera, C. Pulgarin, Photocatalytic activity of N, S co-doped and N-doped commercial anatase TiO_2 powders towards phenol oxidation and E. coli inactivation under simulated solar light irradiation, Solar Energy, 84 (2010) 37-43.

[56] J.A. Rengifo-Herrera, K. Pierzchała, A. Sienkiewicz, L. Forró, J. Kiwi, C. Pulgarin, Abatement of organics and Escherichia coli by N, S co-doped TiO_2 under UV and visible light. Implications of the formation of singlet oxygen (O^2) under visible light, Applied Catalysis B: Environmental, 88 (2009) 398-406.

[57] S.T. Kochuveedu, D.-P. Kim, D.H. Kim, Surface-Plasmon-Induced Visible Light Photocatalytic Activity of TiO_2 Nanospheres Decorated by Au Nanoparticles with Controlled Configuration, The Journal of Physical Chemistry C, 116 (2011) 2500-2506.

[58] X. He, Y. Cai, H. Zhang, C. Liang, Photocatalytic degradation of organic pollutants with Ag decorated free-standing TiO_2 nanotube arrays and interface electrochemical response, J. Mater. Chem., 21 (2011) 475-480.

[59] H. Tran, J. Scott, K. Chiang, R. Amal, Clarifying the role of silver deposits on titania for the photocatalytic mineralisation of organic compounds, Journal of Photochemistry and Photobiology A: Chemistry, 183 (2006) 41-52.

[60] I.M. Arabatzis, T. Stergiopoulos, M.C. Bernard, D. Labou, S.G. Neophytides, P. Falaras, Silver-modified titanium dioxide thin films for efficient photodegradation of methyl orange, Applied Catalysis B: Environmental, 42 (2003) 187-201.

[61] L.G. Devi, R. Kavitha, A review on non metal ion doped titania for the photocatalytic degradation of organic pollutants under UV/solar light: Role of photogenerated charge carrier dynamics in enhancing the activity, Applied Catalysis B: Environmental, 140–141 (2013) 559-587.

[62] H. Park, Y. Park, W. Kim, W. Choi, Surface modification of TiO_2 photocatalyst for environmental applications, Journal of Photochemistry and Photobiology C: Photochemistry Reviews, 15 (2013) 1-20.

[63] S.G. Kumar, L.G. Devi, Review on Modified TiO_2 Photocatalysis under UV/Visible Light: Selected Results and Related Mechanisms on Interfacial Charge Carrier Transfer Dynamics, The Journal of Physical Chemistry A, 115 (2011) 13211-13241.

[64] R. Daghrir, P. Drogui, D. Robert, Modified TiO_2 For Environmental Photocatalytic Applications: A Review, Industrial & Engineering Chemistry Research, 52 (2013) 3581-3599.

[65] Y. Wen, H. Ding, Y. Shan, Preparation and visible light photocatalytic activity of Ag/TiO_2/graphene nanocomposite, Nanoscale, 3 (2011) 4411-4417.

[66] S.S. Rayalu, D. Jose, M.V. Joshi, P.A. Mangrulkar, K. Shrestha, K. Klabunde, Photocatalytic water splitting on Au/TiO_2 nanocomposites synthesized through various routes: Enhancement in photocatalytic activity due to SPR effect, Applied Catalysis B: Environmental, 142–143 (2013) 684-693.

[67] S. Bouhadoun, C. Guillard, F. Dapozze, S. Singh, D. Amans, J. Bouclé, N. Herlin-Boime, One step synthesis of N-doped and Au-loaded TiO_2 nanoparticles by laser pyrolysis: Application in photocatalysis, Applied Catalysis B: Environmental, 174–175 (2015) 367-375.

[68] T. Hirakawa, P.V. Kamat, Charge Separation and Catalytic Activity of $Ag@TiO_2$ Core−Shell Composite Clusters under UV−Irradiation, JACS, 127 (2005) 3928-3934.

[69] A. Kudo, Y. Miseki, Heterogeneous photocatalyst materials for water splitting, Chem. Soc. Rev., 38 (2009) 253-278.

[70] K. Maeda, K. Teramura, D. Lu, N. Saito, Y. Inoue, K. Domen, Noble-Metal/Cr_2O_3 Core/Shell Nanoparticles as a Cocatalyst for Photocatalytic Overall Water Splitting, Angew. Chem., 118 (2006) 7970-7973.

[71] J. Sato, H. Kobayashi, K. Ikarashi, N. Saito, H. Nishiyama, Y. Inoue, Photocatalytic Activity for Water Decomposition of RuO_2-Dispersed Zn_2GeO_4 with d10 Configuration, The Journal of Physical Chemistry B, 108 (2004) 4369-4375.

[72] G. Hu, B. Tang, Photocatalytic mechanism of graphene/titanate nanotubes photocatalyst under visible-light irradiation, Mater. Chem. Phys., 138 (2013) 608-614.

[73] K. Zhou, Y. Zhu, X. Yang, X. Jiang, C. Li, Preparation of graphene-TiO_2 composites with enhanced photocatalytic activity, New J. Chem., 35 (2011) 353-359.

[74] S. Liu, H. Sun, S. Liu, S. Wang, Graphene facilitated visible light photodegradation of methylene blue over titanium dioxide photocatalysts, Chem. Eng. J., 214 (2013) 298-303.

[75] H. Zhang, X. Lv, Y. Li, Y. Wang, J. Li, P25-graphene composite as a high performance photocatalyst, ACS Nano, 4 (2010) 380-386.

[76] S. Malato, J. Blanco, A. Vidal, C. Richter, Photocatalysis with solar energy at a pilot-plant scale: an overview, Applied Catalysis B: Environmental, 37 (2002) 1-15.

[77] J. Petlicki, T.G.M. van de Ven, The equilibrium between the oxidation of hydrogen peroxide by oxygen and the dismutation of peroxyl or superoxide radicals in aqueous solutions in contact with oxygen, J. Chem. Soc., Faraday Trans., 94 (1998) 2763-2767.

[78] J.S. Lee, K.H. You, C.B. Park, Highly Photoactive, Low Bandgap TiO_2 Nanoparticles Wrapped by Graphene, Adv. Mater., 24 (2012) 1084-1088.

[79] G. Li, T. Wang, Y. Zhu, S. Zhang, C. Mao, J. Wu, B. Jin, Y. Tian, Preparation and photoelectrochemical performance of Ag/graphene/TiO_2 composite film, Appl. Surf. Sci., 257 (2011) 6568-6572.

[80] T.-D. Nguyen-Phan, V.H. Pham, E.W. Shin, H.-D. Pham, S. Kim, J.S. Chung, E.J. Kim, S.H. Hur, The role of graphene oxide content on the adsorption-enhanced photocatalysis of titanium dioxide/graphene oxide composites, Chem. Eng. J., 170 (2011) 226-232.

[81] A. Tanaka, S. Sakaguchi, K. Hashimoto, H. Kominami, Preparation of Au/TiO_2 with Metal Cocatalysts Exhibiting Strong Surface Plasmon Resonance Effective for Photoinduced Hydrogen Formation under Irradiation of Visible Light, ACS Catalysis, 3 (2012) 79-85.

[82] Y. Wang, J. Yu, W. Xiao, Q. Li, Microwave-assisted hydrothermal synthesis of graphene based Au-TiO_2 photocatalysts for efficient visible-light hydrogen production, Journal of Materials Chemistry A, 2 (2014) 3847-3855.

[83] V. Subramanian, E.E. Wolf, P.V. Kamat, Catalysis with TiO_2/Gold Nanocomposites. Effect of Metal Particle Size on the Fermi Level Equilibration, JACS, 126 (2004) 4943-4950.

[84] I. Vaz-Moreira, O.C. Nunes, C.M. Manaia, Bacterial diversity and antibiotic resistance in water habitats: searching the links with the human microbiome, FEMS Microbiology Reviews, 38 (2014) 761-778.

[85] C. Baker-Austin, M.S. Wright, R. Stepanauskas, J.V. McArthur, Co-selection of antibiotic and metal resistance, Trends Microbiol, 14 (2006) 176-182.

[86] A. Hernandez, R.P. Mellado, J.L. Martinez, Metal accumulation and vanadium-induced multidrug resistance by environmental isolates of *Escherichia hermannii* and *Enterobacter cloacae*, Appl. Environ. Microbiol., 64 (1998) 4317-4320.

[87] E. Miyahara, M. Nishie, S. Takumi, H. Miyanohara, J. Nishi, K. Yoshiie, H. Oda, M. Takeuchi, M. Komatsu, K. Aoyama, M. Horiuchi, T. Takeuchi, Environmental mutagens may be implicated in the emergence of drug-resistant microorganisms, FEMS Microbiol. Lett., 317 (2011) 109-116.

[88] A.C. Fluit, F.J. Schmitz, Resistance integrons and super-integrons, Clin Microbiol Infect, 10 (2004) 272-288.

[89] B.M. Babior, Phagocytes and oxidative stress, The American Journal of Medicine, 109 (2000) 33-44.

[90] R.A. Miller, B.E. Britigan, Role of oxidants in microbial pathophysiology, Clinical microbiology reviews, 10 (1997) 1-18.

[91] W.D. Splettstoesser, P. Schuff-Werner, Oxidative stress in phagocytes—"The enemy within", Microsc. Res. Tech., 57 (2002) 441-455.

[92] R.A. Clark, The Human Neutrophil Respiratory Burst Oxidase, Journal of Infectious Diseases, 161 (1990) 1140-1147.

[93] J.C. Ireland, P. Klostermann, E.W. Rice, R.M. Clark, Inactivation of *Escherichia coli* by titanium dioxide photocatalytic oxidation, Appl. Environ. Microbiol., 59 (1993) 1668-1670.

[94] Y. Kikuchi, K. Sunada, T. Iyoda, K. Hashimoto, A. Fujishima, Photocatalytic bactericidal effect of TiO_2 thin films: Dynamic view of the active oxygen species responsible for the effect, Journal of Photochemistry and Photobiology a-Chemistry, 106 (1997) 51-56.

[95] P.C. Maness, S. Smolinski, D.M. Blake, Z. Huang, E.J. Wolfrum, W.A. Jacoby, Bactericidal activity of photocatalytic TiO_2 reaction: Toward an understanding of its killing mechanism, Appl. Environ. Microbiol., 65 (1999) 4094-4098.

[96] M. Cho, H. Chung, W. Choi, J. Yoon, Linear correlation between inactivation of *E. coli* and OH radical concentration in TiO_2 photocatalytic disinfection, Water Res., 38 (2004) 1069-1077.

[97] I. Paspaltsis, K. Kotta, R. Lagoudaki, N. Grigoriadis, I. Poulios, T. Sklaviadis, Titanium dioxide photocatalytic inactivation of prions, Journal of General Virology, 87 (2006) 3125-3130.

[98] V. Ramamurthy, Organic Photochemistry, Taylor & Francis, 1997.

[99] J.-J. Huang, H.-Y. Hu, Y.-H. Wu, B. Wei, Y. Lu, Effect of chlorination and ultraviolet disinfection on tetA-mediated tetracycline resistance of *Escherichia coli*, Chemosphere, 90 (2013) 2247-2253.

[100] L. Rizzo, A. Fiorentino, A. Anselmo, Effect of solar radiation on multidrug resistant *E. coli* strains and antibiotic mixture photodegradation in wastewater polluted stream, Sci. Total Environ., 427–428 (2012) 263-268.

[101] V.M. Sousa, C.M. Manaia, A. Mendes, O.C. Nunes, Photoinactivation of various antibiotic resistant strains of *Escherichia coli* using a paint coat, Journal of Photochemistry and Photobiology A: Chemistry, 251 (2013) 148-153.

[102] T.M. Tsai, H.H. Chang, K.C. Chang, Y.L. Liu, C.C. Tseng, A comparative study of the bactericidal effect of photocatalytic oxidation by TiO_2 on antibiotic-resistant and antibiotic-sensitive bacteria, J. Chem. Technol. Biotechnol., 85 (2010) 1642-1653.

[103] C. Coulon, A. Collignon, G. McDonnell, V. Thomas, Resistance of *Acanthamoeba* Cysts to Disinfection Treatments Used in Health Care Settings, J. Clin. Microbiol., 48 (2010) 2689-2697.

[104] W.L. Nicholson, N. Munakata, G. Horneck, H.J. Melosh, P. Setlow, Resistance of *Bacillus* Endospores to Extreme Terrestrial and Extraterrestrial Environments, Microbiology and Molecular Biology Reviews, 64 (2000) 548-572.

[105] D. Gumy, A.G. Rincon, R. Hajdu, C. Pulgarin, Solar photocatalysis for detoxification and disinfection of water: Different types of suspended and fixed TiO_2 catalysts study, Solar Energy, 80 (2006) 1376-1381.

[106] J.S. Wist, J. Dierolf, C. Torres, W. Pulgarin, C., Evaluation of photocatalytic disinfectin of crude water for drinking-water production, Journal of Photochemistry and Photobiology A: Chemistry, (2002) 241-246.

[107] J.C. Yu, W. Ho, J. Yu, H. Yip, P.K. Wong, J. Zhao, Efficient Visible-Light-Induced Photocatalytic Disinfection on Sulfur-Doped Nanocrystalline Titania, Environmental Science & Technology, 39 (2005) 1175-1179.

[108] M. Cho, H. Chung, W. Choi, J. Yoon, Different Inactivation Behaviors of MS-2 Phage and *Escherichia coli* in TiO_2 Photocatalytic Disinfection, Applied and Environmental Microbiology, 71 (2005) 270-275.

[109] D.M. Blake, P.C. Maness, Z. Huang, E.J. Wolfrum, J. Huang, W.A. Jacoby, Application of the photocatalytic chemistry of titanium dioxide to disinfection and the killing of cancer cells, Sep. Purif. Methods, 28 (1999) 1-50.

[110] C. Hu, Y. Lan, J. Qu, X. Hu, A. Wang, Ag/AgBr/TiO$_2$ Visible Light Photocatalyst for Destruction of Azodyes and Bacteria, The Journal of Physical Chemistry B, 110 (2006) 4066-4072.

[111] C. McCullagh, J.M.C. Robertson, D.W. Bahnemann, P.K.J. Robertson, The application of TiO$_2$ photocatalysis for disinfection of water contaminated with pathogenic micro-organisms: a review, Res. Chem. Intermed., 33 (2007) 359-375.

[112] J.A. Ibanez, M.I. Litter, R.A. Pizarro, Photocatalytic bactericidal effect of TiO$_2$ on *Enterobacter cloacae*. Comparative study with other Gram (-) bacteria, Journal of Photochemistry and Photobiology a-Chemistry, 157 (2003) 81-85.

[113] P.S.M. Dunlop, J.A. Byrne, N. Manga, B.R. Eggins, The photocatalytic removal of bacterial pollutants from drinking water, Journal of Photochemistry and Photobiology a-Chemistry, 148 (2002) 355-363.

[114] R. Dillert, U. Siemon, D. Bahnemann, Photocatalytic disinfection of municipal wastewater, Chemical Engineering & Technology, 21 (1998) 356-358.

[115] C.M.B. Carvalho, J.P.C. Tomé, M.A.F. Faustino, M.G.P.M.S. Neves, A.C. Tomé, J.A.S. Cavaleiro, L. Costa, E. Alves, A. Oliveira, Â. Cunha, A. Almeida, Antimicrobial photodynamic activity of porphyrin derivatives: Potential application on medical and water disinfection, J. Porphyrins Phthalocyanines, 13 (2009) 574-577.

[116] J.M.C. Robertson, P.K.J. Robertson, L.A. Lawton, A comparison of the effectiveness of TiO$_2$ photocatalysis and UVA photolysis for the destruction of three pathogenic micro-organisms, Journal of Photochemistry and Photobiology a-Chemistry, 175 (2005) 51-56.

[117] A.G. Rincon, C. Pulgarin, Use of coaxial photocatalytic reactor (CAPHORE) in the TiO$_2$ photo-assisted treatment of mixed *E. coli* and *Bacillus sp.* and bacterial community present in wastewater, Catal. Today, 101 (2005) 331-344.

[118] M. Wainwright, Photoinactivation of viruses, Photochemical and Photobiological Sciences, 3 (2004) 406-411.

[119] M.J. Casteel, K. Jayaraj, A. Gold, L.M. Ball, M.D. Sobsey, Photoinactivation of hepatitis A virus by synthetic porphyrins, Photochem. Photobiol., 80 (2004) 294-300.

[120] J. Gamage, Z.S. Zhang, Applications of Photocatalytic Disinfection, International Journal of Photoenergy, (2010).

[121] Y. Oka, W.C. Kim, T. Yoshida, T. Hirashima, H. Mouri, H. Urade, Y. Itoh, T. Kubo, Efficacy of titanium dioxide photocatalyst for inhibition of bacterial

colonization on percutaneous implants, Journal of Biomedical Materials Research Part B-Applied Biomaterials, 86B (2008) 530-540.

[122] R. Baan, K. Straif, Y. Grosse, B. Secretan, F. El Ghissassi, V. Cogliano, Carcinogenicity of carbon black, titanium dioxide, and talc, The Lancet Oncology, 7 (2006) 295-296.

[123] V.L. Colvin, The potential environmental impact of engineered nanomaterials, Nat Biotech, 21 (2003) 1166-1170.

[124] L. Caballero, K.A. Whitehead, N.S. Allen, J. Verran, Photocatalytic inactivation of *Escherichia coli* using doped titanium dioxide under fluorescent irradiation, Journal of Photochemistry and Photobiology A: Chemistry, 276 (2013) 50-57.

[125] T. Zuccheri, M. Colonna, I. Stefanini, C. Santini, D. Gioia, Bactericidal Activity of Aqueous Acrylic Paint Dispersion for Wooden Substrates Based on TiO_2 Nanoparticles Activated by Fluorescent Light, Materials, 6 (2013) 3270-3283.

[126] K.S. Yao, D.Y. Wang, C.Y. Chang, K.W. Weng, L.Y. Yang, S.J. Lee, T.C. Cheng, C.C. Hwang, Photocatalytic disinfection of phytopathogenic bacteria by dye-sensitized TiO_2 thin film activated by visible light, Surf. Coat. Technol., 202 (2007) 1329-1332.

[127] E.J. Wolfrum, J. Huang, D.M. Blake, P.-C. Maness, Z. Huang, J. Fiest, W.A. Jacoby, Photocatalytic Oxidation of Bacteria, Bacterial and Fungal Spores, and Model Biofilm Components to Carbon Dioxide on Titanium Dioxide-Coated Surfaces, Environmental Science & Technology, 36 (2002) 3412-3419.

[128] A. Vohra, D.Y. Goswami, D.A. Deshpande, S.S. Block, Enhanced photocatalytic inactivation of bacterial spores on surfaces in air, Journal Of Industrial Microbiology & Biotechnology, 32 (2005) 364-370.

[129] E.V. Skorb, L.I. Antonouskaya, N.A. Belyasova, D.G. Shchukin, H. Möhwald, D.V. Sviridov, Antibacterial activity of thin-film photocatalysts based on metal-modified TiO_2 and TiO_2:In_2O_3 nanocomposite, Applied Catalysis B: Environmental, 84 (2008) 94-99.

[130] S. Navalon, M. Alvaro, H. Garcia, D. Escrig, V. Costa, Photocatalytic water disinfection of *Cryptosporidium parvum* and *Giardia lamblia* using a fibrous ceramic TiO_2 photocatalyst, Water Sci. Technol., 59 (2009) 639-645.

[131] J. Lonnen, S. Kilvington, S.C. Kehoe, F. Al-Touati, K.G. McGuigan, Solar and photocatalytic disinfection of protozoan, fungal and bacterial microbes in drinking water, Water Res., 39 (2005) 877-883.

[132] C.-Y. Lin, C.-S. Li, Effectiveness of Titanium Dioxide Photocatalyst Filters for Controlling Bioaerosols, Aerosol Sci. Technol., 37 (2003) 162-170.

[133] K.P. Kühn, I.F. Chaberny, K. Massholder, M. Stickler, V.W. Benz, H.-G. Sonntag, L. Erdinger, Disinfection of surfaces by photocatalytic oxidation with titanium dioxide and UVA light, Chemosphere, 53 (2003) 71-77.

[134] S.-C. Kim, D.-K. Lee, Preparation of TiO_2-coated hollow glass beads and their application to the control of algal growth in eutrophic water, Microchem. J., 80 (2005) 227-232.

[135] M.B. Fisher, D.A. Keane, P. Fernandez-Ibanez, J. Colreavy, S.J. Hinder, K.G. McGuigan, S.C. Pillai, Nitrogen and copper doped solar light active TiO_2 photocatalysts for water decontamination, Applied Catalysis B-Environmental, 130 (2013) 8-13.

[136] A. Erkan, U. Bakir, G. Karakas, Photocatalytic microbial inactivation over Pd doped SnO_2 and TiO_2 thin films, Journal of Photochemistry and Photobiology A: Chemistry, 184 (2006) 313-321.

[137] P.S.M. Dunlop, C.P. Sheeran, J.A. Byrne, M.A.S. McMahon, M.A. Boyle, K.G. McGuigan, Inactivation of clinically relevant pathogens by photocatalytic coatings, Journal of Photochemistry and Photobiology A: Chemistry, 216 (2010) 303-310.

[138] C. Chawengkijwanich, Y. Hayata, Development of TiO_2 powder-coated food packaging film and its ability to inactivate *Escherichia coli* in vitro and in actual tests, Int J Food Microbiol, 123 (2008) 288-292.

[139] J.A. Herrera Melián, J.M. Doña Rodrıguez, A. Viera Suárez, E. Tello Rendón, C. Valdés do Campo, J. Arana, J. Pérez Peña, The photocatalytic disinfection of urban waste waters, Chemosphere, 41 (2000) 323-327.

[140] J. Ângelo, L. Andrade, A. Mendes, Highly active photocatalytic paint for NO_x abatement under real-outdoor conditions, Applied Catalysis A: General, 484 (2014) 17-25.

[141] M. Dizdaroglu, P. Jaruga, M. Birincioglu, H. Rodriguez, Free radical-induced damage to DNA: mechanisms and measurement, Free Radical Biol. Med., 32 (2002) 1102-1115.

[142] T. Matsunaga, R. Tomoda, T. Nakajima, N. Nakamura, T. Komine, Continuous-sterilization system that uses photosemiconductor powders, Applied and Environmental Microbiology, 54 (1988) 1330-1333.

[143] C. Srinivasan, N. Somasundaram, Bactericidal and detoxification effects of irradiated semiconductor catalyst, TiO_2, Current Science 85 (2003) 8.

[144] Z. Huang, P.-C. Maness, D.M. Blake, E.J. Wolfrum, S.L. Smolinski, W.A. Jacoby, Bactericidal mode of titanium dioxide photocatalysis, Journal of Photochemistry and Photobiology A: Chemistry, 130 (2000) 163-170.

[145] K. Sunada, T. Watanabe, K. Hashimoto, Studies on photokilling of bacteria on TiO_2 thin film, Journal of Photochemistry and Photobiology a-Chemistry, 156 (2003) 227-233.

[146] W. Kangwansupamonkon, V. Lauruengtana, S. Surassmo, U. Ruktanonchai, Antibacterial effect of apatite-coated titanium dioxide for textiles applications, Nanomedicine: Nanotechnology, Biology and Medicine, 5 (2009) 240-249.

[147] L. Luo, L. Miao, S. Tanemura, M. Tanemura, Photocatalytic sterilization of TiO_2 films coated on Al fiber, Materials Science and Engineering: B, 148 (2008) 183-186.

[148] R. van Grieken, J. Marugán, C. Pablos, L. Furones, A. López, Comparison between the photocatalytic inactivation of Gram-positive *E. faecalis* and Gram-negative *E. coli* faecal contamination indicator microorganisms, Applied Catalysis B: Environmental, 100 (2010) 212-220.

[149] Z.X. Lu, L. Zhou, Z.L. Zhang, W.L. Shi, Z.X. Xie, H.Y. Xie, D.W. Pang, P. Shen, Cell damage induced by photocatalysis of TiO_2 thin films, Langmuir, 19 (2003) 8765-8768.

[150] P. Demchick, A.L. Koch, The permeability of the wall fabric of *Escherichia coli* and *Bacillus subtilis*, J. Bacteriol., 178 (1996) 768-773.

[151] ISO 27447:2009 Fine ceramics (advanced ceramics, advanced technical ceramics) -- Test method for antibacterial activity of semiconducting photocatalytic materials, in: ISO, 2009.

[152] P. Fernández, J. Blanco, C. Sichel, S. Malato, Water disinfection by solar photocatalysis using compound parabolic collectors, Catal. Today, 101 (2005) 345-352.

[153] A.G. Rincón, C. Pulgarin, Photocatalytical inactivation of *E. coli*: effect of (continuous–intermittent) light intensity and of (suspended–fixed) TiO_2 concentration, Applied Catalysis B: Environmental, 44 (2003) 263-284.

[154] A.K. Benabbou, Z. Derriche, C. Felix, P. Lejeune, C. Guillard, Photocatalytic inactivation of *Escherischia coli*: Effect of concentration of TiO_2 and microorganism, nature, and intensity of UV irradiation, Applied Catalysis B: Environmental, 76 (2007) 257-263.

[155] A. Pal, S.O. Pehkonen, L.E. Yu, M.B. Ray, Photocatalytic Inactivation of Airborne Bacteria in a Continuous-Flow Reactor, Industrial & Engineering Chemistry Research, 47 (2008) 7580-7585.

[156] W.-C.G. Armon R, Bettane P, Disinfection of Bacillus spp. spores in drinking water by TiO_2 photocatalysis as a model for *Bacillus anthracis*, Waterborne Pathog, 4 (2004) 8.

[157] E.S. Tuchina, V.V. Tuchin, TiO_2 nanoparticle enhanced photodynamic inhibition of pathogens, Laser Physics Letters, 7 (2010) 607-612.

[158] Y.W. Cheng, R.C.Y. Chan, P.K. Wong, Disinfection of Legionella pneumophila by photocatalytic oxidation, Water Res., 41 (2007) 842-852.

[159] S. Tanaka, K. Ikeda, H. Miyasaka, Y. Shioi, Y. Suzuki, M. Tamoi, T. Takeda, S. Shigeoka, K. Harada, K. Hirata, Comparison of three Chlamydomonas strains which show distinctive oxidative stress tolerance, Journal of Bioscience and Bioengineering, 112 (2011) 462-468.

[160] S.B. Farr, T. Kogoma, Oxidative stress responses in *Escherichia coli* and Salmonella typhimurium, Microbiological Reviews, 55 (1991) 561-585.

[161] Y.-H. Tsuang, J.-S. Sun, Y.-C. Huang, C.-H. Lu, W.H.-S. Chang, C.-C. Wang, Studies of Photokilling of Bacteria Using Titanium Dioxide Nanoparticles, Artificial Organs, 32 (2008) 167-174.

[162] N.S. Allen, M. Edge, G. Sandoval, J. Verran, J. Stratton, J. Maltby, Photocatalytic coatings for environmental applications, Photochem. Photobiol., 81 (2005) 279-290.

[163] J. Podporska-Carroll, E. Panaitescu, B. Quilty, L. Wang, L. Menon, S.C. Pillai, Antimicrobial properties of highly efficient photocatalytic TiO_2 nanotubes, Applied Catalysis B: Environmental, 176–177 (2015) 70-75.

[164] U. Joost, K. Juganson, M. Visnapuu, M. Mortimer, A. Kahru, E. Nõmmiste, U. Joost, V. Kisand, A. Ivask, Photocatalytic antibacterial activity of nano-TiO$_2$ (anatase)-based thin films: Effects on *Escherichia coli* cells and fatty acids, Journal of Photochemistry and Photobiology B: Biology, 142 (2015) 178-185.

[165] A.C. Miranda, M. Lepretti, L. Rizzo, I. Caputo, V. Vaiano, O. Sacco, W.S. Lopes, D. Sannino, Surface water disinfection by chlorination and advanced oxidation processes: Inactivation of an antibiotic resistant *E. coli* strain and cytotoxicity evaluation, Sci. Total Environ., 554–555 (2016) 1-6.

[166] B. Kim, D. Kim, D. Cho, S. Cho, Bactericidal effect of TiO$_2$ photocatalyst on selected food-borne pathogenic bacteria, Chemosphere, 52 (2003) 277-281.

[167] D. Venieri, E. Markogiannaki, E. Chatzisymeon, E. Diamadopoulos, D. Mantzavinos, Inactivation of *Bacillus anthracis* in water by photocatalytic, photolytic and sonochemical treatment, Photochemical & Photobiological Sciences, 12 (2013) 645-652.

[168] C. Berberidou, I. Paspaltsis, E. Pavlidou, T. Sklaviadis, I. Poulios, Heterogenous photocatalytic inactivation of *B. stearothermophilus* endospores in aqueous suspensions under artificial and solar irradiation, Applied Catalysis B: Environmental, 125 (2012) 375-382.

[169] J.-Y. Choi, K.-H. Kim, K.-C. Choy, K.-T. Oh, K.-N. Kim, Photocatalytic antibacterial effect of TiO$_2$ film formed on Ti and TiAg exposed to *Lactobacillus acidophilus*, Journal of Biomedical Materials Research Part B: Applied Biomaterials, 80B (2007) 353-359.

[170] T. Saito, T. Iwase, J. Horie, T. Morioka, Mode of photocatalytic bactericidal action of powdered semiconductor TiO$_2$ on mutans streptococci, Journal of Photochemistry and Photobiology B: Biology, 14 (1992) 369-379.

[171] C. Sichel, M. de Cara, J. Tello, J. Blanco, P. Fernández-Ibáñez, Solar photocatalytic disinfection of agricultural pathogenic fungi: Fusarium species, Applied Catalysis B: Environmental, 74 (2007) 152-160.

[172] J.H. Lee, M. Kang, S.-J. Choung, K. Ogino, S. Miyata, M.-S. Kim, J.-Y. Park, J.-B. Kim, The preparation of TiO$_2$ nanometer photocatalyst film by a hydrothermal method and its sterilization performance for *Giardia lamblia*, Water Res., 38 (2004) 713-719.

[173] M. Agulló-Barceló, M.I. Polo-López, F. Lucena, J. Jofre, P. Fernández-Ibáñez, Solar Advanced Oxidation Processes as disinfection tertiary treatments for real wastewater: Implications for water reclamation, Applied Catalysis B: Environmental, 136–137 (2013) 341-350.

[174] R.J. Watts, S. Kong, M.P. Orr, G.C. Miller, B.E. Henry, Photocatalytic inactivation of coliform bacteria and viruses in secondary wastewater effluent, Water Res., 29 (1995) 95-100.

[175] J. Araña, J.A. Herrera Melián, J.M. Doña Rodrıguez, O. González Díaz, A Viera, J. Pérez Peña, P.M. Marrero Sosa, V. Espino Jiménez, TiO$_2$-photocatalysis as a tertiary treatment of naturally treated wastewater, Catal. Today, 76 (2002) 279-289.

[176] C.-H. Lin, R.-F. Yu, W.-P. Cheng, C.-R. Liu, Monitoring and control of UV and UV-TiO$_2$ disinfections for municipal wastewater reclamation using artificial neural networks, J. Hazard. Mater., 209–210 (2012) 348-354.

[177] A. Kubacka, M. Ferrer, A. Martínez-Arias, M. Fernández-García, Ag promotion of TiO$_2$-anatase disinfection capability: Study of *Escherichia coli* inactivation, Applied Catalysis B: Environmental, 84 (2008) 87-93.

[178] W.-J. Chen, P.-J. Tsai, Y.-C. Chen, Functional Fe$_3$O$_4$/TiO$_2$ Core/Shell Magnetic Nanoparticles as Photokilling Agents for Pathogenic Bacteria, Small, 4 (2008) 485-491.

[179] V. Rodríguez-González, S.O. Alfaro, L.M. Torres-Martínez, S.-H. Cho, S.-W. Lee, Silver–TiO$_2$ nanocomposites: Synthesis and harmful algae bloom UV-photoelimination, Applied Catalysis B: Environmental, 98 (2010) 229-234.

[180] L. Zhang, M.D. Han, O.K. Tan, M.S. Tse, Y.X. Wang, C.C. Sze, Facile fabrication of Ag/C-TiO$_2$ nanoparticles with enhanced visible light photocatalytic activity for disinfection of *Escherichia coli* and *Enterococcus faecalis*, Journal of Materials Chemistry B, 1 (2013) 564-570.

[181] C.-L. Cheng, D.-S. Sun, W.-C. Chu, Y.-H. Tseng, H.-C. Ho, J.-B. Wang, P.-H. Chung, J.-H. Chen, P.-J. Tsai, N.-T. Lin, M.-S. Yu, H.-H. Chang, The effects of the bacterial interaction with visible-light responsive titania photocatalyst on the bactericidal performance, Journal of Biomedical Science, 16 (2009) 7.

[182] O. Akhavan, E. Ghaderi, Photocatalytic Reduction of Graphene Oxide Nanosheets on TiO$_2$ Thin Film for Photoinactivation of Bacteria in Solar Light Irradiation, The Journal of Physical Chemistry C, 113 (2009) 20214-20220.

[183] A. Pal, S.O. Pehkonen, L.E. Yu, M.B. Ray, Photocatalytic inactivation of Gram-positive and Gram-negative bacteria using fluorescent light, Journal of Photochemistry and Photobiology A: Chemistry, 186 (2007) 335-341.

[184] G. Veréb, L. Manczinger, A. Oszkó, A. Sienkiewicz, L. Forró, K. Mogyorósi, A. Dombi, K. Hernádi, Highly efficient bacteria inactivation and phenol degradation by visible light irradiated iodine doped TiO_2, Applied Catalysis B: Environmental, 129 (2013) 194-201.

[185] O. Akhavan, R. Azimirad, S. Safa, M.M. Larijani, Visible light photo-induced antibacterial activity of CNT-doped TiO_2 thin films with various CNT contents, J. Mater. Chem., 20 (2010) 7386-7392.

[186] Y. Lan, C. Hu, X. Hu, J. Qu, Efficient destruction of pathogenic bacteria with $AgBr/TiO_2$ under visible light irradiation, Applied Catalysis B: Environmental, 73 (2007) 354-360.

[187] D. Venieri, A. Fraggedaki, M. Kostadima, E. Chatzisymeon, V. Binas, A. Zachopoulos, G. Kiriakidis, D. Mantzavinos, Solar light and metal-doped TiO_2 to eliminate water-transmitted bacterial pathogens: Photocatalyst characterization and disinfection performance, Applied Catalysis B: Environmental, 154–155 (2014) 93-101.

[188] K. Pathakoti, S. Morrow, C. Han, M. Pelaez, X. He, D.D. Dionysiou, H.-M. Hwang, Photoinactivation of Escherichia coli by Sulfur-Doped and Nitrogen–Fluorine-Codoped TiO_2 Nanoparticles under Solar Simulated Light and Visible Light Irradiation, Environmental Science & Technology, 47 (2013) 9988-9996.

[189] R. Sadowski, M. Strus, M. Buchalska, P.B. Heczko, W. Macyk, Visible light induced photocatalytic inactivation of bacteria by modified titanium dioxide films on organic polymers, Photochemical & Photobiological Sciences, 14 (2015) 514-519.

[190] P. Gao, A. Li, D.D. Sun, W.J. Ng, Effects of various TiO_2 nanostructures and graphene oxide on photocatalytic activity of TiO_2, J. Hazard. Mater., 279 (2014) 96-104.

[191] H.M. Yadav, T.V. Kolekar, S.H. Pawar, J.-S. Kim, Enhanced photocatalytic inactivation of bacteria on Fe-containing TiO_2 nanoparticles under fluorescent light, Journal of Materials Science: Materials in Medicine, 27 (2016) 1-9.

[192] P. Magalhães, J. Ângelo, V.M. Sousa, O.C. Nunes, L. Andrade, A. Mendes, Synthesis and assessment of a graphene-based composite photocatalyst, Biochem. Eng. J., 104 (2015) 20-26.

[193] D.-H. Kuo, W.-T. Hsu, Y.-Y. Yang, From the fluorescent lamp-induced bactericidal performance of sputtered Ag/TiO_2 films to re-explore the photocatalytic mechanism, Applied Catalysis B: Environmental, 184 (2016) 191-200.

[194] Y.-H. Tseng, D.-S. Sun, W.-S. Wu, H. Chan, M.-S. Syue, H.-C. Ho, H.-H. Chang, Antibacterial performance of nanoscaled visible-light responsive platinum-containing titania photocatalyst in vitro and in vivo, Biochimica et Biophysica Acta (BBA) - General Subjects, (2013).

[195] W.A. Rutala, D.J. Weber, Uses of inorganic hypochlorite (bleach) in health-care facilities, Clinical Microbiology Reviews, 10 (1997) 597-610.

[196] M. Deborde, U. von Gunten, Reactions of chlorine with inorganic and organic compounds during water treatment—Kinetics and mechanisms: A critical review, Water Res., 42 (2008) 13-51.

[197] A.V. Levanov, I.V. Kuskov, E.E. Antipenko, V.V. Lunin, Stoichiometry and products of ozone reaction with chloride ion in an acidic medium, Russ. J. Phys. Chem., 86 (2012) 757-762.

[198] J.C. Crittenden, M.W. Harza, D.W. Hand, K.J. Howe, MWH's Water Treatment: Principles and Design, Wiley, 2012.

[199] W.A. Rutala, D.J. Weber, C.f.D. Control, Guideline for disinfection and sterilization in healthcare facilities, 2008, in, Centers for Disease Control (US), 2008.

[200] V. Lazarova, P. Savoye, M.L. Janex, E.R. Blatchley Iii, M. Pommepuy, Advanced wastewater disinfection technologies: State of the art and perspectives, Water Sci. Technol., 40 (1999) 203-213.

[201] G.P. Winward, L.M. Avery, T. Stephenson, B. Jefferson, Chlorine disinfection of grey water for reuse: Effect of organics and particles, Water Res., 42 (2008) 483-491.

[202] R. Virto, P. Mañas, I. Álvarez, S. Condon, J. Raso, Membrane Damage and Microbial Inactivation by Chlorine in the Absence and Presence of a Chlorine-Demanding Substrate, Applied and Environmental Microbiology, 71 (2005) 5022-5028.

[203] C. Shang, E.R. Blatchley Iii, Chlorination of pure bacterial cultures in aqueous solution, Water Res., 35 (2001) 244-254.

[204] A. Hassen, A. Heyouni, H. Shayeb, M. Cherif, A. Boudabous, Inactivation of indicator bacteria in wastewater by chlorine—a kinetics study, Bioresour. Technol., 72 (2000) 85-93.

[205] L.V. Venczel, M. Arrowood, M. Hurd, M.D. Sobsey, Inactivation of *Cryptosporidium parvum* oocysts and Clostridium perfringens spores by a mixed-oxidant disinfectant and by free chlorine, Applied and Environmental Microbiology, 63 (1997) 1598-1601.

[206] G. Berg, D.R. Dahling, G.A. Brown, D. Berman, Validity of fecal coliforms, total coliforms, and *fecal streptococci* as indicators of viruses in chlorinated primary sewage effluents, Applied and Environmental Microbiology, 36 (1978) 880-884.

[207] J.A. Tree, M.R. Adams, D.N. Lees, Chlorination of Indicator Bacteria and Viruses in Primary Sewage Effluent, Applied and Environmental Microbiology, 69 (2003) 2038-2043.

[208] J. Koivunen, H. Heinonen-Tanski, Inactivation of enteric microorganisms with chemical disinfectants, UV irradiation and combined chemical/UV treatments, Water Res., 39 (2005) 1519-1526.

[209] C.H. King, E.B. Shotts, R.E. Wooley, K.G. Porter, Survival of coliforms and bacterial pathogens within protozoa during chlorination, Applied and Environmental Microbiology, 54 (1988) 3023-3033.

[210] S. Neralla, R.W. Weaver, B.J. Lesikar, R.A. Persyn, Improvement of domestic wastewater quality by subsurface flow constructed wetlands, Bioresour. Technol., 75 (2000) 19-25.

[211] T.E. Agustina, H.M. Ang, V.K. Vareek, A review of synergistic effect of photocatalysis and ozonation on wastewater treatment, Journal of Photochemistry and Photobiology C: Photochemistry Reviews, 6 (2005) 264-273.

[212] J. Hoigné, H. Bader, Rate constants of reactions of ozone with organic and inorganic compounds in water—I: Non-dissociating organic compounds, Water Res., 17 (1983) 173-183.

[213] J.A. Imlay, The molecular mechanisms and physiological consequences of oxidative stress: lessons from a model bacterium, Nat Rev Micro, 11 (2013) 443-454.

[214] C.-S. Li, Y.-C. Wang, Surface Germicidal Effects of Ozone for Microorganisms, AIHA Journal, 64 (2003) 533-537.

[215] H. Liltved, H. Hektoen, H. Efraimsen, Inactivation of bacterial and viral fish pathogens by ozonation or UV irradiation in water of different salinity, Aquacultural Engineering, 14 (1995) 107-122.

[216] C. Nebel, R.D. Gottschling, R.L. Hutchison, T.J. McBride, D.M. Taylor, J.L. Pavoni, M.E. Tittlebaum, H.E. Spencer, M. Fleischman, Ozone Disinfection of Industrial-Municipal Secondary Effluents, Journal (Water Pollution Control Federation), 45 (1973) 2493-2507.

[217] J.C. Joret, J.C. Block, Y. Richard, Wastewater Disinfection : Elimination of Fecal Bacteria and Eneric Viruses By Ozone, Ozone: Science & Engineering, 4 (1982) 91-99.

[218] M.L. Janex, P. Savoye, M. Roustan, Z. Do-Quang, J.M. Laîné, V. Lazarova, Wastewater Disinfection by Ozone: Influence of Water Quality and Kinetics Modeling, Ozone: Science & Engineering, 22 (2000) 113-121.

[219] J.M. Sousa, G. Macedo, M. Pedrosa, C. Becerra-Castro, S. Castro-Silva, M.F.R. Pereira, A.M.T. Silva, O.C. Nunes, C.M. Manaia, Ozonation and UV254 nm radiation for the removal of microorganisms and antibiotic resistance genes from urban wastewater, J. Hazard. Mater.

[220] J.G. Kim, A.E. Yousef, Inactivation Kinetics of Foodborne Spoilage and Pathogenic Bacteria by Ozone, J. Food Sci., 65 (2000) 521-528.

[221] G.R. Burleson, T.M. Murray, M. Pollard, Inactivation of Viruses and Bacteria by Ozone, With and Without Sonication, Applied Microbiology, 29 (1975) 340-344.

[222] G.H.R. Silva, L.A. Daniel, H. Bruning, W.H. Rulkens, Anaerobic effluent disinfection using ozone: Byproducts formation, Bioresour. Technol., 101 (2010) 6981-6986.

[223] J.L. Rennecker, B.J. Mariñas, J.H. Owens, E.W. Rice, Inactivation of Cryptosporidium parvum oocsts with ozone, Water Res., 33 (1999) 2481-2488.

[224] S.K. Sastry, A.K. Datta, R.W. Worobo, Ultraviolet Light, J. Food Sci., 65 (2000) 90-92.

[225] WHO (World Health Organization) Guidelines for Drinking-water Quality, in, WHO, Geneva, Switzerland, 2011.

[226] C. Bouki, D. Venieri, E. Diamadopoulos, Detection and fate of antibiotic resistant bacteria in wastewater treatment plants: A review, Ecotoxicology and Environmental Safety, 91 (2013) 1-9.

[227] M.-T. Guo, Q.-B. Yuan, J. Yang, Microbial selectivity of UV treatment on antibiotic-resistant heterotrophic bacteria in secondary effluents of a municipal wastewater treatment plant, Water Research, (2013).

[228] N. Goosen, G.F. Moolenaar, Repair of UV damage in bacteria, DNA Repair, 7 (2008) 353-379.

[229] R.P. Rastogi, Richa, A. Kumar, M.B. Tyagi, R.P. Sinha, Molecular Mechanisms of Ultraviolet Radiation-Induced DNA Damage and Repair, Journal of Nucleic Acids, 2010 (2010).

[230] R.P. Sinha, D.-P. Hader, UV-induced DNA damage and repair: a review, Photochemical & Photobiological Sciences, 1 (2002) 225-236.

[231] A.L. Santos, C. Moreirinha, D. Lopes, A.C. Esteves, I. Henriques, A. Almeida, M.R.M. Domingues, I. Delgadillo, A. Correia, Â. Cunha, Effects of UV Radiation on the Lipids and Proteins of Bacteria Studied by Mid-Infrared Spectroscopy, Environmental Science & Technology, 47 (2013) 6306-6315.

[232] K.G. McGuigan, R.M. Conroy, H.-J. Mosler, M.d. Preez, E. Ubomba-Jaswa, P. Fernandez-Ibañez, Solar water disinfection (SODIS): A review from bench-top to roof-top, Journal of Hazardous Materials, 235–236 (2012) 29-46.

[233] L. Rizzo, C. Manaia, C. Merlin, T. Schwartz, C. Dagot, M.C. Ploy, I. Michael, D. Fatta-Kassinos, Urban wastewater treatment plants as hotspots for antibiotic resistant bacteria and genes spread into the environment: A review, Science of The Total Environment, 447 (2013) 345-360.

[234] W.A.M. Hijnen, E.F. Beerendonk, G.J. Medema, Inactivation credit of UV radiation for viruses, bacteria and protozoan (oo)cysts in water: A review, Water Res., 40 (2006) 3-22.

[235] T. Bintsis, E. Litopoulou-Tzanetaki, R.K. Robinson, Existing and potential applications of ultraviolet light in the food industry – a critical review, J. Sci. Food Agric., 80 (2000) 637-645.

[236] E. Levetin, R. Shaughnessy, C.A. Rogers, R. Scheir, Effectiveness of Germicidal UV Radiation for Reducing Fungal Contamination within Air-Handling Units, Applied and Environmental Microbiology, 67 (2001) 3712-3715.

[237] W.A. Rutala, M.F. Gergen, D.J. Weber, Room Decontamination with UV Radiation, Infection Control & Hospital Epidemiology, 31 (2010) 1025-1029.

[238] C.W. McKinney, A. Pruden, Ultraviolet Disinfection of Antibiotic Resistant Bacteria and Their Antibiotic Resistance Genes in Water and Wastewater, Environmental Science & Technology, 46 (2012) 13393-13400.

[239] J.C. Chang, S.F. Ossoff, D.C. Lobe, M.H. Dorfman, C.M. Dumais, R.G. Qualls, J.D. Johnson, UV inactivation of pathogenic and indicator microorganisms, Applied and Environmental Microbiology, 49 (1985) 1361-1365.

[240] P. Drogui, S. Elmaleh, M. Rumeau, C. Bernard, A. Rambaud, Hydrogen peroxide production by water electrolysis: Application to disinfection, J. Appl. Electrochem., 31 (2001) 877-882.

[241] F. Haber, J. Weiss, The Catalytic Decomposition of Hydrogen Peroxide by Iron Salts, 1934.

[242] J.P. Kehrer, The Haber–Weiss reaction and mechanisms of toxicity, Toxicology, 149 (2000) 43-50.

[243] E. Linley, S.P. Denyer, G. McDonnell, C. Simons, J.-Y. Maillard, Use of hydrogen peroxide as a biocide: new consideration of its mechanisms of biocidal action, J. Antimicrob. Chemother., 67 (2012) 1589-1596.

[244] M. Finnegan, E. Linley, S.P. Denyer, G. McDonnell, C. Simons, J.-Y. Maillard, Mode of action of hydrogen peroxide and other oxidizing agents: differences between liquid and gas forms, J. Antimicrob. Chemother., 65 (2010) 2108-2115.

[245] G. Fichet, E. Comoy, C. Duval, K. Antloga, C. Dehen, A. Charbonnier, G. McDonnell, P. Brown, C. Ida Lasmézas, J.-P. Deslys, Novel methods for disinfection of prion-contaminated medical devices, The Lancet, 364 (2004) 521-526.

[246] G. Fichet, K. Antloga, E. Comoy, J.P. Deslys, G. McDonnell, Prion inactivation using a new gaseous hydrogen peroxide sterilisation process, Journal of Hospital Infection, 67 (2007) 278-286.

[247] J.A. Otter, G.L. French, Survival of Nosocomial Bacteria and Spores on Surfaces and Inactivation by Hydrogen Peroxide Vapor, J. Clin. Microbiol., 47 (2009) 205-207.

[248] N.A. Klapes, D. Vesley, Vapor-phase hydrogen peroxide as a surface decontaminant and sterilant, Applied and Environmental Microbiology, 56 (1990) 503-506.

[249] M. Ksibi, Chemical oxidation with hydrogen peroxide for domestic wastewater treatment, Chem. Eng. J., 119 (2006) 161-165.

[250] S. Lemmen, S. Scheithauer, H. Häfner, S. Yezli, M. Mohr, J.A. Otter, Evaluation of hydrogen peroxide vapor for the inactivation of nosocomial pathogens on porous and nonporous surfaces, American Journal of Infection Control, 43 (2015) 82-85.

[251] Water treatment manual: disinfection, in, US EPA, United States Environmental Protection Agency, 2011.

[252] J. Gamage, Z. Zhang, Applications of Photocatalytic Disinfection, International Journal of Photoenergy, 2010 (2010).

[253] D. Spasiano, R. Marotta, S. Malato, P. Fernandez-Ibañez, I. Di Somma, Solar photocatalysis: Materials, reactors, some commercial, and pre-industrialized applications. A comprehensive approach, Applied Catalysis B: Environmental, 170–171 (2015) 90-123.

[254] M.S. Siddiqui, G.L. Amy, R.G. Rice, Bromate ion formation: a critical review, Journal of the American Water Works Association, 87 (1995) 58-70.

[255] L. Rizzo, H. Selcuk, A.D. Nikolaou, S. Meriç Pagano, V. Belgiorno, A comparative evaluation of ozonation and heterogeneous photocatalytic oxidation processes for reuse of secondary treated urban wastewater, Desalination and Water Treatment, 52 (2013) 1414-1421.

[256] L. Prieto-Rodríguez, I. Oller, N. Klamerth, A. Agüera, E.M. Rodríguez, S. Malato, Application of solar AOPs and ozonation for elimination of micropollutants in municipal wastewater treatment plant effluents, Water Res., 47 (2013) 1521-1528.

[257] N.F.F. Moreira, J.M. Sousa, G. Macedo, A.R. Ribeiro, L. Barreiros, M. Pedrosa, J.L. Faria, M.F.R. Pereira, S. Castro-Silva, M.A. Segundo, C.M. Manaia, O.C. Nunes, A.M.T. Silva, Photocatalytic ozonation of urban wastewater and surface water using immobilized TiO_2 with LEDs: Micropollutants, antibiotic resistance genes and estrogenic activity, Water Res., 94 (2016) 10-22.

[258] C. Blazejewski, F. Wallet, A. Rouzé, R. Le Guern, S. Ponthieux, J. Salleron, S. Nseir, Efficiency of hydrogen peroxide in improving disinfection of ICU rooms, Critical Care, 19 (2015) 30.

[259] K.E. Wainwright, M. Lagunas-Solar, M.A. Miller, B.C. Barr, I.A. Gardner, C. Pina, A.C. Melli, A.E. Packham, N. Zeng, T. Truong, P.A. Conrad, Physical Inactivation of Toxoplasma gondii Oocysts in Water, Applied and Environmental Microbiology, 73 (2007) 5663-5666.

[260] M.W. LeChevallier, C.D. Cawthon, R.G. Lee, Factors promoting survival of bacteria in chlorinated water supplies, Applied and Environmental Microbiology, 54 (1988) 649-654.

[261] O.K. Dalrymple, E. Stefanakos, M.A. Trotz, D.Y. Goswami, A review of the mechanisms and modeling of photocatalytic disinfection, Applied Catalysis B: Environmental, 98 (2010) 27-38.

[262] G.A. Boorman, Drinking water disinfection byproducts: review and approach to toxicity evaluation, Environ. Health Perspect., 107 (1999) 207-217.

[263] P.S.M. Dunlop, M. Ciavola, L. Rizzo, D.A. McDowell, J.A. Byrne, Effect of photocatalysis on the transfer of antibiotic resistance genes in urban wastewater, Catal. Today, 240, Part A (2015) 55-60.

[264] D. Nozaic, Chlorine: Is it really so bad and what are the alternatives?, Water Sa, 30 (2004) 18-24.

[265] R.G. Rice, Ozone in the United States of America -- State-Of-The-Art, Ozone: Science & Engineering, 21 (1999) 99-118.

[266] V. Camel, A. Bermond, The use of ozone and associated oxidation processes in drinking water treatment, Water Res., 32 (1998) 3208-3222.

[267] Wastewater technology fact sheet [electronic resource] : ozone disinfection, United States Environmental Protection Agency, Office of Water, [Washington, D.C.], 1999.

[268] Wastewater technology fact sheet [electronic resource] : ultraviolet disinfection, United States Environmental Protection Agency, Office of Water, [Washington, D.C.], 1999.

[269] G. McDonnell, A.D. Russell, Antiseptics and Disinfectants: Activity, Action, and Resistance, Clinical Microbiology Reviews, 12 (1999) 147-179.

[270] S. Malato, P. Fernández-Ibáñez, M.I. Maldonado, J. Blanco, W. Gernjak, Decontamination and disinfection of water by solar photocatalysis: Recent overview and trends, Catal. Today, 147 (2009) 1-59.

[271] Q. Li, S. Mahendra, D.Y. Lyon, L. Brunet, M.V. Liga, D. Li, P.J.J. Alvarez, Antimicrobial nanomaterials for water disinfection and microbial control: Potential applications and implications, Water Res., 42 (2008) 4591-4602.

PART II:

PHOTOCATALYSTS

Chapter 2.

Synthesis and Assessment of a Graphene-based Composite Photocatalyst

Pedro Magalhães, Joana Ângelo, Vera M. Sousa, Olga C. Nunes, Luísa Andrade, Adélio Mendes

Abstract

A novel composite photocatalyst prepared from graphene and commercial TiO$_2$ (P25 from Evonik) was synthesized, exhibiting enhanced photocatalytic activity for methylene blue degradation, when compared with pristine P25. Additionally, the new catalyst showed 20% more NO conversion under UV light than P25. The band gap of the catalyst, obtained from diffuse reflectance, was 2.95 eV indicating an extended light absorption up to 420 nm. The novel photocatalyst was further tested for inactivating microorganisms showing better results than the reference photocatalyst. Under visible light, the viability loss of the reference bacterial strain *Escherichia coli* DSM 1103 was two times higher than with the bare P25; it was observed 29 % of inactivation with the P25/graphene composite and 14 % with the P25 sample, following standard ISO 27447:2009.
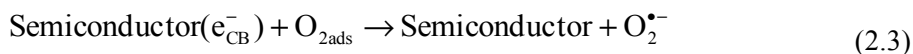
2.1. Introduction

Photocatalysis has attracted the attention of many researchers mainly because it can be used for photoabatement of atmospheric contaminants, water treatment and inactivation of microorganisms both in suspension and on surfaces [1, 2]. More recently, photoinactivation of microorganisms has emerged as an alternative disinfection method [3]; especially the use of titanium dioxide in antimicrobial application has been widely discussed [2, 3]. This special interest on TiO_2 material was fueled by the work by Fujishima *et al.* [4] in 1972, describing for the first time water splitting using a TiO_2 photoelectrode.

Independently of the photocatalytic application, the mechanism behind photocatalyss consists in the generation of electron-hole pairs upon excitation of the photocatalyst with photons showing energy higher than the band gap (in the case of TiO_2 *ca.* 3.2 eV) – Eq. (2.1). These holes and electrons can oxidize and reduce surface-adsorbed molecules, respectively. The strong oxidation potential of the photogenerated valence band holes in anatase TiO_2 (E_{VB} = +3.0 V *vs*. Normal Hydrogen Electrode (NHE), pH = 1) originates the formation of hydroxyl radicals ($OH^\bullet$) when in contact with water – Eq. (2.2). The reduction potential of anatase TiO_2 conduction band electrons is of *ca.* -0.2 V (pH = 1) and reduces O_2 to produce superoxide radical ($O_2^{\bullet-}$) – Eq. (2.3) [5]. These free radicals intermediate the oxidation of organic species at, for example, the surface of microorganisms, originating ultimately their inactivation.

$$\text{Semiconductor} \xrightarrow{\;h\nu\;} e_{CB}^- + h_{VB}^+ \tag{2.1}$$

$$\text{Semiconductor}(h_{VB}^+) + H_2O_{ads} \rightarrow \text{Semiconductor} + HO_{ads}^\bullet + H^+ \tag{2.2}$$

$$\text{Semiconductor}(e_{CB}^-) + O_{2ads} \rightarrow \text{Semiconductor} + O_2^{\bullet-} \tag{2.3}$$

The extensive use of TiO_2 material as photocatalyst can be explained by its thermal and chemical stability, exhibiting no photocorrosion, readily available, relatively cheap and band edges that are well positioned for producing oxidizing/reducing agents [5]. However, TiO_2 absorbs only UV light, preventing its usage under visible spectrum; hence, many efforts have been powered to enhance titanium dioxide photocatalytic activity. Two main actions are being followed: i) narrowing the semiconductor band gap (E_g); and ii) decrease the e^-/h^+ recombination. While the first allows the photocatalyst to absorb a larger fraction of the solar spectrum

and eventually reach the visible spectrum, the later allows improving the redox reactions rate at the photocatalyst surface. Several doping techniques have been described targeting the decrease of the semiconductor band gap [6, 7]. Even though the doping mechanism is not yet fully understood, the two most used dopants of TiO_2 are C and N; these dopants act as substitutional anions (substitute oxygen) or interstitial cations (substitute titanium) [8, 9]. On the other hand, to decrease e^-/h^+ recombination rate several studies suggest the use of carbon-based supports such as carbon nanotubes (CNTs), fullerene or graphene [8]. These materials have the ability to receive and store photoinjected electrons and thus preventing e^-/h^+ recombination. In most of the cases, partially oxidized graphene, known as graphene oxide (GO), is used instead of pure graphene due its tunable optical, conductive and chemical properties. Graphene oxide is obtained functionalizing graphene sheets with carboxylic acid, hydroxyl and/or epoxide groups, and thus its properties can be adjusted via chemical modification [10]. The binding of TiO_2 to graphene sheets allows improved photocatalytic performance when compared with their pristine form mainly because: i) efficient charge separation and transportation; ii) extended light absorption range; and iii) enhanced adsorption [11]. TiO_2/graphene composites slow the rate of e^-/h^+ recombination after light excitation [12], increasing the charge transfer rate of electrons. The extended light absorption can be achieved due to doping of TiO_2 with carbon from the graphene, leading to a narrowing of the semiconductor band gap. The enhanced adsorption of the TiO_2/graphene composite is mainly attributed to its very large π-conjugation system and two-dimensional planar structure [11, 13]. The increase in adsorption may enhance the photocatalytic degradation of methylene blue, assuming the adsorption of reactants is higher than the adsorption of the degradation products. Even though there are some works reporting the use of the TiO_2/graphene composites in areas such as dyes degradation evaluation [14] and microorganism photoinactivation [15], the use of TiO_2/graphene composites for NO deep oxidation has never been reported in literature.

In this work, a composite photocatalyst was prepared from commercial graphene (xGnP® from XG Sciences) and commercial TiO_2 (P25 from Evonik) and its performance compared with commercial photocatalysts – P25 and VLP7101 (Kronos). The band-gap of the prepared photocatalyst was assessed by diffuse reflectance and it was tested for methylene blue degradation and NO deep oxidation under UV-light. The photocatalyst was further tested for inactivating microorganisms both under UV

radiation and visible light. The viability loss of the reference bacterial strain *Escherichia coli* DSM 1103 was obtained for both types of radiation and compared with three commercial photocatalysts: P25, VLP7000 and VLP7101.

2.2. Materials and Methods

2.2.1 Synthesis of P25/graphene composite photocatalyst

P25/graphene composite was prepared as described elsewhere [11] with minor modifications. Briefly, oxidized graphene nano-platelets (GNP_{ox}) - $KMNO_4$ 3:1 graphene nano-platelets (GNP) - were prepared according to a modified Hummer´s method. Shortly, 50 mL of H_2SO_4 were added to 2 g of GNP at room temperature and the solution was cooled using an ice bath, followed by gradual addition of 6 g of $KMnO_4$. Then, 300 mL of distilled water was added, followed by addition of H_2O_2 until oxygen release stopped. GNP_{ox} was washed 5 times with water by centrifugation at 4000 rpm during 15 minutes. The solid was dispersed in 500 mL of water by sonication (Bandelin Sonorex R K512 H) during 5 h and lyophilized during 72 h. Then, the composite was obtained via a hydrothermal method based on the work by Zhang *et al.* [11]. Briefly, 2 mg of GNP_{ox} was dissolved in a solution of distilled H_2O (20 mL) and ethanol (10 mL) by ultrasonic treatment for 1 h, and 0.2 g of P25 was added to the obtained GNP_{ox} solution and stirred for another 2 h to get a homogeneous suspension. The suspension was then placed in a 40 mL Teflon-sealed autoclave and maintained at 120 °C for 3 h to simultaneously achieve the reduction of GO and the deposition of P25 on the carbon support. Finally, the resulting composite was recovered by filtration, rinsed by deionized water several times and dried at room temperature.

The photocatalytic activity of the as-prepared P25/graphene composite was then compared with three different commercial photocatalysts: Aeroxide[®] TiO_2 P25 (Evonik Industries, Germany), Kronos[®] VLP7000 and VLP7101 (KRONOS Worldwide, Inc., United States of America).

2.2.2. Characterization

2.2.2.1 Diffuse reflectance analyses

Diffuse reflectance spectroscopy is often used to determine the absorption properties of both crystalline and amorphous materials [16]. The band gap of a sample can be obtained from the Tauc equation, which relates the diffuse reflectance and the Kubelka–Munk model to the excitation frequency [16]:

$$(h\nu F(R_\infty))^{1/n} = A(h\nu - E_g) \hspace{3cm} (2.4)$$

where, h is the Planck constant, ν is the frequency of vibration, A is a constant and E_g is the band gap energy.

This equation is obtained multiplying the Kubelka–Munk equation by the energy of the incident radiation ($E = h\nu$) and powered to a coefficient n, according to the type of the electronic transition of the material. For indirect transitions n equals 2 and for direct transition n is 1/2. Plotting the modified Kubelka–Munk equation as a function of the incident radiation, the band gap of the semiconductor can be obtained extrapolating the linear part of this curve to the x-axis, the so-called Tauc plot; the band gap energy is read at the intersection. Diffuse reflectance of the different samples were obtained in a Shimatzu UV-3600 UV-VIS-NIR spectrophotometer, equipped with a 150 mm integrating sphere and using $BaSO_4$ as 100 % reflectance standard. The samples were pressed to form a flat disc that fit into the spectrophotometer sample holder.

2.2.2.2 SEM and XRD analyses

The morphology and composition of the photocatalysts was obtained from scanning electron microscopy (SEM) coupled with energy dispersive X-ray (EDX) analysis. A FEI Quanta 400FEG ESEM/EDAX Genesis X4M apparatus equipped with a Schottky field emission gun (for optimal spatial resolution) was used for the characterization of the surface morphology of the photocatalysts with SEM. Images were digitally recorded using a Gatan SC 1000 ORIUS CCD camera (Warrendale, PA, USA). These SEM/EDX analyses were made at Centro de Materiais da Universidade do Porto (CEMUP).

The crystallographic characterization of the samples was performed by X-ray diffraction (XRD). The XRD pattern of the selected samples was obtained using a Denchtop X-Ray Diffractometer RIGAKU, model MiniFlex II using Cu X-ray tube (30 KV/15 mA). The data was obtained at 2θ angles (10–80°), with a step speed of 3.5°/min. Debye–Scherrer equation was used to determine the crystallite size. The obtained X-ray scans were compared to those of standard database and the phases were assigned comparing with data available in literature.

2.2.3 Photoactivity characterization

The photocatalytic performance of the as prepared semiconductors was determined by: a) degradation of dye methylene blue, b) nitrogen oxide (NO) deep oxidation and c) photoinactivation of microorganisms. Each of these techniques is described next.

2.2.3.1 Methylene blue degradation

The photodegradation history of methylene blue (MB) dyes was followed by photospectroscopy. In a typical process, aqueous solution of MB dye (0.01 g/L, i.e. 2.7 × 10^{-5} M, 100 mL) and photocatalysts (50 mg) were placed in a 250 mL cylindrical glass vessel. Under ambient conditions and stirring, the photoreactor vessel was exposed to the UV irradiation produced by an ultraviolet (UV-A, highest emission at 365 nm) lamp with two 6 W black-light-blue bulbs (VL-206-BLB, Vilbert Lourmat, France); the lamp was positioned 10 cm away from the vessel (intensity at the catalyst mixture surface was measured with a UV radiometer (HD 2102.2, Delta/OHM, Italy) being 10 W·m^{-2}). The trial began by putting the mixture during 30 minutes in the dark; the mixture was then illuminated for 4 hours. Samples were collected every 30 minutes, centrifuged and the supernatant was analyzed in an UV-visible absorption spectrophotometer (Shimatzu UV-3600 UV-VIS-NIR spectrophotometer).

2.2.3.2. Nitrogen oxide (NO) deep oxidation

The experimental setup used in NO deep oxidation tests were based on standard ISO 22197-1:2007 [17]. The experimental setup consists of four main sections: i) feed, ii) reactor, iii) NO$_x$ quantification and iv) computer monitoring/control [18]. Semiconductors were tested as powder films pressed on aluminum slabs with an area of 2 cm × 2 cm. A 50 % of relative humidity feed stream was supplied, with a feed rate of 0.7 L·min^{-1} of NO at 1 ppmv in air at 25 °C. The irradiation was provided by a UV lamp (VL-206-BLB, Vilbert Lourmat, France) with an irradiation of 10 W·m^{-2}. The photocatalytic activity was assessed from the NO conversion (Eq. 2.5):

$$X_{NO} = \left(\frac{C_{NO}^{in} - C_{NO}^{out}}{C_{NO}^{in}} \right) \times 100 \qquad (2.5)$$

where X_{NO} is the conversion of NO, C_{NO} stands for NO concentration and the superscripts (*in* and *out*) refer to the inlet and outlet streams.

2.2.3.3 Photoinactivation of microorganisms

a) Bacterial strains and culture conditions

Escherichia coli DSM 1103 was used in the photoinactivation trials. *E. coli* cells were grown overnight (18–20 h) at 30 ºC on Plating Count Agar (PCA, LiofilChem, Italy) and the biomass was used to prepare a suspension in sterile saline solution [0.85 % NaCl (w/v)]. The cell density of the suspension was adjusted to 10^6 CFU·mL^{-1} [19] or 10^3 CFU·mL^{-1} using a calibration curve of optical density versus number of viable cells [colony forming units (CFU)·mL^{-1}].

b) Light source and apparatus

A high intensity, long-wave (highest emission at 365 nm) ultraviolet (UV-A) lamp with two 6 W black-light-blue bulbs (VL-206-BLB, Vilbert Lourmat, France) was employed on the UV trials. The incident photon flux was 10 W·m^{-2} according to the standard [19]. The visible light trials were conducted with a regular fluorescent light (Philips Master TL-Mini Super 80 6W/840) with a light intensity of 50 W·m^{-2}.

c) Experimental procedure for *E. coli* photoinactivation in suspension

The experimental procedure for determining the *E. coli* DSM 1103 photoinactivation is described elsewhere [20]. Briefly, the photocatalyst (P25, P25/graphene, VLP7000 or VLP7101) was added to the cell suspension at a concentration of 0.2 % (w/v). For each photocatalyst two initial cellular densities (10^3 or 10^6 CFU·mL^{-1}) were tested. The mixture was stirred (250 rpm) and irradiated with UV radiation or visible light for 40 minutes. After this time, the mixture was kept in the dark for 20 minutes for ensuring that the photocatalyst had no activity, which usually is still observed for a few minutes after being irradiated [21].

At the initial ($t_i = 0$ min) and final time ($t_f = 40 + 20$ min), the cell suspension was serially diluted in sterile saline solution and aliquots of 100 μL were spread on PCA, as described in Koch [22]. After incubation at 30 ºC for 24 h, the colony forming units, corresponding to the viable cells, were enumerated in plates containing 30 to 300

CFU. The photoinactivation fraction (= viability loss) and log reduction were determined as shown in equation (2.6) and equation (2.7), respectively:

$$\text{viability loss (\%)} = \left(\frac{M_i \text{-} M_f}{M_i}\right) \times 100 \tag{2.6}$$

$$\text{Log reduction} = \log M_i - \log M_f \tag{2.7}$$

where M_i and M_f are the initial and final *E. coli* viable counts, respectively.

d) Controls

Control assays in the dark, under UV radiation and under visible light in the absence of photocatalyst were performed to assess the influence of the experimental conditions and of the irradiation on cell inactivation, respectively. All the assays were performed in triplicate, inside a clean chamber.

2.3 Results and discussion

2.3.1 Photocatalysts characterization

The band gaps of the three photocatalysts used in this work – P25, VLP7101 and P25/graphene - were calculated from the diffuse reflectance spectra (Figure 2.1). The band gap obtained for the composite photocatalyst was 2.95 eV, whilst the values obtained for commercial P25 were 3.03 eV and 3.16 eV, corresponding to the two different crystalline forms of titanium dioxide – respectively rutile and anatase, and for VLP7101 was 2.75 eV. The slight decrease in the band gap between P25/graphene and P25 may be attributed to some doping of TiO_2 by the carbon molecules of graphene [11]. The specific mechanism of carbon doping is not yet fully understood. However, several authors reported that carbon doping leads to a band gap narrowing, causing a red-shift in the absorption spectrum of the photocatalyst [8]. Carbon dopant can be a substitutional anion (substitutes oxygen) or an interstitial cation (substitutes titanium). The substitutional anion behavior of carbon is related to its -4 oxidation state in the Ti–C bond in carbides, and the interstitial cation behavior is related to its +4 state in the C–O bond in carbonates [8]; decreases in the TiO_2 band gap originated by carbon doping can range from 0.1 eV to 1.05 eV [8]. However, there is a threshold for dopant concentration at around 2% of the photocatalyst mass; high dopant concentration leads to a dopant segregation phase [23]. Furthermore, the enhanced photocatalytic activity of VLP7101 can also be ascribed to the presence of an organic sensitizer, as it was already reported [24].
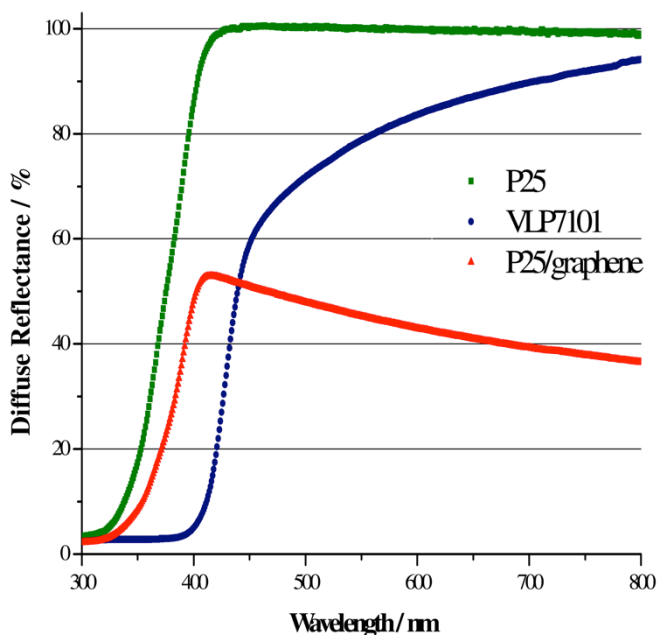
Figure 2.1. Diffuse reflectance spectra of VLP7101, P25 and P25/graphene photocatalysts.

XRD analyses were performed to assess the crystallinity of the photocatalysts – Figure 2.2. XRD allows determining the crystalline structure of the photocatalysts and, in some cases, to determine the crystal size.
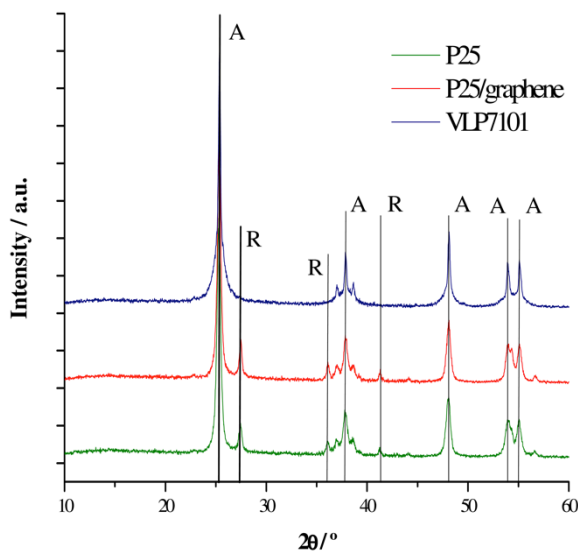

Figure 2.2. XRD patterns of VLP7101, P25 and P25/graphene photocatalysts.

The composite photocatalyst showed similar XRD pattern when compared to P25. Furthermore, no diffraction peaks for carbon species were observed in the composite, which might be due to its low amount and relatively low diffraction intensity of graphene. Furthermore, the similarity of patterns between P25 and the P25/graphene composite evidences that crystallinity, crystal size and modifications on the crystal structure of TiO_2 are not responsible for differences between the photocatalytic activity of these two photocatalysts. It is also possible to observe that VLP7101 is only anatase, contrarily to P25 that is composed by anatase and rutile. Even though it is believed that the interaction between anatase and rutile phases (80/20 wt.%) improve the photoactivity of P25 [25], VLP7101 present normally higher photoactivity than P25 [18]; this higher catalytic activity was ascribed to an aromatic carbon compound photo sensitizer, as reported elsewhere [24].

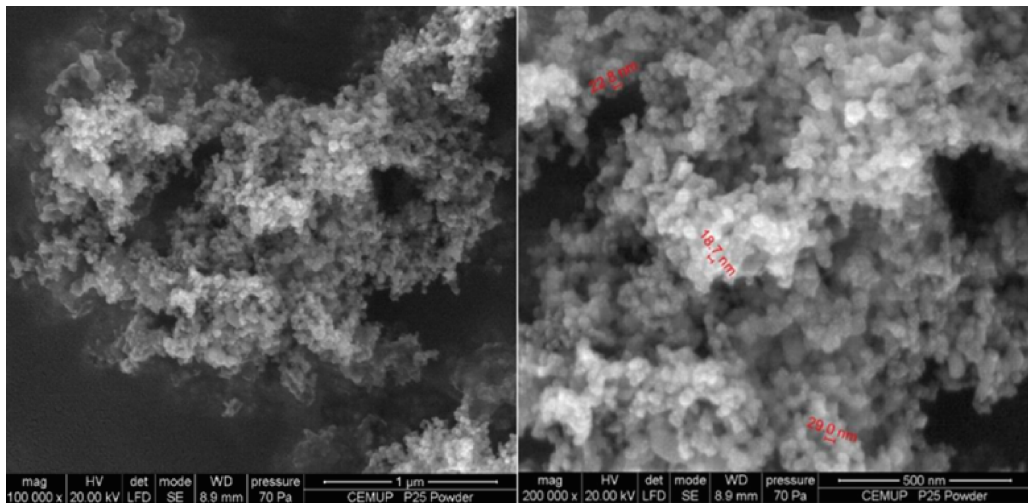SEM images of P25 and V LP7101 are presented in Figure 2.3 and 2.4.

Figure 2.3. SEM images of P25.

Figure 2.3 shows the morphology of P25 sample. The high agglomeration observed is caused by the high surface energy of the nanoparticles [26]. As it can be seen, the primary particles present sizes in nanometer range. These particles agglomerate forming aggregates with different shapes and morphologies, which influence the surface roughness, haze and transparency of the bulk material [26]. The approximate size of the P25 nanoparticles is between 15 to 30 nm, which is in accordance with values presented in literature [27].
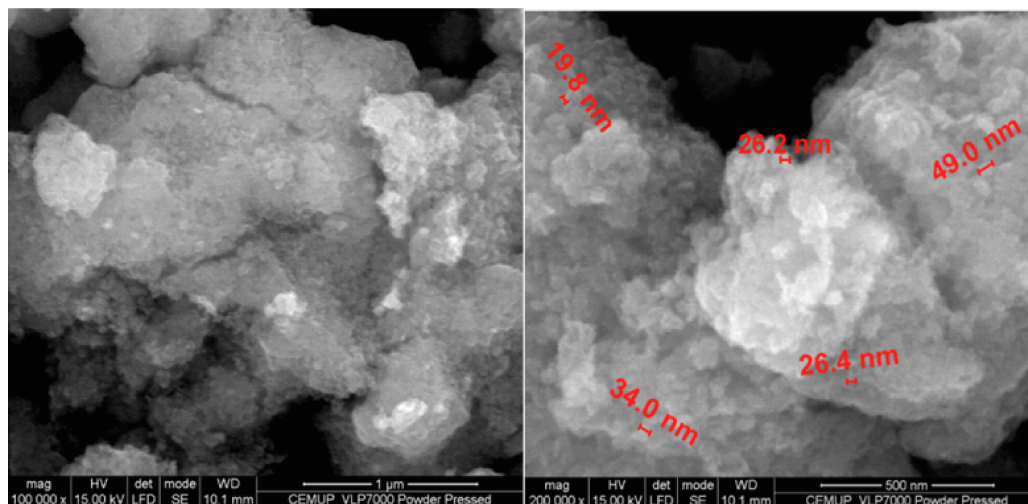
Figure 2.4. SEM images of VLP7101.

Figure 2.4 shows two SEM images of VLP7101 photocatalyst. The particles have a size of 15 to 50 nm and form also large agglomerates. P25/graphene composite, as already shown previously [11], is composed by P25 nanoparticles deposited on the graphene sheets. These particles bond preferably to the wrinkles and edges of the graphene nanoplatelets, initially covered with carboxylic acid groups. These carboxylic acid groups interact with the hydroxyl groups forming chemical P25/graphene bonds [11].

2.3.2 Photoactivity characterization

The photoactivity of the composite photocatalyst, P25 and VLP7101 was assessed based on the methylene blue degradation history and NO photo-conversion. Regarding the methylene blue degradation under UV radiation it is possible to observe in Figure 2.5 an increase in the activity of the composite photocatalyst when compared with commercial P25. Comparing the synthesized photocatalyst with VLP7101, both showed similar activities.
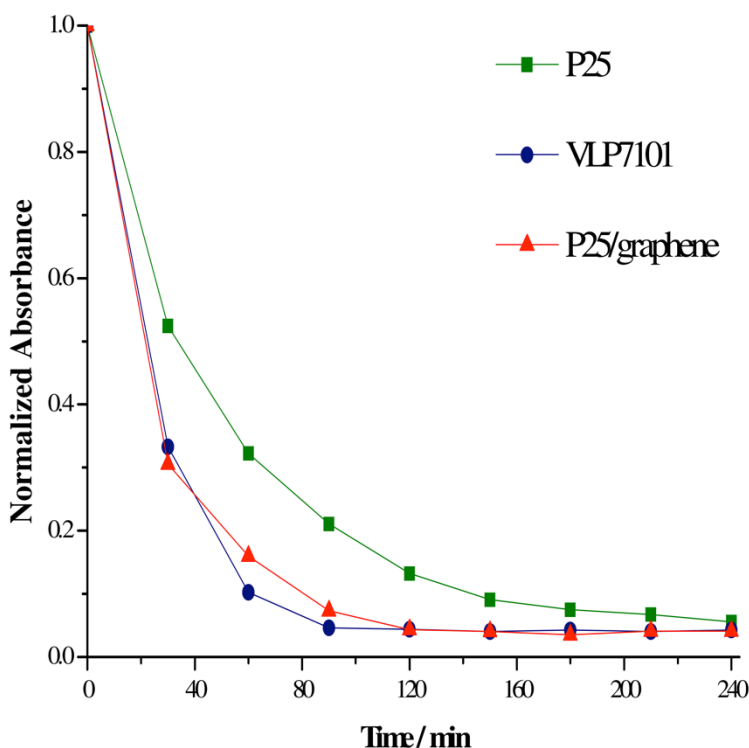
Figure 2.5. Normalized absorbance values of methylene blue degradation during 240 minutes (lines were added to improve the readability) for P25 and VLP70101 commercial photocatalysts and P25/graphene photocatalyst.

The increased photocatalytic activity of the P25/graphene composite to the methylene blue degradation compared to pristine P25 should be ascribed to the decrease of e^-/h^+ recombination, which is related to the ability of graphene to accept photogenerated electrons by P25 [11], and to an increased adsorption of methylene blue in the support graphene sheets. Actually, graphene support has a much higher adsorption capacity compared with P25 particles. For the relevant methylene blue concentrations, the equilibrium adsorbed concentration on P25 was 4 orders of magnitude smaller than on the graphene used, while on P25/graphene composite was 2 orders of magnitude smaller. This points out for the critical role of the graphene support in the P25/graphene photocatalyst concerning the methylene blue adsorption.

Nguyen-Phan *et al.* [28] reported the preparation of TiO_2/graphene composites with enhanced adsorption and photocatalytic activity under both UV and visible radiation. These authors state that the increase in graphene content, from 1 to 10 wt.%,

facilitates the photodegradation rate of methylene blue. The greater photocatalytic performance of TiO_2/graphene composite was attributed to the formation of both π–π conjugations between dye molecules and aromatic rings and to ionic interactions between methylene blue and oxygen-containing functional groups at the edges or on the surfaces of carbon-based nanosheets. Graphene oxide works as adsorbent for the methylene blue, electron acceptor and photosensitizer originating an enhanced dye photodecomposition.

Methylene blue degradation is a technique widely used to assess the photocatalytic activity due to its simplicity and easy use. However, this relevant standard [29] presents limitations. This standard assumes the use of methylene blue with very high purity, which is not always possible to obtain. The pH of the solution should be defined as it influences the adsorption of methylene blue on titanium dioxide. Finally, the standard is mainly applicable to low active photocatalytic films due to problems of stirring and diffusion, among others [30]. Standard ISO 22197-1:2007 [17] uses NO photooxidation to infer about the photoactivity. Since NO is gas, the mass transfer limitations associated to the methylene blue method do not hold here. Because that, this standard is now recommended though its higher complexity. Figure 2.6 shows NO conversion history catalyzed by P25, VLP7101 and P25/graphene, under UV light.
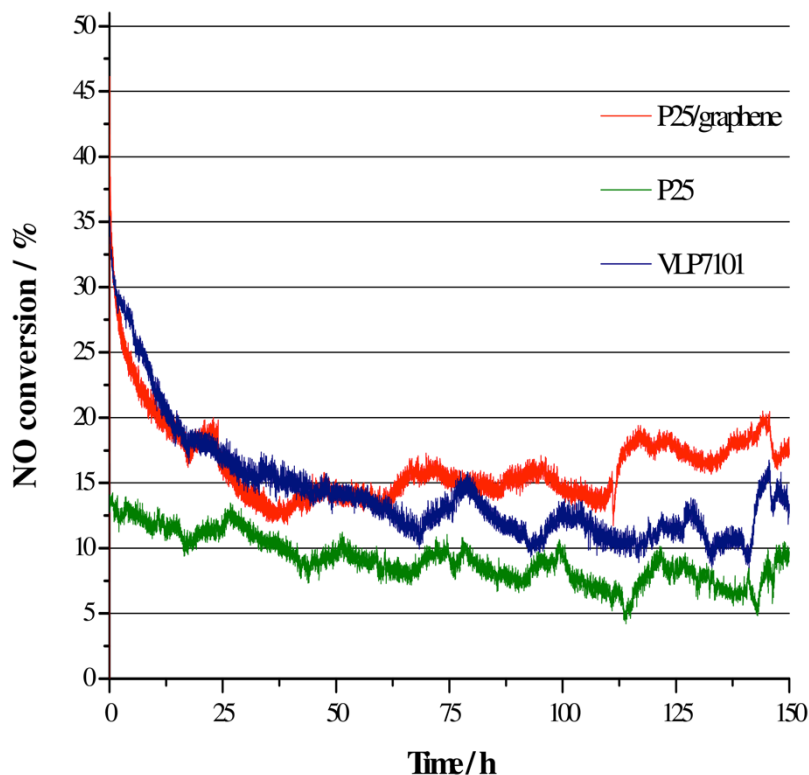
Figure 2.6. NO conversion for P25 and P25/graphene composite during 150 hours under UV radiation.

The prepared photocatalyst presented higher initial and steady state NO conversion than P25 and VLP7101. Furthermore, after the first 24 hours, the prepared photocatalyst showed good stability throughout the 150 hours. This increased conversion can be ascribed to several factors that were already discussed before. P25/graphene composite slows e^-/h^+ recombination rate since graphene support increases the draining rate of electrons. Then, the extended light absorption of P25/graphene, supported by a smaller band gap (2.95 eV), allows the absorption of a broader range of wavelengths.

Finally, aiming for a possible future commercial application of the composite photocatalyst, photoinactivation trials were conducted. The initial value of cellular density used was chosen to be around 1×10^6 CFU·mL^{-1}, based on standard ISO 27447:2009 used for evaluating the antibacterial activity of semiconducting photocatalytic materials [19]. Moreover, the order of magnitude 10^6 is also referred to

in the standard ISO 11137-2:2013, applied to assess the efficiency of a given method on the sterilization of health care products [31].
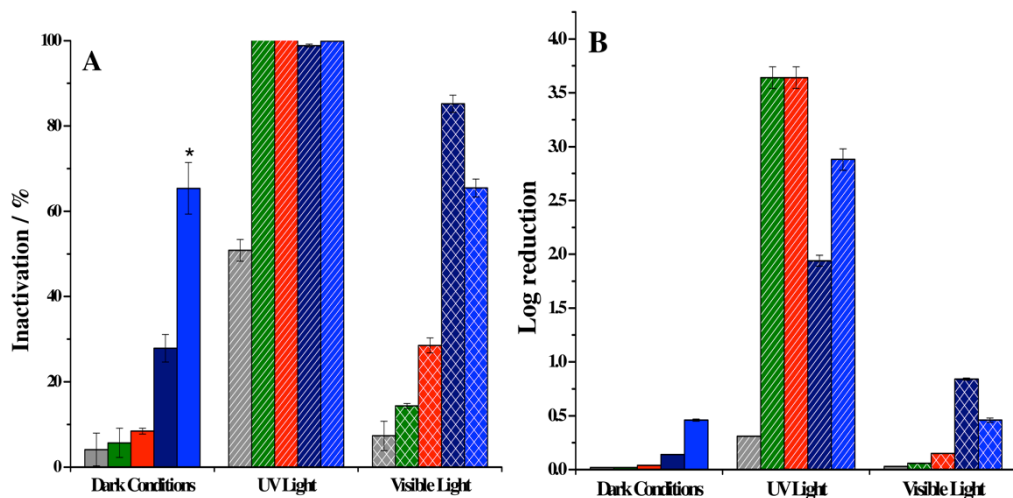

Figure 2.7. *E. coli* viability loss (A) and log reduction (B) under dark, UV radiation and visible light for P25 (■), P25/graphene (■), VLP7101 (■), VLP7000 (■) and without photocatalyst (■). Results are mean values (n = 3) and the error bars represent the standard deviation. Initial Cellular Density - 10^6 CFU·mL^{-1}. *This value ranged from 5.27% to 65.37% in trials conducted over a year.

Under dark conditions the cell inactivation values in the presence of P25 and P25/graphene composite were, as expected, low (around 6% and 8%, respectively) and similar to those obtained in the absence of photocatalyst (around 5%), showing that these photocatalysts do not inhibit *E. coli* in the absence of irradiation – Figure 2.7. Contrarily to what was expected, under the same conditions, the cell inactivation values for the carbon-modified VLP7000 and VLP7101 ranged from ~5 to 65% for assays carried out over one year. These results show that VLP7000 and VLP7101 present some toxicity towards *E. coli* cells in the absence of irradiation. Additionally, these values also point out that these photocatalysts did not present stability, as it was already reported in previous studies [24, 32]. Due to the mutagenic effect of UV irradiation, cell inactivation under UV was approximately 51% – Figure 2.7.

Higher cell viability losses were obtained in the UV-photoinactivation trials. Under these conditions, similar cell inactivation values (99.98%), corresponding to log reduction values of around 3.6, were obtained for P25 and P25/graphene composite.

Comparatively lower cell inactivation values were observed when VLP7000 and VLP7101 were irradiated with UV (99.87% and 98.85%, respectively), corresponding to log reduction values of 2.8 and 1.9, respectively.

Under visible light, the prepared P25/graphene composite produced two times higher viability loss values (~29%), when compared with the commercial P25 (~14%). Under the same conditions, cell inactivation with VLP7000 and VLP 7101 was much higher (~65% and 85%, respectively) than the ones obtained for the produced P25/graphene (~29%). However, as mentioned above, these commercial photocatalysts did not present stability, promoting cell inhibition even under dark conditions.

The influence of the initial cellular density on the photoinactivation was also studied. Additional trials carried out with P25 and the P25/graphene were conducted with an initial cellular density of 10^3 CFU·mL^{-1}. As expected, with this lower initial cellular density, the values of photoinactivation obtained were higher than those obtained with an initial cellular density of 10^6 CFU·mL^{-1} – Figure 2.8. Total inactivation (log reduction value of 3) was verified when both catalysts were irradiated with UV. Under visible light, viability loss values reached around 15% for P25 and 33% for the P25/graphene composite. Although the log reduction values were still low (0.07 and 0.18 for P25 and P25/graphene composite, respectively), the increase in the photoinactivation efficiency of the prepared composite can be ascribed to its slower rate of e$^-$/h$^+$ recombination and extended light absorption range, as suggested by its lower band gap value when compared with that of P25.
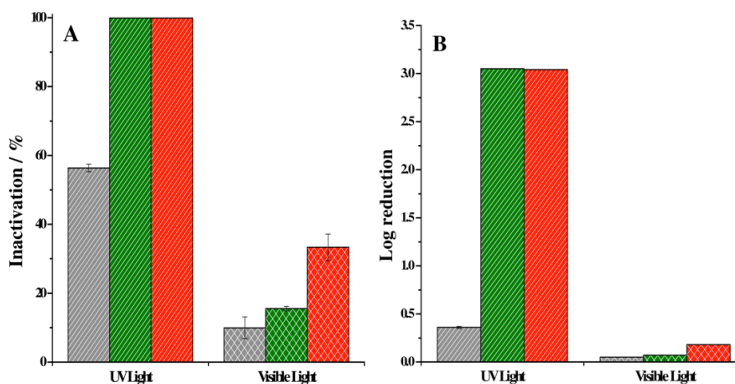

Figure 2.8. *E. coli* viability loss (A) and log reduction (B) under UV radiation and visible light for P25 (■), P25/graphene (■) and without the use of a photocatalyst (■). Results are mean values (n = 3) and the error bars represent the standard deviation. Initial cellular density - 10^3 CFU·mL^{-1}.

2.4 Conclusions

The prepared TiO$_2$/graphene photocatalyst presented better results for methylene blue and NO oxidation under UV radiation when compared with P25. Additionally, regarding photoinactivation of *E. coli* DSM 1103, the new photocatalyst exhibited higher inactivation activity under visible light than the commercial P25. When compared with VPL7101, the prepared photocatalyst showed similar photoactivity for methylene blue degradation and higher photoactivity regarding the NO oxidation. Both VLP7101 and VLP7000 achieved higher values of *E. coli* DSM 1103 inactivation than the prepared TiO$_2$/graphene. However, it was observed that VLP7101 and VLP7000 showed high values of inactivation under dark conditions, suggesting toxic properties of these materials.

Further developments in photoinactivation under visible light using TiO$_2$/graphene composites are expected not only from the improvement of this material but also from the use of suitable co-catalysts.

Acknowledgements

Bibliography

[1] J. Colls, Air Pollution, Spon Press 2002.

[2] H.A. Foster, I.B. Ditta, S. Varghese, A. Steele, Photocatalytic disinfection using titanium dioxide: spectrum and mechanism of antimicrobial activity, Appl. Microbiol. Biotechnol., 90 (2011) 1847-1868.

[3] T. Matsunaga, R. Tomoda, T. Nakajima, H. Wake, Photoelectrochemical sterilization of microbial cells by semiconductor powders, FEMS Microbiol. Lett., 29 (1985) 211-214.

[4] A. Fujishima, K. Honda, Electrochemical Photolysis of Water at a Semiconductor Electrode, Nature, 238 (1972) 37-38.

[5] A. Fujishima, T.N. Rao, D.A. Tryk, Titanium dioxide photocatalysis, J. Photoch. Photobio. C, 1 (2000) 1-21.

[6] S. Banerjee, S.C. Pillai, P. Falaras, K.E. O'Shea, J.A. Byrne, D.D. Dionysiou, New Insights into the Mechanism of Visible Light Photocatalysis, J. Phys. Chem. Lett., 5 (2014) 2543-2554.

[7] P. Magalhães, V.M. Sousa, O.C. Nunes, A. Mendes, Titanium dioxide photocatalysis: fundamentals and application on photoinactivation, Submitted to Chemical Engineering Journal, (2014).

[8] R. Leary, A. Westwood, Carbonaceous nanomaterials for the enhancement of TiO_2 photocatalysis, Carbon, 49 (2011) 741-772.

[9] B. Viswanathan, K.R. Krishanmurthy, Nitrogen Incorporation in TiO_2: Does It Make a Visible Light Photo-Active Material?, Int. J. Photoenergy, 2012 (2012) 10.

[10] Q. Xiang, J. Yu, M. Jaroniec, Graphene-based semiconductor photocatalysts, Chem. Soc. Rev., 41 (2012) 782-796.

[11] H. Zhang, X. Lv, Y. Li, Y. Wang, J. Li, P25-graphene composite as a high performance photocatalyst, ACS Nano, 4 (2010) 380-386.

[12] G. Williams, B. Seger, P.V. Kamat, TiO_2-Graphene Nanocomposites. UV-Assisted Photocatalytic Reduction of Graphene Oxide, ACS Nano, 2 (2008) 1487-1491.

[13] N.T. Khoa, M.W. Pyun, D.H. Yoo, S.W. Kim, J.Y. Leem, E.J. Kim, S.H. Hahn, Photodecomposition effects of graphene oxide coated on TiO$_2$ thin film prepared by electron-beam evaporation method, Thin Solid Films, 520 (2012) 5417-5420.

[14] K. Zhou, Y. Zhu, X. Yang, X. Jiang, C. Li, Preparation of graphene-TiO$_2$ composites with enhanced photocatalytic activity, New J. Chem., 35 (2011) 353-359.

[15] O. Akhavan, E. Ghaderi, Photocatalytic Reduction of Graphene Oxide Nanosheets on TiO$_2$ Thin Film for Photoinactivation of Bacteria in Solar Light Irradiation, J. Phys. Chem. C, 113 (2009) 20214-20220.

[16] A.B. Murphy, Band-gap determination from diffuse reflectance measurements of semiconductor films, and application to photoelectrochemical water-splitting, Sol. Energy Mater. Sol. Cells, 91 (2007) 1326-1337.

[17] ISO 22197-1:2007 Fine ceramics (advanced ceramics, advanced technical ceramics) -- Test method for air-purification performance of semiconducting photocatalytic materials -- Part 1: Removal of nitric oxide, ISO, 2007.

[18] C. Águia, J. Ângelo, L.M. Madeira, A. Mendes, Photo-oxidation of NO using an exterior paint – Screening of various commercial titania in powder pressed and paint films, J Environ. Manage., 92 (2011) 1724-1732.

[19] ISO 27447:2009 Fine ceramics (advanced ceramics, advanced technical ceramics) -- Test method for antibacterial activity of semiconducting photocatalytic materials, ISO, 2009.

[20] V.M. Sousa, C.M. Manaia, A. Mendes, O.C. Nunes, Photoinactivation of various antibiotic resistant strains of *Escherichia coli* using a paint coat, J. Photoch. Photobio. A, 251 (2013) 148-153.

[21] Z. Huang, P.-C. Maness, D.M. Blake, E.J. Wolfrum, S.L. Smolinski, W.A. Jacoby, Bactericidal mode of titanium dioxide photocatalysis, J. Photoch. Photobio. A, 130 (2000) 163-170.

[22] A.L. Koch, Growth Measurement, in: R.G.E.M. P. Gerhardt, W.A. Wood, N.R. Krieg (Ed.) Methods for General and Molecular Bacteriology, ASM Press, Washington DC, 1994, pp. 248-292.

[23] R. Van De Krol, M. Grätzel, Photoelectrochemical Hydrogen Production, Springer 2011, pp. 13-67.

[24] P. Zabek, J. Eberl, H. Kisch, On the origin of visible light activity in carbon-modified titania, Photoch. Photobio. Sci., 8 (2009) 264-269.

[25] M. Pelaez, N.T. Nolan, S.C. Pillai, M.K. Seery, P. Falaras, A.G. Kontos, P.S.M. Dunlop, J.W.J. Hamilton, J.A. Byrne, K. O'Shea, M.H. Entezari, D.D. Dionysiou, A review on the visible light active titanium dioxide photocatalysts for environmental applications, Appl. Catal. B-Environ., 125 (2012) 331-349.

[26] N. Mandzy, E. Grulke, T. Druffel, Breakage of TiO_2 agglomerates in electrostatically stabilized aqueous dispersions, Powder Technol., 160 (2005) 121-126.

[27] B. Ohtani, O.O. Prieto-Mahaney, D. Li, R. Abe, What is Degussa (Evonik) P25? Crystalline composition analysis, reconstruction from isolated pure particles and photocatalytic activity test, J. Photoch. Photobio. A, 216 (2010) 179-182.

[28] T.-D. Nguyen-Phan, V.H. Pham, E.W. Shin, H.-D. Pham, S. Kim, J.S. Chung, E.J. Kim, S.H. Hur, The role of graphene oxide content on the adsorption-enhanced photocatalysis of titanium dioxide/graphene oxide composites, Chem. Eng. J., 170 (2011) 226-232.

[29] ISO 10678: 2010 Fine ceramics, advanced technical ceramics) – Determination of photocatalytic activity of surfaces in an aqueous medium by degradation of methylene blue, ISO, Geneva, 2010.

[30] A. Mills, C. Hill, P.K.J. Robertson, Overview of the current ISO tests for photocatalytic materials, J. Photoche. Photobio. A, 237 (2012) 7-23.

[31] ISO 11137-2:2013 Sterilization of health care products — Radiation, ISO, Geneva, 2010.

[32] R. Quesada-Cabrera, A. Mills, C. O'Rourke, Action spectra of P25 TiO_2 and a visible light absorbing, carbon-modified titania in the photocatalytic degradation of stearic acid, Appl. Catal. B-Environ., 150–151 (2014) 338-344.

Chapter 3.

Synthesis of a novel TiO$_2$/graphene composite under supercritical conditions

Abstract

A novel method for producing TiO$_2$/graphene composites under supercritical conditions is described. This method allows the use of nontoxic reactants to prepare a high quality TiO$_2$/graphene photocatalyst and uses an easily scalable reactor. The produced composite presented a lower band gap -3.0 eV when compared with the TiO$_2$ produced under supercritical conditions -3.2 eV. The morphology of the composite was thoroughly characterized. When compared with pristine TiO$_2$ produced under the same conditions, the composite showed enhanced methylene blue degradation.

Keywords

Photocatalysis, Supercritical conditions, Methylene Blue, TiO$_2$/graphene

3.1. Introduction

Several methods have already been described for the synthesis of TiO_2, from sol–gel methods [1], gas-phase synthesis [2], solvothermal synthesis [3], and hydrothermal techniques [4]. However, these methods are in most cases time-consuming and have in some cases high manufacturing cost, and thereby are not attractive for commercial TiO_2 nanoparticle production. Synthesis in supercritical or near-critical conditions is an efficient method for producing highly crystalline nanoparticles with a controllable size and a narrow size distribution [5]. Supercritical fluids have gas-like transport properties in diffusivity, viscosity and surface tension, while maintaining liquid-like properties such as high-solvation capability and density, and this makes them attractive solvents in chemical processes. Continuous supercritical flow synthesis has been developed for the production of different metal oxides and metal nanoparticles. Moreover, the manufacturing costs of continuous flow synthesis are relatively low and the production can easily be scaled up due to the quick synthesis. It is also important to note their ability to provide rapid heating and short reaction times, suitable for a wide range of nanoparticles. Regarding the application of such nanoparticles for environmental purposes, the fact that the reactants used are in most cases non toxic, presents an advantage to the more traditional methods of production that use toxic and hazardous reactants. A metal precursor is rapidly heated by mixing with a superheated solvent stream to induce rapid nucleation and then led into a reactor for growth and/or further crystallization of the NPs [5, 6]. The synthesis of TiO_2 supercritical or near-critical conditions also leads to the formation of highly crystalline TiO_2 [6], which is a fundamental requirement for a photocatalyst with high activity [7]. However, TiO_2 absorbs only UV light, preventing its usage under visible spectrum; hence, many efforts have been powered to enhance titanium dioxide photocatalytic activity. Two main research paths are being followed: i) narrowing the semiconductor band gap (Eg); and ii) decrease the e^-/h^+ recombination. The use of carbon-based supports such as carbon nanotubes (CNTs), fullerene or graphene make the e^-/h^+ recombination rate to decrease [8]. These materials have the ability to receive and store photoinjected electrons and thus slowing e^-/h^+ recombination. The binding of TiO_2 to graphene sheets allows improved photocatalytic performance when compared with their pristine form mainly because: i) efficient charge separation and transportation; ii)

extended light absorption range; and iii) enhanced adsorption of the reactants [9]. TiO_2/graphene composites slow the rate of e^-/h^+ recombination after light excitation [10], increasing the charge transfer rate of electrons. The extended light absorption is achieved due to doping of TiO_2 with carbon from the graphene, leading to a narrowing of the semiconductor band gap [9]. The enhanced adsorption of the TiO_2/graphene composite is mainly attributed to its very large π-conjugation system and two-dimensional planar structure [9, 11]. Even though the production of TiO_2 under supercritical conditions is well described in literature, the manipulation of graphene and graphene nanoplatelets under supercritical conditions has not yet attracted much attention. However, it is now known that graphene and graphene oxide nanoplatelets should not suffer oxidation during the hydrothermal treatment or at the most extreme cases show minimal erosion after the passage on the supercritical reactor [12].

The aim of this work was to produce a TiO_2/graphene composite under supercritical conditions. The produced composite was characterized regarding its crystalline structure – X-ray diffraction – SEM and TEM imaging, band gap value – diffuse reflectance and for the presence of Ti-O-C bonds – FTIR spectra. The photocatalytic activity of the prepared TiO_2/graphene composite was also assessed based on methylene blue photodegradation and compared with pristine TiO_2 synthesized also under supercritical conditions.

3.2 Materials and Methods

3.2.1 Experimental Setup

A diagram of the dual-stage supercritical flow reactor used is shown in Figure 3.1. A modular design was adopted using straight tube sections with no reducing unions in the heated sections of the system for facilitating the cleaning of these tubes. In the "cold" sections, smaller tube diameters were employed. The preheaters of the setup operate at 300 °C while the main heaters operate at 450 °C; the maximum operation pressure was set to 400 bar.
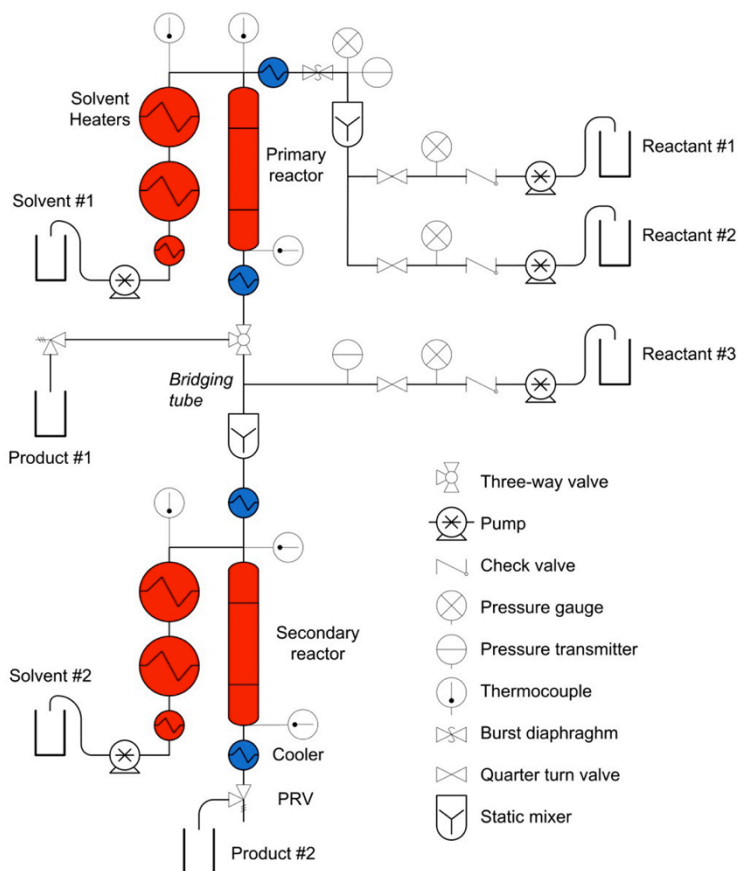

Figure 3.1. Schematic of the supercritical reactor used (from [5] with permission).

Two different types of pumps were used in the system. For the pure solvents, double-acting HPLC-pumps (LabAlliance Prep 36) were chosen due to their constant flow, each up to 36 mL/min; precursors are introduced directly by particle-tolerant

Milton Roy, Milroyal D pumps (stroke volume ≤ 0.71 mL). These are suited for handling corrosive chemicals and suspensions and are robust since few moving parts are in contact with the medium. Pure solvents need to be degassed (ultrasonication, vacuum) to be fed to the HPLC pumps;

The preheaters were constructed of 1/8″ Hastelloy C-276 tubes whereas the supercritical reactors were made of a 3/8″ Inconel-625 tube; downstream the reactors, standard SS316 tubing was chosen. The modular design enables direct exchange of reactor tubes and makes their cleaning easier.

The described reactor can be used in both dual-stage or single-stage mode as previously reported by Hellstern and co-workers [5]. However, for the work conducted, only the single-stage mode was used. The reactor zone is made of a 1.1 m long SS316 tube heated using two separated heating modules (each 45 cm long). Feed flow rates are read based on the weight derivative obtained using balances. The suspensions can cause clogging on some areas of the reactor, which leads to an increase in the total pressure of the system. To minimize this problem a pressure release valve was used, which opens more for higher flow rates decreasing particle sedimentation. A LabView-based program hosted in a computer controls the whole setup.

3.2.2. Characterization

3.2.2.1 Diffuse reflectance analyses

The diffuse reflectance spectrum was used to obtain the band gap of the photocatalysts. Tauc equation relates the diffuse reflectance and the Kubelka–Munk model to the excitation frequency [13]:

$$(h\nu F(R_\infty))^{1/n} = A(h\nu - E_g) \tag{3.1}$$

where, h is the Planck constant, ν is the frequency of vibration, A is a constant and E_g is the band gap energy. This equation is obtained multiplying the Kubelka–Munk equation by the energy of the incident radiation ($E = h\nu$) powered to a coefficient n, according to the type of the electronic transition of the material. For indirect transitions n equals 2 and for direct transition n is 1/2. Plotting the modified Kubelka–Munk equation as a function of the incident radiation, the band gap of the semiconductor can be obtained extrapolating the linear part of this curve to the x-axis, the so-called Tauc plot; the band gap energy is read at the intersection. Diffuse reflectance of the different samples were obtained in a Shimatzu UV-3600 UV-VIS-NIR spectrophotometer,

equipped with a 150 mm integrating sphere and using $BaSO_4$ as 100 % reflectance standard. The samples were pressed to form a flat disc that fit into the spectrophotometer sample holder.

3.2.2.2 SEM and XRD analyses

The morphology and composition of the photocatalysts was obtained from scanning electron microscopy (SEM) coupled with energy dispersive X-ray (EDX) analysis. A FEI Quanta 400FEG ESEM/EDAX Genesis X4M apparatus equipped with a Schottky field emission gun (for optimal spatial resolution) was used for the characterization of the surface morphology of the photocatalysts with SEM. Images were digitally recorded using a Gatan SC 1000 ORIUS CCD camera (Warrendale, PA, USA).

The crystallographic characterization of the samples was performed by X-ray diffraction (XRD). The XRD pattern of the selected samples was obtained using a Benchtop X-Ray Diffractometer RIGAKU, model MiniFlex II using Cu X-ray tube (30 KV/15 mA). The data was obtained at 2θ angles (10–80°), with a step speed of 3.5°/min. Debye–Scherrer equation was used to determine the crystallite size. The obtained X-ray scans were compared to those of standard database and the phases were assigned comparing with data available in literature.

3.2.2.3 Methylene blue degradation trials

The photodegradation history of methylene blue (MB) dyes was followed by photospectroscopy. In a typical process, aqueous solution of MB dye (0.01 g/L, i.e. 2.7×10^{-5} M, 100 mL) and photocatalysts (50 mg) were placed in a 250 mL cylindrical glass vessel. Under ambient conditions and stirring, the photoreactor vessel was exposed to the UV irradiation produced by an ultraviolet (UV-A, highest emission at 365 nm) lamp with two 6 W black-light-blue bulbs (VL-206-BLB, Vilbert Lourmat, France); the lamp was positioned 10 cm away from the vessel (intensity at the catalyst mixture surface was measured with a UV radiometer (HD 2102.2, Delta/OHM, Italy) being 10 $W·m^{-2}$). The trial began by putting the mixture during 30 minutes in the dark; the mixture was then illuminated for 4 hours. Samples were collected every 30 minutes, centrifuged and the supernatant was analyzed in an UV-visible absorption spectrophotometer (Shimatzu UV-3600 UV-VIS-NIR spectrophotometer).

3.3 Results and Discussion

3.3.1 Photocatalyst preparation

Two different photocatalysts were prepared using the supercritical reactor previously described. The TiO_2/graphene sample was produced from titanium isopropoxide (TiO_2 precursor) on 2-isopropanol (0.5 M), both acquired from Sigma-Aldrich®, at a temperature of 400 ºC and under a pressure of around 250 bar. The graphene oxide was obtained partially oxidizing commercial graphene nanoplatelets (xGnP® from XG Sciences) following the modified Hummers method – described in Chapter 2. Then a suspension of the produced graphene oxide on 2-isopropanol is prepared, 400 mg/L. This suspension was then added to the titanium isopropoxide solution (0.5 M) for obtaining a dispersion graphene:Ti of 800 mg/mol, which assuming a 100 % yield should give TiO_2/graphene photocatalyst containing 1 wt.% of graphene. Additionally, TiO_2 was produced under the same operational conditions in order to be properly compared with the produced composite.

3.3.2 Samples Characterization

Figure 3.2 shows TEM images of the prepared TiO_2 particles. Very large agglomerates composed of small TiO_2 nanoparticles (ca. 10 nm) with a very uniform size distribution are observed.
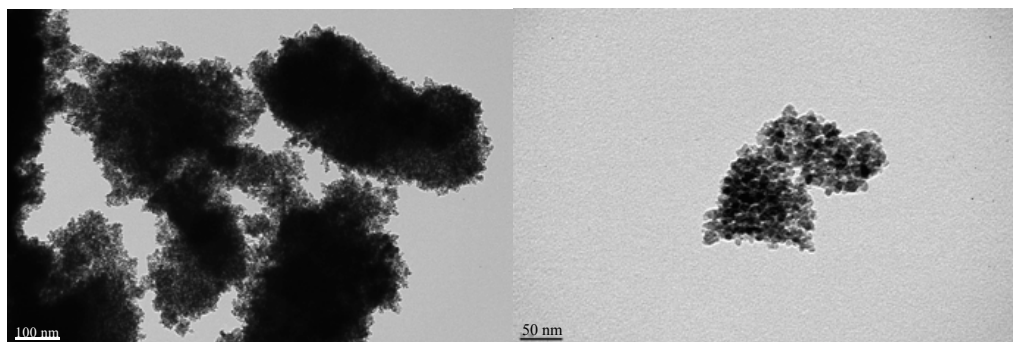

Figure 3.2. TEM images for the TiO_2 produced.

Figure 3.3 shows TEM images of the prepared TiO_2/graphene sample. These images show the TiO_2 nanoparticles on graphene sheets. However, the obtained images

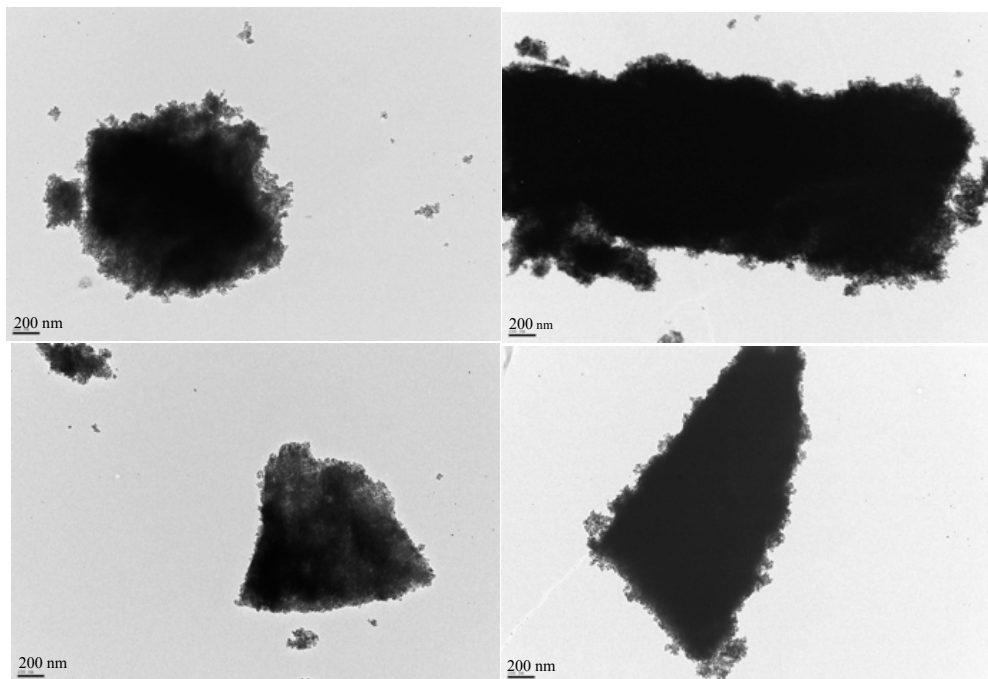do not allow to assess the formation of covalent Ti-O-C bonds between the TiO_2 nanoparticles and the graphene sheets.

Figure 3.3. TEM images for the TiO_2/graphene composite produced.

Figure 3.4 shows a SEM image of TiO_2/graphene particles where the graphene platelets can be seen. In this figure, additionally to the standard image, a backscatter diffraction image is shown. Backscatter electron images are very helpful for obtaining high-resolution elemental maps of a sample and for quickly distinguishing different atomic weights. In this image two different zones are highlighted – a dark grey area (Z1) that should be attributed to the graphene and white zones (Z2), which should be associated with the TiO_2 nanoparticles produced.
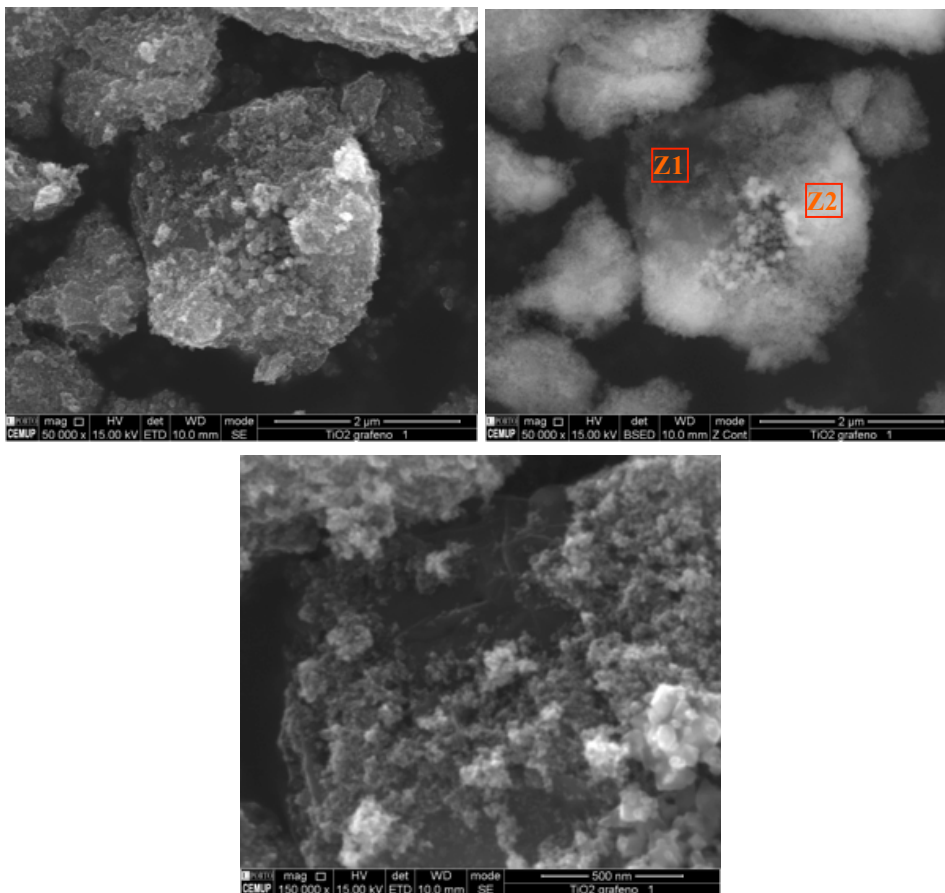
Figure 3.4. SEM images of TiO_2 deposited on a graphene sheet.

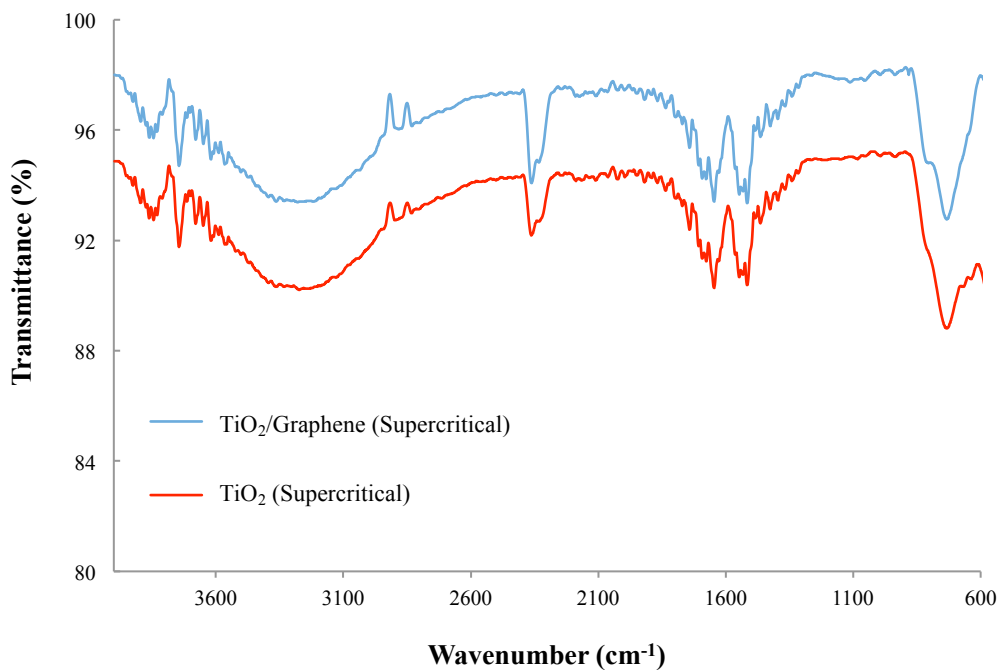The two samples produced – TiO_2 and TiO_2/graphene – were analysed by FTIR – Figure 3.5.

Figure 3.5. FTIR spectra of the analysed samples – transmittance values.

The IR spectra of TiO$_2$/graphene and TiO$_2$ produced under supercritical conditions samples are quite similar, showing the presence of bands at *ca.* 3200 cm^{-1}, 1600 cm^{-1} and 750 cm^{-1}. The very broad band centered at 3220 cm^{-1} can be attributed to the O-H stretching mode of water molecules, while the sharp/narrow band at 1640 cm^{-1} can be ascribed to the H-O-H bending mode of adsorbed water. The intense band noted *ca.* 745 cm^{-1} can be ascribed to the symmetric stretching vibrations of the Ti-O bonds of the TiO$_4$ tetrahedra [14].

Additionally, the second derivative of both spectra was obtained. The second derivative usually allows a better comparison between two or more FTIR spectra [15]. As it is possible to observe from Figure 3.6 there are slight differences between the two spectra at *ca.* 900 cm^{-1} range. Differences in FTIR spectra in this range of wavelengths were previously associated with the formation of the Ti-O-C bonds [9, 16].
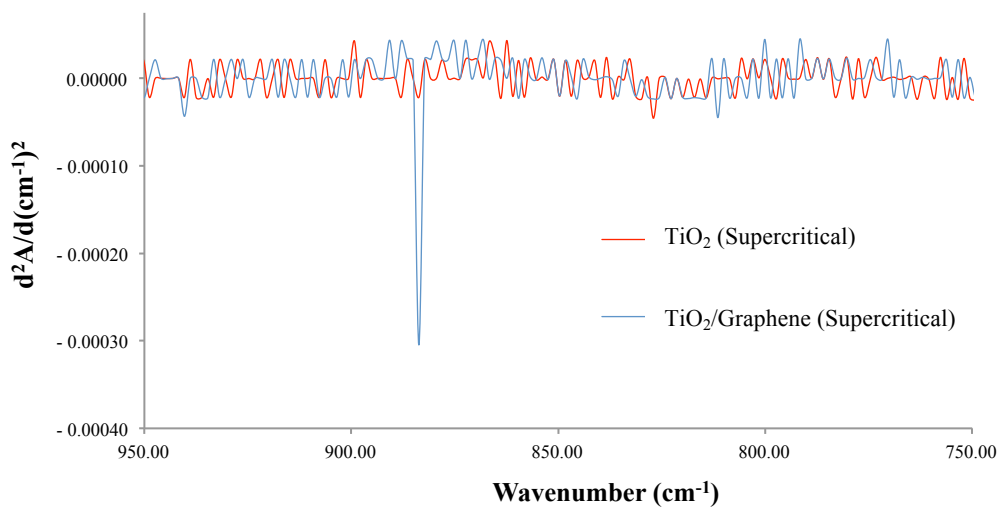
Figure 3.6. Second derivative of the obtained FTIR spectra for the selected wavenumber range.

XRD analyses were conducted for the prepared samples and compared with both the commercial P25 and with stored information for the characteristic peaks of TiO_2 crystalline phases, both anatase and rutile – Figure 3.7.
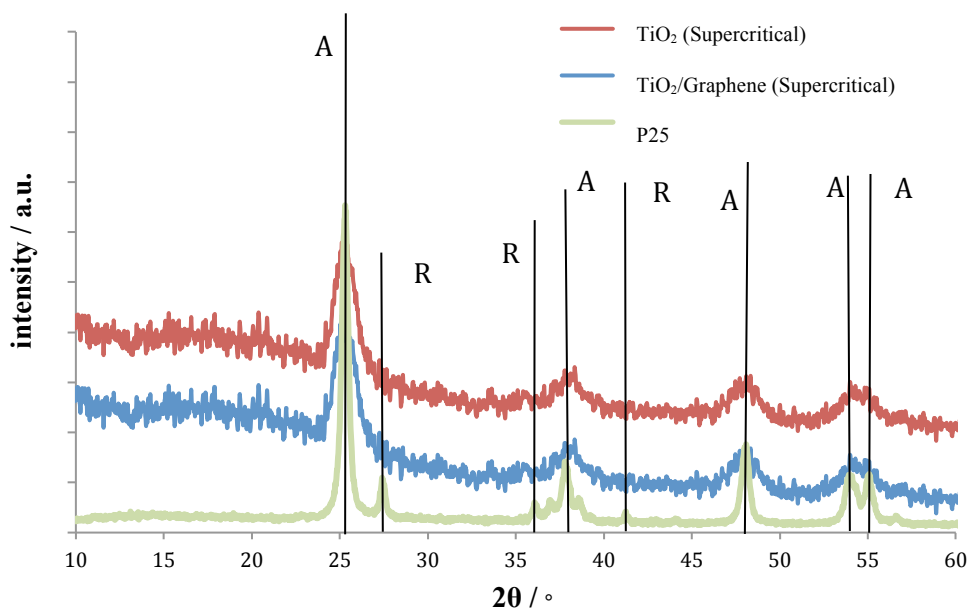

Figure 3.7. XRD spectra of the TiO_2/graphene and TiO_2 samples produced under supercritical conditions and for commercial P25.

Figure 3.7 indicates that there are no noticeable changes on the crystalline structure of titanium dioxide on the TiO_2/graphene sample compared with the corresponding TiO_2 sample. This similarity was expected due to the very low amount of graphene used to produce the TiO_2/graphene composite ($\approx$ 1 wt. %). Analyzing the XRD spectra it is also possible to observe differences between P25 and the produced TiO_2 and TiO_2/graphene under supercritical conditions. Firstly, it is possible to observed that in the case of P25 there are additional peaks that correspond to the presence of rutile. In the case of the produced photocatalysts only anatase peaks are present. Furthermore, it is known that P25 crystallite size is of *ca.* 20 nm. The value obtained for the produced photocatalysts was of *ca.* 7 nm. This difference is noticeable from the width of the peaks in the XRD spectra where the width of the peaks corresponding to the supercritical TiO_2 are wider.

The diffuse reflectance of the TiO_2/graphene and pristine TiO_2 samples was determined for obtaining their band gaps – Figure 3.8 and 3.9.
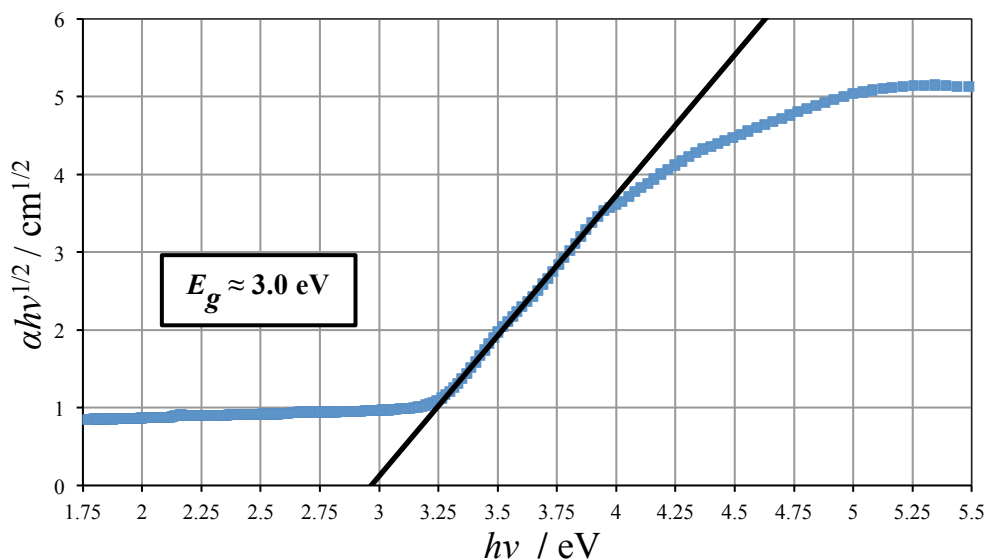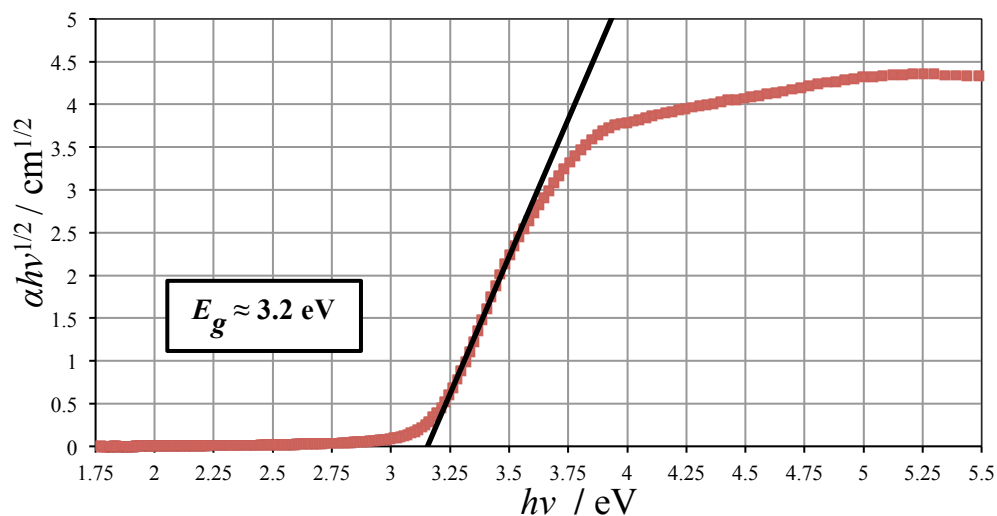

Figure 3.8. Tauc plot of the TiO_2/graphene sample.

Figure 3.9. Band gap calculation for the produced TiO_2.

The value of band gap was estimated to be around 3.0 eV for the TiO_2/graphene composite and of 3.2 eV for the pristine TiO_2. These values show a decrease in the band gap of the TiO_2/graphene sample when compared with TiO_2. The decrease observed for the band gap value can be attributed to the possible formation of Ti-O-C bonds on the TiO_2/graphene sample.

The photocatalytic performance of the both samples was evaluated based on the methylene blue degradation. The results obtained are presented in Figure 3.10.
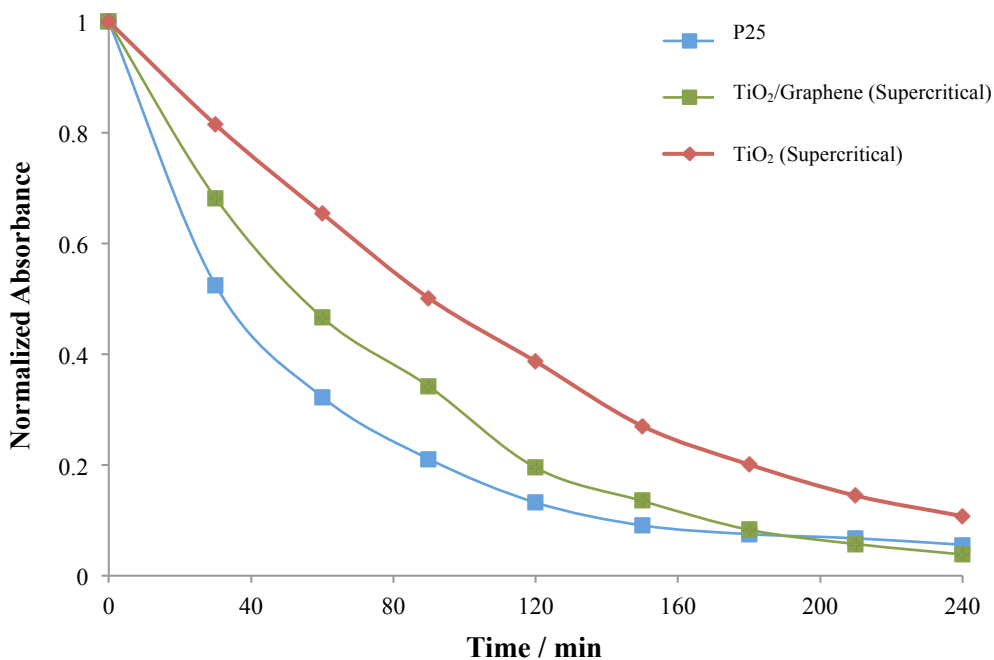
Figure 3.10. Normalized absorbance values for the methylene blue degradation trials conducted with the different photocatalysts. Lines were added to improve readability.

The conducted trials show that commercial P25 presents enhanced methylene blue photodegradation when compared with both the produced composite and the produced TiO_2. Anatase is considered to be the titanium dioxide crystalline phase with higher photocatalytic activity. However, in this case, P25, which is made of anatase and rutile, showed enhanced photocatalytic activity for the methylene blue photodegradation.

Comparing both photocatalysts produced under supercritical conditions, it is possible to observed that the produced TiO_2/graphene sample showed enhanced methylene blue degradation when compared with the pristine TiO_2 sample. As there were not observed any type of difference between the crystalline structures of the TiO_2 and TiO_2/graphene samples, this enhancement should be attributed to the presence of the graphene sheets.

3.4. Conclusions

TiO$_2$/graphene photocatalyst sample was prepared in a supercritical reactor. The SEM and TEM images obtained show the presence of the produced TiO$_2$ nanoparticles on graphene sheets. The XRD analyses performed showed that there is no noticeable differences between the XRD pattern of the produced TiO$_2$ nanoparticles and the TiO$_2$/graphene composite, which indicates an unchanged crystalline structure. The obtained FTIR spectra of both TiO$_2$ and TiO$_2$/graphene are very similar. However, it is not possible to eliminate the possibility of formation of Ti-O-C bonds between TiO$_2$ and the graphene sheets. The band-gap of the produced TiO$_2$ (3.2 eV) and of the produced TiO$_2$/graphene composite (3.0 eV) samples were obtained from the Tauc plots. Finally, the TiO$_2$/graphene sample showed enhanced methylene blue photodegradation compared with TiO$_2$ produced under the same conditions. Further optimization of the TiO$_2$/graphene sample is envisioned.

Acknowledgements

Bibliography

[1] D.M. Antonelli, J.Y. Ying, Synthesis of Hexagonally Packed Mesoporous TiO_2 by a Modified Sol–Gel Method, Angewandte Chemie International Edition in English, 34 (1995), pp. 2014-2017.

[2] A. Goossens, E.-L. Maloney, J. Schoonman, Gas-Phase Synthesis of Nanostructured Anatase TiO_2, Chem. Vap. Deposition, 4 (1998), pp. 109-114.

[3] H.G. Yang, G. Liu, S.Z. Qiao, C.H. Sun, Y.G. Jin, S.C. Smith, J. Zou, H.M. Cheng, G.Q. Lu, Solvothermal Synthesis and Photoreactivity of Anatase TiO_2 Nanosheets with Dominant {001} Facets, JACS, 131 (2009), pp. 4078-4083.

[4] D.V. Bavykin, V.N. Parmon, A.A. Lapkin, F.C. Walsh, The effect of hydrothermal conditions on the mesoporous structure of TiO_2 nanotubes, J. Mater. Chem., 14 (2004), pp. 3370-3377.

[5] H.L. Hellstern, J. Becker, P. Hald, M. Bremholm, A. Mamakhel, B.B. Iversen, Development of a Dual-Stage Continuous Flow Reactor for Hydrothermal Synthesis of Hybrid Nanoparticles, Industrial & Engineering Chemistry Research, 54 (2015), pp. 8500-8508.

[6] J.-L. Mi, S. Johnsen, C. Clausen, P. Hald, N. Lock, L. Sø, B.B. Iversen, Highly controlled crystallite size and crystallinity of pure and iron-doped anatase-TiO2 nanocrystals by continuous flow supercritical synthesis, J. Mater. Res., 28 (2013), pp. 333-339.

[7] M. Kaneko, I. Okura, Photocatalysis: Science and Technology, Kodansha, 2002, pp. 123-155.

[8] R. Leary, A. Westwood, Carbonaceous nanomaterials for the enhancement of TiO_2 photocatalysis, Carbon, 49 (2011), pp. 741-772.

[9] H. Zhang, X. Lv, Y. Li, Y. Wang, J. Li, P25-graphene composite as a high performance photocatalyst, ACS Nano, 4 (2010), pp. 380-386.

[10] G. Williams, B. Seger, P.V. Kamat, TiO_2-Graphene Nanocomposites. UV-Assisted Photocatalytic Reduction of Graphene Oxide, ACS Nano, 2 (2008), pp. 1487-1491.

[11] N.T. Khoa, M.W. Pyun, D.H. Yoo, S.W. Kim, J.Y. Leem, E.J. Kim, S.H. Hahn, Photodecomposition effects of graphene oxide coated on TiO_2 thin film prepared by electron-beam evaporation method, Thin Solid Films, 520 (2012), pp. 5417-5420.

[12] H.P. Mungse, O.P. Sharma, H. Sugimura, O.P. Khatri, Hydrothermal deoxygenation of graphene oxide in sub- and supercritical water, RSC Advances, 4 (2014), pp. 22589-22595.

[13] A.B. Murphy, Band-gap determination from diffuse reflectance measurements of semiconductor films, and application to photoelectrochemical water-splitting, Sol. Energy Mater. Sol. Cells, 91 (2007), pp. 1326-1337.

[14] A.N. Murashkevich, A.S. Lavitskaya, T.I. Barannikova, I.M. Zharskii, Infrared absorption spectra and structure of TiO_2-SiO_2 composites, Journal of Applied Spectroscopy, 75 (2008), pp. 730.

[15] L. Rieppo, S. Saarakkala, T. Närhi, H.J. Helminen, J.S. Jurvelin, J. Rieppo, Application of second derivative spectroscopy for increasing molecular specificity of fourier transform infrared spectroscopic imaging of articular cartilage, Osteoarthritis and Cartilage, 20 (2012), pp. 451-459.

[16] M.R. Whitbeck, Second Derivative Infrared Spectroscopy, Appl. Spectrosc., 35 (1981), pp. 93-95.

PART III:

PHOTOCATALYTIC MECHANISM

Chapter 4

Enhanced methylene blue photodegradation with propylene carbonate as a solvent

Pedro Magalhães, Joana Ângelo, Olga Nunes, Adélio Mendes*

LEPABE - Faculdade de Engenharia, Universidade do Porto, rua Dr. Roberto Frias, 4200-465 Porto, Portugal
*Corresponding author: mendes@fe.up.pt

Abstract

The role of water in the TiO_2-based photocatalytic phenomenon is not yet fully understood. The photocatalysis of methylene blue dissolved in propylene carbonate and different concentrations of water was studied. It was observed that the photocatalytic activity of TiO_2 (P25 from Evonik) peaks when propylene carbonate solvent is used with minute amounts of water; the maximum photodegradation rate was ca. 6.5 times higher than when just water solvent was used. The conventional interpretation of the methylene blue photooxidation intermediated by free radical OH• cannot explain these results. Alternately, the experimental results were interpreted based on the recently proposed "direct–indirect" (D-I) model and a mathematical model was successfully developed and fitted to the experimental results. Finally, new insights on the role of water in the photocatalytic phenomenon were withdrawn.

Keywords: Photocatalysis; D-I model; methylene blue; water; propylene carbonate.

4.1. Introduction

Photocatalysis based on titanium dioxide anatase has attracted the attention of many researchers mainly due to its wide range of applications - photoabatement of atmospheric contaminants, water treatment and the inactivation of microorganisms both in suspension and on surfaces [1-3], among others. This special interest on TiO_2 material was fueled by the pioneer work by Fujishima et al. [4] in 1972, who described for the first time the water splitting using a TiO_2 photoelectrode.

The anatase band gap is ca. 3.2 eV while the band gap of rutile is ca. 3.0 eV. Upon excitation with photons presenting energy higher than the band gap energy, electrons are injected from the valence to the conduction band, generating electron-hole pairs in the conduction and valence bands, respectively – Eq.(4.1). The photogenerated charges diffuse to the surface of the semiconductor particle where they promote redox reactions; holes may generate vacancies on TiO_2 surface or excited reduced species, while excited electrons normally react with oxygen to produce free radical O_2^{-}. These are responsible for the photodegradation of organic compounds, where adsorbed water and oxygen have been described to play a critical important role [5, 6].

The mechanism of photodegradation has been thoroughly studied, and several pathways for the photodegradation of pollutants have been reported [7, 8]. The most commonly assumed photodegradation mechanism is based on Langmuir-Hinshelwood kinetic model, as described by Ollis and Turchi [6]:

$$TiO_2 + h\nu \rightarrow h^+ + e^- \tag{4.1}$$

$$h^+ + e^- \rightarrow heat \tag{4.2}$$

$$h^+ + (H_2O/OH^-)_S \leftrightarrows OH\bullet_{(aq)} \tag{4.3}$$

$$e^- + O_2 \leftrightarrows O_2^- \tag{4.4}$$

$$Reactant_{(aq)} + S \leftrightarrows Reactant \tag{4.5}$$

$$OH\bullet + Reactant \rightarrow Products \tag{4.6}$$

where OH• is the hydroxyl radical, $O_2^{\cdot-}$ is the superoxide radical and S are the active centers of the photocatalyst. This model assumes that the oxidation reactions are intermediated by free radical OH•, which is formed accordingly to Eq. (3). This assumption is based on studies of spin trapping and electron spin resonance (ESR) that evidence high concentrations of OH• radicals in photocatalytic systems [6]. Additionally, the pivotal role of hydroxyl radicals was also supported by the hydroxylated intermediates formed during the photodegradation of the studied compounds [6].

The role of water on the photocatalytic phenomenon has been questioned with increasing emphasis in the recent years. Many authors showed that in gas phase experiments photocatalytic conversion increases with the relative humidity only up to values of ca. 50 % [9, 10]; this effect was assigned to limitations on the UV light availability to form hydroxyl radicals [9, 11]. Ângelo [12] reported recently NO conversions for a dry feed (ca. -20 °C of dew point) of X_{NO} = 75.7 % and for a feed containing 25 % of relative humidity (RH) of X_{NO} = 82.4 %, which is the maximum conversion as a function of the RH. The same work indicates that the water-adsorbed monolayer on the TiO_2 particles is reached for a relative humidity of ca. 25 %. If the main intermediate for the oxidation of NO was OH•, NO conversion for the dry feed would be rather small, see Eq. (3), which seems to be often not the case. Salvador and co-workers [13] also studied the influence of water on the photodegradation of benzene in a dispersion of TiO_2 (anatase sample) in anhydrous acetonitrile. These authors assigned this decrease to the water adsorption on the TiO_2 surface, which hinders the chemical sorption of photogenerated intermediate species. This result, along with other studies reported in literature [14], question the role of hydroxyl radicals in photocatalysis or, otherwise, of Eq. (4.3).

Montoya and co-workers [15] argued strongly against the direct reaction of a photogenerated hole with adsorbed water or OH^- to form OH•. Besides questioning the participation of OH• radicals on the photodegradation mechanism, this work also studied the mechanism that leads to their formation and how these radicals interact with the reactant degradation [15]. These authors [15] suggested a novel pathway for the photocatalytic mechanism named direct-indirect model (D-I). Depending on the

type of electronic interaction of the reactant with the semiconductor surface, the D-I model shows two different types of interfacial charge transfer mechanisms. For strong electronic interaction, D-I model assumes that photo-oxidation is mainly based in an interfacial direct transfer (DT) mechanism of photogenerated valence band free holes to adsorbed species to TiO_2 surface. On the other hand, for weak interactions between reactant and TiO_2 surface, the D-I model assumes an interfacial indirect transfer (IT) mechanism involving two successive steps: first species h_f^+ (surface free hole) are trapped by O_s^{2-} terminal oxygen ions of the TiO_2 surface leading to the generation of terminal $O_s^{\bullet-}$ radicals; next, surface trapped holes are isoenergetically transferred via tunneling to the adsorbed reactant, according to the Marcus-Gerischer model for adiabatic electron transfer at the semiconductor electrolyte interface [16]. Generally DT prevails over IT, although the contribution of both mechanisms can be comparable in some special cases [15]. Figure 1 sketches the D-I model.
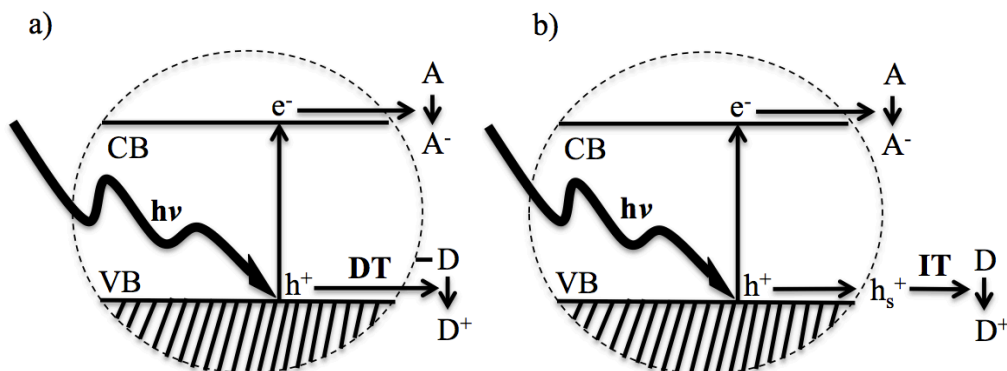
Figure 4.1. Schematic of the direct-indirect model: a) direct transition; b) indirect transition. Adapted from [15] with permission. Copyright American Chemical Society 2014.

Salvador and co-workers [13] also analyzed the importance of oxygen on the photocatalytic phenomenon. The interaction between anatase nanoparticles and adsorbed O_2 was assessed by UV photoinduced oxygen isotopic exchange. The experimental results obtained showed that terminal 2-fold coordinated bridging oxygen ions ($>O_{br}^{2-}$) of the TiO_2 surface are exchanged with oxygen atoms of dissolved O_2 molecules. Furthermore, experimental evidences have recently been reported about the

anaerobic mineralization of benzene dissolved in water using ^{18}O isotope-labeled titania ($Ti^{18}O_2$) as photocatalyst. The generation of $^{16}C^{18}O_2$ as mineralization product allowed to conclude that one-fold coordinated bridging oxygen radicals ($-^{18}O_{br}{}^{\bullet-}$), via inelastic trapping of holes ($h_f{}^+$) by terminal ($>^{18}O_{br}{}^{2-}$) ions, behave as structural oxygen species able to capture electrons from adsorbed benzene on $Ti^{18}O_2$ via an adiabatic interfacial charge transfer mechanism [13]. Dillert et al. [17] and Ângelo et al. [12] also demonstrated the importance of oxygen for the photocatalytic phenomenon, showing that without oxygen there is no NO conversion. Thus, though several models have been proposed to explain the photocatalytic phenomenon, a definitive model has yet to be established.

In this work, the photocatalytic efficiency for the photodegradation of methylene blue was studied using propylene carbonate as solvent with different water concentrations. Additionally, a mechanism based on the D-I model is proposed for explaining the photodegradation of methylene blue and a mathematical model developed and fitted to the experimental results.

4.2. Materials and Methods

4.2.1. Propylene carbonate

Propylene carbonate (Sigma-Aldrich, reagent grade) was used as a solvent for the photodegradation of methylene blue. The propylene carbonate was previously dehydrated heating at 120 °C one and half hour while bubbling nitrogen from a cylinder (nitrogen 99.999 % from Air Liquide). Methylene blue was dissolved in the propylene carbonate and used in the photocatalytic studies immediately after the dehydration process.

4.2.2. Titanium dioxide

Pristine and dehydrated anatase (P25 from Evonik) was used. The dehydration was conducted at 300 ºC during two hours under a nitrogen atmosphere. The sample was then stored in a container previously cleaned with nitrogen flow.

4.2.3. Methylene blue degradation

The photodegradation rate of methylene blue (MB) was followed by spectrophotometry. In a typical experiment, MB dye (10 and 18 $mg \cdot dm^{-3}$) dissolved in an organic solvent – propylene carbonate - and photocatalyst (12.5 mg) were placed in a 50 mL cylindrical glass vessel. Under inert conditions (mixture was bubbled with a low nitrogen flow) and stirring, the photoreactor vessel was exposed to the UV irradiation produced by an ultraviolet (UV-A, highest emission at 365 nm) lamp with two 6 W black-light-blue bulbs (VL-206-BLB, Vilbert Lourmat, France); the lamp was positioned 10 cm away from the vessel (irradiance of 10 $W \cdot m^{-2}$ measured at the reactant mixture surface using a UV radiometer (HD 2102.2, Delta/OHM, Italy)). Each experiment began putting the mixture during 30 minutes in the dark; the mixture was then illuminated for 15 minutes. Aliquots of ca. 2 cm3 were centrifuged (Microcentrifuge, MiniStar silverline from VWR collection) for 5 minutes at 6000 rpm and the supernatant was analyzed in an UV-visible absorption spectrophotometer (Shimatzu UV-3600 UV-VIS-NIR spectrophotometer).

4.2.4. Quantification of hydroxyl radicals

The concentration of hydroxyl radicals produced by P25 were determined by photoluminescence (PL). Coumarin (COU) was chosen as probe molecule since this species reacts stoichiometrically with OH• producing a highly fluorescent product, 7-hydroxycoumarin (7HC) [18, 19]. First, different concentrations of 7-hydroxycoumarin aqueous solutions were prepared and the photoluminescence signal was measured at 456 nm (PL signal of 7HC) to obtain the photoluminescence calibration curve. Then, titanium dioxide (P25) was dispersed in 25 mL of a 1 mM coumarin aqueous solution and kept in dark for 30 min to reach the adsorption-desorption equilibrium. This dispersion was then irradiated (UV light - 10 W·m^{-2}) during fifteen minutes and samples collected each 5 min. They were then centrifuged and analyzed on a spectrofluorophotometer (RF-5301, Shimadzu) at 456 nm. The samples were then evaluated with an excitation wavelength of 332 nm, setting the emission and excitation slits to 3.0 nm. Trials were conducted with propylene carbonate with minute concentration of water and with water in the absence of oxygen.

4.3. Results and discussion

As previously mentioned, few works revisited the role of water in the photocatalytic phenomenon. The direct-indirect model by Salvador and co-workers [13, 15] pointed to a different mechanism for photocatalysis when compared to the traditional mechanism intermediated by hydroxyl radicals formed through Eq. (3) [6]. Until now, the presence of water was considered to be of utmost importance for forming hydroxyl radicals and thus fundamental for the photocatalytic phenomenon. Aiming at a deeper understanding of the role of water on the photocatalytic phenomenon, propylene carbonate, an organic solvent with a very large redox window, 6.6 V, high boiling point, 242 °C, and high relative permittivity, 64.9, was used instead of water [20]. The MB degradation rate was obtained based on the derivative of the absorption light (665 nm) extrapolated for the initial instant – initial rate method. The reaction rate was then obtained transforming the absorption light at 665 nm in methylene blue concentrations.

Figure 4.2 shows the oxidation rate of methylene blue as a function of the solvent used – pure water and different concentrations of water in propylene carbonate. The oxidation rate was obtained for two different initial concentrations of methylene blue – 10 mg dm^{-3} and 18 mg dm^{-3}. The value for dried solvent was also obtained though not inserted in the semi-logarithm plot; the obtained value was 9.6 x 10^{-5} mol dm^{-3} s^{-1} for a methylene blue concentration of 18 mg dm^{-3}. In the absence of water, and as it can be concluded analyzing the pathway degradation shown in Figure 4, there should be no photodegradation of methylene blue. Minute amounts of water should then be present, despite the efforts to keep the system as dry as possible.
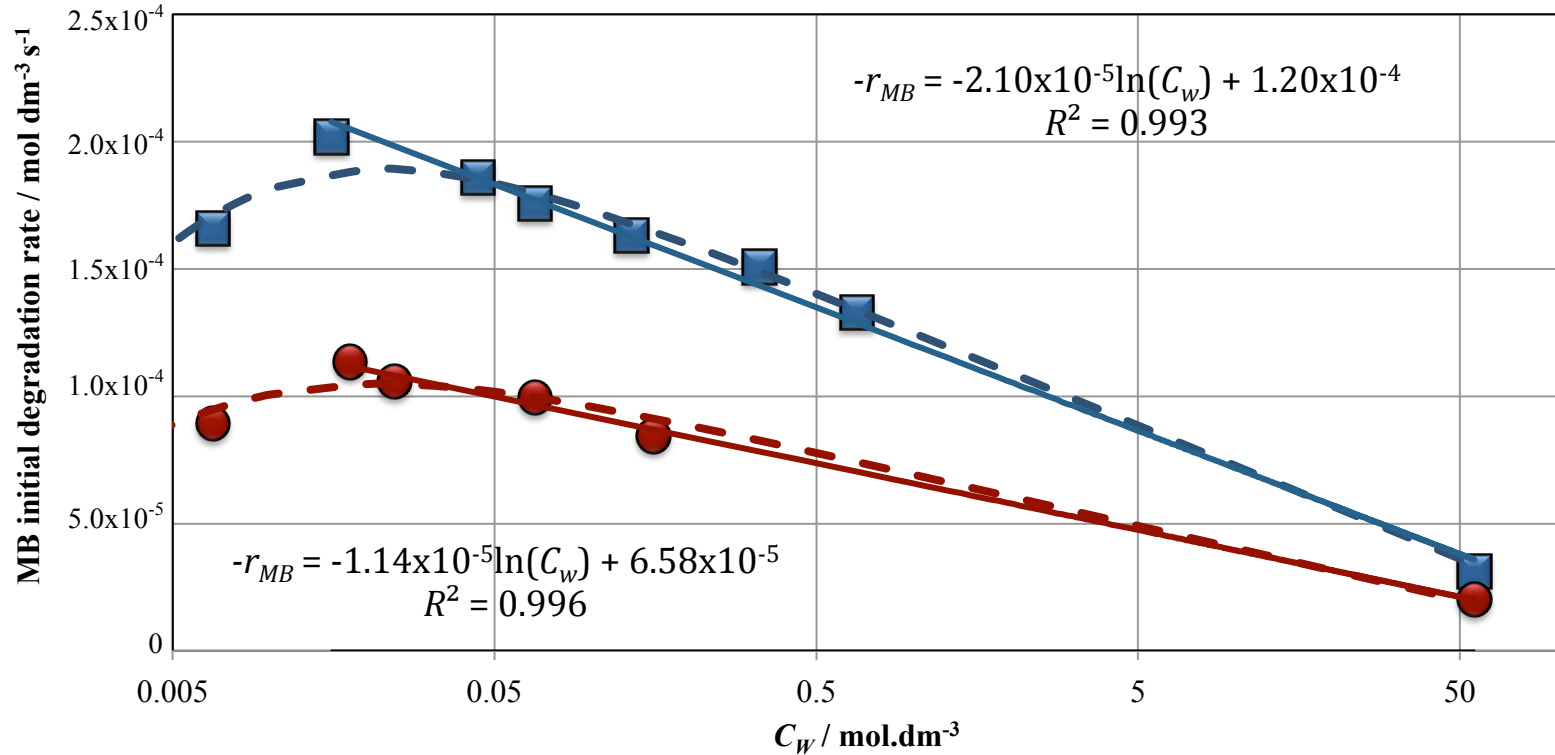
Figure 4.2. Degradation rate of methylene blue as a function of the water concentration for two different initial methylene blue concentrations - 10 mg dm^{-3} (⬤) and 18 mg dm^{-3} (■). Results for the proposed equations are also presented - Equation (4.10) in the continuous line and Equation (4.14) in the dotted line.

The results show that the photodegradation rate peaks for very low water concentration, $C_W \approx 0.016$ mol·dm^{-3} of water in propylene carbonate. Additionally, towards high water contents, the photooxidation rate decreases exponentially with the water concentration.

Assuming that MB has to adsorb on the TiO$_2$ particles surface to oxidize (direct transfer mechanism), the MB degradation rate should be proportional to the active sites concentration and to the MB concentration:

$$-r_{MB} = kSC_{MB} \tag{4.7}$$

where $-r_{MB}$ is the methylene blue reaction rate, S is the available concentration of active sites at TiO$_2$ particles surface for adsorbing methylene blue, C_{MB} is the methylene blue surface concentration and k is the reaction kinetic constant. Since MB is present at low concentrations and should display a moderate adsorption affinity to the photocatalyst surface, Eq. (4.7) assumes that the MB adsorption follows a Henry's law equation. From Figure 4.2 it can be observed that for $C_W > 0.016$ M, S can be written as:

$$S = S_0 - b \ln(C_w) \tag{4.8}$$

where C_W is the water concentration in the solvent and S_0 and b parameters of the empirical model. This equation states that the available active sites concentration depends on the total active sites concentration and on the concentration of water, which should be the species with more adsorption affinity to the surface of the TiO$_2$ particles.

Introducing now Eq. (4.8) into Eq. (4.7), the following expression is obtained:

$$-r_{MB} = k[S_0 - b \ln(C_w)]C_{MB} \tag{4.9}$$

Finally, for a given concentration of methylene blue, one obtains:

$$-r_{MB} = k'_0 + k' \ln(C_w) \tag{4.10}$$

where $k'_0 = kC_{MB}S_0$ and $k' = C_{MB}kb$, named as apparent reaction kinetic constants.

Equation (4.10) was used for fitting the experimental values in Figure 2 for $C_W > 0.016$ M; the determination coefficients obtained for both sets of values are higher than 0.99. According to this model, the apparent kinetic constants are $k' = 2.1 \times 10^{-5}$ s^{-1} and $k'_0 = 1.2 \times 10^{-4}$ mol·dm^{-3}·s^{-1} for an initial methyl blue concentration of 18 mg·dm^{-3}

and $k' = 1.1$ x 10^{-5} s^{-1} and $k'_0 = 6.6$ x 10^{-5} mol·dm^{-3}·s^{-1} for an initial concentration of 10 mg·dm^{-3}.

For $C_W < 0.016$ M, Eq. (4.7) is no longer valid and the surface water concentration has to be considered:

$$-r_{MB} = k_w S C_{MB} C_W^S \qquad (4.11)$$

where k_w is the reaction kinetic constant and C_W^S is the surface water concentration, adsorbed on the photocatalyst particles. For high water concentration values, the water concentration at the photocatalyst surface is mostly constant and the reaction rate depends only on the surface concentration of MB, as taught by Eq. (4.9). For low water concentration, the reaction rate equation becomes second order, with the reaction rate depending on the MB and water surface concentrations. The water adsorption isotherm that best fits the experimental results is the Langmuir equation:

$$-r_{MB} = k_w S C_{MB} \left(\frac{C_W}{C_W \alpha + 1} \right) \qquad (4.12)$$

where α is a constant.

Introducing now Eq. (4.8) into Eq. (4.12), the reaction rate becomes:

$$-r_{MB} = k_w [S_0 - b \ln(C_W)] C_{MB} \left(\frac{C_W}{C_W \alpha + 1} \right) \qquad (4.13)$$

and rearranging, one obtains the reaction rate for the photodegradation of methylene blue:

$$-r_{MB} = k_w C_{MB} \frac{S_0 - b \ln(C_W)}{\alpha + 1/C_W} \qquad (4.14)$$

The reaction rate limit for null water concentration is:

$$\lim_{C_W \to 0} (-r_{MB}) = k_w C_{MB} \frac{S_0 - b \ln(C_W)}{\alpha + 1/C_W} = 0 \qquad (4.15)$$

as it was expected.

Eq. (4.14) was used for fitting the experimental results for the entire range of water concentration and for both initial MB concentration – Figure 4.2. The parameters of the fitting model are given in Table 4.1.

**Table 4.1.** Parameters of the fitting model to the experimental results.

C_{MB}	10 mg/L	18 mg/L
K_W	$32.76 \ dm^6 \cdot mol^{-2} \cdot s^{-1}$	
S_0	$25.45 \ mol \cdot dm^{-3}$	
b	4.63	
α	$375.07 \ dm^3 \cdot mol^{-1}$	
R^2	0.972	0.986

The complete model is able to fit the experimental values for whole range of water concentrations.

Two experiments were conducted for assessing the concentration of the free hydroxyl radicals, namely for pure water and for $C_W \approx 0.016$ M, which corresponds to the highest photocatalytic activity, both in the absence of oxygen. For $C_W \approx 0.016$ M no hydroxyl radicals were detected (concentration $< 7 \times 10^{-6}$ µM), while for pure water a concentration of 0.03 µM was obtained. The concentration of free radicals was also assessed when oxygenated water was used and in this case a concentration of 0.045 µM was measured. On the other hand, the photodegradation rate of methylene blue in deaerated and oxygenated water was, respectively, 2.03×10^{-5} mol·dm^{-3}·s^{-1} and 2.19×10^{-5} mol·dm^{-3}·s^{-1}. This result along with the fact that when the photocatalytic activity was the highest no free hydroxyl radicals were detected are evidences that free hydroxyl radicals should play a minor role in the photodegradation of methylene blue, supporting the mechanism proposed hereafter and based on D-I model.

4.4. Methylene blue photodegradation pathway

The methylene blue ($C_{16}H_{18}ClN_3S$) photodegradation pathway has been described as intermediated by hydroxyl radicals formed according to Eq. (4.3). This pathway starts with the following equation [21]:

$$R - S^+ = R' + OH\bullet \longrightarrow R - S(=O) - R' + H^+ \tag{4.16}$$
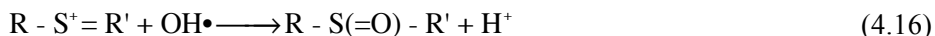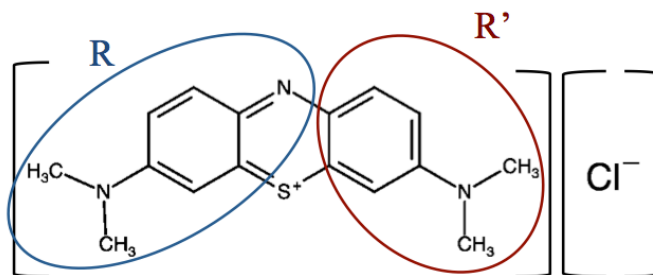
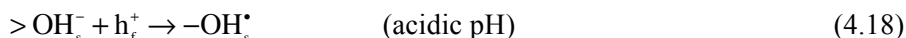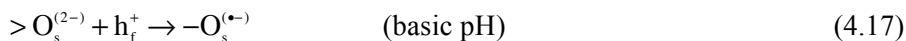where R is and R' are depicted in Figure 4.3.

Figure 4.3. Methylene blue structure.

However, and as mentioned before, it is now believed that the formation of hydroxyl radicals through Eq. (4.3) is thermodynamically and kinetically unfavorable [14, 22]. According to Montoya and co-workers [23] the top of TiO_2 valence band is made of energy levels of O:2p orbitals associated with 3-fold-coordinate bulk oxygen atoms, while the bottom of the bandgap region is composed by those associated with 2-fold-coordinated bridging oxygen atoms of the TiO_2 surface ($> O_s^{2-}$). Upon irradiation, h_f^+ holes are trapped by $>O_s^{2-}$ surface oxygen atoms, giving rise to surface trapped holes, h_s^+ associated with either 1-fold coordinated bridging oxygen radicals $-O_s^{(\bullet-)}$ or bridging hydroxyl radicals $-OH_s^{\bullet}$, depending on the electrolyte pH. Therefore,

$$> O_s^{(2-)} + h_f^+ \rightarrow -O_s^{(\bullet-)} \qquad \text{(basic pH)} \tag{4.17}$$

$$> OH_s^- + h_f^+ \rightarrow -OH_s^{\bullet} \qquad \text{(acidic pH)} \tag{4.18}$$

In the case of acidic pH, as the formed radical is the hydroxyl radical, the mechanism of degradation can be considered the traditional one [21] considering, however, a different mechanism for forming the hydroxyl radical – Eq. (4.18). Otherwise, for alkaline media the mechanism sketched in Figure 4.4 is proposed.
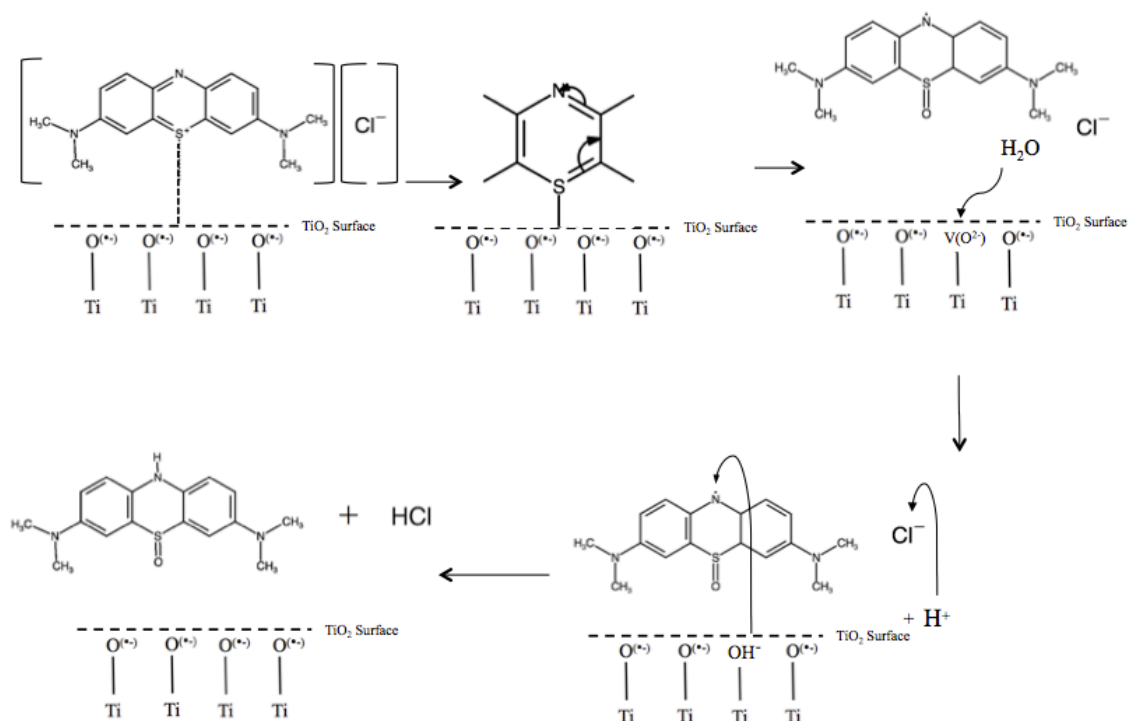
a)
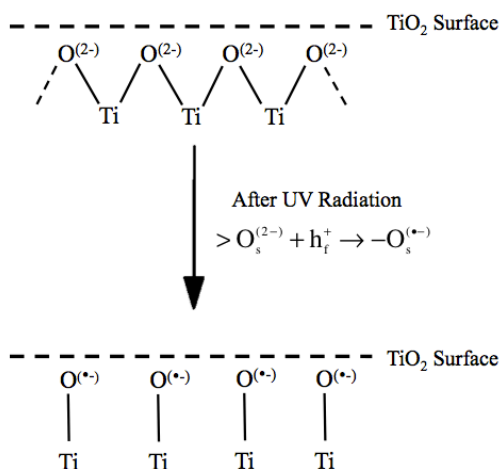
b)

Figure 4.4. Proposed methylene blue photodegradation mechanism for alkaline media: a) TiO$_2$ surface upon irradiation; b) First step of the methylene blue photodegradation and the role of water on this process.

A bridge between the sulfur of the methylene blue molecule and the surface oxygen of TiO$_2$ should be formed. This bond will ultimately lead to the migration of the oxygen from TiO$_2$ surface to the new molecule, forming a double bond with sulfur and causing also a reorganization of the aromatic ring – formation of an intermediate with the phenothiazine structure [21]. Additionally, the presence of water in this system is needed to fill the vacancies formed on both the methylene blue molecule and on the surface of TiO$_2$. Water fills the vacancy on the TiO$_2$ surface and one of the hydrogen atoms splits off leaving a bridging hydroxyl group (OH$_s$) at the vacancy. The split hydrogen atom sits on a nearby bridging O atom, forming another OH$_s$ species [24]. The dissociation of water on the formed vacancies of TiO$_2$ is a well-known phenomenon. The thermodynamic preference is for recombination to reform water instead of H$_2$ formation [25] – equations (4.19) and (4.20):

$$H_2O + V(O_s^{2-}) + O_s^{2-} \rightarrow 2OH_s^- \tag{4.19}$$

$$2OH_s^- \rightarrow H_2O + V(O_s^{2-}) + O_s^{2-} \tag{4.20}$$

4.5. Conclusions

In this work, the photocatalytic oxidation of methylene blue dissolved in propylene carbonate and water mixtures using TiO$_2$ (P25 from Evonik) was studied. It was observed that the photocatalytic activity of P25 increases as the fraction of water in propylene carbonate decreases; a catalytic activity 6.5 times higher than when pure water is used was observed for a water concentration of 0.016 mol·dm^{-3}. Beyond this threshold, the photocatalytic activity decreases to eventually vanishing for the limiting case of complete absence of water – water is a reactant on the photodegradation of methylene blue and thus a requisite for the photodegradation of methylene blue. Even though the MB degradation mechanism requires water as reactant, it was observed that water concentration over *ca.* 0.016 mol·dm^{-3} is prejudicial for the photocatalytic activity. This phenomenon was assigned to the saturation of the TiO$_2$ active centers with water molecules; as there are less active centers available, the photocatalytic activity decreases. The recently proposed D-I model was used to explain the photodegradation mechanism of methylene blue. Furthermore, a phenomenological

mathematical model of the photodegradation of methylene blue was proposed and assessed experimentally; it was concluded that the model fits quite well to the experimental data.

Acknowledgements

Bibliography

[1] J. Colls, Air Pollution, Spon Press, 2002.

[2] H.A. Foster, I.B. Ditta, S. Varghese, A. Steele, Photocatalytic disinfection using titanium dioxide: spectrum and mechanism of antimicrobial activity, Applied microbiology and biotechnology 90 (2011) 1847-1868.

[3] T. Matsunaga, R. Tomoda, T. Nakajima, H. Wake, Photoelectrochemical sterilization of microbial cells by semiconductor powders, FEMS Microbiology Letters 29 (1985) 211-214.

[4] A. Fujishima, K. Honda, Electrochemical Photolysis of Water at a Semiconductor Electrode, Nature 238 (1972) 37-38.

[5] H. Gerischer, A. Heller, The role of oxygen in photooxidation of organic molecules on semiconductor particles, The Journal of Physical Chemistry 95 (1991) 5261-5267.

[6] C.S. Turchi, D.F. Ollis, Photocatalytic degradation of organic water contaminants: Mechanisms involving hydroxyl radical attack, Journal of Catalysis 122 (1990) 178-192.

[7] A. Mills, C. O'Rourke, K. Moore, Powder semiconductor photocatalysis in aqueous solution: An overview of kinetics-based reaction mechanisms, Journal of Photochemistry and Photobiology A: Chemistry 310 (2015) 66-105.

[8] B. Liu, X. Zhao, C. Terashima, A. Fujishima, K. Nakata, Thermodynamic and kinetic analysis of heterogeneous photocatalysis for semiconductor systems, Physical Chemistry Chemical Physics 16 (2014) 8751-8760.

[9] S. Chin, E. Park, M. Kim, J. Jeong, G.-N. Bae, J. Jurng, Preparation of TiO_2 ultrafine nanopowder with large surface area and its photocatalytic activity for gaseous nitrogen oxides, Powder Technology 206 (2011) 306-311.

[10] S. Devahasdin, C. Fan Jr, K. Li, D.H. Chen, TiO_2 photocatalytic oxidation of nitric oxide: transient behavior and reaction kinetics, Journal of Photochemistry and Photobiology A: Chemistry 156 (2003) 161-170.

[11] J. Jeong, J. Jurng, S. Jin, Y. Kim, Optimization of the removal efficiency of nitrogen oxides in the air using a low-pressure Hg lamp, Journal of Photochemistry and Photobiology A: Chemistry 197 (2008) 50-54.

[12] J. Ângelo, Development and Characterization of Titania-based Photocatalysts and their Incorporation in Paint Coatings, Chemical Engineering Department, Faculty of Engineering of the University of Porto, Porto, 2016.

[13] J.F. Montoya, D.W. Bahnemann, J. Peral, P. Salvador, Catalytic Role of TiO_2 Terminal Oxygen Atoms in Liquid-Phase Photocatalytic Reactions: Oxidation of Aromatic Compounds in Anhydrous Acetonitrile, ChemPhysChem 15 (2014) 2311-2320.

[14] P. Salvador, On the Nature of Photogenerated Radical Species Active in the Oxidative Degradation of Dissolved Pollutants with TiO_2 Aqueous Suspensions: A Revision in the Light of the Electronic Structure of Adsorbed Water, The Journal of Physical Chemistry C 111 (2007) 17038-17043.

[15] J.F. Montoya, M.F. Atitar, D.W. Bahnemann, J. Peral, P. Salvador, Comprehensive Kinetic and Mechanistic Analysis of TiO_2 Photocatalytic Reactions According to the Direct–Indirect Model: (II) Experimental Validation, The Journal of Physical Chemistry C 118 (2014) 14276-14290.

[16] R.A. Marcus, On the theory of oxidation-reduction reactions involving electron transfer. I, The Journal of Chemical Physics 24 (1956) 966-978.

[17] R. Dillert, A. Engel, Gro, P. Lindner, D.W. Bahnemann, Light intensity dependence of the kinetics of the photocatalytic oxidation of nitrogen(ii) oxide at the surface of TiO_2, Physical Chemistry Chemical Physics 15 (2013) 20876-20886.

[18] J. Marques, L.F. Oliveira, R.T. Pinto, P.J.G. Coutinho, P. Parpot, J.R. Góis, J.F.J. Coelho, F.D., Magalhães, C.J. Tavares, Release of Volatile Compounds from Polymeric Microcapsules Mediated by Photocatalytic Nanoparticles, International Journal of Photoenergy 2013 (2013) 9.

[19] H. Czili, A. Horváth, Applicability of coumarin for detecting and measuring hydroxyl radicals generated by photoexcitation of TiO2 nanoparticles, Applied Catalysis B: Environmental 81 (2008) 295-302.

[20] K. Gong, Q. Fang, S. Gu, S.F.Y. Li, Y. Yan, Nonaqueous redox-flow batteries: organic solvents, supporting electrolytes, and redox pairs, Energy & Environmental Science 8 (2015) 3515-3530.

[21] A. Houas, H. Lachheb, M. Ksibi, E. Elaloui, C. Guillard, J.-M. Herrmann, Photocatalytic degradation pathway of methylene blue in water, Applied Catalysis B: Environmental 31 (2001) 145-157.

[22] A. Imanishi, T. Okamura, N. Ohashi, R. Nakamura, Y. Nakato, Mechanism of Water Photooxidation Reaction at Atomically Flat TiO_2 (Rutile) (110) and (100) Surfaces: Dependence on Solution pH, Journal of the American Chemical Society 129 (2007) 11569-11578.

[23] J.F. Montoya, J. Peral, P. Salvador, Comments on the published article "Effects of hydroxyl radicals and oxygen species on the 4-chlorophenol degradation by photoeletrocatalytic reactions with TiO_2-film electrodes by J. Yang, J. Dai, Ch. Chen, J. Zhao; J. Photochem. Photobiol. A: Chem. 208 (2009) 66–77", Journal of Photochemistry and Photobiology A: Chemistry 210 (2010) 215-216.

[24] C. Lun Pang, R. Lindsay, G. Thornton, Chemical reactions on rutile TiO_2(110), Chemical Society Reviews 37 (2008) 2328-2353.

[25] M.A. Henderson, A surface science perspective on photocatalysis, Surface Science Reports 66 (2011) 185-297.

PART IV:

GENERAL CONCLUSIONS AND FUTURE WORK SUGGESTIONS

Chapter 5

GENERAL CONCLUSIONS AND FUTURE WORK SUGGESTIONS

TiO_2-anatase is presently the most used photocatalyst for environmental applications due to its high stability, good location of the band edges, moderate charge mobility, high photocatalytic activity, high chemical and thermal stability, low toxicity and low price. However, to increase the usefulness of titanium dioxide, it is necessary to red-shift the light absorption spectrum. This thesis presents an overview of the fundamentals of photocatalysis and strategies to enhance the photocatalytic activity of TiO_2, aiming the indoor photoinactivation of harmful biological agents. Since TiO_2 may contribute to prevent nosocomial infections, its practical application in this field is envisaged. TiO_2 photocatalysis, similarly to the phagocytic cells of the human immune system, use the cytotoxic effects of Reactive Oxygen Species (ROS) to inactivate microorganisms. ROS are highly reactive with biological molecules and thus they are effective for the inactivation various different types of microorganisms.

This thesis consisted on the development of TiO_2/graphene composites by two different methods: hydrothermal and supercritical method. Both composites were characterized and their photocatalytic efficiency evaluated. Additionally, a novel understanding of methylene blue photodegradation and photocatalytic mechanism was suggested based on the DT-IT model.

The prepared TiO_2/graphene photocatalyst presented enhanced methylene blue and NO oxidation rates under UV radiation when compared with P25. Additionally, regarding photoinactivation of *E. coli* DSM 1103, the new photocatalyst exhibited higher inactivation activity under visible light than the commercial P25. When compared with VPL7101, the prepared photocatalyst showed similar photoactivity for methylene blue degradation and higher photoactivity regarding the NO oxidation. Both VLP7101 and VLP7000 achieved higher values of *E. coli* DSM 1103 inactivation than the prepared TiO_2/graphene. However, it was observed that VLP7101 and VLP7000 showed high values of inactivation under dark conditions, suggesting toxic properties of these materials.

137

TiO$_2$/graphene photocatalyst sample was prepared in a supercritical reactor. The SEM and TEM images obtained show the presence of the produced TiO$_2$ nanoparticles on graphene sheets. The XRD analyses performed showed that there is no noticeable difference between the XRD pattern of the produced TiO$_2$ nanoparticles and the TiO$_2$/graphene composite, which indicates an unchanged crystalline structure. The obtained FTIR spectra of both TiO$_2$ and TiO$_2$/graphene are very similar. However, it is not possible to eliminate the possibility of formation of Ti-O-C bonds between TiO$_2$ and the graphene sheets. The band-gap of the produced TiO$_2$ (3.2 eV) and of the produced TiO$_2$/graphene composite (3.0 eV) samples were obtained from the Tauc plots. Finally, the TiO$_2$/graphene sample showed enhanced methylene blue photodegradation compared with TiO$_2$ produced under the same conditions. Further optimization of the TiO$_2$/graphene sample is envisioned.

Aiming a deeper understanding of the role of water on the photocatalytic phenomenon, the photocatalytic oxidation of methylene blue dissolved in propylene carbonate and water solvent using TiO$_2$ (P25 from Evonik) was studied. It was observed that the photocatalytic activity of P25 increases as the fraction of water in propylene carbonate decreases; a catalytic activity 6.5 times higher than when pure water is used was observed for a water concentration of 0.016 mol·dm^{-3}. Beyond this threshold, the photocatalytic activity decreases to eventually vanishing for the limiting case of complete absence of water – water is a reactant on the photodegradation of methylene blue and thus a requisite for the photodegradation of methylene blue. Even though the MB degradation mechanism requires water as reactant, it was observed that water concentration over *ca.* 0.016 mol·dm^{-3} is prejudicial for the photocatalytic activity. This phenomenon was assigned to the saturation of the TiO$_2$ active centers with water molecules; as there are less active centers available, the photocatalytic activity decreases. The recently proposed D-I model was used to explain the photodegradation mechanism of methylene blue. Furthermore, a phenomenological mathematical model of the photodegradation of methylene blue was proposed and assessed experimentally; it was concluded that the model fits quite well to the experimental data.

Targeting future commercial applications, the research should focus on the development of engineered TiO_2 photocatalysts active under visible light, quite import for indoor applications on improving the photoinactivation of harmful microorganisms. In the case of TiO_2/graphene composite photocatalyst, the decoration of TiO_2 with ultrananoparticles of Au has been suggested, since it promotes a decrease in charge recombination, show plasmonic effect and reduce the redox overpotentials leading to more efficient photocatalysts. Furthermore, it is believed that the use of Au does not promote the propagation of antibiotic resistance. The synthesis of TiO_2/graphene in a supercritical reactor is a promising approach for producing monodisperse particles with highly crystalline TiO_2 at industrial scale. Moreover, compared with some of the more traditional methods, this method uses harmless reactants. Thus, the optimization of the process should be accomplished aiming to obtain a photocatalyst useful for environmental applications such as the photoabatement of air and water born pollutants.

Although promising, photocatalysis still faces some drawbacks when imposing itself as a reference disinfection technique. There are still some limitations on the optimization of photocatalysts towards reaching visible light activity, hindering the development of effective commercial photocatalysts. Furthermore, the absence of knowledge on the propagation of both antibiotic and photoinactivation resistant microorganisms needs to be thoroughly addressed before using photoinactivation as a reference disinfection technique.

APPENDIX

TITANIUM DIOXIDE PHOTOCATALYSIS: FUNDAMENTALS AND APPLICATION ON PHOTOINACTIVATION

Pedro Magalhães, Luísa Andrade, Olga C. Nunes and Adélio Mendes

LEPABE, Departamento de Engenharia Química, Faculdade de Engenharia, Universidade do Porto, rua Dr. Roberto Frias, 4200-465 Porto, Portugal

Abstract. TiO_2 semiconductor is being investigated and used for different applications such as energy production, photoinactivation, photoabatement, self-cleaning and water desalination. TiO_2 has, however, a large band gap, *ca.* 3.2 eV, which limits its absorption to UV light range that accounts only for *ca.* 5% of the solar spectrum energy. Therefore, strategies for reducing its band gap aiming to enhance visible light harvesting and making TiO_2 usable for indoors applications are being studied; this reduction is mainly achieved by doping and decoration. More recently, TiO_2/graphene composite proved to be an interesting material for photocatalytic purposes, presenting enhanced energy harvesting properties and an improved photocatalytic activity. Furthermore, the micro size of the composite graphene platelets allows its use without the potential health hazards associated to TiO_2 nanoparticles. TiO_2 may contribute to prevent nosocomial infections because, similarly to the phagocytic cells of the human immune system, it uses the cytotoxic effects of Reactive Oxygen Species (ROS) to inactivate microorganisms. These ROS are known to be highly reactive with biological molecules and thus they are effective for the inactivation of various types of microorganisms. The photocatalysis fundamentals and the preparation of more efficient TiO_2 photocatalysts suitable for indoor applications are reviewed aiming their application for the photoinactivation of microorganisms. Additionally, a comparison of the effectiveness of photoinactivation with traditionally used disinfection methods is also made. Finally, gaps in the knowledge on the long-term effect of the utilization of TiO_2 based materials are identified.

1. INTRODUCTION

In the past four decades photocatalysis fundamentals and applications developed tremendously. Presently, there is a deeper understanding of the photocatalysis fundamentals and, consequently, the use of photocatalysts in several emergent fields such as energy production (*e.g.* photocatalytic water splitting [1]), environmental protection (*e.g.* self-cleaning materials [2] and photo abatement of atmospheric pollutants such as NO_x [3], volatile and halogenated hydrocarbons [4]), water purification (*e.g.* photooxidation of micropollutants [5], volatile organohalide compounds, pesticides [6]) and for microorganisms inactivation [7].

Even though the environmental applications are leading the photocatalysis, microorganism photoinactivation is also catching more and more attention within the scientific community. In fact, there is an alarming increase in the number of hospital-acquired infections, also known as nosocomial infections [8]. This increase was caused by an uncontrolled use of substances that promote the propagation of antibiotic resistance, strongly motivated by a lack of adequate legislation [9]. Infectious diseases are becoming again a real threat, with new infections appearing at an alarming rate [10], and the exponential movement of people across coun-

Corresponding author: O.C. Nunes, e-mail opnunes@fe.up.pt and A. Mendes, e-mail: mendes@fe.up.pt

tries, oceans and continents are intensively contributing to their propagation.

In the past decade many studies reported the photocatalysis use for disinfection purposes; especially the antimicrobial application of titanium dioxide has been widely discussed in many reviews and research papers [11]. In this work, the microorganism photoinactivation main issues will be reviewed, namely regarding the development of materials with enhanced visible light harvesting to foster photocatalysis for indoor applications (*e.g.* hospitals, health centres, etc.). Since the use of TiO_2 for disinfection purposes is being limited to its ability of absorbing only UV light and by the rapid recombination of separated positive and negative charges, doping, decoration and the use of TiO_2/graphene composites are addressed below as mechanisms for mitigating these drawbacks.
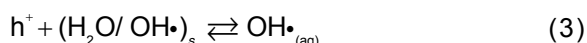
2. FUNDAMENTALS OF PHOTOCATALYSIS

The pioneer work developed by Fujishima *et al.* [12] describing water splitting with a TiO_2 photoelectrode caught the attention of several research groups working on this field and rapidly TiO_2 became the most used semiconductor for photocatalysis. Titanium dioxide exhibits three crystalline structures: rutile, anatase and brookite. Rutile is the most thermodynamically stable crystal structure of titanium dioxide but anatase is the preferred form for photocatalysis because it presents higher photocatalytic activity and it is easier to prepare. Brookite is the least stable phase and normally not used in photocatalysis. There are studies that indicate the benefits of mixings different crystalline phases of TiO_2 for obtaining a higher photoactivity [13,14]. When different crystalline phases are coupled, it is mostly believed that the movement of electrons from the rutile phase to the anatase phase occurs, which causes a more efficient e^-/h^+ separation and consequently an increased photocatalytic activity [15]. However, there are other studies defending that the electron movement is from anatase to rutile [16].

The anatase band gap is *ca.* 3.2 eV while the band gap of rutile is *ca.* 3.0 eV. Upon excitation with photons presenting energy higher than the band gap energy, an electron is injected from the valence to the conduction band, generating an electron-hole pair in the conduction and valence bands, respectively – Eq. (1). The photogenerated charges diffuse to the surface of the semiconductor particle where they promote redox reactions; holes may generate vacancies on TiO_2 surface or excited reduced spe-

cies, while excited electrons normally react with oxygen to produce free radical $O^{2\bullet}$. These are responsible for the photodecomposition of organic compounds, where adsorbed water and oxygen have been described to play an important role.

There are, nowadays, several proposed pathways for the photodegradation of pollutants [17,18]. The most commonly assumed photodegradation mechanism is based on Langmuir-Hinshelwood kinetic model, as described by Ollis and Turchi [19]:

$$TiO_2 + h\nu \rightarrow h^+ + e^- \tag{1}$$

$$h^+ + e^- \rightarrow heat \tag{2}$$

$$h^+ + (H_2O/OH\bullet)_s \rightleftarrows OH\bullet_{(aq)} \tag{3}$$

$$e^- + O_2 \rightleftarrows O_2^- \tag{4}$$

$$Reactant_{sol} + S \rightleftarrows Reactant \tag{5}$$

$$OH\bullet + Reactant \rightarrow Products \tag{6}$$

where OH• is the hydroxyl radical, O_2^- is the superoxide radical and S is an active center of the photocatalyst. This kinetic model was proposed based on studies of spin trapping and electron spin resonance (ESR) showing high concentrations of OH• radicals in photocatalytic systems [19]; the presence of hydroxylated intermediates formed during the photodegradation of the studied compounds also supports the suggested model. However, Ângelo [20] reported recently a maximum of NO conversion of 82.4% for a feed containing 25% of RH and of X_{NO} = 75.7% for a feed with a dew point of -20 °C; the same work indicates that the water-adsorbed monolayer is reached for a relative humidity of *ca.* 25%. If the main intermediate oxidation species of NO is OH• the NO conversion for the dry feed should be quite smaller, see Eq. (3). This result along with other studies reported in literature [21] question the role of hydroxyl radicals in photocatalysis or, otherwise, of the equation (3). Montoya and co-workers [22] made a strong case against the direct reaction of a photogenerated hole with adsorbed water or OH⁻ to form OH•, suggesting a novel direct-indirect model (D-I) – Fig. 1. The D-I model shows two different types of interfacial charge transfer mechanisms. For strong electronic interaction, D-I model assumes that photo-oxidation is mainly based in an interfacial direct transfer (DT) mechanism of photogenerated valence band free holes to adsorbed species to TiO_2 surface. On the
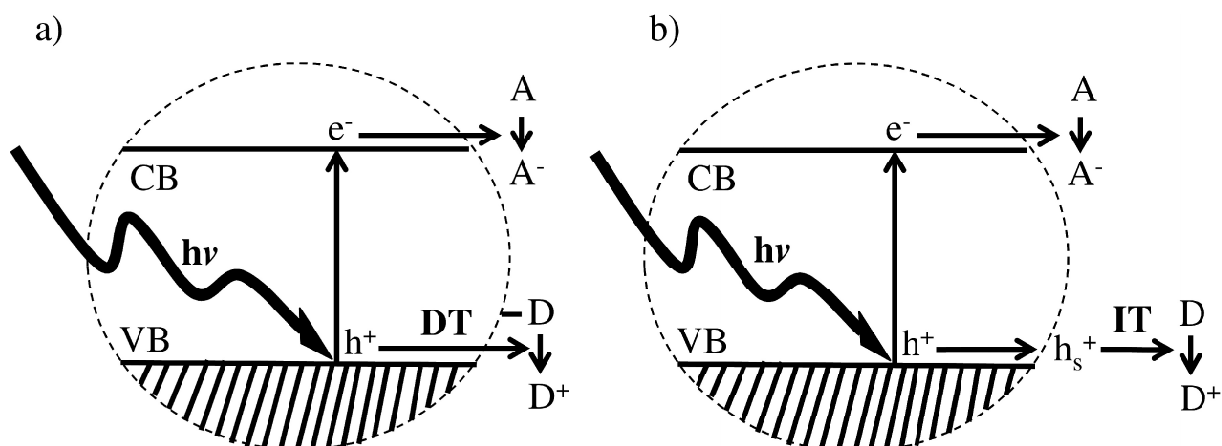
a)

b)

Fig. 1. Schematic of the Direct-Indirect Model: a) Direct Transition; b) Indirect Transition. Adapted from [13] with permission.

other hand, for weak interactions between reactant and TiO_2 surface, the D-I model assumes an interfacial indirect transfer (IT) mechanism involving two successive steps: at the first step, h_f^+ species are trapped by O_s^{2-} terminal oxygen ions of the TiO_2 surface leading to generation of terminal O_s^{-} radicals; at a second step, surface trapped holes are isoenergetically transferred via tunneling to the adsorbed reactant, according to the Marcus-Gerischer model for adiabatic electron transfer at the semiconductor electrolyte interface [23].

The study conducted by Salvador and co-workers [24] analyze the importance of oxygen on the photocatalytic phenomenon. Dillert et al. [25] and Ângelo et al. [20], also highlighted the importance of oxygen on the photocatalytic phenomenon, showing that without oxygen there is no NO conversion. Thus, the photooxidation mechanisms still a matter of debate.

As previously mentioned, improving the TiO_2 photocatalytic activity for attaining visible light activity is being targeted; this improvement can be achieved by: i) avoiding the recombination of photogenerated electrons/holes; ii) narrowing the semiconductor band gap (E_g) [26]. While the first permits to efficiently generate more free radicals, the later allows the photocatalyst to absorb a larger fraction of the solar spectrum. Even though the recombination rate of e^-/h^+ has been neglected in many works due to difficulties in its estimation, it has been proved that the recombination rate has a strong contribution for the net photocatalytic activity [27,28]. The majority of the authors working on this topic defend that the crystal structure of the photocatalyst is a dominant factor of the photocatalytic activity since the recombination of e^- and h^+ is

facilitated at the traps on the surface and in the bulk of the particles [29]. Indeed, it is assumed that the recombination process occurs at the crystal defects, explaining why amorphous TiO_2 presents almost negligible photocatalytic activity. Nevertheless, there are few works discussing this point since the defects of the photocatalytic powders are very difficult to determine. Anatase absorbs only wavelengths smaller than 386 nm, which falls in the UV range. Sunlight spectrum comprises only 5-7 % of UV light, 46% of visible light and 47% of infrared radiation [30]. So, TiO_2 modifications to allow visible absorption are fundamental to enhance the photocatalytic rate. Targeting this enhancement the research was directed for the use visible light instead of only UV radiation, and of proper immobilization of the photocatalyst. TiO_2 doping and/or decoration with the objective of increasing photoactivity and photoabsorbance is addressed below. Doping concerns adding foreign chemical elements (impurities) to modify in the inner-structure of the photocatalyst, while decoration concerns adding materials to the photocatalyst surface. Both modifications target the same objectives: preventing e^-/h^+ recombination and red-shift of the light absorption. TiO_2/graphene composite photocatalysts reduces the charge recombination and originates Ti-O-C bonds that promotes significant red-shift.

2.1. Doping and decoration

Doping of TiO_2 can help the improvement of photocatalytic activity by enhancing the optical absorption of wide band gap semiconductors, increasing the minority carrier diffusion length or enhancing the catalytic activity at the surface of the semiconduc-

tor [31]. However, in some cases, these dopants can also promote e⁻/h⁺ recombination with the creation of mid gap surface states that actually act as recombination centres [31]. High values of dopant concentration (not above 10^6 mol·dm³ [31]) should be avoided since may lead to segregation of the dopant phase. There are two possible doping sites in TiO$_2$: at the titanium site (cation doping) or at the oxygen site (anion doping). Thus, there are two main types of TiO$_2$ doping: cation-doping [32-41] and anion-doping [42-51]. Various studies have been performed to explain the band gap narrowing mechanism in TiO$_2$ doping [30,42,52]. Nitrogen doping is the most used approach for obtaining visible light activity; [53-55] however, there is no established mechanism that explains the visible light activity of N-doped TiO$_2$. While some authors state that substitutional N-doping results in band gap narrowing due to the efficient mixing of orbitals 2p of N and O, others argue that band gap narrowing through modifications in the energy levels of valence and conduction bands can only occur with high concentrations of dopants and strong interactions among impurity energy states, valence and conduction bands [54]. Di Valentin and co-workers [56] based on the density functional theory (DFT) predicted that N atoms could occupy either substitutional or interstitial sites in the TiO$_2$ lattice and thus generate localized energy states. When substitutional sites are occupied, a higher energy level extending the valence band is formed, while in the case of interstitial sites occupation, discrete energy levels above the valence band are created. Doping with other anions, such as carbon, can also show gap narrowing [57]. Some authors suggest that the use of doping agents results in modifications of (101) TiO$_2$ surface [58]. These modifications can increase the transfer of photogenerated electrons to the outer surface regions, facilitating the photocatalytic reactions and improving the quantum efficiency of the photocatalytic processes.

Another approach used for obtaining visible light activity is metal ion doping. Some theories explain the visible light response obtained with this type of doping such as, the occurrence of band gap narrowing and intrinsic defects by either substitutional or interstitial substitution in the TiO$_2$ matrix [54]. Metal ion doping induces, however, recombination of charge carriers lowering the overall efficiency of photocatalysis. Additionally, some reports point to differences in the photocatalytic phenomena under visible light and UV radiation. For UV radiation, as discussed in Section 2, both superoxide and hydroxyl radicals are produced. Nevertheless, for the case of visible light activity, a less oxidative superoxide radical was suggested to be formed and being the main responsible for the photocatalytic activity [54,59,60]. Renguifo-Herrera and co-workers [59] developed N and S co-doped TiO$_2$ presenting an intense visible-light absorption. However, its photocatalytic activity was low, similar to P25 under solar simulated light. These results can be ascribed to the fact that the photogenerated holes on the intermediary energy levels formed by N and S co-doping under visible light do not present sufficient redox potential to oxidize water and thus are not able to produce OH· radicals.

The main difference between doping and decoration is related to which part of the TiO$_2$ is modified. In the case of doping, the modifications are conducted inside the crystalline structure of TiO$_2$, while in the case of decoration the modifications are made on the TiO$_2$ surface. After excitation of TiO$_2$, electrons migrate to the attached decorating particle where they become trapped, minimizing the electron-hole recombination [61]. The migration of electrons to the decorating particles was confirmed in several studies [62-64], which showed an improved photocatalytic activity of the decorated TiO$_2$ when compared to pristine TiO$_2$; the holes migrate then to the semiconductor surface without recombining [62-64]. Few review articles analysing doping and decorating effects on photocatalysis have been published recently [65-68].

An effect that worth to be explained and that has been gathering interest in the scientific community is the surface plasmon resonance effect - SPR effect. When a metal nanoparticle is subjected to an oscillating electric field as the case of incident light, the free electrons in the nanoparticle will answer to that electric field also by oscillating. This behavior is called localized surface plasmon resonance and it can be adjusted by manipulating the size, shape and dielectric environment to change the interaction of the nanoparticles with incident light. Thus, it is possible to scatter the incident light with metal nanoparticles and increase the optical path of photons, leading to an absorption enhancement in certain wavelengths. SPR effect also promotes changes in the energy of the Fermi level caused by the electron storage effects in the metal nanoparticle [54]. Localized SPR of gold and silver nanoparticles normally results in strong and broad absorption bands in the visible light region, which can be exploited to attain visible light-activated photocatalysts [61,69-71].

Important to mention that one of the possible disadvantages of TiO$_2$ decoration is the corrosion

and dissolution of decorating metal particles during the photocatalytic reaction [72]. The decorative particles can also act as co-catalysts, reducing the overvoltage of the redox reactions involved in photocatalysis. The use of co-catalysts allow a given electrochemical reaction to progress faster [73]. For instance, in photoelectrochemical water splitting, the lower level of the conduction band must be more negative than the redox potential of H^+/H_2 (0 V vs. NHE, at pH = 0) and the top level of the valence band must be more positive than the redox potential of O_2/H_2O (1.23 V, at pH = 0). Since this reaction is very difficult to accomplish using TiO_2 photocatalyst, the use of co-catalysts such as Pt, Au and Rh for H_2 evolution [74] and RuO_2 for O_2 evolution [75] is essential.

2.2. TiO_2/graphene composite

TiO_2 photoactivity can also be enhanced with the production of TiO_2 composites. The most notable case is the production of TiO_2/graphene composites. In TiO_2/graphene composites, the electron–hole pairs are generated upon TiO_2 excitation under UV light irradiation. These photogenerated electrons are then injected into graphene due to the more positive Fermi level of graphene [76]. The high carrier mobility of graphene accelerates excited electron transport that enhances the photocatalytic performance [77]. Simultaneously, Ti-O-C bonds formed in the TiO_2/graphene photocatalyst originate a red shift of few dozens of nanometers in the solar spectrum, reducing its bandgap and making it sensitive to longer-wavelength light [78,79]. The resulted photocatalyst presents then an extended photoresponse of up to *ca.* 440 nm

TiO_2 photooxidation is normally assigned intermediated free radicals $OH^{\cdot}$ (oxidation potential of 2.8 V [80]) and $O_2^{\cdot-}$ (reduction potential of -0.137 V [81]), making necessary a thermodynamic minimum band gap of 2.94 eV for generating both radicals. Since most of band gap shortening approaches consider the creation of intermediate energy levels, cf. section 3, making the electron energy gain a stepwise process, the lowest and highest energy levels are still available. This means that, despite the band gap shortening below e.g. 2.8 eV, the photocatalyst is still active towards $OH^{\cdot}$ and $O_2^{\cdot-}$ generation [82]. Nevertheless, the visible light activity of the TiO_2/graphene composites is not fully understood [83,84]. When graphene is bounded to TiO_2 the overall photocatalytic performance is largely improved. This is mainly attributed to three effects: i) efficient charge separation and transportation; ii)

extended light absorption range; and iii) enhanced adsorptivity of the reactant species [79].

For photocatalytic indoor applications, such as for photoinactivation of microorganisms, a very promising photocatalyst is Au/TiO_2/graphene. The use of gold nanoparticles is expected to promote increased values of photoactivity due to the high surface plasmon resonance effect observed with these nanoparticles [61,85]. The Au/TiO_2/graphene, already described for the H_2 production [86], shows enhanced photocatalytic activity due to the surface plasmon resonance effect of the Au nanoparticles, that broadens the visible light response of the TiO_2, and the excellent electron transport properties of graphene, which decreases the recombination of electron and hole pairs. Au nanoparticles, as explained before, can also reduce redox overpotentials [87].

3. PHOTOINACTIVATION

3.1. Rationale of using TiO_2 photocatalysis as the basis of new disinfection methods

The intensive use of antimicrobial agents, including antibiotics in human and veterinary chemobiotherapy, aquaculture and animal husbandry have been pointed out as the main cause behind the tremendous increase of antibiotic resistance in clinical settings and in the environment [88]. The emergence and spread of antibiotic resistant bacteria is not only of paramount public health concern, but it leads also to high costs for the national health services. Organic disinfectants are among the substances that may promote antibiotic resistance dissemination, given the occurrence of co-selection due to genetic linkage between antibiotics and biocides [89-92]. Therefore, the development of new disinfection techniques based on biocides naturally occurring in the human immune system is very attractive.

Phagocytic cells of the human immune system use the cytotoxic effects of ROS as a component of their host defence mechanism [93-95]. When a phagocyte encounters a microorganism, a portion of the phagocyte membrane surrounds it – the first step of a phagolysosome formation. This process leads to increased phagocyte oxygen consumption and activates a unique membrane-associated NADPH-dependent oxidase complex [96]. This enzymatic complex univalently reduces O_2 to $O_2^{\cdot-}$, which further dismutes to H_2O_2 [96]. Another mecha-

nism involved in phagocyte-mediated oxidant generation and microbial toxicity involves the iron-catalysed intra- or extracellular reaction of $O_2^{\cdot-}$ and H_2O_2 to form $OH^{\cdot}$ [94]. These ROS are known to be highly reactive with biological molecules and various authors proposed that $OH^{\cdot}$ radical is the most toxic [97-100]. During the photocatalysis process similar ROS are formed. Hence, photoinactivation seems a good alternative to commonly used disinfection methods.

Matsunaga and co-workers in 1985 were the first authors assessing the feasibility of using UV-activated TiO_2 for photoinactivation [7]. This study reported the successful photoinactivation of both Gram negative and Gram positive bacteria (*Escherichia coli* and *Lactobacillus acidophilus,* respectively) and yeasts (*Saccharomyces cerevisiae*) cells by a semiconductor powder (platinum-doped titanium dioxide, $Pt-TiO_2$). This pioneer work triggered numerous studies to assess the efficiency of TiO_2 photocatalysis on the inactivation of microorganisms and viruses (Tables 1-3) as well as microbial toxins and prions [11,101]. A representative summary of the studies performed up to now on photoinactivation, as well as a comparison of this technique with traditional disinfection methods is given below.

3.2. Target test organisms and TiO_2 matrices

Given the commercial availability of TiO_2 nanoparticles, most of the studies assessing the efficacy of photoinactivation have been carried out with P25 (Table 1), which shows high performance and stability when excited with UV radiation [102]. Most of the studies used axenic suspensions of bacteria as target organisms, being *Escherichia coli*, the well characterized and universally used faecal contamination indicator, the most used. However, domain *Bacteria* accommodates an immense diversity of organisms, reflected in a wide variety of phylogenetic, genotypic and phenotypic groups. Therefore, differences in cellular structure, metabolism, pathogenicity, or tolerance against stressful conditions, including resistance to antimicrobial agents, may influence the susceptibility of bacteria to photocatalysis. This explains why other bacteria, including Gram positive bacteria (phyla *Firmicutes* and *Actinobacteria*), endospore formers (a restricted group of *Firmicutes,* including genera such as *Bacillus* and *Clostridium*), pathogens or opportunistic pathogens (such as *Legionella pneumophila* and *Pseudomonas aeruginosa*)*,* and antibiotic resistant bacteria have been used as test organisms in photoinactivation trials (Table 1, [103-106]). Given the complexity of the bacterial communities in natural environments, some studies assessed the efficacy of photocatalysis in mixed suspensions of known composition, or in a more realistic way, in wastewater (Table 1). The efficacy of photocatalysis in the inactivation of eukaryotic microorganisms, both in axenic or mixed suspensions has also been assessed. In fact, the differences in the cellular structure of prokaryotic and eukaryotic organisms may lead to distinct tolerances to photocatalysis. Similar reasons are behind the studies performed with prokaryotic and eukaryotic dormant forms (spores, cysts). Indeed, the inactivation of these structures, particularly the bacterial endospores, has been a challenge due to their well-known resistance to chemical and physical antimicrobial agents [107,108].

TiO_2 photoinactivation is expected to be the basis of different processes and materials compatible with commercial applications for disinfection. Indeed, photocatalysis-based new disinfection processes can be potentially used in several fields, such as water disinfection [97,109-121], medical applications [119,122-125], and pharmaceutical and food industry [124]. Given the wide variety of potential applications, assessment of photoinactivation has been carried out in different matrices. The majority of the studies assessed the efficacy of TiO_2 nanoparticles in aqueous suspension. This happens mainly because it is well known that the photoinactivation process is favored when cells are in direct contact with the photocatalyst. However, and primarily due to the potential harmful effects of nanoparticles in human health [126] and environment [127], immobilization of TiO_2 has been studied (Tables 1-3). Indeed, TiO_2 immobilization is very important for commercial applications [128], also due to two main reasons. Firstly, it is difficult to recover the photocatalyst when used as powder; this requires a post-treatment solid-liquid separation stage, which will add complexity and costs to the overall process [109]. Secondly, when it is not possible to recover the photocatalyst, the total loss of this material implies economical losses and it becomes itself a pollutant.

TiO_2 has been immobilized in different materials such as glass (plates, beads), polymers (polypropylene, polycarbosilane, cellulose acetate), paint and quartz disks [128-142]. These materials have been employed in surface coatings (glass, cellulose acetate sheets), paint coating and impregnated membranes. These approaches can be used for the inactivation of organisms in aqueous solu-

Table 1. Photoinactivation studies conducted under the influence of UV radiation (<380 nm).

Suspension type	Domain	Phylum	Organism	Initial cellular density (CFU/mL)	Photo catalyst	Photocatalyst concentration (mg/L)	Irradiance (W/m²)	Contact time (min)	Reduction (%)	Type of Trial	Ref.
Axenic	*Bacteria*	*Proteo-bacteria*	Susceptible and multidrug resistant *Acinetobacter baumannii*	$10^3 - 10^5$	TiO_2 (P25, other commercial TiO_2 and produced TiO_2)	62.5 and 125	4 and 8	5 to 80	99	Suspension	[106]
			Enterobacter cloacae	10^6-10^7		100	55	40	99.9	Suspension	[116]
			Susceptible and multiantibiotic resistant *Escherichia coli*	10^3 to 10^9, [a,b]		25 to 2500, [c,d]	2 to 1000, [e,f,g]	5 to 8640	99-100 (20[h])	Surface coating / Suspension / Paint Coating	[106,116, 120,131, 137,141, 142,156-159,161, 165-169]
				10^6		9000	10	40	98.7 -99	Paint coating	[105]
			Salmonella typhimurium	10^6-10^7		100	55	40	99.9	Suspension	[116]
			Legionella pneumophila	10^7		1000	1.65	1	100	Suspension	[162]
			Pseudomonas aeruginosa	10^3-10^7		1000 - 10000	8 - 30, [c,i]	60 - 120	99.9 - 100	Surface coating / Suspension	[120,137, 141,165]
			Salmonella enteritidis	10^7		1000	[c]	120	99.9	Suspension	[120]

a - 1.3 mg/mL, b - 1000 microbial cells (mc)/mL, c - 0.02% suspension of uncovered 100-nm TiO_2 nanoparticles, d - 15-25 mg of TiO_2 per disk, e - 3.42 x 10^{-15} Einsteins.s⁻¹, f - 100 W high-pressure Hg lamp, g - 3900 lux, h – reduction in CO_2 mass balance, i - 2 x15 W, white light 356 nm peak emission, n.a. – not available

Suspension type	Domain	Phylum	Organism	Initial cellular density (CFU/mL)	Photo catalyst	Photo-catalyst concentration (mg/L)	Irradiance (W/m²)	Contact time (min)	Reduction (%)	Type of Trial	Ref.
Axenic	Bacteria	Proteo-bacteria	Salmonella choleraesuis	10^7		250 - 1250	1	180	> 99	Suspension	[170]
			Vibrio parahaemolyticus	10^7		250 - 1250	1	180	> 99	Suspension	[170]
		Firmicutes	Bacillus anthracis	10^3-10^6		1000, 1500	j	60, 90	4^k	Suspension	[171]
			Bacillus cereus endospores	10^5		250	34	540	$> 5^k$	Suspension	[160]
			Bacillus subtilis	$10^{5,l}$		d	74-318	8640	> 80, 20^h	Surface coating Impregnated Membrane	[131,136]
			Bacillus subtilis endospores	10^6		250	70	540	$> 5^k$	Suspension	[160]
			Geobacillus stearother-mophilus endospores	10^7	TiO$_2$ (P25, other commercial TiO$_2$ and produced TiO$_2$)	50 to 1000	91± 2	90	100	Suspension	[172]
			Clostridium difficile endospores	10^3		n.a.	30	300	3^a	Surface coating	[141]
			Enterococcus hirae	10^7		10 000	8	60	100	Suspension	[165]
			Lactobacillus acidophilus	10^7		n.a.	b	60	100	Surface coating	[173]
			Listeria monocytogenes	10^7		250 - 1250	1	180	> 99	Suspension	[170]

a- 15-25 mg of TiO$_2$ per disk, b - UVA - 9 W lamp; UVC -11 W lamp, c - log reduction, l - 1.5 mg/mL, d- UVA light, n.a. – not available

Suspension type	Domain	Phylum	Organism	Initial cellular density (CFU/mL)	Photo catalyst	Photo-catalyst concentration (mg/L)	Irradiance (W/m²)	Contact time (min)	Reduction (%)	Type of Trial	Ref.
Axenic	*Bacteria*	*Firmicutes*	Susceptible and Vancomycin-resistant *Enterococcus faecalis*	10^3–10^5		62.5 and 125	4 and 8	5 to 80	99	Suspension	[160]
			Enterococcus faecium	10^7		n.a.	c	n.a.	3^a	Surface coating	[137]
			Staphylococcus aureus	10^3–10^7		62.5 - 10 000	4 and 8	5 to 80	99 - 100	Suspension	[106,161, 165,167]
				10^5		n.a.	c	n.a.	$>4^a$	Surface coating	[137]
			Methicillin resistant	10^3–10^5		62.5 and 125	4 - 330	5 to 80	99	Suspension	[106]
			Staphylococcus aureus	10^3		n.a.	30	80	99.8	Surface coating	[141]
			Streptococcus sobrinus	10^5		1000	d	3	5^a	Suspension	[174]
		Actinobacteria	*Micrococcus luteus*	h		e	104	8640	20^f	Surface coating	[131]
		Bacteroidetes	*Bacteroides fragilis*	10^7		10 000	8	60	100	Suspension	[165]
		Cyanobacteria	*Anabaena Microcystis*	n.a.		n.a.	6 and 43	60	100^g	Surface coating	[138]

a - log reduction, b - 2 x15 W, white light 356 nm peak emission, c - UV light (300–400 nm, peak emission: 352 nm), d - 15-25 mg of TiO_2 per disk, e - reduction in CO_2 mass balance, f - relative ^{14}C–assimilation, g – 1.77 mg/mL, n.a. – not available

P. Magalhães, L. Andrade, O.C. Nunes and A. Mendes

Table 1 (Continuation). Photoinactivation studies conducted under the influence of UV radiation (<380 nm).

Suspension type	Domain	Phylum	Organism	Initial cellular density (CFU/mL)	Photo catalyst	Photo-catalyst concentration (mg/L)	Irradiance (W/m²)	Contact time (min)	Reduction (%)	Type of Trial	Ref.
Axenic	*Eukarya*	*Ascomycota*	*Candida albicans*	10^3-10^5	TiO$_2$(P25, other commercial	20 (n.a.)	315 and 330, [a]	30, n.a.	96 (1.2[b])	Suspension Surface coating	[137,161]
			Aspergillus niger spores	[c]	TiO$_2$ and produced	[d]	104	8640	0[e]	Surface coating	[131]
			Fusarium (5 different strains)	10^3	TiO$_2$)	35	34	360	3[b]	Suspension	[175]
			Penicillium citrinum	10^5		n.a.	74 and 318	n.a.	< 60	Impregnated membrane	[136]
		Apicomplexa	*Cryptosporidium parvum*	Variable		n.a.	100	Variable	100	Impregnated membrane	[134]
		Stramenopiles	*Melosira*	n.a.		n.a.	6 and 43	60	60[f]	Surface coating	[138]
		Metamonada	*Giardia lamblia*	10^5		[g]	24 and 100	60	100	Surface coating Impregnated membrane	[134,176]

a - 2 x15 W, white light 356 nm peak emission, b - log reduction, c – 0.6 mg/mL, d - 25 mg of TiO$_2$ per disk, e - reduction in CO$_2$ mass balance, f - relative ^{14}C-assimilation, g - 3 % colloidal solution, n.a. – not available.

Table 1 (Continuation). Photoinactivation studies conducted under the influence of UV radiation (<380 nm).

Suspension type	Domain	Phylum	Organism	Initial cellular density (CFU/mL)	Photo catalyst	Photo-catalyst concentration (mg/L)	Irradiance (W/m²)	Contact time (min)	Reduction (%)	Type of Trial	Ref.
Mixed	Bacteria	Proteo-bacteria	*Escherichia coli*	10^5	TiO$_2$(P25, other commercial TiO$_2$ and produced TiO$_2$)	25[b]	[c]	90	5.5[a]	Surface coating	[135]
			Pseudomonas aeruginosa	10^4				120	5[a]		
		Firmicutes	*Bacillus subtilis* endospores	10^6				480	1.7[a]		
	Eukarya	Amoebozoa	*Acanthamoeba Polyphaga* (Trophozoites)	10^4				120	4[a]		
		Acanthamoeba	*Polyphaga*(Cysts)	10^4				480	0		
		Ascomycota	*Candida albicans*	10^5				240	5.4[a]		
			Fusarium solani (Conidia)	10^5				240	5.5[a]		
Wastewater	Bacteria	Proteo-bacteria	*Escherichia coli*	Variable		100	38	360	100	Suspension	[177]
		Firmicutes	*Enterococcus faecalis*	n.a.		250	[d]	180	99.6	Impregnated membrane	[143]
		Proteo-bacteria	Total coliforms	10^4 - 10^7		0.2 - 2000	1.5 (n.a.),[e]	3 - 150	100	Suspension	[121, 178-180]
		-	Total heterotrophic bacteria	10^4		5000	[f]	360	100	Suspension	[118]

a - log reduction, b - mg/cm², c - 70 W/m² in the 300 nm–10 mm range, 200W/m² in the 300–400nm UV range, d - 800 W UV lamp, e - 36 W UV Lamp, f-Photon flux: 0.2 mmol/h < 280 nm, 18 mmol/h 280±315 nm, 390 mmol/h 315±380 nm or 5 mmol/h < 280 nm, 150 mmol/h 280±315 nm, 220 mmol/h 315±380 nm, n.a. – not available

Table 2. Photoinactivation studies conducted under the influence of UV radiation (<380 nm) with TiO_2 modified photocatalysts. The modification types are: doping (x-TiO_2) and decoration (x/TiO_2).

Suspension type	Domain	Phylum	Organism	Initial cellular density (CFU/mL)	Photocatalyst	Photocatalyst concentration (mg/L)	Irradiance (W/m²)	Contact time (min)	Reduction (%)	Type of Trial	Ref.
Axenic	Bacteria	Proteobacteria	*Escherichia coli*	10^9	Ag/TiO_2	1000	0.5	35	6[a]	Suspension	[181]
		Firmicutes	*Bacillus cereus endospores*	10^4 - 10^5	Ag-TiO_2	n.a.	50	1440	100	Surface coating	[132]
			Staphylococcus aureus	$10^9 – 10^{10}$	Fe_3O_4@TiO_2[b]	2500	4	20	93	Suspension	[182]
			Streptococcus pyogenes						96		
			Staphylococcus saprophyticus						99.5		
			Lactococcus lactis	10^4	TiO_2, In_2O_3-TiO_2, Ag/TiO_2, Ag/Ni/TiO_2	n.a.	150	10	99.98	Surface coating	[133]
		Proteobacteria	*Pseudomonas fluorescens*								
			Escherichia coli	10^3	Pt -P25	250	c	60 and 120	100 100	Suspension	[7]
		Firmicutes	*Lactobacillus acidophilus*								
	Eukarya	Ascomycota	*Saccharomyces cerevisiae*						100		
		Chlorophyta	*Chlorella vulgaris*						45		
		Dinoflagellata	*Tetraselmis suecica*	10^3	Ag/TiO_2, Ag-TiO_2	500	d	60	100	Suspension	[183]
			Amphidinium carterae								

a –log reduction, b – core/shell magnetic nanoparticles, c -300-W xenon lamp, a 400-W metal halide lamp and a 500-W white fluorescent lamp, d - 20 W A-type UV lamps, n.a. - not available.

Table 3. Photoinactivation studies conducted under the influence of visible light (>380 nm) with TiO$_2$ modified photocatalysts.

SSuspension type	Domain	Phylum	Organism	Initial cellular density (CFU/mL)	Photo catalyst	Photocatalyst concentration (mg/L)	Irradiance (W/m²)	Contact time (min)	Reduction (%)	Type of Trial	Ref.
Axenic	Bacteria	Proteo-bacteria	*Escherichia coli*	10^2–10^9	Ag/C–TiO$_2$, AgBr/TiO$_2$, I–TiO$_2$, PdO-TiO$_2$, CNT-doped TiO$_2$, N–TiO$_2$, C–TiO$_2$, Pt-TiO$_2$, S–TiO$_2$, N-F- TiO$_2$, Mn–TiO$_2$, Co–TiO$_2$, Fe–TiO$_2$, Mn/Co-TiO$_2$, Cathecol/TiO$_2$ TiO$_2$/Graphene	10–1000, [a]	1.31×10^2–1100, 3900-15 000 [b], [c,d,e]	15-1440, [f]	100	Impregnated Membrane Suspension Surface coating	[128,129,139,140,184,186-197]
			Erwinia Carotovora	10^4–10^5	Synthesized TiO$_2$	n.a.	724 [b]	20-60	> 90	Thin films	[130]
			Enterobacter cloacae	10^4–10^5	Synthesized TiO$_2$	n.a.	724 [b]	20-60	> 90	Thin films	[130]
			Shigella flexneri	10^4	C-TiO$_2$	200	100 and 900, 5	> 80	Suspension	Suspension	[185]
			Klebsiella pneumoniae	10^2 – 10^8	Mn–TiO$_2$, Co–TiO$_2$, Mn/Co–TiO$_2$	25-250	1.31×10^2	60	100	Suspension	[191]
			Acinetobacter baumannii	10^4 – 10^5	C–TiO$_2$, Pt-TiO$_2$	50, 200	100 - 900	5, 75	< 90	Suspension	[185,198]
			Staphylococcus aureus	10^3–10^8	P25, PdO-TiO$_2$, C–TiO$_2$, AgBr/TiO$_2$, Pt-TiO$_2$, Cathecol/TiO$_2$	50 – 200, [c]	10 - 900	5 - 1440	100	Paint coating Surface coating Suspension	[129,140,185,190,193,198]
			Streptococcus pyogenes	10^5	Pt-TiO$_2$	50	480	75	> 90	Suspension	[198]

		Organism	Conc.	Photocatalyst					Method	Ref.
		Enterococcus faecalis	10^6-10^9	Ag/C-TiO$_2$, N-TiO$_2$, C-TiO$_2$	1000	450-500, 15 000[b]	300	4[g]	Suspension Surface coating	[139,184]
Eukarya	*Ascomycota*	*Saccharomyces cerevisiae*	10^2	PdO-TiO$_2$	n.a.	100	180	65	Thin films	[140]
		Aspergilus niger spores	10^2	PdO-TiO$_2$	n.a.	100	480	0	Thin films	[140]

a - 2 wt.% in paint, b - lux, c - 4 x 24 W fluorescence lamps, d - portion of UV (290–400 nm) of 0.05–0.12 W m^{-2} intensity, and visible light (400–700 nm) with a range of intensity 2.70–3.99 W m^{-2}, e - UVA - 3 mW/cm^2, e - UVA - 3 mW/cm^2 (SSL) VL–162 370 lux, f - months of May–September in Tehran (IRAN) at around noon, g – log reduciton, n.a. – not available.
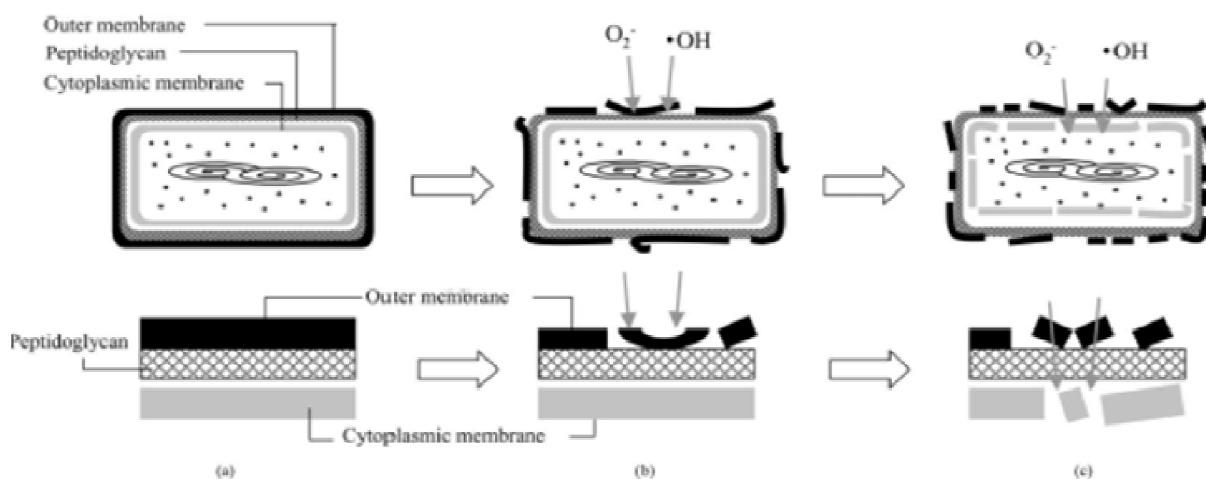
Fig. 2. Free radicals mode of action (reprinted with permission from M. Dizdaroglu, P. Jaruga, M. Birincioglu and H. Rodriguez // *Free Radical Biol. Med.* **32** (2002) 1102. (c) 2002 Elsevier).

tions (e.g. reactor wall), air (e.g. air filters) and fomites (e.g. paint coating). In the specific case of water treatment, the advantage of using coated glass beads is the larger specific surface area, which allows a more efficient photoinactivation of microorganisms. However, the use of glass beads can increase the cost and complexity of the process. In impregnated membranes, TiO_2 is deposited in the interstices of the membrane, improving the surface contact area between TiO_2 and the microorganisms. This method seems to be useful for wastewater treatment [143] but can also be used for the photoinactivation of air microorganisms [136]. Paint coating seems to be, currently, the most promising immobilization matrix for commercial applications. Paint is a readily available material, easy to be applied onto surfaces and does not react with the photocatalyst nor interfere with the photocatalytic efficiency [144]. Furthermore, paint provides a good support for the photocatalyst in a 3D arrangement and can be applied in hospitals and other buildings where infections should be prevented.

3.3. Photoinactivation mechanism

To better understand the effect of TiO_2 photocatalysis on the differential inactivation of the cells and thereof dormant forms, the mechanism of action of photoinactivation is summarized as follows. All the cellular constituents, such as polysaccharides, lipids, proteins and nucleic acids can be attacked by ROS formed during photocatalysis. However, cell wall is the initial target for the photocatalytic attack. Considering as example the Gram-negative bacteria, the oxidation of components of the outer membrane by ROS promotes an increase in cell perme-

ability. Consequently, ROS easily reach the cytoplasmic membrane, where peroxidation of membrane lipids also occurs. The consequent structural and functional disorders of the cytoplasmic membrane lead to ROS entrance in the cell, where they negatively interfere with DNA replication [11,145] and respiratory activity [7,146] due to the direct oxidation of coenzyme A into its dimeric form. Ultimately, ROS attack leads to the loss of cell viability and cell death [147-149]. The initial process of *E. coli* photoinactivation by the action of TiO_2 photocatalysis is depicted in Fig. 2. Evidences indicate that the TiO_2 photocatalytic reaction results in continued bactericidal activity, well after the UV illumination terminates [148].

In what concerns Gram-positive bacteria, the majority of the studies showed that they are more resistant to photocatalytic inactivation than Gram-negative [11]. However, some authors reported opposite observations [141,150,151]. Some of the differences encountered in the susceptibility to photoinactivation between Gram-negative and Gram-positive bacteria may be caused by the experimental conditions. For instance, van Grieken and co-workers [152] showed that the susceptibility of *E. coli* and *Enterococcus faecalis* to photocatalysis in natural waters was similar, whereas in distilled water the Gram-positive was more resistant. Nevertheless, the different cell wall structure of Gram-negative and positive bacteria is actually cited as the main reason for the distinction on ROS attack susceptibility. Gram-negative bacteria have a triple-layer, with an inner cytoplasmic membrane, and a cell wall composed by a thin peptidoglycan layer and an outer membrane. Besides the inner cyto-

plasmic membrane, the Gram-positive bacteria have a thick peptidoglycan layer. The high porosity of peptidoglycan allows solutes, such as ROS, to permeate. Therefore, also Gram-positive cells become susceptible to radical attack [153,154]. However, the thickness of the peptidoglycan layer in these bacteria may allow a delay in the loss of cell permeability, and/or retard oxidants diffusion to vital sites. Indeed, both mechanisms would explain the higher resistance of Gram-positive bacteria to TiO_2 photoinactivation when compared with Gram-negative ones. On the other hand, the presence of an outer membrane in Gram-negative cells may explain why under certain circumstances these bacteria are more resistant to ROS attack than Gram-positive cells [7,141,150]. The rigid cell wall of filamentous and unicellular fungi, composed mainly of soluble and insoluble polysaccharide polymers, make them more resistant to ROS attack than bacterial cells [11,135]. Generally, dormant forms, such as fungal spores [131], cysts [135], and bacterial endospores [131], are even more resistant than the vegetative cells which proves the role of cell wall thickness and complexity in ROS defence.

3.4. Efficiency of photoinactivation

In this section, a summary of the studies carried out on the efficiency of photoinactivation under UV and visible radiation is given. Given the high number of studies published up to now in this field, a selection was made. The selection criteria included the type of tested microorganism, light sources and testing conditions, and the utilization of novel TiO_2 based photocatalysts. A more extensive literature review on this topic can be found elsewhere [11].

The factors affecting cell death, caused by an antimicrobial agent, include the agent concentration, time of exposure, and type and density of cells. Therefore, for a rigorous comparison of efficiency among antimicrobial agents and/or type of target organisms, standardized methods should be used. Even though there is already a standard for testing photocatalytic materials [155], most studies does not follow this standard, probably because this standard is referred to surfaces and most of studies are based on the use of suspensions, as previously mentioned. Hence, it is very difficult to compare the photoinactivation efficiency against different target organisms in different conditions, even when the same photocatalyst (e.g., P25) is used (Tables 1-3). For example, studies reporting the inactivation of *E. coli* in suspension used photocatalyst concentrations ranging from 50 to 1000 mg/L, values of

UV irradiance from 2 to 1000 W/m^2, time of contact from 5 min up to 144 h, and cell densities ranging between 10^3 to 10^7 colony forming units (CFU)/mL. In addition, different strains of this species were used ([105,106,116,120,131,137,141,156-159], Table 1). Nevertheless, most of the studies performed up to now included controls and, in some cases, the inactivation of different organisms or matrices were tested under the same conditions allowing a better comparative assessment and thus valuable data to conclude on the efficacy of photoinactivation.

3.4.1. UV-TiO$_2$ photoinactivation

Photocatalytic experiments under UV radiation produce high levels of photoinactivation for the majority of the different microorganisms tested. As mentioned previously, P25 has been the most used photocatalyst. However, synthetized, pristine, doped or decorated TiO_2 were also reported.

As referred to above, despite the difficulties encountered on comparing the results obtained in the different studies shown in Tables 1 and 2, some conclusions can be drawn. UV-TiO_2 photocatalysis seems to be effective on the inactivation of all the types of microorganisms. Studies carried out by Herrera Mélian *et al.* [143], Dillert *et al.* [118] and Rincón *et al.* [121] should be highlighted since high values of inactivation of total heterotrophic bacteria and coliforms were reported for real wastewater samples.

But care must be taken to define the operating conditions since organisms with different cellular structure and complexity, such as *E. coli*, *Bacillus subtilis* endospores and the yeast *Candida albicans*, have very different susceptibility to photoinactivation. Total inactivation of *E. coli* cellular at a density of 10^6 CFU/mL was achieved within 40 minutes of contact in suspension, with a photocatalyst concentration of 0.1 g/L and irradiance of 55 W/m^2 [116]. However, to completely inactivate *Bacillus subtilis* endospores at a similar initial spore density (10^6 spore/mL), a photocatalyst concentration of 0.25 g/L, an irradiance of 70 W/m^2 and 540 minutes were needed [160]. Despite of shorter time of contact (30 minutes) and photocatalyst concentration (0.02 g/L) a very high irradiance value (330 W/m^2) was necessary to achieve 96% inactivation of *Candida albicans* at and initial cellular density of 10^3 CFU/mL [161]. On the contrary, pathogenicity seems to have less influence on bacterial susceptibility against photoinactivation. For example, Cheng et al. [162] reported that total inactivation of pathogenic *Legionella pneumophila* serotype 1 at an ini-

tial cellular density of 10^7 CFU/mL was attained after 105 minutes with a photocatalyst concentration of 0.2 g/L and an irradiance of 1.65 W/m², conditions comparable to the ones used by Ibañez et al. [116] for the photoinactivation of *E. coli.*

Some antibiotic resistant bacteria are also susceptible to TiO_2 photocatalytic inactivation. Photoinactivation values of susceptible and antibiotic resistant strains of *E. coli* [105] and *S. aureus* (MRSA) [106] were not significantly different (Table 1). However, differences between antibiotic resistant and sensitive counterparts have also been reported [106]. A multidrug-resistant *Acinetobacter baumannii* (MDRAB) was ca. 2 times more susceptible to photoinactivation than the antibiotic sensitive *Acinetobacter baumannii* control strain. Opposite results were obtained for *Enterococcus faecalis,* where the vancomycin resistant strain (VRE) showed ca. 2 times less susceptibility against photoinactivation than the susceptible strain [106]. Indeed, different susceptibility against oxidative stress was already reported among strains of the same microbial species [163,164]. Hence, despite the utmost importance of comparing the response of a wide variety of these organisms against photoinactivation, to the best of our knowledge, such studies were not reported yet.

Even though efficient, high photocatalyst concentrations, powerful light sources or high contact times are needed when P25 or other synthetized pristine TiO_2 are used. Thus, in order to achieve higher photoinactivation performances with less severe conditions, modified titanium dioxide (doped and/or decorated) has been studied (Table 2). As discussed in detail in Section 3, these TiO_2 modifications enhance the photocatalytic activity of the photocatalyst. Much lower irradiance (0.5 *versus* 55 W/m², respectively) and lower contact times (35 *versus* 40 minutes) were necessary to achieve total inactivation of *E. coli* at a higher cellular density (10^9 *versus* 10^6 CFU/mL, respectively) with a TiO_2 decorated with silver nanoparticles [181] compared with pristine TiO_2 [116]. However, a final conclusion concerning the performance of the modified photocatalyst cannot be retrieved because a 10 times higher concentration of TiO_2 decorated with Ag (1 g/L) [181] than of pristine TiO_2 [116] was used. Nevertheless, other studies suggest that modification of the photocatalyst improve, in fact, their inactivation performance. For the complete inactivation of *S. aureus* at an initial cellular density of 10^6 CFU/mL, 10 g/L of synthetized pristine TiO_2 and irradiance of 8 W/m² for 60 minutes were necessary [165], while 2.5 g/L of Fe_3O_4 decorated TiO_2 and an irradiance of 4 W/m² for 20 minutes were sufficient to inactivate 93 % of *S. aureus* viable cells at an initial higher concentration (10^9 CFU/mL).

3.5. Visible light-TiO_2 photoinactivation

Despite the success of UV-photocatalysis in disinfection, the mutagenic action of this type of radiation hampers its use in the majority of the indoor spaces [113]. On the other hand, the negligible UV irradiancy under common internal lighting conditions prevents the use of pure photocatalytic TiO_2 in indoor spaces. Even in outdoor events, the low fraction of solar UV compared to the total solar irradiation advises the use of visible light photocatalysts. To overcome this major drawback, several studies focused on the development of modified titanium dioxide with enhanced visible light photoactivity have been conducted, as mentioned in Section 3.

Among the modified photocatalysts tested up to now, carbon doped TiO_2, decorated [184] or not [185] with silver nanoparticles was shown to respectively fully inactivate *E. coli* and *S. aureus* under visible light. Also manganese-, cobalt doped or co-doped Mn/Co-TiO_2 was shown to fully inactivate *Klebsiella pneumonia* [100]. As mentioned in Section 4, the use of graphene for photocatalytic applications by Akhavan *et al.* [186] resulted in a novel graphene oxide/TiO_2 composite with an increased antibacterial activity under solar light irradiation when compared to bare TiO_2 (roughly 7.5 times more).

Nevertheless, the disinfection performance of modified TiO_2 under visible light is still lower than under UV radiation. Indeed, the inactivation fraction of vegetative cells of a wide variety of microorganisms under UV irradiation varies between 96% and 100% (Table 1), while under visible light ranges from 65% to 90% (Table 3). Moreover, to attain these inactivation values extreme conditions were necessary, i.e, very high values of irradiance (up to 15 000 lux), photocatalyst concentration (1 g/L) and/or contact time (1440 minutes). Finally, inactivation of dormant forms such as spores of *Aspergillus niger* under visible light was also not attained yet (Table 3).

Thus, optimization of photoinactivation under visible light envisaging a future commercial application of this technique is still needed.

3.6. Traditional disinfection methods

Traditional disinfection methods are based on the utilization of heat, radiation or chemical compounds.

Chlorine, hydrogen peroxide, ozone, and UV radiation are amongst the most used agents currently used to disinfect water, air or fomites. The disinfection methods based on each of these antimicrobial agents will be briefly overviewed next.

3.6.1. Chlorination

Chlorination as a disinfection technique is mainly based on the use of gaseous chlorine and/or hypochlorite. Chlorine gas (Cl_2) is the elemental form of chlorine at standard temperature and pressure. Chlorine gas is approximately 2.5 times heavier than air and is highly toxic. Hypochlorite (ClO^-) is usually obtained from sodium hypochlorite and calcium hypochlorite [199].

Chlorine gas hydrolyzes in water according to the following reaction (Eq. (7)):
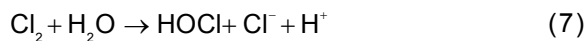
$$Cl_2 + H_2O \rightarrow HOCl + Cl^- + H^+ \qquad (7)$$

while hypochlorous acid, resulting from the previous reaction, is a weak acid, which dissociates in aqueous solution:

$$HOCl \rightarrow ClO^- + H^+ \qquad (8)$$

Under typical water treatment conditions in the pH range 6–9, hypochlorous acid and hypochlorite are the main chlorine species. Depending on the temperature and pH level, different distributions of aqueous chlorine species (Cl_2, HOCl, and ClO^-) are observed [200]. In addition to these major chlorine species, other chlorine intermediates including trichloride (Cl_3^-) and chlorine hemioxide (Cl_2O) can also be formed – Fig. 3. In solution, ratios of these intermediates are a function of temperature, pH and chloride concentration. Under typical water treatment conditions, the concentrations of Cl_3^- and Cl_2O are very low, accounting, at most, to 20% of all the chlorine species in solution [200,201].

Chlorination as a water disinfection method was first introduced in 1902 in Middlekerke, Belgium [202]. Chlorination is mainly used in water disinfection, however, hypochlorite is also used for the disinfection of some surfaces (mostly for countertops and floors), mainly in health care facilities [203]. A leading advantage of chlorination is that it is effective against a wide variety of bacteria and viruses. However, it cannot inactivate all microbes, being some protozoan cysts resistant to the effects of chlorine [204]. In cases where protozoan cysts are not a major concern, chlorination seems to be a good water disinfection method because it is inexpensive.
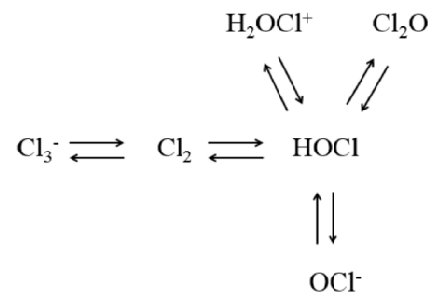
Fig. 3. Equilibrium of chlorine and its derivatives in solution at 25 °C (adapted from [196]).

The precise mechanism by which microorganisms are inactivated by chlorine has not yet been fully explained. However, some studies show that the bacterial cell membrane changes its permeability in the presence of chlorine [205,206]. The presence of suspended solids influences the action of chlorine because the particles and organic compounds usually provide protection to microorganisms. This protection usually comes from stabilization of the cell membranes, which reduces the access of chlorine to key cellular components for inactivation [206]. Indeed, microbial aggregates or microorganisms attached to or embedded in particles have been shown to have increased resistance to inactivation by chlorine, when compared to non-attached, free-swimming microorganisms. Dietrich and co-workers [206] reported, however, that chlorine is capable of penetrating particles in wastewater by radial diffusion. Greater chlorine penetration into wastewater particles was observed with increasing initial chlorine concentration, indicating that chlorine application could be tailored to penetrate particles of known size in order to achieve inactivation [206].

Some of the studies reported in the literature on the efficiency of chlorination on disinfection are summarized in Table 4. Koivunen and co-workers [207] studied the chlorination of *Enterococcus faecalis, Escherichia coli*, and *Salmonella enteritidis* in aqueous solution. In this work, concentrations of chlorine of 12 mg/L with a contact time of 10 minutes were used in order to achieve a log reduction value of around 3 for *Enterococcus faecalis.* But, even with a higher chlorine concentration (18 mg/L), lower reduction values were registered for *Escherichia coli* and *Salmonella enteritidis* (0.3 and 0.44, respectively) for the same contact time, demonstrating that microorganisms have distinct tolerance against chlorination. In wastewater samples, Hassen and co-workers [208] registered log reduction values up to 3.7 and 4.4 for fecal coliforms and enterococci, re-

Table 4. Inactivation of several microorganisms by chlorination.

Domain	Phylum	Organism	Type of suspension	Type of Trial	Chlorine concentration (mg/l)	Contact time (min)	Final chlorine concentration (mg/L)	Initial cellular density (CFU/mL)	Reduction (log)	Reference
Bacteria	Firmicutes	Clostridium perfringens Spores	Axenic	Suspension	5	1440	n.a.	10^4	4	[209]
		Enterococci	Wastewater	Suspension	6.5-25	15-40	1.2-3	10^4-10^5	4.5(99[a])	[208,210]
		Enterococcus faecalis	Axenic Wastewater	Suspension	8-30	30	0.2-0.3	10^5-10^7	5	[211,212]
		Staphylococcus aureus	Axenic	Suspension	1-5	30	0.5-3	10^8-10^9	b	[207]
		Enterococcus faecalis	Axenic	Suspension	1-5	30	0.5-3	10^8-10^9	b	[207]
	Proteo-bacteria	Campylobacter jejuni	Axenic	Suspension	0-4	120	n.a.	10^3-10^4	99[a]	[213]
		Citrobacter freundii	Axenic	Suspension	0-10	120	n.a.	10^3-10^4	99[a]	[213]
		Enterobacter agglomerans	Axenic	Suspension	0-10	120	n.a.	10^3-10^4	99[a]	[213]
		Enterobacter cloacae	Axenic	Suspension	0-10	120	n.a.	10^3-10^4	99[a]	[213]
		Escherichia coli	Axenic Wastewater	Suspension	1-30	2.5-120	0.2-3	10^5-10^9	>5 (99[a])[b]	[169,207, 211-213]
		Fecal coliforms	Wastewater	Suspension	6.5-25	15-5760	1.2-3	10^4-10^{5c}	7(99[a])	[208,210, 214]
		Klebsiella oxytoca	Axenic	Suspension	0-10	120	n.a.	10^3-10^4	99[a]	[213]
		Klebsiella pneumoniae	Axenic	Suspension	0-10	120	n.a.	10^3-10^4	99[a]	[213]
		Legionella gormanii	Axenic	Suspension	0-4	120	n.a.	10^3-10^4	99[a]	[213]

		Pseudomonas aeruginosa	Axenic	Suspension	1 - 5	30	0.5-3	10^8-10^9	b	[207]
		Salmonella enterica	Axenic	Suspension	0-4	120	n.a.	10^3-10^4	99[a]	[213]
		Salmonella enteritidis	Axenic	Suspension	18	n.a.	0.2-0.3	10^5-10^7	0.5	[212]
		Shigella sonnei	Axenic	Suspension	0-4	120	n.a.	10^3-10^4	99[a]	[213]
		Total coliforms	Wastewater	Suspension	11-21	15-5760	n.a.	c	7(99[a])	[210,241]
		Yersinia enterocolitica	Axenic	Suspension	0–4	120	n.a.	10^3-10^4	99[a]	[213]
Eukarya	Apicomplexa	Cryptosporidium parvum Cysts	Axenic	Suspension	5	1440	n.a.	10^4	4	[209]

a -%, b – evaluated through the consumption of chlorine and presence of residual chlorine, c- 1 million to 20 millions per 100 ml, n.a. – not available.
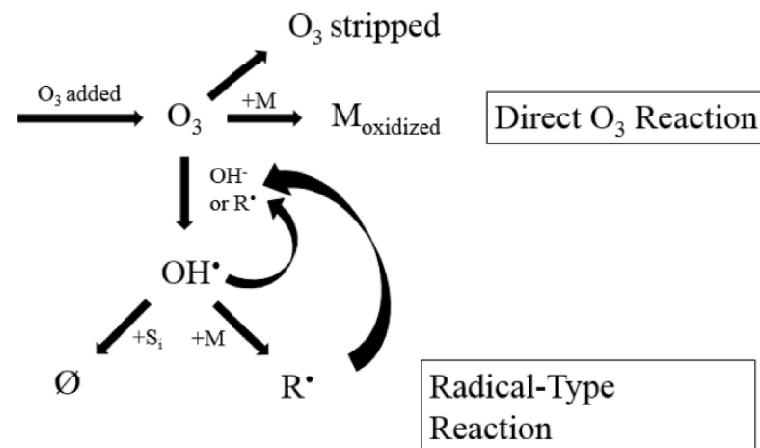
Fig. 4. Mechanisms involved in the ozonation process. In the figure, M is referred to the solute, M_{oxid} to the oxidized solute, S_i to the free radical scavenger, Ø to products that do not catalyze the ozone decomposition and R to the free radicals that catalyze the ozone decomposition. (Reprinted with permission from J. Koivunen and H. Heinonen-Tanski // *Water Res.* **39** (2005) 1519. (c) 2005 Elsevier).

spectively, when using chlorine concentrations ranging from 6.5 and 13.6 mg/L and contact times up to 40 minutes.

3.6.2. Ozonation

Ozone is produced when oxygen molecules are dissociated by an energy source into oxygen atoms and subsequently collide with the non-dissociated oxygen molecules. Ozone is one of the most powerful oxidizing agents (E^0 = 2.07 V) and it is mostly used to destroy organic compounds [215].

The oxidation of the target compounds can occur through two different mechanisms: i) direct reaction with molecular ozone or ii) indirect reaction with secondary oxidants formed upon the decomposition of ozone in water. Such decomposition is catalyzed by hydroxide ions (OH⁻) and other solutes. Highly reactive secondary oxidants, such as hydroxyl radicals (OH·), are thereby formed. These radicals and their reaction products can cause the decomposition of ozone. Consequently, radical-type chain reactions may occur, which consume ozone concurrently with the direct reaction of ozone with dissolved organic material and contributing to the formation of additional hydroxyl radicals – Fig. 4 [216].

Ozone reacts with polysaccharides slowly, leading to breakage of glycosidic bonds and formation of aliphatic acids and aldehydes. The reaction of ozone with primary and secondary aliphatic alcohols may lead to formation of hydroxy-hydroperoxides, precursors to hydroxyl radicals, which in turn react strongly with the hydrocarbons [217]. However, it was already shown that N-acetyl glucosamine, a compound present in the peptidoglycan of bacterial cell walls, was resistant to the action of ozone in aqueous solution at pH 3 to 7. This explains the higher resistance of Gram-positive bacteria compared to Gram negative ones, because the former contains higher amounts of peptidoglycan in their cell walls than the later. Ozone can react significantly with amino acids and peptides, especially at neutral and basic pH. Furthermore, ozone reacts quickly with nucleobases, especially thymine, guanine, and uracil. Reaction of ozone with the nucleotides releases the carbohydrate and phosphate ions [217].

Ozone is mainly used for water treatment, however the use of ozone for surface disinfection was already reported [218]. Water disinfection by ozonation has been extensively reported, and some of the works are summarized in Table 5. Low ozone concentrations (0.15-0.20 mg/L) and contact time (180 s) were sufficient to inactivate several Gram negative bacteria in suspension to values up to 99.99% [219]. Nebel and co-workers [220] reported one of the first works describing the treatment of wastewater by ozonation. In this work, with an ozone dose of 14 mg/L and a contact time of 5 minutes it was possible to achieve log reduction values of up to 3 log for enterococci, total coliforms and fecal coliforms.

3.6.3. UV

Ultraviolet processing involves the use of radiation from the ultraviolet region of the electromagnetic spectrum for purposes of disinfection. Usually, the range of UV refers to wavelengths between 100 and

P. Magalhães, L. Andrade, O.C. Nunes and A. Mendes

Table 5. Inactivation of several microorganisms by ozonation.

Domain	Phylum	Organism	Type of suspension	Type of Trial	Disinfection O$_3$ dose (mg/l)	Contact time (min)	Final Ozone Concentrations (mg/L)	Initial cellular density (CFU/mL)	Reduction (log)	Reference
Bacteria	Firmicutes	Bacillus subtilis spores	Axenic	Surface	16	150	n.a.	10^5-10^6	0.5	[218]
		Enterococci	Wastewater	Suspension	2-14	5-30	0.05-0.4	n.a.	1-3	[220-223]
		Leuconostoc mesenteroides	Axenic	Suspension	0.2 – 3.8	2	0	10^9	7	[224]
		Listeria monocytogenes	Axenic	Suspension	0.2 – 3.8	2	0	10^9	7	[224]
		Staphylococcus aureus	Axenic	Suspension	a	n.a.	2	10^7	7	[225]
	Proteobacteria	Aeromonas salmonicida	Axenic	Suspension	0.15-0.20	3	0.05-0.07	10^9	4	[219]
		Escherichia coli	Axenic / Wastewater	Surface / Suspension	0.2 – 4	2-30	0.1-0.4	10^5-10^9	2-7	[218,221, 223-2236]
		Fecal coliforms	Wastewater	Suspension	7-14	5	0.05	n.a.	1-3	[220]
		Pseudomonas fluorescens	Axenic	Suspension	0.2 – 3.8[a]	2	2	10^9	7	[224,225]
		Salmonella enterica	Axenic	Suspension	a	n.a.	2	10^7	7	[225]
		Shigella flexneri	Axenic	Suspension	a	n.a.	2	10^7	7	[225]
		Total coliforms	Wastewater	Suspension	7-14	5	0.05	n.a.	2-3	[220,226]
		Vibrio anguillarum	Axenic	Suspension	0.15-0.20	3	0.05-0.07	10^9	4	[219]
		Vibrio cholerae	Axenic	Suspension	a	n.a.	2	10^7	7	[225]
		Vibrio salmonicida	Axenic	Suspension	0.15-0.20	3	0.05-0.07	10^9	4	[219]
		Yersinia ruckeri	Axenic	Suspension	0.15-0.20	3	0.05-0.07	10^9	4	[219]

										Ref.
	-	Total heterotrophic bacteria	Treated Wastewater	Suspension	50^b	30	10^6	0	6	[223]
Eukarya	Apicomplexa	*Cryptosporidium parvum*	Axenic	Suspension	0.36-2.2	1	n.a.	n.a.	6	[227]
	Ascomycota	*Aspergillus niger*	Wastewater	Suspension	50^b	30	10^3	0	3	[223]
		Penicillium citrinum	Axenic	Surface	16	120	10^5-10^9	n.a.	2	[218]
	Basidiomycota	*Rhodotorula rubra*	Wastewater	Suspension	50^b	30	10^3	0	3	[223]

a – Flow rate of 152.4 cm^3/h, b - grams of ozone per normal cubic meter, n.a. – not available

400 nm. This range can be further subdivided. UVA corresponds to wavelengths between 315 and 400 nm and it is normally responsible for change in human skin that cause tanning; UVB refers to wavelengths between 280 and 315 nm and is the main responsible for skin burning and can also lead ultimately to skin cancer. UVC – 200 to 280 nm – is called the germicidal range, because it is considered to be the most effective towards the inactivation of bacteria and viruses. Finally, the vacuum UV range (100 to 200 nm), can be absorbed by almost all substance and can only be transmitted in the vacuum [228].

Among the above mentioned disinfection methods, UV light has been adopted as the most appropriate treatment process for drinking water because it is simple to use, highly effective for inactivating microbes and it does not introduce chemicals or cause the production of harmful disinfection by-products in the water [229]. This method promotes additional security after traditional treatment processes [230,231]. UV radiation is responsible for a wide range of biological effects [232-234], including modifications in the protein structure and in the DNA [235]. Regarding DNA damage, it may result on inhibition of cell replication and, in case of lethal doses, on the loss of ability to reproduce. Although the UV-A wavelengths bordering on visible light are not sufficiently energetic to directly modify DNA bases, cellular membrane damage can be induced through the production of ROS, such as singlet oxygen, superoxide, hydrogen peroxide and hydroxyl radical, generated via excitation of dissolved oxygen in water [177,236]. Furthermore, according to several authors, the damage induced by UV radiation continues even after the end of the irradiation period [236,237]. Bacterial DNA is a critical target of UV radiation and its effects depend on several parameters, such as UV spectrum, dissolved oxygen concentration, salt concentration and post-irradiation growth conditions [236]. Different microorganisms respond differently to the lethal effects of UV. It is known that the effectiveness of a UV disinfection system depends on the sensitivity of the target microorganisms to UV, microbial content, antibiotic resistance phenotypes, light source, UV radiation intensity, exposure time of microorganisms to radiation and their ability to re-growth [120,223,236-238]. UV treatment can be used for the inhibition of microorganisms in surfaces, in the air or in water [239-241].

Some works reporting the use of UV radiation on the inactivation of microorganisms are presented in Table 6. When using a light intensity of 2 W/m^2, it was possible to achieve high values of inactivation of different microorganisms in wastewater samples. A contact time of 50 seconds permitted to achieve log reductions of 4 to 5 for methicillin-resistant *Staphylococcus aureus* (MRSA), *E. coli,* and *Pseudomonas aeruginosa.* A higher contact time (100 s) was needed to reach similar log reduction values for vancomycin resistant *Enterococcus faecium* (VRE) [242]. In a study assessing the effectiveness of UV radiation on the inactivation of several vegetative bacteria (*Staphylococcus aureus, Enterococcus faecalis, E. coli, Salmonella enterica, Shigella sonnei) Bacillus subtilis* spores*, Acanthamoeba castellanii* cysts and viruses (poliovirus type 1 and simian rotavirus SAil), Chang and co-workers [243] reported that viruses, spores and cysts were 3-4, 9 and 15 times more resistant than the vegetative bacteria, respectively.

3.6.4. Hydrogen peroxide

Hydrogen peroxide is a metastable molecule – it easily decomposes into water and oxygen - with high redox potential (1.77 V) [244]. Even though the mechanism of hydrogen peroxide inactivation towards cells is usually attributed to the production of highly reactive hydroxyl radical, hydrogen peroxide itself presents some cytotoxicity towards cells. H_2O_2 can directly oxidize the catalytic iron atom of dehydratase clusters, precipitating iron loss and enzyme inactivation. H_2O_2 poisons the Isc system, which is responsible for the transfer of [4Fe-4S] clusters to newly synthesized apoenzymes. However, the mechanism of cytotoxic activity of H_2O_2 is generally reported as based on the production of highly reactive hydroxyl radicals from the interaction of the superoxide ($O_2^{\cdot-}$) radical and H_2O_2, a reaction first proposed by Haber and Weiss [245] (Eq. (9)):

$$O_2^- + H_2O_2 \rightarrow O_2 + OH + OH^- \qquad (9)$$

Further, it is believed that the production of extremely short-lived hydroxyl radicals within the cell by the Haber–Weiss cycle is catalyzed in vivo by the presence of transition metal ions (particularly iron-II) according to Fenton chemistry [246] (Eq. (10)):
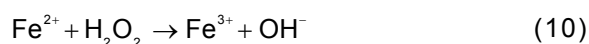
$$Fe^{2+} + H_2O_2 \rightarrow Fe^{3+} + OH^- \qquad (10)$$

The iron released from oxidized metalloproteins enlarges its intracellular pool, favoring the production of hydroxyl radical through the Fenton reaction [247]. The production of hydroxyl radical is, as described before, of utmost importance in the inactivation of microorganisms, accelerating the process of DNA damaging [217].

Table 6. Inactivation of several microorganisms with the use of UV radiation.

Domain	Phylum	Microorganism	Type of suspension	Type of trial	Irradiance (W/m²)	Contact time (min)	Initial cellular density (CFU/mL)	Log reduction	Reference
Bacteria	Firmicutes	Bacillus subtilis spores	Axenic	Suspension	45[a]	a	10^5–10^6	99.9[b]	[243]
		Clostridium difficile Spores	Axenic	Surface	36000[c]	17	10^6–10^7	3	[241]
		Enterococci	Wastewater	Suspension	e,g	180	10^5	2	[143,223]
		Vancomycin-resistant Enterococcus (VRE)	Wastewater	Surface	12000[c]	17(100[d])	10^5–10^7	5	[241,242]
		Enterococcus faecalis	Axenic	Suspension	80–100 (45[a])	10 (a)	10^5–10^7	1.2 (99.9[b])	[212,243]
		Staphylococcus aureus	Axenic	Suspension	45[a]	a	10^5–10^6	99.9[b]	[243]
		Methicillin-resistant Staphylococcus aureus (MRSA)	Wastewater	Surface	12000[c]	17(50[d])	10^5–10^7	4	[241,242]
	Proteobacteria	Acinetobacter baumannii	Axenic	Surface	12000[c]	17	10^6–10^7	4	[241]
		Escherichia coli	Wastewater Axenic	Suspension	100–140[f,g]	10–120(50[d])	10^5–10^7	5	[120,212, 223,242, 243]
		Pseudomonas aeruginosa	Wastewater Axenic	Suspension	f	120(50[d])	10^7	5	[120,242]
		Salmonella enterica	Axenic	Suspension	f	120	10^7	3	[120,243]
		Salmonella enteritidis	Axenic	Suspension	60–100	10	10^5–10^7	3	[212]
		Shigella sonnei	Axenic	Suspension	45[a]	a	10^5–10^6	99.9[b]	[243]
		Total Coliforms	Wastewater Axenic	Suspension	1.5–45[a] (e)	2, a	10^5–10^6	3 (99.9[b])	[143,180, 243]
		Vibrio anguillarum	Axenic	Suspension	30	n.a.	10^7	5	[219]
		Vibrio salmonicida	Axenic	Suspension	30	n.a.	10^7	5	[219]
		Yersinia ruckeri	Axenic	Suspension	30	n.a.	10^7	5	[219]

		Organism	Matrix					Ref.
-		Total heterotrophic bacteria	Wastewater	Suspension	g	30	10^6	6	[223]
Eukarya		*Acanthamoeba castellanii* cysts	Axenic	Suspension	45^a	a	10^5-10^6	99.9^b	[243]
	Ascomycota	*Aspergillus niger*	Wastewater	Suspension	g	30	10^3	3	[223]
	Basidiomycota	*Rhodotorula rubra*	Wastewater	Suspension	g	30	10^3	3	[223]

a- UV dose – $mW.s/cm^2$, b- %, c- mWs/cm^2, d – seconds, e - 800 W UV-lamp, f –3.42×10^{-5} Einsteins s^{-1}, g - low-pressure mercury lamp (emission line at 254 nm), n.a. – not available.

H_2O_2 can be used in both liquid and vapor phases. Hence, it is used in water disinfection (liquid phase) or in the disinfection of surfaces (vapor phase). Indeed, it is believed that the vapor phase has higher kinetic energies and is uncharged, so it can surround and penetrate the three-dimensional protein structures more easily, oxidizing buried cysteine residues and breaking vulnerable bonds between subunits [248]. Thus, an enhanced antimicrobial activity of hydrogen peroxide vapor when compared to its liquid state is usually reported [249-252].

Some studies reporting the utilization of hydrogen peroxide as a disinfectant are summarized in Table 7. Otter and co-workers [251] studied the effectiveness of hydrogen peroxide on the inactivation of nosocomial bacteria and spores on surfaces. After 90 minutes of contact with hydrogen peroxide vapor, all of the tested microorganisms were completely inactivated (Log reduction of 6). However, differences on the resistance against the hydrogen peroxide vapor treatment were observed. *Acinetobacter* showed the highest resistance to this treatment, while vancomycin-resistant enterococci were the first to be completely inactivated, after only 10 minutes of treatment. Hydrogen peroxide is also suitable to disinfect wastewater. Indeed, the density of total coliforms in wastewater was reduced 4 fold when using H_2O_2 up to 2.5 mL/L and a contact time of 3 h [253].

3.7. Comparison between photoinactivation and traditional disinfection methods

In contrast with the traditional disinfection methods described above, TiO_2-UV photocatalysis is not yet considered as an established water disinfection technology [255]. However, until this date, several reports showed the potential of this technique for disinfecting. Indeed, photocatalysis is a versatile and effective process that can be adapted for use in many applications for disinfection in both air and water matrices. Additionally, improved photocatalytic coatings are being developed, tested and even commercialized for use in the context of "self-disinfecting" materials. In this sense, the strength of photocatalytic disinfection lies in its versatility for use in many different applications [256]. Indeed, photocatalytic-based products already reached a global volume of US$848 Million in 2009 of which over 87% were related to products with self-cleaning activity used for construction [257]. Among these are glass coatings, cements and textile fibers [257],

commercialized by companies such as Pilkington, Italcementi Group and Taiheiyou Cement. Coatings and ceramics with antimicrobial activity are also commercialized by several companies. Deutsche Steinzeug company, which commercializes flags, tiles and sanitary ceramics and, company Kurare, which commercializes textile fibers containing TiO_2 photocatalysts, should be highlighted. Japanese Arc-Flash, the first company commercializing photocatalyst-based materials in 1992, uses a photocatalyst fixation technology that allows spraying the photocatalytic product directly on surfaces. The photocatalytic coating produced by Arc-Flash uses titania nanoparticles as main ingredient and is used to sterilize mildew, sanitize environments such as hospitals, residential kitchens, schools, and floors, killing bacteria with over 98% efficiency [257].

The versatility mentioned for photocatalysis is also reported for UV radiation. Advances in the optimization of UV reactors permitted to inactivate a high variety of waterborne microorganisms in few seconds [242]. However, there are still some limitations on the use of this technique. Very high values of irradiation (in most cases over 50 W/m^2) must be used to inactivate some microorganisms (Table 6), and even under these harsh conditions, inactivation of some microbial forms, such as *Clostridium difficile* spores, is not possible. Several studies where the effectiveness of UV treatment was directly compared with photocatalysis demonstrated that, as expected, UV treatment was less efficient than TiO_2-UV [105,116,118]. The use of a photocatalyst, in most cases decreases the need of high irradiation intensity and promotes the decrease of contact times. Ibanez and co-workers [116] verified that it was not possible to inactivate *Enterobacter cloacae, E. coli, P. aeruginosa* and *Salmonella typhimurium* with an UV irradiance of 55 W/m^2. However, when coupling UV irradiation with 0.1 g/L TiO_2, log reduction values around 6 were achieved for all the tested strains for the same time of contact. The decrease of contact time from 360 to 50 minutes to achieve 3 log reduction of the total heterotrophic bacteria of wastewater was also reported [118], when using a photon flux of approximately 390 mmol/h and 5 g/L of photocatalyst. More recently, Lin and co-workers [180] showed that it was possible to reduce the load of the total coliforms in wastewater 4 fold, when irradiance of 1.5 W/m^2 and a contact time of 120 s was coupled with the presence of a TiO_2 coated reactor, while a 3 fold reduction was obtained in the absence of the photocatalyst.

Ozonation is a technique that can promote total inactivation of most types of microorganisms under

Table 7. Inactivation of several microorganisms with the use hydrogen peroxide.

Domain	Phylum	Organism	Type of suspension	Type of trial	Hydrogen peroxide concentration (mL/L)	Contact time(min)	Initial cellular density (CFU/mL)	Log reduction	Reference
Bacteria	Firmicutes	*Bacillus subtilis*	Axenic	Surface	a	32	10^6	100^b	[252]
		Enterococcus faecalis	Axenic	Suspension	3-150	10	10^5-10^7	0.1	[212]
		Enterococcus faecium	Axenic	Surface	a	90	10^6	6	[251]
		Geobacillus stearothermophilus	Axenic	Surface	a	32-50	10^4-10^6	$4\,(100^b)$	[252,254]
		Staphylococcus aureus (MRSA)	Axenic	Surface	a	50-90	10^4-10^6	6	[251,254]
		Vancomycin-resistant *Enterococcus* (VRE)	Axenic	Surface	a	50 - 90	10^4 - 10^6	6	[251,254]
		Clostridium difficile	Axenic	Surface	a	50 - 90	10^4 - 10^6	6	[251,254]
	Proteobacteria	*Acinetobacter baumannii*	Axenic	Surface	a	90	10^6	6	[251]
		Acinetobacter sp.	Axenic	Surface	a	90	10^6	6	[251]
		Fecal Coliforms	Wastewater	Suspension	2.5	240	10^6	4	[253]
		Klebsiella pneumoniae	Axenic	Surface	a	90	10^6	6	[251]

a- Hydrogen Peroxide Vapor (HPV) was used, b -%.

low contact times, in most cases under 20 minutes, and with low O_3 doses, at most 4 mg/L – Table 5. However, it is important to note that ozonation may cause the formation of very harmful by-products, specially bromide and other brominated compounds [258]. Rizzo and co-workers [259] compared the efficiency of ozonation and photocatalysis for the treatment of urban wastewaters. In this work, it was shown that it was possible to obtain increased degradation of organic matter with the photocatalytic oxidation process, even at low TiO_2 concentrations. Furthermore, a 30 min photocatalytic treatment was found to produce an effluent complying with the trihalomethanes limit set by Italian regulation for wastewater reuse. Furthermore, the cost associated to the use of ozonation is still very high [260]. Additionally, the coupling of ozonation with photocatalysis was already studied. Moreira and co-workers [261] reported the use of photocatalytic ozonation for the disinfection of urban treated wastewaters. In this study, a photocatalytic ozonation system using TiO_2-coated glass Raschig rings with LEDs irradiation - two 10 W UV high intensity LEDs with dominant emission line at 382 nm - was tested in continuous mode. This study reported the reduction of enterococci, enterobacteria, and fungi from 10^5 - 10^6 CFU/100 mL to values around or below 10^1 CFU/100 mL; total heterotrophs presented lower reductions, but still reaching values of around 10^2 CFU/100 mL after the treatment.

The use of hydrogen peroxide to disinfect water requires, usually, high contact times (up to 240 minutes) or concentrations (up 150 mL/L) (Table 7). Lower contact times (90 minutes) are required to inactivate the microorganisms when the vapor phase is used (Table 7), suggesting that hydrogen peroxide is a good technique to disinfect surfaces. However, the toxic effects of H_2O_2, require the interdiction of the site to be disinfected [262] for periods up to 1 hour and 40 minutes. Also chlorination requires high contact times (up to 120 minutes) to be effective on the inactivation of microorganisms (Table 4). Additionally, some microorganisms are resistant to chlorination treatments [263,264]. Nevertheless, it is important to note that nowadays chlorination remains as the most used disinfection method [265]. This is mainly due to the fact that the new alternative processes require expensive chemicals or costly equipment to generate the disinfectant onsite. However, chlorination causes the formation of several highly toxic by-products. Among these, it is important to highlight the formation of trihalomethanes and dichloroacetic acid that are believed to be carcinogenic 266]. The existence of

these dangerous by-products leads to the necessity of coming up with suitable alternatives to chlorination. The main advantages and disadvantages of each of these techniques are summarized in Table 8.

Although promising, photocatalysis still faces some drawbacks when imposing itself as a reference disinfection technique. As for other disinfection methods, re-growth after photocatalytic treatment may occur [223,261]. In addition, one of the main problems, usually disregarded by most of works conducted up to now in this field, is the absence of knowledge on the long time effect of photoinactivation. Little is known on the type of organisms able to tolerate the oxidative stress imposed by photocatalysis; however, increased tolerance of antibiotic resistant bacteria when compared with the susceptible counterpart is reported [106]. This observation points out for the need of further studies on the type and fate of the organisms surviving the treatment. This is particularly important, because under real conditions it may be not economically feasible to use conditions guaranteeing the inactivation without regrowth of potentially dangerous microorganisms [267]. Furthermore, and in order to be applied in full scale, the optimization of the photocatalyst to fully take advantage of the visible light spectrum should be achieved. This optimization should be focused in the future either by the optimization of the photocatalytic material (TiO_2) or by the use of suitable supports (for example graphene).

Although being a very promising disinfection technology, the massive use of TiO_2 nanoparticles without a proper evaluation concerning of their antimicrobial potential can produce negative drawbacks. Indeed, using TiO_2 nanoparticles, even in those products not directly designed for disinfection, may cause the propagation of the aforementioned antibiotic and oxidative stress resistant microorganism in a worrisome scale. Thus, the definition of new standards to test the efficacy of photocatalytic systems, including organisms with high tolerance to oxidative stress and antibiotics, is a subject of utmost importance in nowadays society.

4. CONCLUSIONS

TiO_2-anatase is presently the most used photocatalyst for environmental applications due to its high stability, good location of the band edges, low charge transport resistance, high photocatalytic activity, high chemical and thermal stability, low toxicity and low price. However, to increase the usefulness of

Table 8. Comparison between the different disinfection techniques.

Disinfection Technique	Chlorination	Ozonation	Ultraviolet radiation	Hydrogen Peroxide	Photocatalysis
Advantages	· Inexpensive; · Relatively easy to handle, simple to dose, measure and control; · Proven to be effective against a wide variety of bacteria and viruses;	· One of the most effective disinfectants; widely used to inactivate pathogens in drinking water; · Needs short contact times; · Generated onsite, leading to fewer safety issues than other techniques;	· Simple to use · Highly effective for inactivating microorganisms; · Does not introduce chemicals or cause the production of harmful disinfection by-products in the water; · High versatility – can be applied to waster, air and surfaces treatment;	· Considered environmentally friendly because it can rapidly degrade into the innocuous products water and oxygen; · Demonstrates broad-spectrum efficacy against viruses, bacteria, yeasts, and bacterial spores	· Capable of inactivating microorganisms, including viruses, bacteria, spores and protozoa; · Does not cause the production of harmful disinfection by-products in water; · TiO_2 is cheap, innocuous and can be attached to different types of inert matrices; · Useful in developing countries where electricity is not available; · High versatility – can be applied to disinfect water, air and surfaces;
Disadvantages	· Some organisms tend to develop resistance and require a concentration higher than normal, diminishing the quality of water; · Formation of hazardous disinfection by-products, specially trihalomethanes (THMs) and nitrosamines; · Residuals are highly toxic to aquatic life; hence, a dechlorination step is needed;	· Formation of potentially harmful byproducts including bromate and other brominated disinfection by-products; · Due to its instability, ozone must be generated before use, which leads to high equipment and operating costs; · Low dosage may not effectively inactivate some viruses, spores and cysts;	· Needs shortwave radiation (<280 nm), which requires the set up of expensive lighting equipment and is associated with increased energy utilization; · Organisms can sometimes repair and reverse the destructive effects of UV (photo-reactivation); · The presence of solid particles in water can affect severely the UV efficiency;	· The presence of catalase or other peroxidases in these organisms can increase tolerance, when conjugated with lower concentrations of H_2O_2; · Higher concentrations of H_2O_2, between 10 and 30 %, and longer contact times are required for inactivation of spores; · During the H_2O_2 treatments the sites where	· Uses nanoparticles than can be harmful for the general health; · Its mainly active in the UV range, presenting still some limitations using visible light; · When used in suspension, brings complexity to the process for the recuperation of the photocatalyst;

· Mainly applied and limited to water treatment and surface cleaning;	· Lacks long residual activity, limiting its application in large distribution systems; · Mainly limited to water treatment, but can be use also for surface disinfection;	· Low dosage may not effectively inactivate some viruses, spores, and cysts; · During the UV treatments the sites where the treatments are applied are interdicted to humans due to the harmful effect of this type of radiation;	the treatments are applied are interdicted to humans due to the harmful effect of this chemical compound;	
References	[207,268]	[269-271]	[229,232-234,272]	[247,273]	[265,274,275]

titanium dioxide, it is necessary to increase its photoactivity and ability to absorb visible light. This review article presents an overview of the fundamentals of photocatalysis and briefly reviews the most relevant strategies to enhance the photocatalytic activity of TiO_2, aiming ultimately the indoor photoinactivation of harmful biological agents. Since TiO_2 may contribute to prevent nosocomial infections, its practical application in this field is strongly envisaged. TiO_2 photocatalysis, similarly to the phagocytic cells of the human immune system, use the cytotoxic effects of Reactive Oxygen Species (ROS) to inactivate microorganisms. These ROS are known to be highly reactive with biological molecules and thus they are effective for the inactivation various different types of microorganisms.

Photoinactivation of microorganisms under UV radiation using TiO_2 has been thoroughly studied with great success; a wide diversity of microorganisms has been studied, Gram-negative and Gram-positive bacteria, including dormant forms (cysts, spores) fungi, algae and protozoa. Targeting future commercial applications, the research was directed to the use of visible light instead of only on UV radiation, and of proper immobilization of the photocatalyst. TiO_2 doping and/or decoration with the objective of increasing photoactivity and photoabsorbance were briefly reviewed as well as the use of TiO_2/graphene composite photocatalysts. The use of graphene reduces the risks of health hazards because in TiO_2/graphene composites TiO_2 nanoparticles are attached to micro-size graphene platelets that prevent the catalyst to be absorbed by the human body. In the case of TiO_2/graphene composite photocatalyst, the decoration of TiO_2 with metals such as Ag and Au further decrease charge recombination, show plasmonic effect and reduce the redox overpotentials.

Although promising, photocatalysis still faces some drawbacks when imposing itself as a reference disinfection technique. Besides the mentioned limitations regarding the optimization of photocatalysts to attain visible light activity, the absence of knowledge on the long time effect of photoinactivation on microorganisms should be a matter of concern.

ACKNOWLEDGEMENTS

REFERENCES

[1] M. Ni, M.K.H. Leung, D.Y.C. Leung and K. Sumathy // *Renew. Sust. Energ. Rev.* **11** (2007) 401.

[2] S. Banerjee, D.D. Dionysiou and S.C. Pillai // *Appl. Catal. B-Environ.* **176–177** (2015) 396.

[3] F. Kapteijn, J. Rodriguez-Mirasol and J.A. Moulijn // *Appl. Catal. B-Environ* **9** (1996) 25.

[4] M. Kaneko and I. Okura, In: *Photocatalysis: Science and Technology* (Kodansha, 2002), p. 123.

[5] J.H. Carey, J. Lawrence and H.M. Tosine // *Bull. Environ. Contam. Toxicol.* **16** (1976) 697.

[6] M. Kaneko and I. Okura, In: *Photocatalysis: Science and Technology* (Kodansha, 2002), p. 157.

[7] T. Matsunaga, R. Tomoda, T. Nakajima and H. Wake // *FEMS Microbiol. Lett.* **29** (1985) 211.

[8] B. Meyer and B. Cookson // *J. Hosp. Infect.* **76** (2010) 200.

[9] B. Spellberg, R. Guidos, D. Gilbert, J. Bradley, H.W. Boucher, W.M. Scheld, J.G. Bartlett and J. Edwards // *Clin. Infect. Dis.* **46** (2008) 155.

[10] World Health Organization, *The world health report 2007 - A safer future: global public health security in the 21st century* (World Health Organization, Geneva, Switzerland, 2007).

[11] H.A. Foster, I.B. Ditta, S. Varghese and A. Steele // *Appl. Microbiol. Biotechnol.* **90** (2011) 1847.

[12] A. Fujishima and K. Honda // *Nature* **238** (1972) 37.

[13] A. Di Paola, M. Bellardita and L. Palmisano // *Catalysts* **3** (2013) 36.

[14] T.A. Kandiel, L. Robben, A. Alkaim and D. Bahnemann // *Photoch. Photob. Sci.* **12** (2013) 602.

[15] D.C. Hurum, A.G. Agrios, K.A. Gray, T. Rajh and M.C. Thurnauer // *J. of Phys. Chem. B* **107** (2003) 4545.

[16] T. Kawahara, Y. Konishi, H. Tada, N. Tohge, J. Nishii and S. Ito // *Angew. Chem.* **114** (2002) 2935.

[17] A. Mills, C. O'Rourke and K. Moore // *J. Photoch. Photobio. A* **310** (2015) 66.

[18] B. Liu, X. Zhao, C. Terashima, A. Fujishima and K. Nakata // *PCCP* **16** (2014) 8751.

[19] C.S. Turchi and D.F. Ollis // *J. Catal.* **122** (1990) 178.

[20] J. Ângelo, *Development and Characterization of Titania-based Photocatalysts and their Incorporation in Paint Coatings* (Chemical Engineering Department, Faculty of Engineering of the University of Porto, Porto, 2016).

[21] P. Salvador // *J. of Phys. Chem. C* **111** (2007) 17038.

[22] J.F. Montoya, M.F. Atitar, D.W. Bahnemann, J. Peral and P. Salvador // *J. of Phys. Chem. C* **118** (2014) 14276.

[23] R.A. Marcus // *J. Chem. Phys.* **24** (1956) 966.

[24] J.F. Montoya, J. Peral and P. Salvador // *J. of Phys. Chem. C* **118** (2014) 14266.

[25] R. Dillert, A. Engel, Gro, P. Lindner and D.W. Bahnemann // *PCCP* **15** (2013) 20876.

[26] A. Zaleska // *Recent Patents on Engineering* **2** (2008) 157.

[27] B. Ohtani, Y. Ogawa and S.I. Nishimoto // *J. Phys. Chem. B* **101** (1997) 3746.

[28] B. Ohtani, K. Iwai, S.I. Nishimoto and S. Sato // *J. Phys. Chem. B* **101** (1997) 3349.

[29] N. Wu, J. Wang, D.N. Tafen, H. Wang, J.G. Zheng, J.P. Lewis, X. Liu, S.S. Leonard and A. Manivannan // *JACS* **132** (2010) 6679.

[30] S. Rehman, R. Ullah, A.M. Butt and N.D. Gohar // *J. Hazard. Mater.* **170** (2009) 560.

[31] R. Van De Krol and M. Grätzel, In: *Photoelectrochemical Hydrogen Production* (Springer, 2011), p. 13.

[32] J. Blanco-Galvez, P. Fernandez-Ibanez and S. Malato-Rodriguez // *J. Sol. Energy Eng.* **129** (2007) 4.

[33] G. Fu, P.S. Vary and C.-T. Lin // *J. of Phys. Chem. B* **109** (2005) 8889.

[34] A. Ghicov, B. Schmidt, J. Kunze and P. Schmuki // *Chem. Phys. Lett.* **433** (2007) 323.

[35] J.-M. Herrmann, J. Disdier and P. Pichat // *Chem. Phys. Lett.* **108** (1984) 618.

[36] S.T. Martin, C.L. Morrison and M.R. Hoffmann // *J. Phys. Chem.* **98** (1994) 13695.

[37] J. Moser, M. Grätzel and R. Gallay // *Helv. Chim. Acta* **70** (1987) 1596.

[38] K. Wilke and H.D. Breuer // *J. Photoch. Photobio. A* **121** (1999) 49.

[39] J.C.S. Wu and C.-H. Chen // *J. Photoch. Photobio. A* **163** (2004) 509.

[40] J. Choi, H. Park and M.R. Hoffmann // *J. of Phys. Chem. C* **114** (2009) 783.

[41] S.N.R. Inturi, T. Boningari, M. Suidan and P.G. Smirniotis // *Appl. Catal. B-Environ.* **144** (2014) 333.

[42] R. Asahi, T. Morikawa, T. Ohwaki, K. Aoki and Y. Taga // *Science* **293** (2001) 269.

[43] D. Chen, Z. Jiang, J. Geng, Q. Wang and D. Yang // *Ind. Eng. Chem. Res.* **46** (2007) 2741.

[44] T. Lindgren, J.M. Mwabora, E. Avendaño, J. Jonsson, A. Hoel, C.-G. Granqvist and S.-E. Lindquist // *J. of Phys. Chem. B* **107** (2003) 5709.

[45] R. Nakamura, T. Tanaka and Y. Nakato // *J. of Phys. Chem. B* **108** (2004) 10617.

[46] W. Zhu, X. Qiu, V. Iancu, X.Q. Chen, H. Pan, W. Wang, N.M. Dimitrijevic, T. Rajh, H.M. Meyer, M.P. Paranthaman, G.M. Stocks, H.H. Weitering, B. Gu, G. Eres and Z. Zhang // *Phys. Rev. Lett.* **103** (2009) 226401.

[47] C. Burda, Y. Lou, X. Chen, A.C.S. Samia, J. Stout and J.L. Gole // *Nano Lett.* **3** (2003) 1049.

[48] T. Tachikawa, S. Tojo, K. Kawai, M. Endo, M. Fujitsuka, T. Ohno, K. Nishijima, Z. Miyamoto and T. Majima // *J. Phys. Chem. B* **108** (2004) 19299.

[49] J. Xu, Y. Ao, D. Fu and C. Yuan // *Appl. Surf. Sci.* **254** (2008) 3033.

[50] J.G. Yu, J.C. Yu, B. Cheng, S.K. Hark and K. Iu // *J. Solid State Chem.* **174** (2003) 372.

[51] H. Barndõk, D. Hermosilla, C. Han, D.D. Dionysiou, C. Negro and Á. Blanco // *Appl. Catal. B-Environ* **180** (2016) 44.

[52] N. Serpone // *J. of Phys. Chem. B* **110** (2006) 24287.

[53] M. Pelaez, N.T. Nolan, S.C. Pillai, M.K. Seery, P. Falaras, A.G. Kontos, P.S.M. Dunlop, J.W.J. Hamilton, J.A. Byrne, K. O'Shea, M.H. Entezari and D.D. Dionysiou // *Appl. Catal. B-Environ* **125** (2012) 331.

[54] S. Banerjee, S.C. Pillai, P. Falaras, K.E. O'Shea, J.A. Byrne and D.D. Dionysiou // *J. Phys. Chem. Lett.* **5** (2014) 2543.

[55] X. Li, P. Liu, Y. Mao, M. Xing and J. Zhang // *Appl. Catal. B-Environ* **164** (2015) 352.

[56] C. Di Valentin, G. Pacchioni, A. Selloni, S. Livraghi and E. Giamello // *J. Phys. Chem. B* **109** (2005) 11414.

[57] W. Ren, Z. Ai, F. Jia, L. Zhang, X. Fan and Z. Zou // *Appl. Catal. B-Environ* **69** (2007) 138.

[58] X. Ma, Y. Dai, M. Guo and B. Huang // *J. Phys. Chem. C* **117** (2013) 24496.

[59] J.A. Rengifo-Herrera and C. Pulgarin // *Sol. Energy* **84** (2010) 37.

[60] J.A. Rengifo-Herrera, K. Pierzchała, A. Sienkiewicz, L. Forró, J. Kiwi and C. Pulgarin // *Appl. Catal. B-Environ* **88** (2009) 398.

[61] S.T. Kochuveedu, D.-P. Kim and D.H. Kim // *J. Phys. Chem. C* **116** (2011) 2500.

[62] X. He, Y. Cai, H. Zhang and C. Liang // *J. Mater. Chem.* **21** (2011) 475.

[63] H. Tran, J. Scott, K. Chiang and R. Amal // *J. Photoch. Photobio. A* **183** (2006) 41.

[64] I.M. Arabatzis, T. Stergiopoulos, M.C. Bernard, D. Labou, S.G. Neophytides and P. Falaras // *Appl. Catal. B-Environ* **42** (2003) 187.

[65] L.G. Devi and R. Kavitha // *Appl. Catal. B-Environ* **140–141** (2013) 559.

[66] H. Park, Y. Park, W. Kim and W. Choi // *J. Photoch. Photobio. C* **15** (2013) 1.

[67] S.G. Kumar and L.G. Devi // *J. Phys. Chem. A* **115** (2011) 13211.

[68] R. Daghrir, P. Drogui and D. Robert // *Ind. Eng. Chem. Res.* **52** (2013) 3581.

[69] Y. Wen, H. Ding and Y. Shan // *Nanoscale* **3** (2011) 4411.

[70] S.S. Rayalu, D. Jose, M.V. Joshi, P.A. Mangrulkar, K. Shrestha and K. Klabunde // *Appl. Catal. B-Environ* **142–143** (2013) 684.

[71] S. Bouhadoun, C. Guillard, F. Dapozze, S. Singh, D. Amans, J. Bouclé and N. Herlin-Boime // *Appl. Catal. B-Environ* **174–175** (2015) 367.

[72] T. Hirakawa and P.V. Kamat // *JACS* **127** (2005) 3928.

[73] A. Kudo and Y. Miseki // *Chem. Soc. Rev.* **38** (2009) 253.

[74] K. Maeda, K. Teramura, D. Lu, N. Saito, Y. Inoue and K. Domen // *Angew. Chem.* **118** (2006) 7970.

[75] J. Sato, H. Kobayashi, K. Ikarashi, N. Saito, H. Nishiyama and Y. Inoue // *J. Phys. Chem. B* **108** (2004) 4369.

[76] G. Hu and B. Tang // *Mater. Chem. Phys.* **138** (2013) 608.

[77] K. Zhou, Y. Zhu, X. Yang, X. Jiang and C. Li // *New J. Chem.* **35** (2011) 353.

[78] S. Liu, H. Sun, S. Liu and S. Wang // *Chem. Eng. J.* **214** (2013) 298.

[79] H. Zhang, X. Lv, Y. Li, Y. Wang and J. Li // *ACS Nano* **4** (2010) 380.

[80] S. Malato, J. Blanco, A. Vidal and C. Richter // *Appl. Catal. B-Environ* **37** (2002) 1.

[81] J. Petlicki and T.G.M. van de Ven // *J. Chem. Soc., Faraday Trans.* **94** (1998) 2763.

[82] J.S. Lee, K.H. You and C.B. Park // *Adv. Mater.* **24** (2012) 1084.

[83] G. Li, T. Wang, Y. Zhu, S. Zhang, C. Mao, J. Wu, B. Jin and Y. Tian // *Appl. Surf. Sci.* **257** (2011) 6568.

[84] T.-D. Nguyen-Phan, V.H. Pham, E.W. Shin, H.-D. Pham, S. Kim, J.S. Chung, E.J. Kim and S.H. Hur // *Chem. Eng. J.* **170** (2011) 226.

[85] A. Tanaka, S. Sakaguchi, K. Hashimoto and H. Kominami // *ACS Catalysis* **3** (2012) 79.

[86] Y. Wang, J. Yu, W. Xiao and Q. Li // *J. Mater. Chem. A* **2** (2014) 3847.

[87] V. Subramanian, E.E. Wolf and P.V. Kamat // *JACS* **126** (2004) 4943.

[88] I. Vaz-Moreira, O.C. Nunes and C.M. Manaia // *FEMS Microbiology Reviews* **38** (2014) 761.

[89] C. Baker-Austin, M.S. Wright, R. Stepanauskas and J.V. McArthur // *Trends Microbiol* **14** (2006) 176.

[90] A. Hernandez, R.P. Mellado and J.L. Martinez // *Appl. Environ. Microbiol.* **64** (1998) 4317.

[91] E. Miyahara, M. Nishie, S. Takumi, H. Miyanohara, J. Nishi, K. Yoshiie, H. Oda, M. Takeuchi, M. Komatsu, K. Aoyama, M. Horiuchi and T. Takeuchi // *FEMS Microbiol. Lett.* **317** (2011) 109.

[92] A.C. Fluit and F.J. Schmitz // *Clin. Microbiol. Infect.* **10** (2004) 272.

[93] B.M. Babior // *Am. J. Med.* **109** (2000) 33.

[94] R.A. Miller and B.E. Britigan // *Clin. Microbiol. Rev.* **10** (1997) 1.

[95] W.D. Splettstoesser and P. Schuff-Werner // *Microsc. Res. Tech.* **57** (2002) 441.

[96] R.A. Clark // *J. Infect. Dis.* **161** (1990) 1140.

[97] J.C. Ireland, P. Klostermann, E.W. Rice and R.M. Clark // *Appl. Environ. Microbiol.* **59** (1993) 1668.

[98] Y. Kikuchi, K. Sunada, T. Iyoda, K. Hashimoto and A. Fujishima // *J. Photochem. Photobio. A* **106** (1997) 51.

[99] P.C. Maness, S. Smolinski, D.M. Blake, Z. Huang, E.J. Wolfrum and W.A. Jacoby // *Appl. Environ. Microbiol.* **65** (1999) 4094.

[100] M. Cho, H. Chung, W. Choi and J. Yoon // *Water Res.* **38** (2004) 1069.

[101] I. Paspaltsis, K. Kotta, R. Lagoudaki, N. Grigoriadis, I. Poulios and T. Sklaviadis // *J. Gen. Virol.* **87** (2006) 3125.

[102] V. Ramamurthy, *Organic Photochemistry* (Taylor & Francis, 1997).

[103] J.-J. Huang, H.-Y. Hu, Y.-H. Wu, B. Wei and Y. Lu // *Chemosphere* **90** (2013) 2247.

[104] L. Rizzo, A. Fiorentino and A. Anselmo // *Sci. Total Environ.* **427–428** (2012) 263.

[105] V.M. Sousa, C.M. Manaia, A. Mendes and O.C. Nunes // *J. Photochem. Photobio. A* **251** (2013) 148.

[106] T.M. Tsai, H.H. Chang, K.C. Chang, Y.L. Liu and C.C. Tseng // *J. Chem. Technol. Biotechnol.* **85** (2010) 1642.

[107] C. Coulon, A. Collignon, G. McDonnell and V. Thomas // *J. Clin. Microbiol.* **48** (2010) 2689.

[108] W.L. Nicholson, N. Munakata, G. Horneck, H.J. Melosh and P. Setlow // *Microbiol. Mol. Biol. R.* **64** (2000) 548.

[109] D. Gumy, A.G. Rincon, R. Hajdu and C. Pulgarin // *Solar Energy* **80** (2006) 1376.

[110] J.S. Wist, J. Dierolf, C. Torres and W. Pulgarin // *J. Photoch. Photobio. A* (2002) 241.

[111] J.C. Yu, W. Ho, J. Yu, H. Yip, P.K. Wong and J. Zhao // *Environ. Sci. Technol.* **39** (2005) 1175.

[112] M. Cho, H. Chung, W. Choi and J. Yoon // *Appl. Environ. Microb.* **71** (2005) 270.

[113] D.M. Blake, P.C. Maness, Z. Huang, E.J. Wolfrum, J. Huang and W.A. Jacoby // *Sep. Purif. Methods* **28** (1999) 1.

[114] C. Hu, Y. Lan, J. Qu, X. Hu and A. Wang // *J. Phys. Chem. B* **110** (2006) 4066.

[115] C. McCullagh, J.M.C. Robertson, D.W. Bahnemann and P.K.J. Robertson // *Res. Chem. Intermed.* **33** (2007) 359.

[116] J.A. Ibanez, M.I. Litter and R.A. Pizarro // *J. Photoch. Photobio. A* **157** (2003) 81.

[117] P.S.M. Dunlop, J.A. Byrne, N. Manga and B.R. Eggins // *J. Photoch. Photobio. A* **148** (2002) 355.

[118] R. Dillert, U. Siemon and D. Bahnemann // *Chem. Eng. Technol.* **21** (1998) 356.

[119] C.M.B. Carvalho, J.P.C. Tomé, M.A.F. Faustino, M.G.P.M.S. Neves, A.C. Tomé, J.A.S. Cavaleiro, L. Costa, E. Alves, A. Oliveira, Â. Cunha and A. Almeida // *J. Porphyrins Phthalocyanines* **13** (2009) 574.

[120] J.M.C. Robertson, P.K.J. Robertson and L.A. Lawton // *J. Photoch. Photobio. A* **175** (2005) 51.

[121] A.G. Rincon and C. Pulgarin // *Catal. Today* **101** (2005) 331.

[122] M. Wainwright // *Photoch. Photobio. Sci.* **3** (2004) 406.

[123] M.J. Casteel, K. Jayaraj, A. Gold, L.M. Ball and M.D. Sobsey // *Photochem. Photobiol.* **80** (2004) 294.

[124] J. Gamage and Z.S. Zhang // *Int. J. Photoenergy* (2010) Article ID 764870.

[125] Y. Oka, W.C. Kim, T. Yoshida, T. Hirashima, H. Mouri, H. Urade, Y. Itoh and T. Kubo // *J. Biomed. Mater. Res. B* **86B** (2008) 530.

[126] R. Baan, K. Straif, Y. Grosse, B. Secretan, F. El Ghissassi and V. Cogliano // *Lancet Oncol.* **7** (2006) 295.

[127] V.L. Colvin // *Nat. Biotech.* **21** (2003) 1166.

[128] L. Caballero, K.A. Whitehead, N.S. Allen and J. Verran // *J. Photoch. Photobio. A* **276** (2013) 50.

[129] T. Zuccheri, M. Colonna, I. Stefanini, C. Santini and D. Gioia // *Materials* **6** (2013) 3270.

[130] K.S. Yao, D.Y. Wang, C.Y. Chang, K.W. Weng, L.Y. Yang, S.J. Lee, T.C. Cheng and C.C. Hwang // *Surf. Coat. Technol.* **202** (2007) 1329.

[131] E.J. Wolfrum, J. Huang, D.M. Blake, P.-C. Maness, Z. Huang, J. Fiest and W.A. Jacoby // *Environ. Sci. Technol.* **36** (2002) 3412.

[132] A. Vohra, D.Y. Goswami, D.A. Deshpande and S.S. Block // *J. Ind. Microbiol. Biot.* **32** (2005) 364.

[133] E.V. Skorb, L.I. Antonouskaya, N.A. Belyasova, D.G. Shchukin, H. Möhwald and D.V. Sviridov // *Appl. Catal. B-Environ* **84** (2008) 94.

[134] S. Navalon, M. Alvaro, H. Garcia, D. Escrig and V. Costa // *Water Sci. Technol.* **59** (2009) 639.

[135] J. Lonnen, S. Kilvington, S.C. Kehoe, F. Al-Touati and K.G. McGuigan // *Water Res.* **39** (2005) 877.

[136] C.-Y. Lin and C.-S. Li // *Aerosol Sci. Technol.* **37** (2003) 162.

[137] K.P. Kühn, I.F. Chaberny, K. Massholder, M. Stickler, V.W. Benz, H.-G. Sonntag and L. Erdinger // *Chemosphere* **53** (2003) 71.

[138] S.-C. Kim and D.-K. Lee // *Microchem. J.* **80** (2005) 227.

[139] M.B. Fisher, D.A. Keane, P. Fernandez-Ibanez, J. Colreavy, S.J. Hinder, K.G. McGuigan and S.C. Pillai // *Appl. Catal. B-Environ.* **130** (2013) 8.

[140] A. Erkan, U. Bakir and G. Karakas // *J. Photoch. Photobio. A* **184** (2006) 313.

[141] P.S.M. Dunlop, C.P. Sheeran, J.A. Byrne, M.A.S. McMahon, M.A. Boyle and K.G. McGuigan // *J. Photoch. Photobio. A* **216** (2010) 303.

[142] C. Chawengkijwanich and Y. Hayata // *Int. J. Food Microbiol.* **123** (2008) 288.

[143] J.A. Herrera Melián, J.M. Doña Rodríguez, A. Vera Suárez, E. Tello Rendón, C. Valdés do Campo, J. Arana and J. Pérez Peña // *Chemosphere* **41** (2000) 323.

[144] J. Ângelo, L. Andrade and A. Mendes // *Appl. Catal. A-Gen.* **484** (2014) 17.

[145] M. Dizdaroglu, P. Jaruga, M. Birincioglu and H. Rodriguez // *Free Radical Biol. Med.* **32** (2002) 1102.

[146] T. Matsunaga, R. Tomoda, T. Nakajima, N. Nakamura and T. Komine // *Appl. Environ. Microb.* **54** (1988) 1330.

[147] C. Srinivasan and N. Somasundaram // *Curr. Sci. India* **85** (2003) 8.

[148] Z. Huang, P.-C. Maness, D.M. Blake, E.J. Wolfrum, S.L. Smolinski and W.A. Jacoby // *J. Photoch. Photobio. A* **130** (2000) 163.

[149] K. Sunada, T. Watanabe and K. Hashimoto // *J. Photoch. Photobio. A* **156** (2003) 227.

[150] W. Kangwansupamonkon, V. Lauruengtana, S. Surassmo and U. Ruktanonchai // *Nanomed-Nanotechnol.* **5** (2009) 240.

[151] L. Luo, L. Miao, S. Tanemura and M. Tanemura // *Mat. Sci. Eng. B* **148** (2008) 183.

[152] R. van Grieken, J. Marugán, C. Pablos, L. Furones and A. López // *Appl. Catal. B-Environ* **100** (2010) 212.

[153] Z.X. Lu, L. Zhou, Z.L. Zhang, W.L. Shi, Z.X. Xie, H.Y. Xie, D.W. Pang and P. Shen // *Langmuir* **19** (2003) 8765.

[154] P. Demchick and A.L. Koch // *J. Bacteriol.* **178** (1996) 768.

[155] ISO 27447:2009 *Fine ceramics (advanced ceramics, advanced technical ceramics) — Test method for antibacterial activity of semiconducting photocatalytic materials* (ISO, 2009).

[156] P. Fernández, J. Blanco, C. Sichel and S. Malato // *Catal. Today* **101** (2005) 345.

[157] A.G. Rincón and C. Pulgarin // *Appl. Catal. B-Environ.* **44** (2003) 263.

[158] A.K. Benabbou, Z. Derriche, C. Felix, P. Lejeune and C. Guillard // *Appl. Catal. B-Environ.* **76** (2007) 257.

[159] A. Pal, S.O. Pehkonen, L.E. Yu and M.B. Ray // *Ind. Eng. Chem. Res.* **47** (2008) 7580.

[160] W.-C.G. Armon and P. Bettane // *Waterborne Pathog.* **4** (2004) 8.

[161] E.S. Tuchina and V.V. Tuchin // *Laser Phys. Lett.* **7** (2010) 607.

[162] Y.W. Cheng, R.C.Y. Chan and P.K. Wong // *Water Res.* **41** (2007) 842.

[163] S. Tanaka, K. Ikeda, H. Miyasaka, Y. Shioi, Y. Suzuki, M. Tamoi, T. Takeda, S. Shigeoka, K. Harada and K. Hirata // *J. Biosci. Bioeng.* **112** (2011) 462.

[164] S.B. Farr and T. Kogoma // *Microbiol. Rev.* **55** (1991) 561.

[165] Y.-H. Tsuang, J.-S. Sun, Y.-C. Huang, C.-H. Lu, W.H.-S. Chang and C.-C. Wang // *Artif. Organs* **32** (2008) 167.

[166] N.S. Allen, M. Edge, G. Sandoval, J. Verran, J. Stratton and J. Maltby // *Photochem. Photobiol.* **81** (2005) 279.

[167] J. Podporska-Carroll, E. Panaitescu, B. Quilty, L. Wang, L. Menon and S.C. Pillai // *Appl. Catal. B-Environ.* **176–177** (2015) 70.

[168] U. Joost, K. Juganson, M. Visnapuu, M. Mortimer, A. Kahru, E. Nõmmiste, U. Joost, V. Kisand and A. Ivask // *J. Photoch. Photobio. B* **142** (2015) 178.

[169] A.C. Miranda, M. Lepretti, L. Rizzo, I. Caputo, V. Vaiano, O. Sacco, W.S. Lopes and D. Sannino // *Sci. Total Environ.* **554–555** (2016) 1.

[170] B. Kim, D. Kim, D. Cho and S. Cho // *Chemosphere* **52** (2003) 277.

[171] D. Venieri, E. Markogiannaki, E. Chatzisymeon, E. Diamadopoulos and D. Mantzavinos // *Photoch. Photobio. Sci.* **12** (2013) 645.

[172] C. Berberidou, I. Paspaltsis, E. Pavlidou, T. Sklaviadis and I. Poulios // *Appl. Catal. B-Environ.* **125** (2012) 375.

[173] J.-Y. Choi, K.-H. Kim, K.-C. Choy, K.-T. Oh and K.-N. Kim // *J. Biomed. Mater. Res. B* **80B** (2007) 353.

[174] T. Saito, T. Iwase, J. Horie and T. Morioka // *J. Photoch. Photobio. B* **14** (1992) 369.

[175] C. Sichel, M. de Cara, J. Tello, J. Blanco and P. Fernández-Ibáñez // *Appl. Catal. B-Environ.* **74** (2007) 152.

[176] J.H. Lee, M. Kang, S.-J. Choung, K. Ogino, S. Miyata, M.-S. Kim, J.-Y. Park and J.-B. Kim // *Water Res.* **38** (2004) 713.

[177] M. Agulló-Barceló, M.I. Polo-López, F. Lucena, J. Jofre and P. Fernández-Ibáñez // *Appl. Catal. B-Environ.* **136–137** (2013) 341.

[178] R.J. Watts, S. Kong, M.P. Orr, G.C. Miller and B.E. Henry // *Water Res.* **29** (1995) 95.

[179] J. Araña, J.A. Herrera Melián, J.M. Doña Rodriguez, O. González, Pérez Peña, P.M. Marrero Sosa and V. Espino Jiménez // *Catal. Today* **76** (2002) 279.

[180] C.-H. Lin, R.-F. Yu, W.-P. Cheng and C.-R. Liu // *J. Hazard. Mater.* **209–210** (2012) 348.

[181] A. Kubacka, M. Ferrer, A. Martínez-Arias and M. Fernández-García // *Appl. Catal. B-Environ.* **84** (2008) 87.

[182] W.-J. Chen, P.-J. Tsai and Y.-C. Chen // *Small* **4** (2008) 485.

[183] V. Rodríguez-González, S.O. Alfaro, L.M. Torres-Martínez, S.-H. Cho and S.-W. Lee // *Appl. Catal. B-Environ.* **98** (2010) 229.

[184] L. Zhang, M.D. Han, O.K. Tan, M.S. Tse, Y.X. Wang and C.C. Sze // *J. Mater. Chem. B* **1** (2013) 564.

[185] C.-L. Cheng, D.-S. Sun, W.-C. Chu, Y.-H. Tseng, H.-C. Ho, J.-B. Wang, P.-H. Chung, J.-H. Chen, P.-J. Tsai, N.-T. Lin, M.-S. Yu and H.-H. Chang // *J. Biomed. Sci.* **16** (2009) 7.

[186] O. Akhavan and E. Ghaderi // *J. Phys. Chem. C* **113** (2009) 20214.

[187] A. Pal, S.O. Pehkonen, L.E. Yu and M.B. Ray // *J. Photoch. Photobio. A* **186** (2007) 335.

[188] G. Veréb, L. Manczinger, A. Oszkó, A. Sienkiewicz, L. Forró, K. Mogyorósi, A. Dombi and K. Hernádi // *Appl. Catal. B-Environ* **129** (2013) 194.

[189] O. Akhavan, R. Azimirad, S. Safa and M.M. Larijani // *J. Mater. Chem.* **20** (2010) 7386.

[190] Y. Lan, C. Hu, X. Hu and J. Qu // *Appl. Catal. B-Environ.* **73** (2007) 354.

[191] D. Venieri, A. Fraggedaki, M. Kostadima, E. Chatzisymeon, V. Binas, A. Zachopoulos, G. Kiriakidis and D. Mantzavinos // *Appl. Catal. B-Environ* **154–155** (2014) 93.

[192] K. Pathakoti, S. Morrow, C. Han, M. Pelaez, X. He, D.D. Dionysiou and H.-M. Hwang // *Environ. Sci. Technol.* **47** (2013) 9988.

[193] R. Sadowski, M. Strus, M. Buchalska, P.B. Heczko and W. Macyk // *Photoch. Photobio. Sci.* **14** (2015) 514.

[194] P. Gao, A. Li, D.D. Sun and W.J. Ng // *J. Hazard. Mater.* **279** (2014) 96.

[195] H.M. Yadav, T.V. Kolekar, S.H. Pawar and J.-S. Kim // *J. Mater. Sci-Mater. M.* **27** (2016) 1.

[196] P. Magalhães, J. Ângelo, V.M. Sousa, O.C. Nunes, L. Andrade and A. Mendes // *Biochem. Eng. J.* **104** (2015) 20.

[197] D.-H. Kuo, W.-T. Hsu and Y.-Y. Yang // *Appl. Catal. B-Environ* **184** (2016) 191.

[198] Y.-H. Tseng, D.-S. Sun, W.-S. Wu, H. Chan, M.-S. Syue, H.-C. Ho and H.-H. Chang // *BBA - Gen. Subjects* (2013).

[199] W.A. Rutala and D.J. Weber // *Clin. Microbiol. Rev.* **10** (1997) 597.

[200] M. Deborde and U. von Gunten // *Water Res.* **42** (2008) 13.

[201] A.V. Levanov, I.V. Kuskov, E.E. Antipenko and V.V. Lunin // *Russ. J. Phys. Chem.* **86** (2012) 757.

[202] J.C. Crittenden, M.W. Harza, D.W. Hand and K.J. Howe, *MWH's Water Treatment: Principles and Design* (Wiley, 2012).

[203] W.A. Rutala and D.J. Weber, *C.f.D. Control, Guideline for disinfection and sterilization in healthcare facilities* (Centers for Disease Control, 2008).

[204] V. Lazarova, P. Savoye, M.L. Janex, E.R. Blatchley Iii and M. Pommepuy // *Water Sci. Technol.* **40** (1999) 203.

[205] G.P. Winward, L.M. Avery, T. Stephenson and B. Jefferson // *Water Res.* **42** (2008) 483.

[206] R. Virto, P. Mañas, I. Álvarez, S. Condon and J. Raso // *Appl. Environ. Microb.* **71** (2005) 5022.

[207] C. Shang and E.R. Blatchley Iii // *Water Res.* **35** (2001) 244.

[208] A. Hassen, A. Heyouni, H. Shayeb, M. Cherif and A. Boudabous // *Bioresour. Technol.* **72** (2000) 85.

[209] L.V. Venczel, M. Arrowood, M. Hurd and M.D. Sobsey // *Appl. Environ. Microb.* **63** (1997) 1598.

[210] G. Berg, D.R. Dahling, G.A. Brown and D. Berman // *Appl. Environ. Microb.* **36** (1978) 880.

[211] J.A. Tree, M.R. Adams and D.N. Lees // *Appl. Environ. Microb.* **69** (2003) 2038.

[212] J. Koivunen and H. Heinonen-Tanski // *Water Res.* **39** (2005) 1519.

[213] C.H. King, E.B. Shotts, R.E. Wooley and K.G. Porter // *Appl. Environ. Microb.* **54** (1988) 3023.

[214] S. Neralla, R.W. Weaver, B.J. Lesikar and R.A. Persyn // *Bioresour. Technol.* **75** (2000) 19.

[215] T.E. Agustina, H.M. Ang and V.K. Vareek // *Appl. Environ. Microb.* **6** (2005) 264.

[216] J. Hoigné and H. Bader // *Water Res.* **17** (1983) 173.

[217] J.A. Imlay // *Nat. Rev. Micro.* **11** (2013) 443.

[218] C.-S. Li and Y.-C. Wang // *AIHA Journal* **64** (2003) 533.

[219] H. Liltved, H. Hektoen and H. Efraimsen // *Aquacult. Eng.* **14** (1995) 107.

[220] C. Nebel, R.D. Gottschling, R.L. Hutchison, T.J. McBride, D.M. Taylor, J.L. Pavoni, M.E. Tittlebaum, H.E. Spencer and M. Fleischman // *J. Water Pollut. Control. Fed.* **45** (1973) 2493.

[221] J.C. Joret, J.C. Block and Y. Richard // *Ozone-Sci. Eng.* **4** (1982) 91.

[222] M.L. Janex, P. Savoye, M. Roustan, Z. Do-Quang, J.M. Laîné and V. Lazarova // *Ozone-Sci. Eng.* **22** (2000) 113.

[223] J.M. Sousa, G. Macedo, M. Pedrosa, C. Becerra-Castro, S. Castro-Silva, M.F.R. Pereira, A.M.T. Silva, O.C. Nunes and C.M. Manaia // *J. Hazard. Mater.* **323A** (2017) 434.

[224] J.G. Kim and A.E. Yousef // *J. Food Sci.* **65** (2000) 521.

[225] G.R. Burleson, T.M. Murray and M. Pollard // *Appl. Microbiol.* **29** (1975) 340.

[226] G.H.R. Silva, L.A. Daniel, H. Bruning and W.H. Rulkens // *Bioresour. Technol.* **101** (2010) 6981.

[227] J.L. Rennecker, B.J. Mariñas, J.H. Owens and E.W. Rice // *Water Res.* **33** (1999) 2481.

[228] S.K. Sastry, A.K. Datta and R.W. Worobo // *J. Food Sci.* **65** (2000) 90.

[229] *WHO (World Health Organization) Guidelines for Drinking-water Quality* (WHO, Geneva, Switzerland, 2011).

[230] C. Bouki, D. Venieri and E. Diamadopoulos // *Ecotox. Environ. Safe.* **91** (2013) 1.

[231] M.-T. Guo, Q.-B. Yuan and J. Yang // *Water Res.* **47** (2013) 6388.

[232] N. Goosen and G.F. Moolenaar // *DNA Repair* **7** (2008) 353.

[233] R.P. Rastogi, Richa, A. Kumar, M.B. Tyagi and R.P. Sinha // *J. Nucleic Acids* **2010** (2010).

[234] R.P. Sinha and D.-P. Hader // *Photoch. Photobio. Sci.* **1** (2002) 225.

[235] A.L. Santos, C. Moreirinha, D. Lopes, A.C. Esteves, I. Henriques, A. Almeida, M.R.M. Domingues, I. Delgadillo, A. Correia and Â. Cunha // *Environ. Sci. Technol.* **47** (2013) 6306.

[236] K.G. McGuigan, R.M. Conroy, H.-J. Mosler, M.d. Preez, E. Ubomba-Jaswa and P. Fernandez-Ibañez // *J. Hazard. Mater.* **235–236** (2012) 29.

[237] L. Rizzo, C. Manaia, C. Merlin, T. Schwartz, C. Dagot, M.C. Ploy, I. Michael and D. Fatta-Kassinos // *Sci. Total Environ.* **447** (2013) 345.

[238] W.A.M. Hijnen, E.F. Beerendonk and G.J. Medema // *Water Res.* **40** (2006) 3.

[239] T. Bintsis, E. Litopoulou-Tzanetaki and R.K. Robinson // *J. Sci. Food Agric.* **80** (2000) 637.

[240] E. Levetin, R. Shaughnessy, C.A. Rogers, R. Scheir // Appl. Environ. Microb., 67 (2001) 3712-3715.

[241] W.A. Rutala, M.F. Gergen and D.J. Weber // *Infect. Cont. Hosp. Ep.* **31** (2010) 1025.

[242] C.W. McKinney and A. Pruden // *Environ. Sci. Technol.* **46** (2012) 13393.

[243] J.C. Chang, S.F. Ossoff, D.C. Lobe, M.H. Dorfman, C.M. Dumais, R.G. Qualls and J.D. Johnson // *Appl. Environ. Microb.* **49** (1985) 1361.

[244] P. Drogui, S. Elmaleh, M. Rumeau, C. Bernard and A. Rambaud // *J. Appl. Electrochem.* **31** (2001) 877.

[245] F. Haber and J. Weiss, *The Catalytic Decomposition of Hydrogen Peroxide by Iron Salts* (1934).

[246] J.P. Kehrer // *Toxicology* **149** (2000) 43.

[247] E. Linley, S.P. Denyer, G. McDonnell, C. Simons and J.-Y. Maillard // *J. Antimicrob. Chemother.* **67** (2012) 1589.

[248] M. Finnegan, E. Linley, S.P. Denyer, G. McDonnell, C. Simons and J.-Y. Maillard // *J. Antimicrob. Chemother.* **65** (2010) 2108.

[249] G. Fichet, E. Comoy, C. Duval, K. Antloga, C. Dehen, A. Charbonnier, G. McDonnell, P. Brown, C. Ida Lasmézas and J.-P. Deslys // *The Lancet* **364** (2004) 521.

[250] G. Fichet, K. Antloga, E. Comoy, J.P. Deslys and G. McDonnell // *J. Hosp. Infect.* **67** (2007) 278.

[251] J.A. Otter and G.L. French // *J. Clin. Microbiol.* **47** (2009) 205.

[252] N.A. Klapes and D. Vesley // *Appl. Environ. Microb.* **56** (1990) 503.

[253] M. Ksibi // *Chem. Eng. J.* **119** (2006) 161.

[254] S. Lemmen, S. Scheithauer, H. Häfner, S. Yezli, M. Mohr and J.A. Otter // *Am. J. Infect. Control* **43** (2015) 82.

[255] *Water treatment manual: disinfection* (United States Environmental Protection Agency, 2011).

[256] J. Gamage and Z. Zhang // *Int. J. Photoenergy* **2010** (2010).

[257] D. Spasiano, R. Marotta, S. Malato, P. Fernandez-Ibañez and I. Di Somma // *Appl. Catal. B-Environ* **170–171** (2015) 90.

[258] M.S. Siddiqui, G.L. Amy and R.G. Rice // *J. Am. Water Works Ass.* **87** (1995) 58.

[259] L. Rizzo, H. Selcuk, A.D. Nikolaou, S. Meriç Pagano and V. Belgiorno // *Desalin. Water Treat.* **52** (2013) 1414.

[260] L. Prieto-Rodríguez, I. Oller, N. Klamerth, A. Agüera, E.M. Rodríguez and S. Malato // *Water Res.* **47** (2013) 1521.

[261] N.F.F. Moreira, J.M. Sousa, G. Macedo, A.R. Ribeiro, L. Barreiros, M. Pedrosa, J.L. Faria, M.F.R. Pereira, S. Castro-Silva, M.A. Segundo, C.M. Manaia, O.C. Nunes and A.M.T. Silva // *Water Res.* **94** (2016) 10.

[262] C. Blazejewski, F. Wallet, A. Rouzé, R. Le Guern, S. Ponthieux, J. Salleron and S. Nseir // *Critical Care* **19** (2015) 30.

[263] K.E. Wainwright, M. Lagunas-Solar, M.A. Miller, B.C. Barr, I.A. Gardner, C. Pina, A.C. Melli, A.E. Packham, N. Zeng, T. Truong and P.A. Conrad // *Appl. Environ. Microb.* **73** (2007) 5663.

[264] M.W. LeChevallier, C.D. Cawthon and R.G. Lee // *Appl. Environ. Microb.* **54** (1988) 649.

[265] O.K. Dalrymple, E. Stefanakos, M.A. Trotz and D.Y. Goswami // *Appl. Catal. B-Environ* **98** (2010) 27.

[266] G.A. Boorman // *Environ. Health Perspect.* **107** (1999) 207.

[267] P.S.M. Dunlop, M. Ciavola, L. Rizzo, D.A. McDowell and J.A. Byrne // *Catal. Today* **240 Part A** (2015) 55.

[268] D. Nozaic // *Water Sa* **30** (2004) 18.

[269] R.G. Rice // *Ozone-Sci. Eng.* **21** (1999) 99.

[270] V. Camel and A. Bermond // *Water Res.* **32** (1998) 3208.

[271] *Wastewater technology fact sheet [electronic resource]: ozone disinfection* (United States Environmental Protection Agency, Office of Water, Washington, D.C., 1999).

[272] *Wastewater technology fact sheet [electronic resource] : ultraviolet disinfection* (United States Environmental Protection Agency, Office of Water, Washington, D.C., 1999).

[273] G. McDonnell and A.D. Russell // *Clin. Microbiol. Rev.* **12** (1999) 147.

[274] S. Malato, P. Fernández-Ibáñez, M.I. Maldonado, J. Blanco and W. Gernjak // *Catal. Today* **147** (2009) 1.

[275] Q. Li, S. Mahendra, D.Y. Lyon, L. Brunet, M.V. Liga, D. Li and P.J.J. Alvarez // *Water Res.* **42** (2008) 4591.

Contents lists available at ScienceDirect

Biochemical Engineering Journal

Synthesis and assessment of a graphene-based composite photocatalyst

Pedro Magalhães, Joana Ângelo, Vera M. Sousa, Olga C. Nunes, Luísa Andrade, Adélio Mendes *

LEPABE – Faculdade de Engenharia, Universidade do Porto, Rua Dr. Roberto Frias, 4200-465 Porto, Portugal

ARTICLE INFO

ABSTRACT

A novel composite photocatalyst prepared from graphene and commercial TiO_2 (P25 from Evonik) was synthesized, exhibiting enhanced photocatalytic activity for methylene blue degradation, when compared with pristine P25. Additionally, the new catalyst showed 20% more NO conversion under UV light than P25. The band gap of the catalyst, obtained from diffuse reflectance, was 2.95 eV indicating an extended light absorption up to 420 nm. The novel photocatalyst was further tested for inactivating microorganisms showing better results than the reference photocatalyst. Under visible light, the viability loss of the reference bacterial strain *Escherichia coli* DSM 1103 was two times higher than with the bare P25; it was observed 29% of inactivation with the P25/graphene composite and 14% with the P25 sample, following standard ISO 27447:2009.

© 2015 Elsevier B.V. All rights reserved.

1. Introduction

Photocatalysis has attracted the attention of many researchers mainly because it can be used for photoabatement of atmospheric contaminants, water treatment and inactivation of microorganisms both in suspension and on surfaces [1,2]. More recently, photoinactivation of microorganisms has emerged as an alternative disinfection method [3]; especially the use of titanium dioxide in antimicrobial application has been widely discussed [2,3]. This special interest on TiO_2 material was fueled by the work by Fujishima and Honda [4] in 1972, describing for the first time water splitting using a TiO_2 photoelectrode.

Independently of the photocatalytic application, the mechanism behind photocatalysis consists in the generation of electron–hole pairs upon excitation of the photocatalyst with photons showing energy higher than the band gap (in the case of TiO_2 *ca.* 3.2 eV) – Eq. (1). These holes and electrons can oxidize and reduce surface-adsorbed molecules, respectively. The strong oxidation potential of the photogenerated valence band holes in anatase TiO_2 (E_{VB} = +3.0 V *vs.* normal hydrogen electrode (NHE), pH 1) originates the formation of hydroxyl radicals (OH$^\bullet$) when in contact with water – Eq. (2). The reduction potential of anatase TiO_2 conduction band electrons

is of *ca.* −0.2 V (pH 1) and reduces O_2 to produce superoxide radical ($O_2^{\bullet-}$) – Eq. (3) [5]. These free radicals intermediate the oxidation of organic species at, for example, the surface of microorganisms, originating ultimately their inactivation.

$$Semiconductor \xrightarrow{h\nu} e_{CB}^- + h_{VB}^+ \qquad (1)$$

$$Semiconductor\,(h_{VB}^+) + H_2O_{ads} \rightarrow Semiconductor + HO_{ads}^\bullet + H^+ \quad (2)$$

$$Semiconductor\,(e_{CB}^-) + O_{2ads} \rightarrow Semiconductor + O_2^{\bullet-} \qquad (3)$$

The extensive use of TiO_2 material as photocatalyst can be explained by its thermal and chemical stability, exhibiting no photocorrosion, readily available, relatively cheap and band edges that are well positioned for producing oxidizing/reducing agents [5]. However, TiO_2 absorbs only UV light, preventing its usage under visible spectrum; hence, many efforts have been powered to enhance titanium dioxide photocatalytic activity. Two main actions are being followed: (i) narrowing the semiconductor band gap (E_g); and (ii) decrease the e$^-$/h$^+$ recombination. While the first allows the photocatalyst to absorb a larger fraction of the solar spectrum and eventually reach the visible spectrum, the later allows improving the redox reactions rate at the photocatalyst surface. Several doping techniques have been described targeting the decrease of the semiconductor band gap [6,7]. Even though the doping mechanism is not yet fully understood, the two most used dopants of TiO_2 are C and N; these dopants act as substitutional anions (sub-

stitute oxygen) or interstitial cations (substitute titanium) [8,9]. On the other hand, to decrease e^-/h^+ recombination rate several studies suggest the use of carbon-based supports such as carbon nanotubes (CNTs), fullerene or graphene [8]. These materials have the ability to receive and store photoinjected electrons and thus preventing e^-/h^+ recombination. In most of the cases, partially oxidized graphene, known as graphene oxide (GO), is used instead of pure graphene due its tunable optical, conductive and chemical properties. Graphene oxide is obtained functionalizing graphene sheets with carboxylic acid, hydroxyl and/or epoxide groups, and thus its properties can be adjusted via chemical modification [10]. The binding of TiO_2 to graphene sheets allows improved photocatalytic performance when compared with their pristine form mainly because: (i) efficient charge separation and transportation; (ii) extended light absorption range; and (iii) enhanced adsorption [11]. TiO_2/graphene composites slow the rate of e^-/h^+ recombination after light excitation [12], increasing the charge transfer rate of electrons. The extended light absorption can be achieved due to doping of TiO_2 with carbon from the graphene, leading to a narrowing of the semiconductor band gap. The enhanced adsorption of the TiO_2/graphene composite is mainly attributed to its very large π-conjugation system and two-dimensional planar structure [11,13]. The increase in adsorption may enhance the photocatalytic degradation of methylene blue, assuming the adsorption of reactants is higher than the adsorption of the degradation products. Even though there are some works reporting the use of the TiO_2/graphene composites in areas such as dyes degradation evaluation [14] and microorganism photoinactivation [15], the use of TiO_2/graphene composites for NO deep oxidation has never been reported in literature.

In this work, a composite photocatalyst was prepared from commercial graphene (xGnP® from XG Sciences) and commercial TiO_2 (P25 from Evonik) and its performance compared with commercial photocatalysts – P25 and VLP7101 (Kronos). The band-gap of the prepared photocatalyst was assessed by diffuse reflectance and it was tested for methylene blue degradation and NO deep oxidation under UV-light. The photocatalyst was further tested for inactivating microorganisms both under UV radiation and visible light. The viability loss of the reference bacterial strain *E. coli* DSM 1103 was obtained for both types of radiation and compared with three commercial photocatalysts: P25, VLP7000 and VLP7101.

2. Materials and methods

2.1. Synthesis of P25/graphene composite photocatalyst

P25/graphene composite was prepared as described elsewhere [11] with minor modifications. Briefly, oxidized graphene nano-platelets (GNP_{ox}) – $KMnO_4$ 3:1 graphene nano-platelets (GNP) – were prepared according to a modified Hummer's method. Shortly, 50 mL of H_2SO_4 were added to 2 g of GNP at room temperature and the solution was cooled using an ice bath, followed by gradual addition of 6 g of $KMnO_4$. Then, 300 mL of distilled water was added, followed by addition of H_2O_2 until oxygen release stopped. GNP_{ox} was washed 5 times with water by centrifugation at 4000 rpm during 15 min. The solid was dispersed in 500 mL of water by sonication (Bandelin Sonorex R K512H) during 5 h and lyophilized during 72 h. Then, the composite was obtained *via* a hydrothermal method based on the work by Zhang et al. [11]. Briefly, 2 mg of GNP_{ox} was dissolved in a solution of distilled H_2O (20 mL) and ethanol (10 mL) by ultrasonic treatment for 1 h, and 0.2 g of P25 was added to the obtained GNP_{ox} solution and stirred for another 2 h to get a homogeneous suspension. The suspension was then placed in a 40 mL Teflon-sealed autoclave and maintained at 120 °C for 3 h to simultaneously achieve the reduction of GO and the deposition of P25 on

the carbon support. Finally, the resulting composite was recovered by filtration, rinsed by deionized water several times and dried at room temperature.

The photocatalytic activity of the as-prepared P25/graphene composite was then compared with three different commercial photocatalysts: Aeroxide® TiO_2 P25 (Evonik Industries, Germany), Kronos® VLP7000 and VLP7101 (KRONOS Worldwide, Inc., United States of America).

2.2. Characterization

2.2.1. Diffuse reflectance analyses

Diffuse reflectance spectroscopy is often used to determine the absorption properties of both crystalline and amorphous materials [16]. The band gap of a sample can be obtained from the Tauc equation, which relates the diffuse reflectance and the Kubelka–Munk model to the excitation frequency [16]:

$$(h\nu F(R_\infty))^{1/n} = A\left(h\nu - E_g\right) \tag{4}$$

where, h is the Planck constant, ν is the frequency of vibration, A is a constant and E_g is the band gap energy.

This equation is obtained multiplying the Kubelka–Munk equation by the energy of the incident radiation ($E = h\nu$) and powered to a coefficient n, according to the type of the electronic transition of the material. For indirect transitions n equals 2 and for direct transition n is 1/2. Plotting the modified Kubelka–Munk equation as a function of the incident radiation, the band gap of the semiconductor can be obtained extrapolating the linear part of this curve to the x-axis, the so-called Tauc plot; the band gap energy is read at the intersection. Diffuse reflectance of the different samples were obtained in a Shimatzu UV-3600 UV–vis-NIR spectrophotometer, equipped with a 150 mm integrating sphere and using $BaSO_4$ as 100% reflectance standard. The samples were pressed to form a flat disc that fit into the spectrophotometer sample holder.

2.2.2. SEM and XRD analyses

The morphology and composition of the photocatalysts was obtained from scanning electron microscopy (SEM) coupled with energy dispersive X-ray (EDX) analysis. A FEI Quanta 400FEG ESEM/EDAX Genesis X4 M apparatus equipped with a Schottky field emission gun (for optimal spatial resolution) was used for the characterization of the surface morphology of the photocatalysts with SEM. Images were digitally recorded using a Gatan SC 1000 ORIUS CCD camera (Warrendale, PA, USA). These SEM/EDX analyses were made at Centro de Materiais da Universidade do Porto (CEMUP).

The crystallographic characterization of the samples was performed by X-ray diffraction (XRD). The XRD pattern of the selected samples was obtained using a Denchtop X-Ray Diffractometer RIGAKU, model MiniFlex II using Cu X-ray tube (30 KV/15 mA). The data was obtained at 2θ angles (10–80°), with a step speed of 3.5°/min. Debye–Scherrer equation was used to determine the crystallite size. The obtained X-ray scans were compared to those of standard database and the phases were assigned comparing with data available in literature.

2.3. Photoactivity characterization

The photocatalytic performance of the as prepared semiconductors was determined by: (a) degradation of dye methylene blue, (b) nitrogen oxide (NO) deep oxidation and (c) photoinactivation of microorganisms. Each of these techniques is described next.

2.3.1. Methylene blue degradation

The photodegradation history of methylene blue (MB) dyes was followed by photospectroscopy. In a typical process, aqueous

solution of MB dye (0.01 g/L, *i.e.* 2.7×10^5 M, 100 mL) and photocatalysts (50 mg) were placed in a 250 mL cylindrical glass vessel. Under ambient conditions and stirring, the photoreactor vessel was exposed to the UV irradiation produced by an ultraviolet (UV-A, highest emission at 365 nm) lamp with two 6 W black-light-blue bulbs (VL-206-BLB, Vilbert Lourmat, France); the lamp was positioned 10 cm away from the vessel (intensity at the catalyst mixture surface was measured with a UV radiometer (HD 2102.2, Delta/OHM, Italy) being 10 W m^{-2}). The trial began by putting the mixture during 30 min in the dark; the mixture was then illuminated for 4 h. Samples were collected every 30 min, centrifuged and the supernatant was analyzed in an UV–vis absorption spectrophotometer (Shimatzu UV-3600 UV–vis-NIR spectrophotometer).

2.3.2. Nitrogen oxide (NO) deep oxidation

The experimental setup used in NO deep oxidation tests were based on standard ISO 22197-1:2007 [17]. The experimental setup consists of four main sections: (i) feed, (ii) reactor, (iii) NO$_x$ quantification and (iv) computer monitoring/control [18]. Semiconductors were tested as powder films pressed on aluminum slabs with an area of 2 cm × 2 cm. A 50% of relative humidity feed stream was supplied, with a feed rate of 0.7 L min^{-1} of NO at 1 ppmv in air at 25 °C. The irradiation was provided by a UV lamp (VL-206-BLB, Vilbert Lourmat, France) with an irradiation of 10 W m^{-2}. The photocatalytic activity was assessed from the NO conversion (Eq. (5)):

$$X_{NO} = \left(\frac{C_{NO}^{in} - C_{NO}^{out}}{C_{NO}^{in}} \right) \times 100 \tag{5}$$

where X_{NO} is the conversion of NO, C_{NO} stands for NO concentration and the superscripts (in and out) refer to the inlet and outlet streams.

2.3.3. Photoinactivation of microorganisms

(a) Bacterial strains and culture conditions

E. coli DSM 1103 was used in the photoinactivation trials. *E. coli* cells were grown overnight (18–20 h) at 30 °C on Plating Count Agar (PCA, LiofilChem, Italy) and the biomass was used to prepare a suspension in sterile saline solution [0.85% NaCl (w/v)]. The cell density of the suspension was adjusted to 10^6 CFU mL^{-1} [19] or 10^3 CFU mL^{-1} using a calibration curve of optical density *versus* number of viable cells [colony forming units (CFU) mL^{-1}].

(b) Light source and apparatus

A high intensity, long-wave (highest emission at 365 nm) ultraviolet (UV-A) lamp with two 6 W black-light-blue bulbs (VL-206-BLB, Vilbert Lourmat, France) was employed on the UV trials. The incident photon flux was 10 W m^{-2} according to the standard [19]. The visible light trials were conducted with a regular fluorescent light (Philips Master TL-Mini Super 80 6 W/840) with a light intensity of 50 W m^{-2}.

(c) Experimental procedure for *E. coli* photoinactivation in suspension

The experimental procedure for determining the *E. coli* DSM 1103 photoinactivation is described elsewhere [20]. Briefly, the photocatalyst (P25, P25/graphene, VLP7000 or VLP7101) was added to the cell suspension at a concentration of 0.2% (w/v). For each photocatalyst two initial cellular densities (10^3 or 10^6 CFU mL^{-1}) were tested. The mixture was stirred (250 rpm) and irradiated with UV radiation or visible light for 40 min. After this time, the mixture was kept in the dark for 20 min for ensuring that the photocatalyst had no activity, which usually is still observed for a few minutes after being irradiated [21].

At the initial (t_i = 0 min) and final time (t_f = 40 + 20 min), the cell suspension was serially diluted in sterile saline solution and aliquots of 100 μL were spread on PCA, as described in Koch [22]. After incubation at 30 °C for 24 h, the colony forming units, corresponding to the viable cells, were enumerated in plates containing 30–300 CFU. The photoinactivation fraction (=viability loss) and log reduction were determined as shown in Eq. (6) and Eq. (7), respectively:
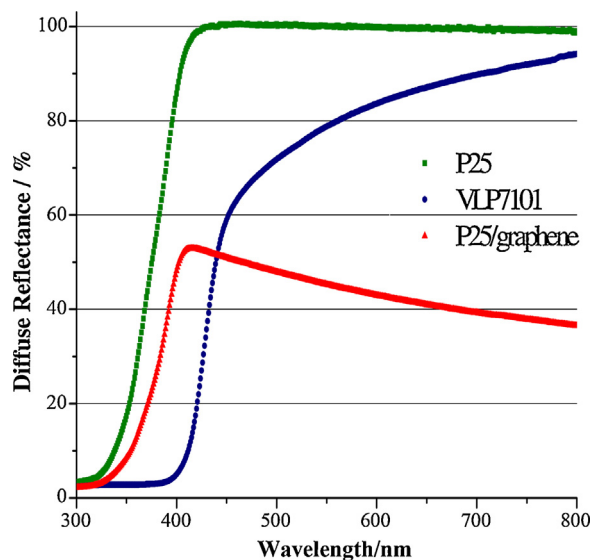
$$\text{Viability loss}(\%) = \left(\frac{M_i - M_f}{M_i} \right) \times 100 \tag{6}$$

$$\text{Log reduction} = \log M_i - \log M_f \tag{7}$$

where M_i and M_f are the initial and final *E. coli* viable counts, respectively.

(d) Controls

Control assays in the dark, under UV radiation and under visible light in the absence of photocatalyst were performed to assess the influence of the experimental conditions and of the irradiation on cell inactivation, respectively. All the assays were performed in triplicate, inside a clean chamber.

3. Results and discussion

3.1. Photocatalysts characterization

The band gaps of the three photocatalysts used in this work – P25, VLP7101 and P25/graphene – were calculated from the diffuse reflectance spectra (Fig. 1). The band gap obtained for the composite photocatalyst was 2.95 eV, whilst the values obtained for commercial P25 were 3.03 eV and 3.16 eV, corresponding to the two different crystalline forms of titanium dioxide – respectively, rutile and anatase, and for VLP7101 was 2.75 eV. The slight decrease in the band gap between P25/graphene and P25 may be attributed to some doping of TiO$_2$ by the carbon molecules of graphene [11]. The specific mechanism of carbon doping is not yet fully understood. However, several authors reported that carbon doping leads to a band gap narrowing, causing a red-shift in the absorption spectrum of the photocatalyst [8]. Carbon dopant can be a substitutional anion (substitutes oxygen) or an interstitial cation (substitutes titanium). The substitutional anion behavior of carbon is related to its −4 oxidation state in the Ti—C bond in carbides, and the interstitial cation behavior is related to its +4 state in the C—O bond in carbonates [8]; decreases in the TiO$_2$ band gap originated by carbon doping can range from 0.1 eV to 1.05 eV [8]. However, there is a threshold for dopant concentration at around 2% of the photocatalyst mass; high dopant concentration leads to a dopant segregation
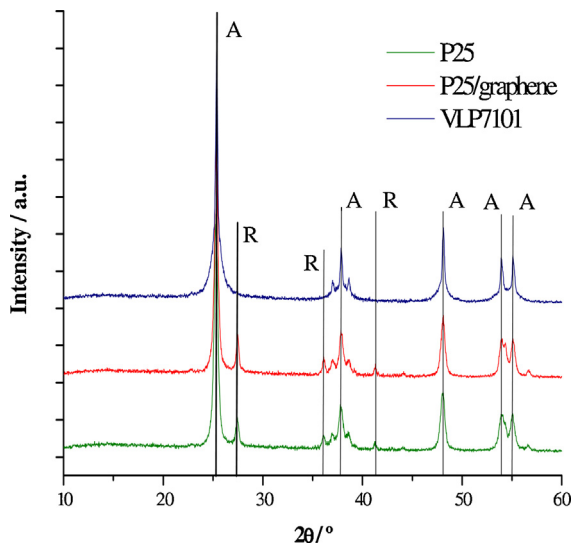

Fig. 1. Diffuse reflectance spectra of VLP7101, P25 and P25/graphene photocatalysts.

Fig. 2. XRD patterns of VLP7101, P25 and P25/graphene photocatalysts.

phase [23]. Furthermore, the enhanced photocatalytic activity of VLP7101 can also be ascribed to the presence of an organic sensitizer, as it was already reported [24].

XRD analyses were performed to assess the crystallinity of the photocatalysts – Fig. 2. XRD allows determining the crystalline structure of the photocatalysts and, in some cases, to determine the crystal size.

The composite photocatalyst showed similar XRD pattern when compared to P25. Furthermore, no diffraction peaks for carbon species were observed in the composite, which might be due to its low amount and relatively low diffraction intensity of graphene. Furthermore, the similarity of patterns between P25 and the P25/graphene composite evidences that crystallinity, crystal size and modifications on the crystal structure of TiO_2 are not responsible for differences between the photocatalytic activity of these two photocatalysts. It is also possible to observe that VLP7101 is only anatase, contrarily to P25 that is composed by anatase and rutile. Even though it is believed that the interaction between anatase and rutile phases (80/20 wt.%) improve the photoactivity of P25 [25], VLP7101 present normally higher photoactivity than P25 [18]; this higher catalytic activity was ascribed to an aromatic carbon compound photo sensitizer, as reported elsewhere [24].

SEM images of P25 and VLP7101 are presented in Figs. 3 and 4.

Fig. 3 shows the morphology of P25 sample. The high agglomeration observed is caused by the high surface energy of the nanoparticles [26]. As it can be seen, the primary particles present sizes in nanometer range. These particles agglomerate forming aggregates with different shapes and morphologies, which influence the surface roughness, haze and transparency of the bulk material [26]. The approximate size of the P25 nanoparticles is between 15 and 30 nm, which is in accordance with values presented in literature [27].
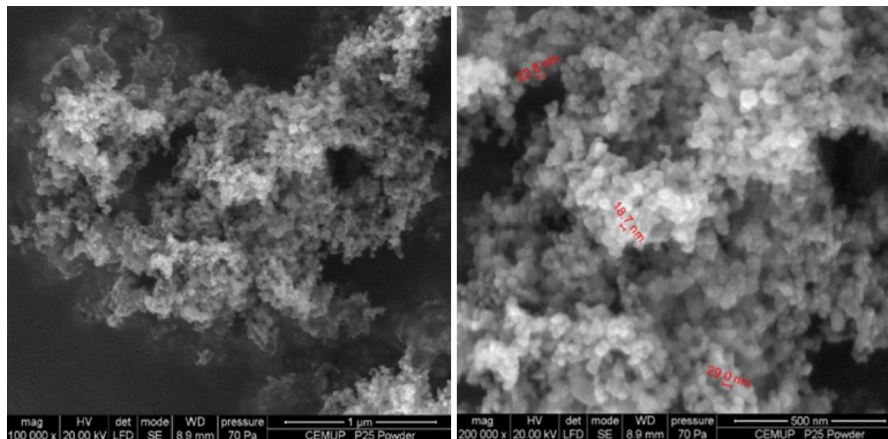
Fig. 3. SEM images of P25.
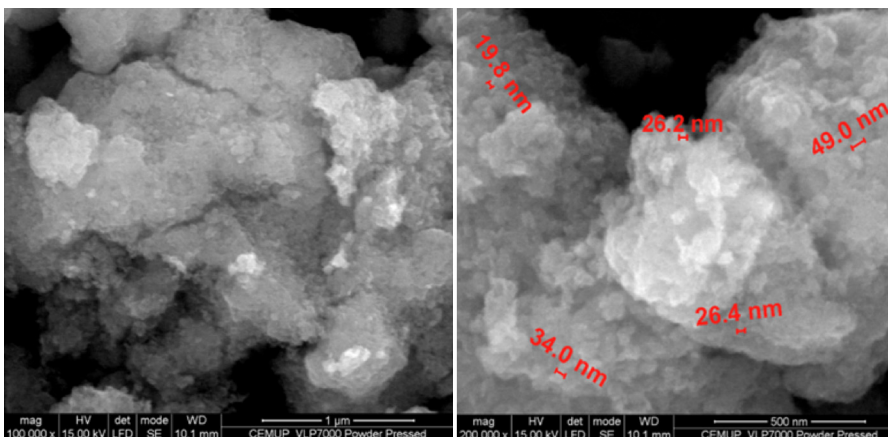
Fig. 4. SEM images of VLP7101.
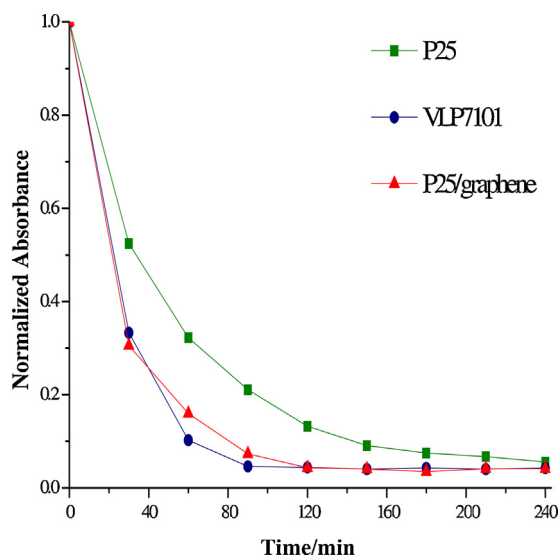
Fig. 5. Normalized absorbance values of methylene blue degradation during 240 min (lines were added to improve the readability) for P25 and VLP70101 commercial photocatalysts and P25/graphene photocatalyst.

Fig. 6. NO conversion for P25 and P25/graphene composite during 150 h under UV radiation.

Fig. 4 shows two SEM images of VLP7101 photocatalyst. The particles have a size of 15–50 nm and form also large agglomerates. P25/graphene composite, as already shown previously [11], is composed by P25 nanoparticles deposited on the graphene sheets. These particles bond preferably to the wrinkles and edges of the graphene nanoplatelets, initially covered with carboxylic acid groups. These carboxylic acid groups interact with the hydroxyl groups forming chemical P25/graphene bonds [11].

3.2. Photoactivity characterization

The photoactivity of the composite photocatalyst, P25 and VLP7101 was assessed based on the methylene blue degradation history and NO photo-conversion. Regarding the methylene blue degradation under UV radiation it is possible to observe in Fig. 5 an increase in the activity of the composite photocatalyst when compared with commercial P25. Comparing the synthesized photocatalyst with VLP7101, both showed similar activities.

The increased photocatalytic activity of the P25/graphene composite to the methylene blue degradation compared to pristine P25 should be ascribed to the decrease of e^-/h^+ recombination, which is related to the ability of graphene to accept photogenerated electrons by P25 [11], and to an increased adsorption of methylene blue in the support graphene sheets. Actually, graphene support has a much higher adsorption capacity compared with P25 particles. For the relevant methylene blue concentrations, the equilibrium adsorbed concentration on P25 was 4 orders of magnitude smaller than on the graphene used, while on P25/graphene composite was 2 orders of magnitude smaller. This points out for the critical role of the graphene support in the P25/graphene photocatalyst concerning the methylene blue adsorption.

Nguyen-Phan et al. [28] reported the preparation of TiO$_2$/graphene composites with enhanced adsorption and photocatalytic activity under both UV and visible radiation. These authors state that the increase in graphene content, from 1 to 10 wt.%, facilitates the photodegradation rate of methylene blue. The greater photocatalytic performance of TiO$_2$/graphene composite was attributed to the formation of both π–π conjugations between dye molecules and aromatic rings and to ionic interactions between methylene blue and oxygen-containing functional groups at the edges or on the surfaces of carbon-based nanosheets.

Graphene oxide works as adsorbent for the methylene blue, electron acceptor and photosensitizer originating an enhanced dye photodecomposition.

Methylene blue degradation is a technique widely used to assess the photocatalytic activity due to its simplicity and easy use. However, this relevant standard [29] presents limitations. This standard assumes the use of methylene blue with very high purity, which is not always possible to obtain. The pH of the solution should be defined as it influences the adsorption of methylene blue on titanium dioxide. Finally, the standard is mainly applicable to low active photocatalytic films due to problems of stirring and diffusion, among others [30]. Standard ISO 22197-1:2007 [17] uses NO photooxidation to infer about the photoactivity. Since NO is gas, the mass transfer limitations associated to the methylene blue method do not hold here. Because that, this standard is now recommended though its higher complexity. Fig. 6 shows NO conversion history catalyzed by P25, VLP7101 and P25/graphene, under UV light.

The prepared photocatalyst presented higher initial and steady state NO conversion than P25 and VLP7101. Furthermore, after the first 24 h, the prepared photocatalyst showed good stability throughout the 150 h. This increased conversion can be ascribed to several factors that were already discussed before. P25/graphene composite slows e^-/h^+ recombination rate since graphene support increases the draining rate of electrons. Then, the extended light absorption of P25/graphene, supported by a smaller band gap (2.95 eV), allows the absorption of a broader range of wavelengths.

Finally, aiming for a possible future commercial application of the composite photocatalyst, photoinactivation trials were conducted. The initial value of cellular density used was chosen to be around 1×10^6 CFU mL^{-1}, based on standard ISO 27447:2009 used for evaluating the antibacterial activity of semiconducting photocatalytic materials [19]. Moreover, the order of magnitude 10^6 is also referred to in the standard ISO 11137-2:2013, applied to assess the efficiency of a given method on the sterilization of health care products [31].

Under dark conditions the cell inactivation values in the presence of P25 and P25/graphene composite were, as expected, low (around 6% and 8%, respectively) and similar to those obtained in the absence of photocatalyst (around 5%), showing that these photocatalysts do not inhibit *E. coli* in the absence of irradiation – Fig. 7 and Fig. S1. Contrarily to what was expected, under the same conditions, the cell inactivation values for the carbon-modified VLP7000 and VLP7101 ranged from ~5 to 65% for assays
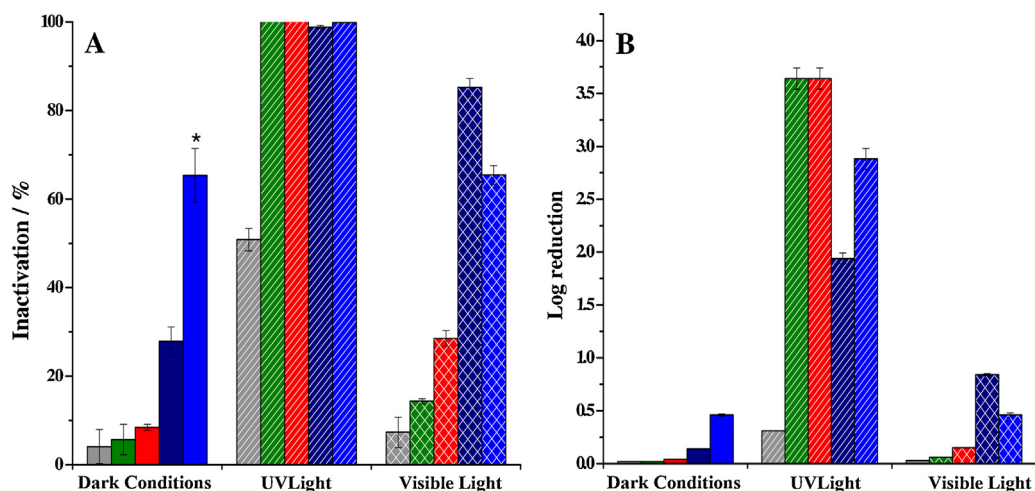
Fig. 7. *E. coli* viability loss (A) and log reduction (B) under dark, UV radiation and visible light for P25 (■), P25/graphene (■), VLP7101 (■), VLP7000 (■) and without photocatalyst (■). Results are mean values (*n* = 3) and the error bars represent the standard deviation. Initial cellular density – 10^6 CFU mL^{-1}. *This value ranged from 5.27% to 65.37% in trials conducted over a year.
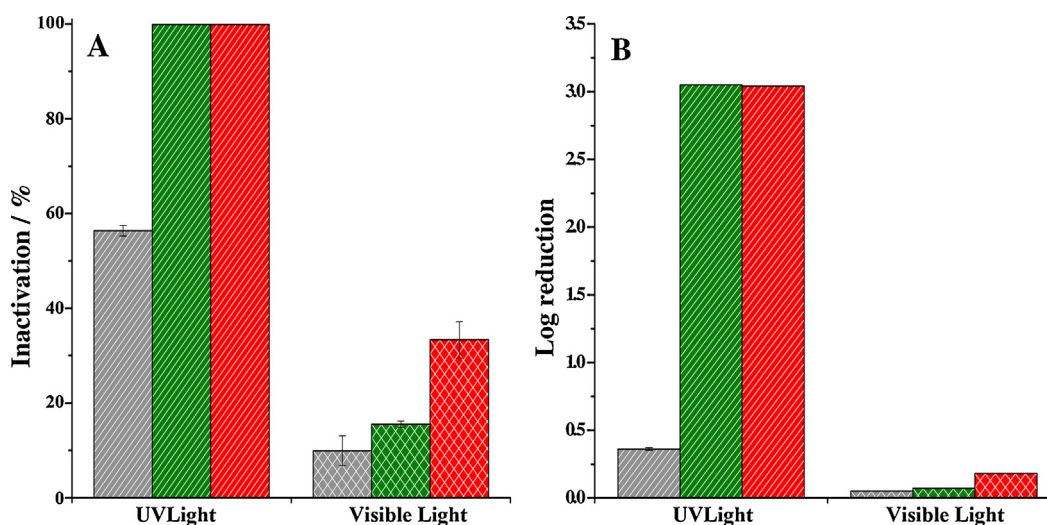

Fig. 8. *E. coli* viability loss (A) and log reduction (B) under UV radiation and visible light for P25 (■), P25/graphene (■) and without the use of a photocatalyst (■). Results are mean values (*n* = 3) and the error bars represent the standard deviation. Initial cellular density – 10^3 CFU mL^{-1}.

carried out over one year. These results show that VLP7000 and VLP7101 present some toxicity towards *E. coli* cells in the absence of irradiation. Additionally, these values also point out that these photocatalysts did not present stability, as it was already reported in previous studies [24,32]. Due to the mutagenic effect of UV irradiation, cell inactivation under UV was approximately 51% – Fig. 7 and Fig. S1.

Higher cell viability losses were obtained in the UV-photoinactivation trials. Under these conditions, similar cell inactivation values (99.98%), corresponding to log reduction values of around 3.6, were obtained for P25 and P25/graphene composite. Comparatively lower cell inactivation values were observed when VLP7000 and VLP7101 were irradiated with UV (99.87% and 98.85%, respectively), corresponding to log reduction values of 2.8 and 1.9, respectively.

Under visible light, the prepared P25/graphene composite produced two times higher viability loss values (∼29%), when compared with the commercial P25 (∼14%). Under the same conditions, cell inactivation with VLP7000 and VLP 7101 was much higher (∼65% and 85%, respectively) than the ones obtained for the pro-

duced P25/graphene (∼29%). However, as mentioned above, these commercial photocatalysts did not present stability, promoting cell inhibition even under dark conditions.

The influence of the initial cellular density on the photoinactivation was also studied. Additional trials carried out with P25 and the P25/graphene were conducted with an initial cellular density of 10^3 CFU mL^{-1}. As expected, with this lower initial cellular density, the values of photoinactivation obtained were higher than those obtained with an initial cellular density of 10^6 CFU mL^{-1} – Fig. 8 and Fig. S2. Total inactivation (log reduction value of 3) was verified when both catalysts were irradiated with UV. Under visible light, viability loss values reached around 15% for P25 and 33% for the P25/graphene composite. Although, the log reduction values were still low (0.07 and 0.18 for P25 and P25/graphene composite, respectively), the increase in the photoinactivation efficiency of the prepared composite can be ascribed to its slower rate of e^-/h^+ recombination and extended light absorption range, as suggested by its lower band gap value when compared with that of P25.

4. Conclusion

The prepared TiO$_2$/graphene photocatalyst presented better results for methylene blue and NO oxidation under UV radiation when compared with P25. Additionally, regarding photoinactivation of *E. coli* DSM 1103, the new photocatalyst exhibited higher inactivation activity under visible light than the commercial P25. When compared with VPL7101, the prepared photocatalyst showed similar photoactivity for methylene blue degradation and higher photoactivity regarding the NO oxidation. Both VLP7101 and VLP7000 achieved higher values of *E. coli* DSM 1103 inactivation than the prepared TiO$_2$/graphene. However, it was observed that VLP7101 and VLP7000 showed high values of inactivation under dark conditions, suggesting toxic properties of these materials.

Further developments in photoinactivation under visible light using TiO$_2$/graphene composites are expected not only from the improvement of this material but also from the use of suitable co-catalysts.

Acknowledgements

Appendix A. Supplementary data

Supplementary data associated with this article can be found, in the online version, at http://dx.doi.org/10.1016/j.bej.2015.05.016

References

[1] J. Colls, Air Pollution, Spon Press, 2002.
[2] H.A. Foster, I.B. Ditta, S. Varghese, A. Steele, Photocatalytic disinfection using titanium dioxide: spectrum and mechanism of antimicrobial activity, Appl. Microbiol. Biotechnol. 90 (2011) 1847–1868.
[3] T. Matsunaga, R. Tomoda, T. Nakajima, H. Wake, Photoelectrochemical sterilization of microbial cells by semiconductor powders, FEMS Microbiol. Lett. 29 (1985) 211–214.
[4] A. Fujishima, K. Honda, Electrochemical photolysis of water at a semiconductor electrode, Nature 238 (1972) 37–38.
[5] A. Fujishima, T.N. Rao, D.A. Tryk, Titanium dioxide photocatalysis, J. Photochem. Photobiol. C 1 (2000) 1–21.
[6] S. Banerjee, S.C. Pillai, P. Falaras, K.E. O'shea, J.A. Byrne, D.D. Dionysiou, New insights into the mechanism of visible light photocatalysis, J. Phys. Chem. Lett. 5 (2014) 2543–2554.
[7] P. Magalhães, L. Andrade, V.M. Sousa, O.C. Nunes, A. Mendes, Titanium dioxide photocatalysis: fundamentals and application on photoinactivation, Chem. Eng. J. (2014).
[8] R. Leary, A. Westwood, Carbonaceous nanomaterials for the enhancement of TiO$_2$ photocatalysis, Carbon 49 (2011) 741–772.
[9] B. Viswanathan, K.R. Krishanmurthy, Nitrogen incorporation in TiO$_2$: does it make a visible light photo-active material? Int. J. Photoenergy 2012 (2012) 10.
[10] Q. Xiang, J. Yu, M. Jaroniec, Graphene-based semiconductor photocatalysts, Chem. Soc. Rev. 41 (2012) 782–796.
[11] H. Zhang, X. Lv, Y. Li, Y. Wang, J. Li, P25-graphene composite as a high performance photocatalyst, ACS Nano 4 (2010) 380–386.
[12] G. Williams, B. Seger, P.V. Kamat, TiO$_2$-graphene nanocomposites. UV-assisted photocatalytic reduction of graphene oxide, ACS Nano 2 (2008) 1487–1491.
[13] N.T. Khoa, M.W. Pyun, D.H. Yoo, S.W. Kim, J.Y. Leem, E.J. Kim, S.H. Hahn, Photodecomposition effects of graphene oxide coated on TiO$_2$ thin film prepared by electron-beam evaporation method, Thin Solid Films 520 (2012) 5417–5420.
[14] K. Zhou, Y. Zhu, X. Yang, X. Jiang, C. Li, Preparation of graphene-TiO$_2$ composites with enhanced photocatalytic activity, New J. Chem. 35 (2011) 353–359.
[15] O. Akhavan, E. Ghaderi, Photocatalytic reduction of graphene oxide nanosheets on TiO$_2$ thin film for photoinactivation of bacteria in solar light irradiation, J. Phys. Chem. C 113 (2009) 20214–20220.
[16] A.B. Murphy, Band-gap determination from diffuse reflectance measurements of semiconductor films, and application to photoelectrochemical water-splitting, Sol. Energy Mater. Sol. Cells 91 (2007) 1326–1337.
[17] ISO 22197-1:2007 Fine ceramics (advanced ceramics, advanced technical ceramics) – Test method for air-purification performance of semiconducting photocatalytic materials – Part 1: Removal of nitric oxide, ISO (2007).
[18] C. Águia, J. Ângelo, L.M. Madeira, A. Mendes, Photo-oxidation of NO using an exterior paint – screening of various commercial titania in powder pressed and paint films, J. Environ. Manage. 92 (2011) 1724–1732.
[19] ISO 27447:2009 Fine ceramics (advanced ceramics, advanced technical ceramics) – Test method for antibacterial activity of semiconducting photocatalytic materials, ISO (2009).
[20] V.M. Sousa, C.M. Manaia, A. Mendes, O.C. Nunes, Photoinactivation of various antibiotic resistant strains of *E. coli* using a paint coat, J. Photochem. Photobiol. A 251 (2013) 148–153.
[21] Z. Huang, P.-C. Maness, D.M. Blake, E.J. Wolfrum, S.L. Smolinski, W.A. Jacoby, Bactericidal mode of titanium dioxide photocatalysis, J. Photochem. Photobiol. A 130 (2000) 163–170.
[22] A.L. Koch, Growth measurement, in: R.G.E.M.P. Gerhardt, W.A. Wood, N.R. Krieg (Eds.), Methods for General and Molecular Bacteriology, ASM, Press, Washington DC, 1994, pp. 248–292.
[23] R. Van De Krol, M. Grätzel, Photoelectrochemical Hydrogen Production, Springer, 2011, pp. 13–67.
[24] P. Zabek, J. Eberl, H. Kisch, On the origin of visible light activity in carbon-modified titania, Photochem. Photobiol. Sci. 8 (2009) 264–269.
[25] M. Pelaez, N.T. Nolan, S.C. Pillai, M.K. Seery, P. Falaras, A.G. Kontos, P.S.M. Dunlop, J.W.J. Hamilton, J.A. Byrne, K. O'Shea, M.H. Entezari, D.D. Dionysiou, A review on the visible light active titanium dioxide photocatalysts for environmental applications, Appl. Catal. B 125 (2012) 331–349.
[26] N. Mandzy, E. Grulke, T. Druffel, Breakage of TiO$_2$ agglomerates in electrostatically stabilized aqueous dispersions, Powder Technol. 160 (2005) 121–126.
[27] B. Ohtani, O.O. Prieto-Mahaney, D. Li, R. Abe, What is Degussa (Evonik) P25? Crystalline composition analysis, reconstruction from isolated pure particles and photocatalytic activity test, J. Photochem. Photobiol. A 216 (2010) 179–182.
[28] T.-D. Nguyen-Phan, V.H. Pham, E.W. Shin, H.-D. Pham, S. Kim, J.S. Chung, E.J. Kim, S.H. Hur, The role of graphene oxide content on the adsorption-enhanced photocatalysis of titanium dioxide/graphene oxide composites, Chem. Eng. J. 170 (2011) 226–232.
[29] ISO 10678: 2010, Fine Ceramics, Advanced Technical Ceramics – Determination of Photocatalytic Activity of Surfaces in an Aqueous Medium by Degradation of Methylene Blue, ISO, Geneva, 2010.
[30] A. Mills, C. Hill, P.K.J. Robertson, Overview of the current ISO tests for photocatalytic materials, J. Photochem. Photobiol. A 237 (2012) 7–23.
[31] ISO 1137-2:2013, Sterilization of Health Care Products — Radiation, ISO, Geneva, 2010.
[32] R. Quesada-Cabrera, A. Mills, C. O'Rourke, Action spectra of P25 TiO$_2$ and a visible light absorbing, carbon-modified titania in the photocatalytic degradation of stearic acid, Appl. Catal. B Environ. 150–151 (2014) 338–344.
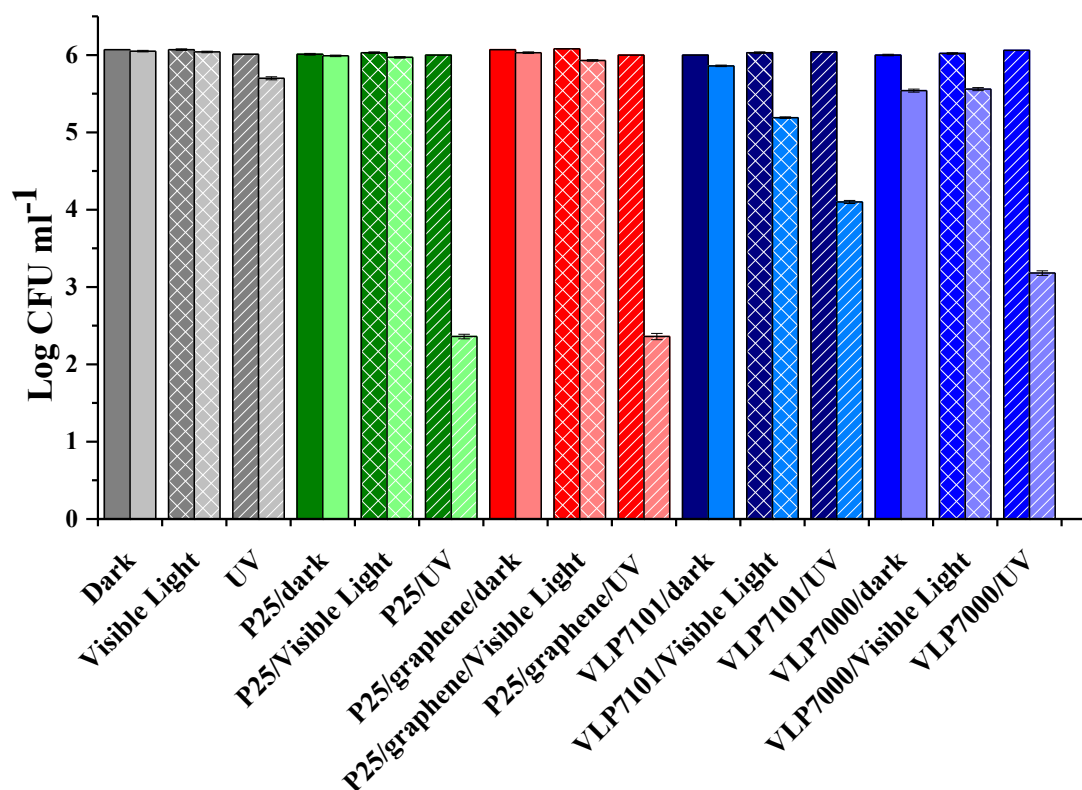
Supplementary Information

Photoinactivation Results

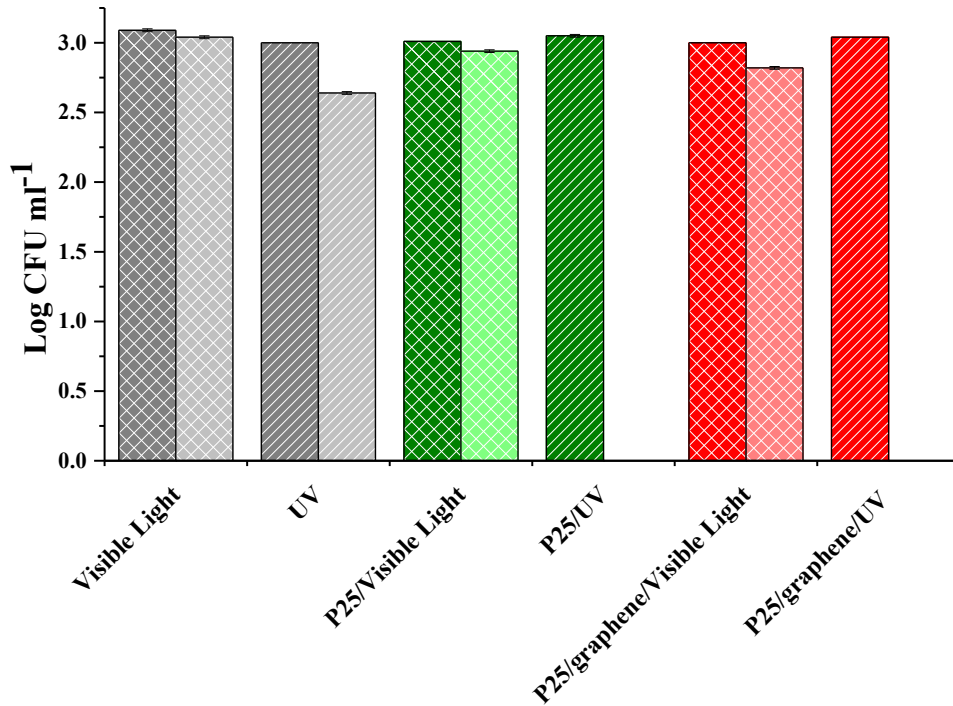**Figure S1.** Logarithmic *E. coli* cell counts under different conditions. Dark (⬛), in the presence of P25 (⬛), P25/graphene (⬛), VLP7101 (⬛) and VLP7000 (⬛). TiO$_2$/UV-A photocatalysis, in the presence of P25 (⬛), P25/graphene (⬛), VLP7101 (⬛), VLP7000 (⬛) and without the presence of photocatalyst (⬛). Visible light in the presence of P25 (⬛), P25/graphene (⬛), VLP7101 (⬛), VLP7000 (⬛) and without the presence of photocatalyst (⬛). t_i, initial instant (0 min) – darker colors; t_f, final instant (40 + 20 min) – lighter colors. Results are mean values (n = 3) and the error bars represent the standard deviation. Initial cellular density - 10^6 CFU·mL^{-1}.

Figure S2. Logarithmic *E. coli* cell counts under different conditions. Dark (⬛), in the presence of P25 (⬛), P25/graphene. TiO$_2$/UV-A photocatalysis, in the presence of P25 (▨), P25/graphene (▨) and without the presence of photocatalyst (▨). Visible light in the presence of P25 (▨), P25/graphene (▨), and without the presence of photocatalyst. t_i, initial instant (0 min) – darker colors; t_f, final instant (40 + 20 min) – lighter colors. Results are mean values (n = 3) and the error bars represent the standard deviation. Initial cellular density – 10^3 CFU·mL^{-1}.

Product information

AEROXIDE® TiO₂ P 25

Hydrophilic fumed titanium dioxide

Characteristic physico-chemical data

Properties and test methods	Unit	Value
Specific surface area (BET)	m²/g	35 - 65
pH value in 4% dispersion		3.5 - 4.5
Loss on drying* 2 hours at 105 °C	%	≤ 1.5
Tamped density*	g/l	100 - 180
Titanium dioxide based on ignited material	%	≥ 99.50
Al₂O₃ content based on ignited material	%	≤ 0.300
SiO₂ content based on ignited material	%	≤ 0.200
Fe₂O₃ content based on ignited material	%	≤ 0.010
HCl content based on ignited material	%	≤ 0.300
Sieve residue (by Mocker, 45μm)	%	≤ 0.050

* ex plant
The data represents typical values (no product specification)

Registrations (substance or product components)

AEROXIDE® TiO₂ P 25

CAS-No.	13463-67-7
REACH (Europe)	registered
TSCA (USA) DSL (Canada)	registered
ENCS (Japan) IECSC (China) KECI (Korea)	registered
AICS (Australia)	registered

AEROXIDE® TiO₂ P 25 is a fine-particulate, pure titanium dioxide (TiO₂) with high specific surface area and marked aggregate and agglomerate structure. Because of its high purity, high specific surface area, and unique combination of anatase and rutile crystal structure, the product is suitable for many catalytic and photocatalytic applications. Its structure also makes it suitable for use as an effective UV filter.

Applications and properties

Properties

- High specific surface area and high purity
- Crystalline TiO₂ with predominantly anatase structure
- Very good thermal and chemical stability
- Outstanding catalytic and photocatalytic efficiency
- Photoactive under UV-B radiation
- Heat-stabilizing effect in silicone elastomers through the influence of titanium dioxide on redox processes

Applications

- Raw material for catalyst substrates with high thermal and hydrothermal stability
- Efficient catalyst substrate with good thermal and hydrothermal stability
- Efficient photocatalyst for formulation of self-cleaning construction materials, such as concrete or mineral plasters
- Suitable for the construction of efficient dye-sensitized solar cells
- Efficient and overdyable heat stabilizer for silicone vulcanizates at process temperatures to more than 200 °C
- Improvement of the flammability protection of silicone vulcanizates
- Additive and raw material for ceramic and metal materials as bonding agent, sintering additive, or structural component

Packaging and storage

AEROXIDE® TiO₂ P 25 is supplied in multiple layer 10 kg bags. We recommend to store the product in closed containers under dry conditions and to protect the material from volatile substances. AEROXIDE® TiO₂ P 25 should be used within 2 years after production.

Safety and handling

A safety data sheet will be provided with your first delivery and with subsequent revisions. Additionally, the Product Safety Department of Evonik Resource Efficiency GmbH can be contacted via mail at sds-hu@evonik.com for specific questions. We recommend to reach the safety data sheer carefully prior to use of the product.

Customer Service

Europe/ Middle-East/ Africa/ Latin America
Evonik Resource Efficiency GmbH
Business Line Silica
PB 010-A410
Rodenbacher Chaussee 4
63457 Hanau-Wolfgang
Germany
PHONE +49 6181 59 12532
FAX +49 6181 59 712532
aerosil@evonik.com
www.aerosil.com

North America
Evonik Corporation
Business Line Silica
299 Jefferson Road
Parsippany, NJ 07054-0677
USA
PHONE +1 800-233-8052
FAX +1 973-929-8502
aerosil@evonik.com
www.aerosil.com

Asia (excluding Japan)
Evonik (SEA) Pte. Ltd.
Business Line Silica
3 International Business Park
Nordic European Centre, #07-18
Singapore 609927
PHONE +65 6809-6877
FAX +65 6809-6677
aerosil@evonik.com
www.aerosil.com

Japan
NIPPON AEROSIL CO., LTD.
Marketing & Sales Division
P.O. Box 7015
Shinjuku Monolith 13F
3-1, Nishi-Shinjuku 2-chrome
Shinjuku-ku, Tokyo
163-0913 Japan
PHONE +81 3 3342-1789
FAX +81 3 3342-1761
infonac@evonik.com
www.aerosil.jp

Technical Service

Europe/ Middle-East/ Africa/ Latin America
Evonik Resource Efficiency GmbH
Business Line Silica
HPC 911-221 A
Rodenbacher Chaussee 4
63457 Hanau-Wolfgang
Germany
PHONE +49 6181 59-3936
FAX +49 6181 59 4489
technical.service.aerosil@evonik.com
www.aerosil.com

North America
Evonik Corporation
Business Line Silica
2 Turner Place
Piscataway, NJ 08855-0365
USA
PHONE +1 888 SILICAS
PHONE +1 732 981-5000
FAX +1 732 981-5275
technical.service.aerosil@evonik.com
www.aerosil.com

Asia (excluding Japan)
Evonik Specialty Chemicals (Shanghai) Co.,Ltd
Business Line Silica
55 Chundong Road
Xinzhuang Industry Park
Shanghai 201108
P.R. China
PHONE +86 21 6119-1151
FAX +86 21 6119-1075
technical.service.aerosil@evonik.com
www.aerosil.com

Japan
NIPPON AEROSIL CO., LTD.
Applied Technology Group
3 Mita-Cho
Yokkaichi, Mie
510-0841 Japan
PHONE +81 59 345-5270
FAX +81 59 346-4657
infonac@evonik.com
www.aerosil.jp

EVONIK
POWER TO CREATE

KRONOS

Limpieza por medio de la luz

La innovación para la
supresión catalítica
de contaminantes:

KRONOS vlp 7000

KRONOS vlp 7000 –
La innovación para la supresión catalítica de contaminantes
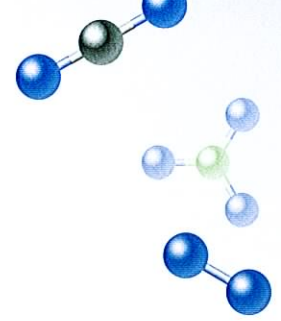
KRONOS vlp 7000 es un fotocatalizador basado en el bióxido de titanio. Este producto cataliza – es decir, propicia y acelera – la descomposición de moléculas orgánicas y la mineralización de compuestos inorgánicos como los óxidos de nitrógeno (NO_X) bajo la radiación con luz visible, así como bajo la acción de la radiación ultravioleta (luz solar). Las substancias nocivas se convierten en componentes inocuos, como el agua y el bióxido de carbono.

KRONOS vlp 7000 actúa donde los catalizadores convencionales no pueden actuar, y desarrolla su acción:
- **detrás de capas de cristal**
- **con bombillas normales y lámparas de bajo consumo eléctrico**
- **bajo la luz del crepúsculo**
- **con luz difusa**

y, naturalmente, como hasta ahora, también bajo la acción de la luz ultravioleta.

Es suficiente una pintura de emulsión para interiores con KRONOS vlp 7001 para mejorar la calidad del aire ambiental.
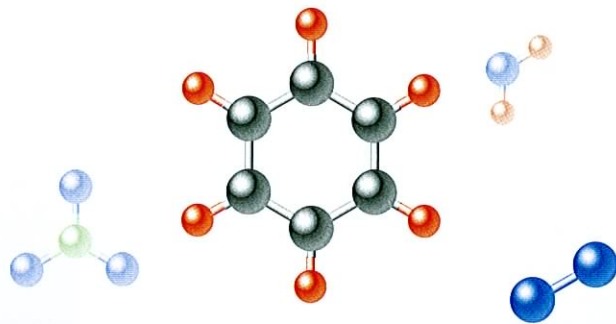
Gama de fotocatalizadores KRONOS

	Fotocatalizador a base de TiO_2 …	optimizado para …
KRONOS vlp 7000	… activado por luz visible	… una elevada fotoactividad
KRONOS vlp 7001	… activado por luz visible	… una relación ideal entre propiedades ópticas y fotoactividad
KRONOS uvlp 7500	… activado por luz ultravioleta	… fotoactividad bajo rayos ultravioleta
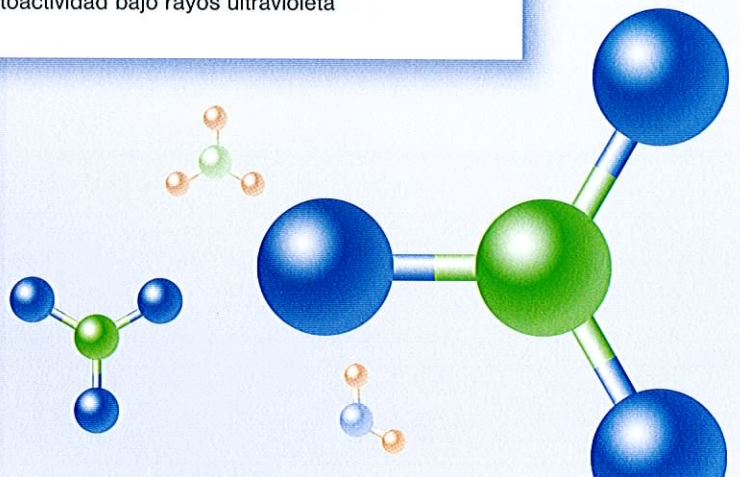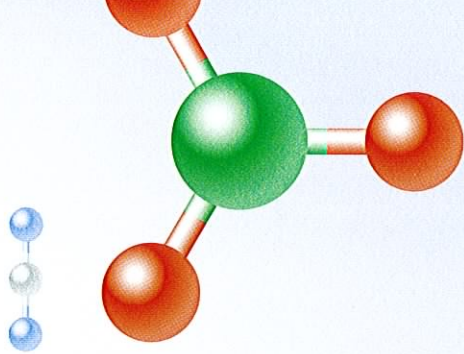
KRONOS vlp 7000 se utiliza para suprimir olores molestos, manchas de origen orgánico y suciedad depositada sobre superficies.

Está documentada su eficacia en la eliminación de numerosos contaminantes:

- nicotina y alquitrán
- amoniaco y aminas
- aldehídos y alcoholes, como formaldehído, acetaldehído y metanol
- fenoles y otros compuestos aromáticos, como por ejemplo benceno, p-clorofenol, bifenilenos policlorados
- óxidos de nitrógeno y monóxido de carbono

Además, se ha podido constatar que los sistemas a base de KRONOS vlp 7000 contribuyen a reducir la contaminación con distintos tipos de algas, mohos y bacterias.

KRONOS vlp 7000 se utiliza en todos los campos de aplicación de los catalizadores convencionales bajo luz ultravioleta: por ejemplo, como catalizador para la conversión de NO_X, con el fin de mejorar la calidad del aire en núcleos urbanos.
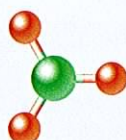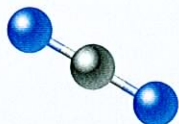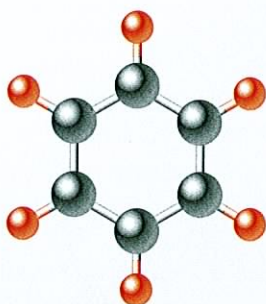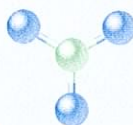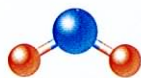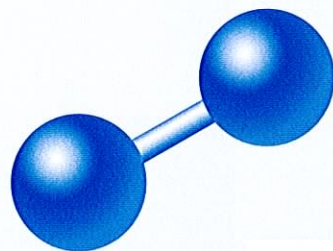
KRONOS vlp 7000

Forma de suministro	polvo beige pálido
Contenido en TiO_2	~ 95 %
Tamaño de cristalita (anatasa)	~15 nm
Superficie específica BET	> 250 m^2/g
Densidad (ISO 787, parte 10)	3,9 g/cm^3
Densidad aparente	~ 350 kg/m^3
Embalaje	sacos de 10 kg
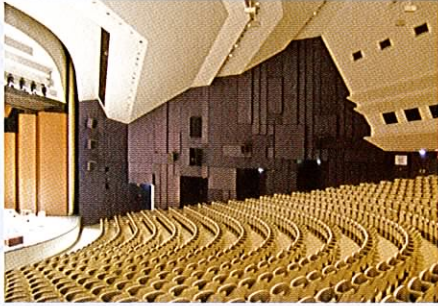
Principio de actuación
El mecanismo de activación con KRONOS vlp 7000

El bióxido de titanio es un producto conocido, como pigmento y absorbente de la luz ultravioleta, que protege la matriz de polímero de su disgregación directa bajo la acción de los rayos ultravioleta. Los pigmentos de bióxido de titanio convencionales están optimizados para garantizar una actividad fotocatalítica mínima. Es decir, la energía de la luz absorbida se convierte en calor. En cambio, en los fotocatalizadores, la energía se utiliza con gran eficiencia para la formación de radicales del tipo del $°OH$ y el $HO_2°$ sobre la superficie del TiO_2. KRONOS vlp 7000 pone estos radicales a disposición para la supresión de substancias indeseadas. A diferencia de los fotocatalizadores convencionales a base de TiO_2, en este caso no se requiere una exposición a la radiación ultravioleta.
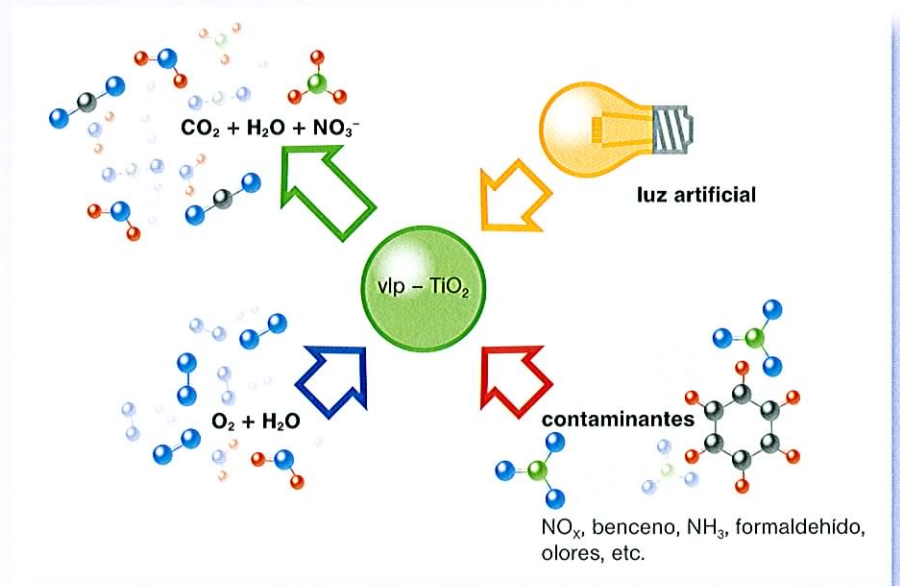
Fig. 1: Supresión de contaminantes con ayuda de fuentes de luz artificial
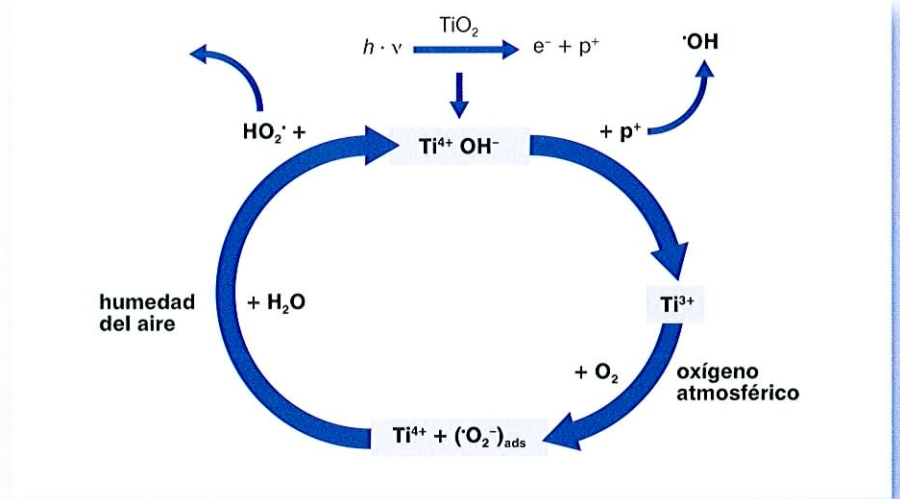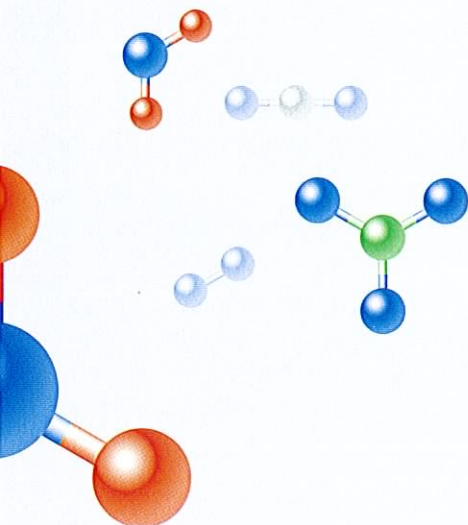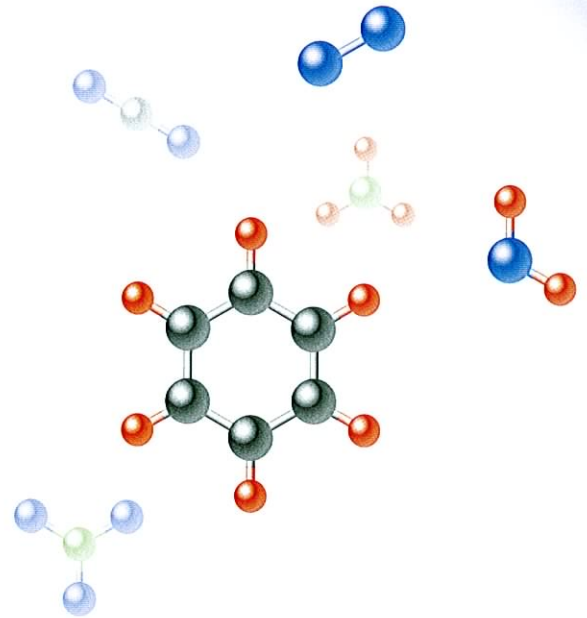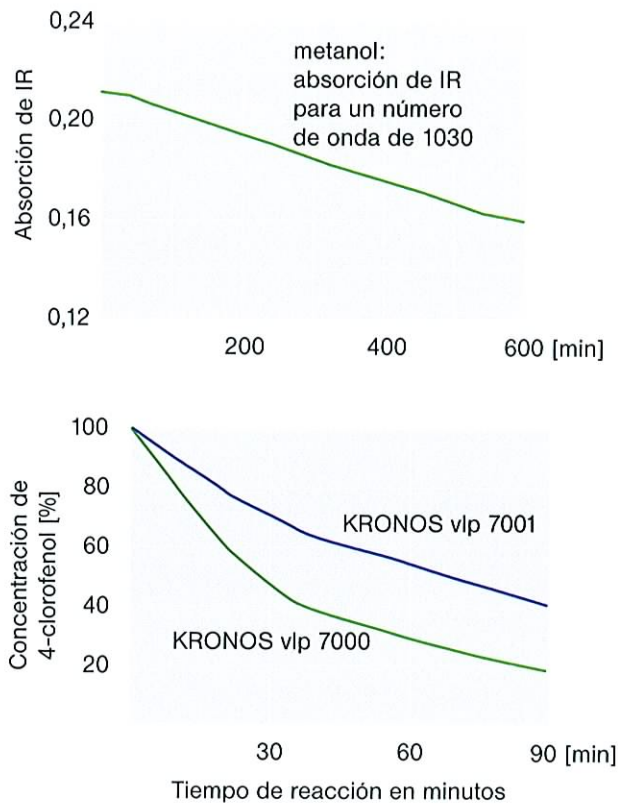

Fig. 2: Fotocatálisis con TiO_2

Fig. 3 a y b: Supresión de diversos contaminantes por acción de los fotocatalizadores KRONOS bajo la acción de la luz visible
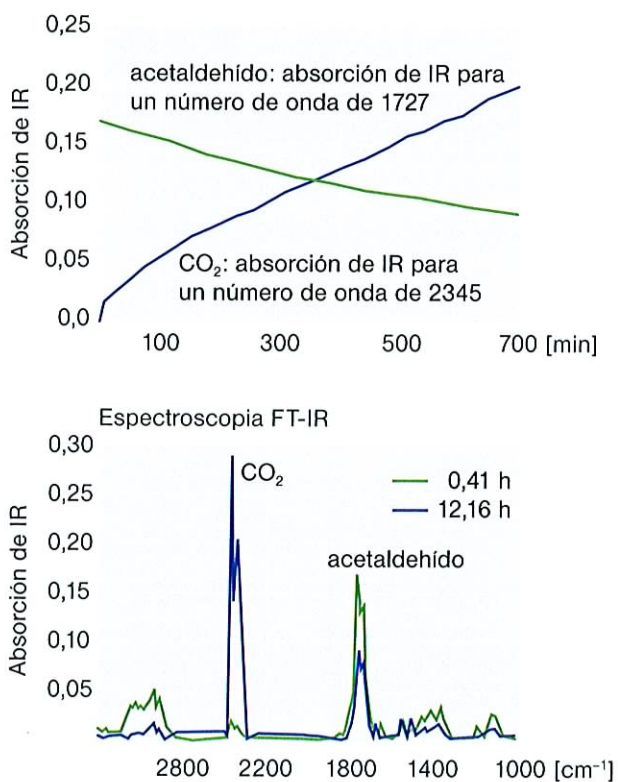

Fig. 4 a y b: Supresión del acetaldehído y formación de bióxido de carbono con KRONOS vlp 7000 bajo la acción de la luz visible

Una diferencia decisiva

Los fotocatalizadores convencionales suelen utilizar sólo la radiación ultravioleta, hasta una longitud de onda aproximada de 400 nm. Por lo tanto, aprovechan menos de un 6% de la energía irradiada sobre la tierra. La gama de luz visible entre los 400 nm y 800 nm constituye un 52% aproximadamente de la energía solar disponible.

Gracias a una modificación especial, KRONOS vlp 7000 está en condiciones de aprovechar, no sólo la radiación ultravioleta, sino también una parte de la luz visible en la gama de longitud de onda mayor de 400 nm. Con KRONOS vlp 7000 se amplía considerablemente el margen de eficiencia de los fotocatalizadores de TiO_2. Ahora pueden aprovecharse, por ejemplo, las horas del crepúsculo, en las que los fotocatalizadores convencionales no muestran prácticamente eficiencia alguna. Los fotocatalizadores KRONOS para luz visible se utilizan ya con éxito en interiores.
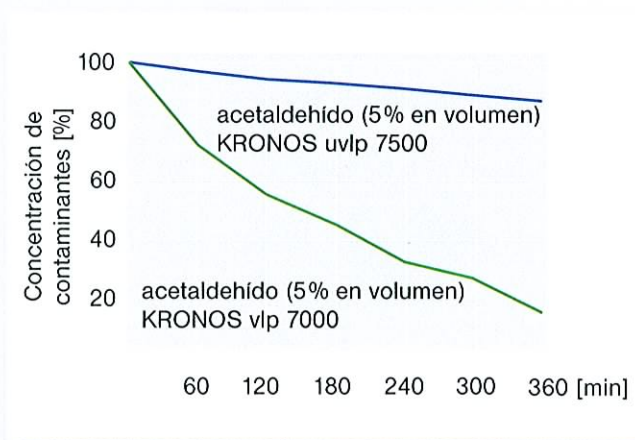

Fig. 5: Supresión del acetaldehído por medio de KRONOS vlp 7000 bajo la acción de la luz visible en comparación con los fotocatalizadores convencionales, como KRONOS uvlp 7500
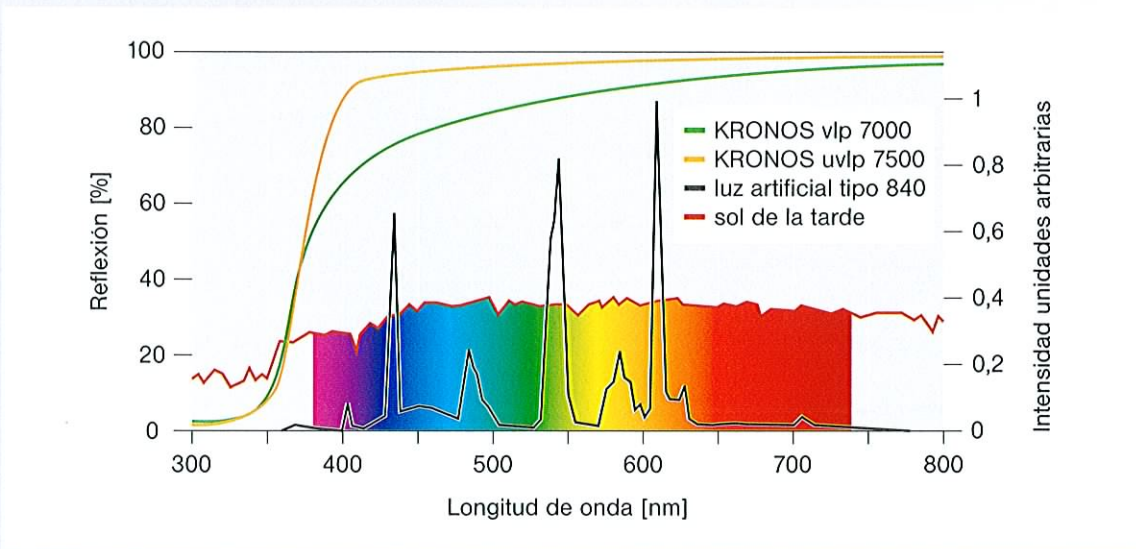

Fig. 6: Espectros de radiación de la luz artificial y la luz solar y espectros de reflexión de KRONOS vlp 7000 en comparación con los fotocatalizadores convencionales, como KRONOS uvlp 7500

El fotocatalizador y su uso correcto

KRONOS vlp 7000 es un polvo de color beige pálido y carece de propiedades pigmentarias en la concentración necesaria habitualmente. La temperatura no tiene que superar los 150 °C durante el procesado.

El fotocatalizador debe su eficiencia a los cristales de unos 15 nm de tamaño, aglomerados en el polvo, y responsables de una superficie específica muy grande de unos 300 m²/g (Fig. 8). La eficiencia del catalizador depende considerablemente de la calidad de la distribución en el sistema concreto, y por lo tanto de la calidad de la molienda y de la estabilización las partículas en la substancia ligante.

La concentración necesaria depende de la aplicación concreta. Recomendamos utilizar en los primeros ensayos una concentración del 5 % en la capa activa a título de orientación. En los sistemas fotocatalíticos, el fotocatalizador tiene que entrar en contacto directo con los contaminantes que deben suprimirse, y con la luz en una gama adecuada de longitud de onda. Esto se consigue generalmente mediante la integración de KRONOS vlp 7000 en una matriz porosa, similar a una esponja, o mediante su fijación sobre la superficie del sistema. Un ejemplo del aumento de la eficiencia mediante optimización de la porosidad del substrato se muestra en las gráficas 9, 10 y 11.
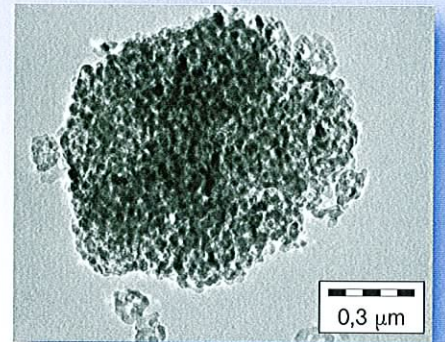

Fig. 7: KRONOS vlp 7000

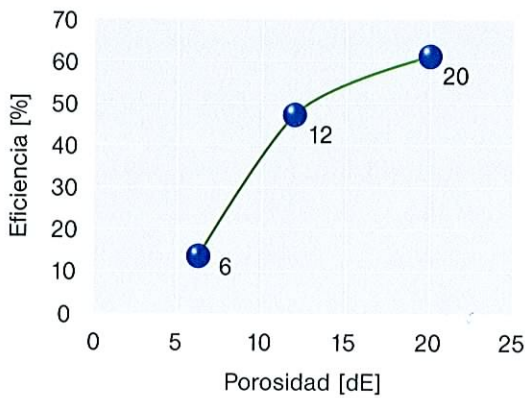Fig. 8: Análisis de KRONOS vlp 7000 bajo el microscopio electrónico

Fig. 9

Fig. 9: Eficiencia de KRONOS vlp 7000 en la conversión del óxido de nitrógeno en recubrimientos de distinta porosidad (CVP 72,3 %, pigmento de TiO₂ 10 %, KRONOS vlp 7000 10 %, espesor de la capa 60 μm)
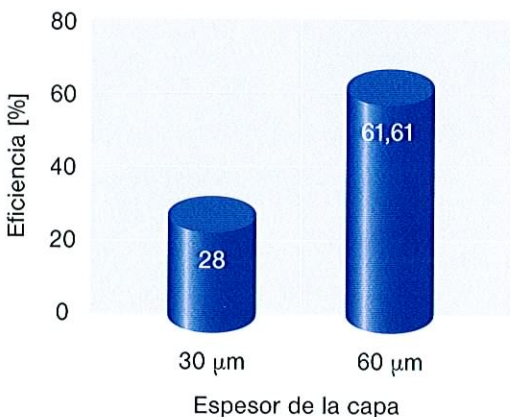
Fig. 10: Eficiencia de KRONOS vlp 7000 en la conversión del óxido de nitrógeno en recubrimientos con distinto espesor de la capa (CVP 72,3 %, pigmento de TiO₂ 10 %, catalizador de TiO₂ 10 %)

Fig. 11: Eficiencia de KRONOS vlp 7000 en la conversión del óxido de nitrógeno en función de la concentración en recubrimientos con distinta porosidad (pigmento de TiO₂ 10 %, espesor de la capa 60 μm)
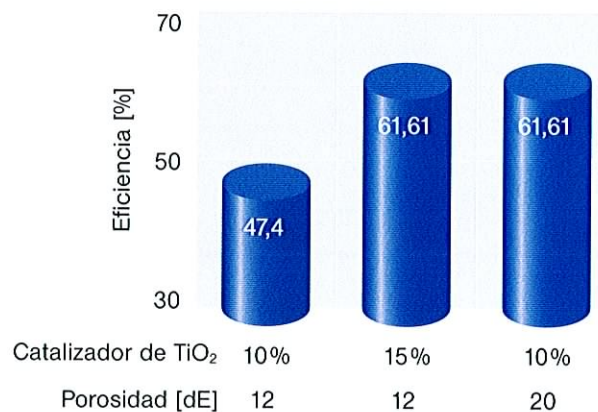

Fig. 10

Fig. 11

KRONOS® vlp 7000
TiO₂ Photocatalyst

KRONOS
TITANIUM DIOXIDE

10 kg

KRONOS WORLDWIDE, Inc. · Dallas/TX · USA
KRONOS CANADA, Inc. · Varennes · Canada
KRONOS EUROPE S.A./N.V. · Ghent · Belgium
KRONOS TITAN AS. · Fredrikstad · Norway
KRONOS TITAN GmbH · Leverkusen · Germany

KRONOS®
vlp 7000
TiO₂ Photocatalyst

HMIS Rating
Health   1
Flammability   0
Reactivity   0

Servicio Técnico de Aplicación – KRONOS TiO₂

KRONOS INTERNATIONAL, Inc.
Peschstr. 5
D-51373 Leverkusen • Alemania
Tel. (+49 214) 356-0
Fax (+49 214) 3562412
kronos.tsd.leverkusen@kronosww.com

Oficinas de ventas de TiO₂ KRONOS

Europa

*Alemania/Austria/Suiza/
Italia/Este de Europa*

KRONOS TITAN GmbH
Peschstr. 5 • D-51373 Leverkusen
Tel. (+49 214) 356-0
Fax (+49 214) 3562585
kronos.sales.leverkusen@kronosww.com

Benelux

KRONOS EUROPE S.A./N.V.
Langerbruggekaai 10, Haven 8160A
B-9000 Ghent • Bélgica
Tel. (+32 9) 2540368
Fax (+32 9) 2540369
kronos.sales.belux@kronosww.com

KRONOS B.V.
Guldenwaard 133 b
NL-3078 AJ Rotterdam • Holanda
Tel. (+31 10) 4136310
Fax (+31 10)4046399
kronos.sales.netherlands@kronosww.com

Dinamarca

KRONOS DENMARK ApS
Hanne Nielsens Vej 10 • DK-2840 Holte
Tel. (+45) 45461206 • Fax (+45) 45461226
kronos.sales.denmark@kronosww.com

España

ZEUS QUIMICA S.A.
Santalo 152-154, bajos
E-08021 Barcelona
Tel. (+34 932) 402222
Fax (+34 932) 402223
zeus@zeusquimica.com

Europa septentrional/Países bálticos

KRONOS TITAN AS
Titangaten 1 • N-1602 Fredrikstad • Noruega
Tel. (+47) 69309000 • Fax (+47)69309001
kronos.sales.scandinavia@kronosww.com

Francia/Portugal/Grecia/África del norte

SOCIETE INDUSTRIELLE DU TITANE
45, rue de Courcelles • F-75008 Paris
Tel. (+33) 153839360
Fax (+33) 142252263
kronos.sales.france@kronosww.com

Gran Bretaña/Irlanda

KRONOS Limited
Barons Court • Manchester Road
Wilmslow, Cheshire SK9 1BQ • UK
Tel. (+44 1625) 547200
Fax (+44 1625) 533123
kronos.sales.uk@kronosww.com

América del norte

Canadá

KRONOS CANADA, Inc.
2000, McGill College Avenue, Suite 1610
Montreal, Quebec H3A 3H3
Tel. (+1 514) 397-3501
Fax (+1 514) 393-1186
kronos.canada@kronosww.com

Estados Unidos/México

KRONOS, Inc.
5 Cedarbrook Drive
Cranbury, NJ 08512 • USA
Tel. (+1 609) 860-6200
Fax (+1 609) 860-6258
kronos.marketing@kronosww.com

Demás países

KRONOS INTERNATIONAL, Inc.
KRONOS Export Department
Peschstr. 5 • D-51373 Leverkusen • Alemania
Tel. (+49 214) 356-0
Fax (+49 214) 3562208
kronos.export@kronosww.com

Estas informaciones contienen indicaciones y sugerencias para el usuario. No pretenden ser completas y se presentan sin compromiso. Deben observarse en cada caso las disposiciones legales vigentes, incluyendo posibles derechos de terceros. Nuestros laboratorios están a disposición de los clientes para tratar y estudiar los problemas y consultas relacionados con el empleo de nuestros productos.

KRONOS INTERNATIONAL, Inc.
Peschstr. 5 · D-51373 Leverkusen · Alemania
Teléfono (+49 214) 356-0 · Telefax (+49 214) 42150
kronos.international@kronosww.com

DS2140S/107.5S